New Ruthenium (II)-Chloroquine Complexes and Metal-Free Aminoquinolines: Synthesis, Antimalarial Activity and Mechanism of Biological Action

By

Chandima Shashikala Kumari Rajapakse

A dissertation submitted to the Graduate Faculty in Chemistry in partial fulfillment of the requirements for the degree of Doctor of Philosophy, The City University of New York

2010

This manuscript has been read and accepted for the

Graduate Faculty in Chemistry in satisfaction of the

dissertation requirements for the degree of Doctor of Philosophy.

Prof. Roberto A. Sanchez-Delgado

_____ _____

Date Chair of Examining Committee

Professor Mehesh K. Lakshman

_____ _____

Date Executive Officer

Professor Roberto A. Sanchez-Delgado

_____

Professor Richard Magliozzo

_____

Professor Wayne W. Harding

_____

Supervisory Committee

THE CITY UNIVERSITY OF NEW YORK

ABSTRACT

New Ruthenium (II)-Chloroquine Complexes and Metal-Free Aminoquinolines:

Synthesis, Antimalarial Activity and Mechanism of Biological Action

by

Chandima S. K. Rajapakse

Advisor – Professor Roberto A. Sanchez-Delgado

Malaria is widespread in many tropical and subtropical regions and causes between one and three million deaths annually. The disease is caused by a protozoan parasite of the genus *Plasmodium* that is transmitted primarily by the female Anopheles mosquito. Chloroquine (CQ) is the most commonly used antimalarial drug, but resistant strains of *P. falciparum* have emerged and thus improved chemotherapies are required. Modifications of the molecular structure of chloroquine led to other effective quinoline based drugs but unfortunately, resistance to these drugs is now also common in many parts of the world.

The success of cisplatin and other platinum anticancer drugs has stimulated a renaissance of inorganic medicinal chemistry and the search for complexes of other transition metals with better biological properties. Among them, ruthenium complexes are attracting increasing attention as potential chemotherapeutic agents against a variety of diseases.

Complexation of CQ to Ru has been previously shown by our group to enhance the activity against resistant strains of the malaria parasite, as for instance the complex $[RuCl_2(CQ)]_2$. In the first phase of this thesis we adopted a molecular design based on

Ru(II) forming coordinate bonds to CQ through one of the basic nitrogen atoms. A series of new organo-Ru^{II}-CQ complexes were synthesized and characterized by use of a combination of NMR and FTIR spectroscopy with DFT calculations.

All the new complexes were active against CQ-resistant (Dd2, K1, and W2) and CQ sensitive (FcB1, PFB, F32 and 3D7) malaria parasites (*Plasmodium falciparum*); importantly, the potency of these complexes against resistant parasites is consistently higher than that of the standard drug chloroquine diphosphate (CQDP). In order to understand the origin of the improved antimalarial activity, we have measured water/*n*-octanol partition coefficients, pK_a values, heme binding constants, and heme aggregation inhibition activity of the new (π-arene)-Ru-CQ complexes. Measurements of heme aggregation inhibition activity of the metal complexes atq water/*n*-octanol interfaces qualitatively predict their superior antiplasmodial action against resistant parasites, in relation to CQ. Some interesting tendencies emerge from our data, indicating that the antiplasmodial activity is related to a balance of effects associated with the lipophilicity, basicity, and structural details of the compounds studied.

We concluded that the increase in the lipophilicity of CQ caused by coordination to the Ru-containing fragments is beneficial for overcoming resistance but the reduction in basicity due to the blocking of one active nitrogen atom by the metal limits the therapeutic potential of the complexes.

Therefore, new compounds combining the desired basicity and lipophilicity are needed. Based on this new model, two new metal free 4-aminoquinoline derivatives were synthesized and characterized by 1D/2D NMR spectroscopy, elemental analysis and mass

spectrometry. Both compounds are highly active *in vitro* against CQ-resistant strains of *P. falciparum* (K1, K14 and Dd2) as well as a CQ-sensitive strain (D6). Both compounds are more basic and more lipophilic than the standard drug CQ. Our mechanistic studies demonstrate the validity of our hypothesis: that the structural and physicochemical modifications of 4-aminoquinoline imposed by the presence of the lipophilic substituent as a side chain lead to an enhanced activity against malaria parasites, while retaining heme aggregation as the main target of action.

Dedicated to my Beloved Parents

ACKNOWLEDGMENTS

I am grateful to many people who have helped me in numerous ways towards the completion of my educational endeavor. Foremost, I would like to express my sincere thanks and gratitude to my advisor Prof. Roberto Sanchez-Delgado. His ever-willing support, guidance, and constant encouragement enabled successful completion of my doctoral study. Without his encouragement, it would have been impossible to complete my graduate work and develop adequate understanding of the research subjects, which is necessary for my professional growth and development. He gave me many opportunities to grow not only as a scientist but also as an individual.

I would also like to thank my committee members, Prof. Richard Magliozzo, Prof. Wayne Harding and Prof. Rajeev Muthyala. Their critical questions and insightful suggestions motivated me to evaluate my research from different perspectives.

A special thanks to Dr. Alberto Martinez who helped and guided my research work and a very sincere thanks to Prof. Andrzej Jarzecki who helped me with computational studies.

I would like to express my heart-felt gratitude to our collaborator Prof. Joseph Schrevel, who evaluated the biological activity of our new complexes.

I also thank all my teachers and colleagues who helped, supported and encouraged me along the way. In particular, I like to thank Becky Naoulou, Dalanda Jalloh, Cula Dautriche, Minfeng Fang, Lei Chen, Reena Rahi, Nancy Medina, Mahendran Adaickkapillai and Vijay Ramalingam.

I like to extend special thanks to my family, especially, my parents and brother who gave their unconditional support and love. Finally, I acknowledge the financial support from Brooklyn College of CUNY for providing the teaching assistance.

Table of Contents

Page

List of Symbols and Abbreviations

P	Plasmodium
A	Anopheles
Fe(III)PPIX	Ferriprotoporphyrin IX
Fe(II)PPIX	Ferrousprotoporphyrin IX
DNA	Deoxyribonucleic acid
CQ	Chloroquine
CQDP	Chloroquine diphosphate
HAP	Histoaspartic protease
M	Molarity
nm	Nanometer
μm	Micrometer
mM	Millimolar
μScm^2Mol^{-1}	Micro Siemens square centimeter per mole
Kcal/Mol	Kilocalories per mole
TEM	Transmission electron microscopy
HRP II	Histidine rich protein II
MMG	Monomyristoylglycerol
HDP	Heme detoxification protein
PfCRT	*Plasmodium falciparum* chloroquine resistance transporter
Pgh1	P-glycoprotein homologue 1
RBC	Red blood cell
FV	Food vacuole
Me	Methyl
Im	Imidazole
CTZ	Clotrimazole
KTZ	Ketoconazole

Ar	Arene
FTIR	Fourier transforms infrared spectroscopy
UV	Ultraviolet- visible
DFT	Density functional theory
B3LYP	Becke, three-parameter, Lee-Yang-Parr
LANL2DZ	Los Alamos National Laboratory 2 double ζ
ECP	Effective core potential
PCM	Polarizable continuum model
D	Distribution coefficient
DMSO	Dimethyl sulfoxide
HAIA	Heme aggregation inhibition activity
SCRF	Self – consistent reaction field
COSY	Correlated spectroscopy
HMBC	Heteronuclear multiple bond correlation spectroscopy
HSQC	Heteronuclear single quantum coherence spectroscopy
NMR	Nuclear magnetic resonance
Δδ	Variations in chemical shifts
T_1	Proton relaxation time
ΔE	Energy difference
MD	Molecular dynamics
pK_a	Log value of acid dissociation constant
VAR	Vacuolar accumulation ratio

List of Figures

Chapter 1

Chapter 2

Figure **Page**

Chapter 3

Figure **Page**

Chapter 4

Figure **Page**

Chapter 5

Figure **Page**

List of Tables

Chapter 1

Chapter 2

Chapter 3

Chapter 4

Table **Page**

Chapter 5

Table **Page**

List of Schemes

Chapter 2

Chapter 5

Chapter 1

An Overview: Malaria

1.1 What is malaria – History

Malaria is the world's most important tropical parasitic disease, since it kills more people than any other communicable disease except for tuberculosis. According to the World Health Organization, 300-500 million people become infected and close to a million die of malaria each year, mostly children under 5 years of age. About 40% of the world's population is at risk of contracting malaria, particularly in the poorest countries.[1]

Malaria is an infectious disease caused by a parasite of the genus *Plasmodium*, which infects red blood cells. *Plasmodium* is a protozoan, a single-celled organism able to divide only within a host cell. Malaria is characterized by cycles of chills, fever, pain and sweating. It is believed that malaria has infected humans since the beginning of mankind. The name "mal 'aria" (meaning "bad air" in Italian) was first used in English in 1740 by H. Walpole. The term malaria evolved into the name of the disease only during the 20th century and until then various names such as jungle fever, marsh fever, paludal fever, or swamp fever were used to name this disease.[2] In 1880, C. Laveran identified the parasites in human blood.[3] In 1889, R. Ross discovered that mosquitoes transmitted malaria.[2] Four different parasites of the *Plasmodium* genus affect humans - *Plasmodium falciparum*, *Plasmodium vivax, Plasmodium malariae,* and *Plasmodium ovale;* the first two are the most common and *P. falciparum* (Figure 1) causes the most deadly form of the disease. The other three species of malaria are generally not life-threatening and less serious. Malaria is a curable disease if promptly diagnosed and adequately treated.

Figure 1. *Plasmodium falciparum*[4]

1.2 How is malaria transmitted?

The life cycle of the parasite involves two hosts, humans and *Anopheles* mosquitoes. The disease is transmitted to humans when an infected female *Anopheles* mosquito bites a person and injects the malaria parasites (sporozoites) into the blood stream (Figure 2). Only female mosquitoes (Figure 3) feed on blood, hence males do not transmit the disease. The females of the *Anopheles* mosquito enter houses between 5 p.m. and 9.30 p.m. and again in early hours of the morning.[3] They start biting by late evening, reaching a peak of biting activity at midnight and early hours of morning.[5] Various species have been found to be the vectors in different parts of the world. *A. gambiae* is the chief vector in Africa and *A. freeborni* in North America.[5] Nearly 45 species of the mosquito have been found in India and *A. culicifacies, A. fluviatilis, A. minimus, A. philippinensis, A. stephensi, A. sundaicus and A. leucosphyrus* have been implicated in the transmission of malaria.[6]

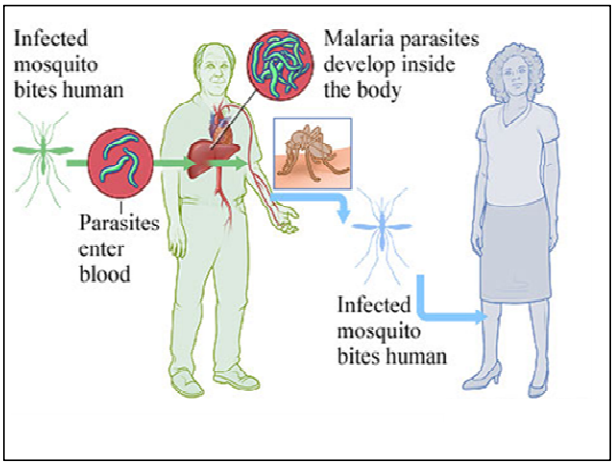

Figure 2. Infected mosquito transmits the disease

Figure 3. *Anopheles* mosquito[7]

Mosquitoes have four stages in their life cycle as represented in Figure 4; egg, larva, pupa and adult. The female mosquito lays 30-150 eggs every 2-3 days and breeds in natural water collections. She needs human blood to nourish these eggs. The average life span of a mosquito is 2-3 weeks and usually it takes about a week for the eggs to develop into adults.

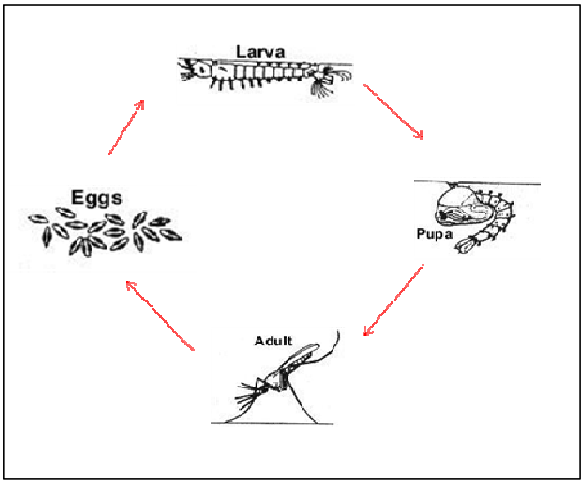

Figure 4. The life cycle of mosquito

1.3 The life cycle of the parasite

There are three major stages in the life cycle of the parasite: the mosquito, liver and blood (Figure 5). Following the bite of an infected mosquito, *P. falciparum* invades human liver cells, emerging into the blood stream after 7 to 10 days, when it enters into the red blood cells of the host. While in red blood cells, the parasites again develop until a mosquito takes a blood meal from an infected human and ingests human red blood cells containing the parasites. Then the parasites reach the *Anopheles* mosquito's stomach and invade the mosquito's salivary glands. When an *Anopheles* mosquito bites a human, these sporozoites complete and repeat the complex *Plasmodium* life cycle.[8] Most of the curative drugs act on the blood stage of the parasite.

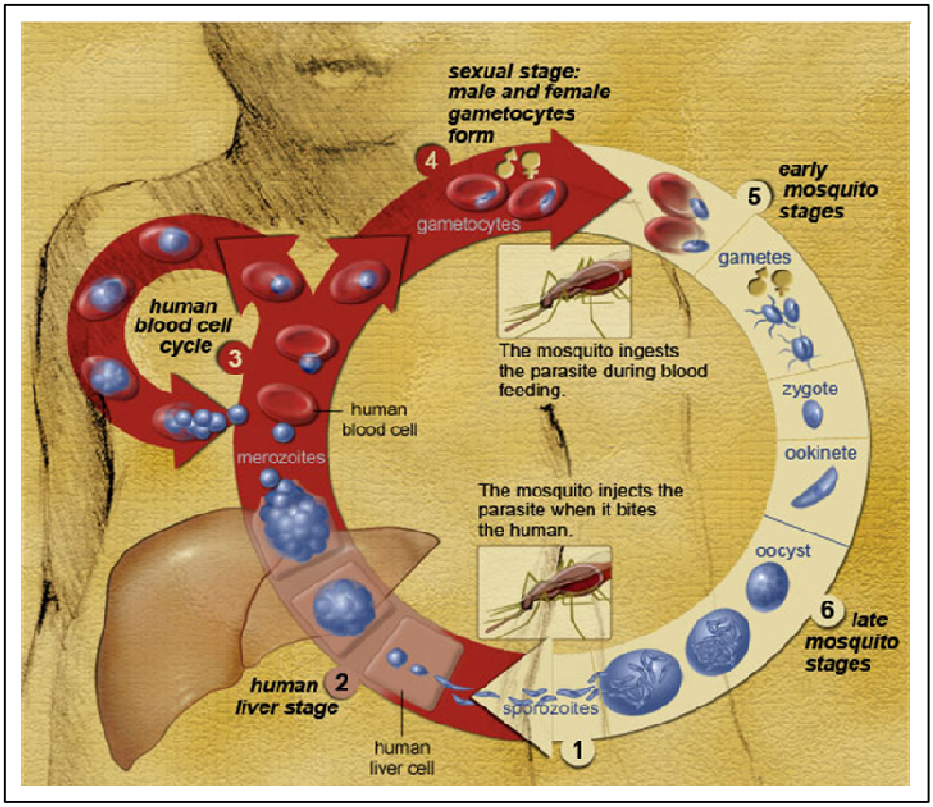

Figure 5. The complete life cycle of the parasite[9]

1.4 Distribution of malaria

It is believed that malaria originated in West and Central Africa and spread all across the globe to become the worst killer disease (Figure 6). The parasites spread to other areas through human migrations. Malaria seems to have been known in China for almost 5,000 years (men from ancient China, who traveled to areas with malaria, were advised to arrange for their wives to be remarried[10]). Today malaria is a major problem in areas of Africa, China, South East Asia, Central and South America.

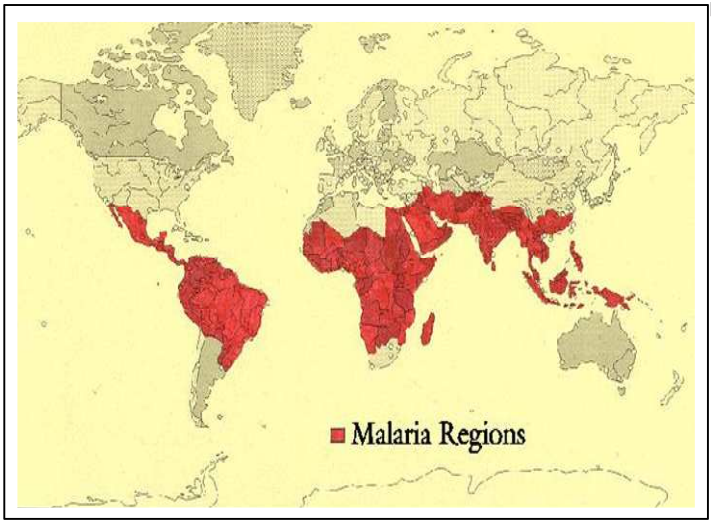

Figure 6. Distribution of malaria in the world[11]

1.5 Signs and symptoms of malaria

The time from the initial malaria infection until symptoms appear (incubation period) generally ranges from 9 to 14 days for *P. falciparum*. The clinical symptoms of malaria are exclusively caused by the erythrocytic parasite stages and in the early stages; the symptoms are sometimes similar to those of many other infections caused by bacteria, viruses, or parasites.[12]

Symptoms may include: flu-like illness with fever, chills, muscle aches, and headache. Some patients develop nausea, vomiting, cough, and diarrhea and there can be yellowing of the skin and whites of the eyes due to destruction of red blood cells and liver cells. Cycles of chills, fever, and sweating that repeat every one, two, or three days are typical. The cyclic pattern of malaria symptoms is due to the life cycle of malaria parasites as they develop, reproduce, and are released from the red blood cells and liver cells (cell debris) in the human body.[13] This cycle of symptoms is also one of the major indicators that you are infected with malaria. Without treatment, the cycle of red blood cell destruction and fever will continue and may lead to death. People with severe *P. falciparum* malaria can develop bleeding problems, shock, liver or kidney failure, central nervous system problems, coma, and can die from the infection.

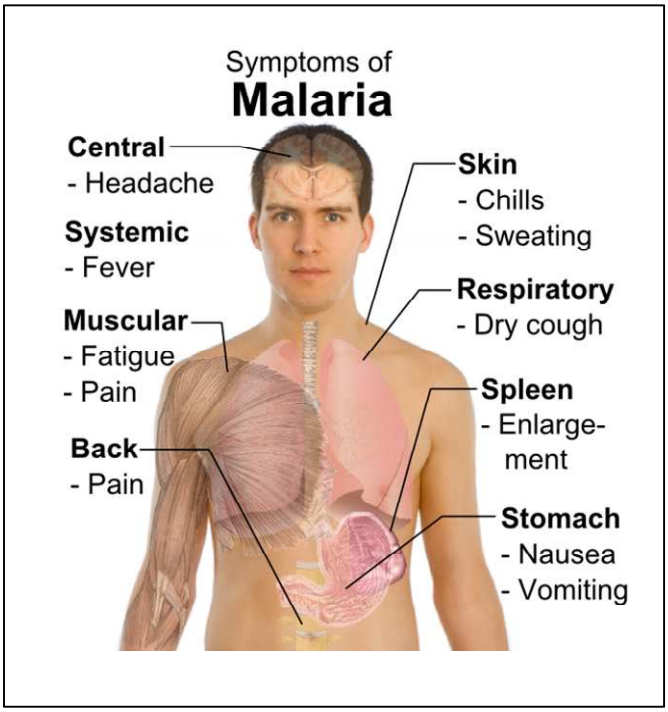

Figure 7. Symptoms of malaria[13]

1.6 Treatments

Antimalarial drugs are designed to prevent or cure malaria. Indians and South Americans have used the bark of Cinchona, a plant native to South America (Figures 8, 9), as a treatment for malaria long before any treatments were available in Europe. In 1639, Jesuit missionaries introduced the bark of this plant to Europe, where it became the main treatment for malaria fever.[14] In 1820 the French chemists Pierre Joseph Pelletier and Joseph Bienaime Caventou identified quinine, an alkaloid, as the active ingredient of the bark of Cinchona.[15] This is the only drug largely effective for treating the disease over a long period of time (Figure 10).

Figure 8. Cinchona tree[16]

Figure 9. Bark of cinchona[17]

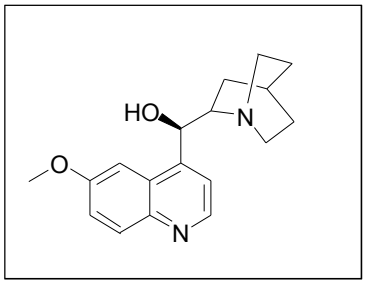

(a)

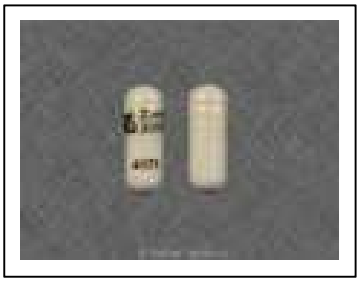

(b)

Figure 10. (a) The structure of quinine, (b) quinine tablets[18]

Until World War I, quinine was the only drug used to treat malaria for more than three centuries. It is now only used for treating severe *falciparum* malaria because of undesirable side effects.[19] Hence there was a continous search for new antimalarials and in1920, a 9 -aminoacrinidine was synthesized and it was commercialized in 1930 with the name of Atabrine (Figure 11).

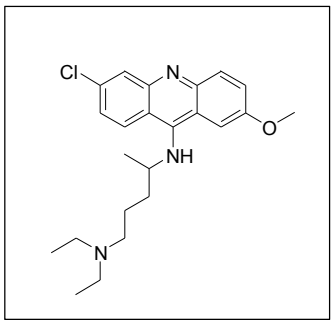

Figure 11. Atabrine

During World War II many drugs were developed to protect the troops from malaria, such as chloroquine, primaquine, proguanil, amodiaquine and sulfadoxine /pyrimethamine (Figure 12). Among those, chloroquine (CQ) has been uniquely successful owing to low cost, mild side effects, good tolerance, which makes it adequate for treating pregnant women and most importantly, highly effective in curing the disease. It was first used in the 1940s shortly after the Second World War.

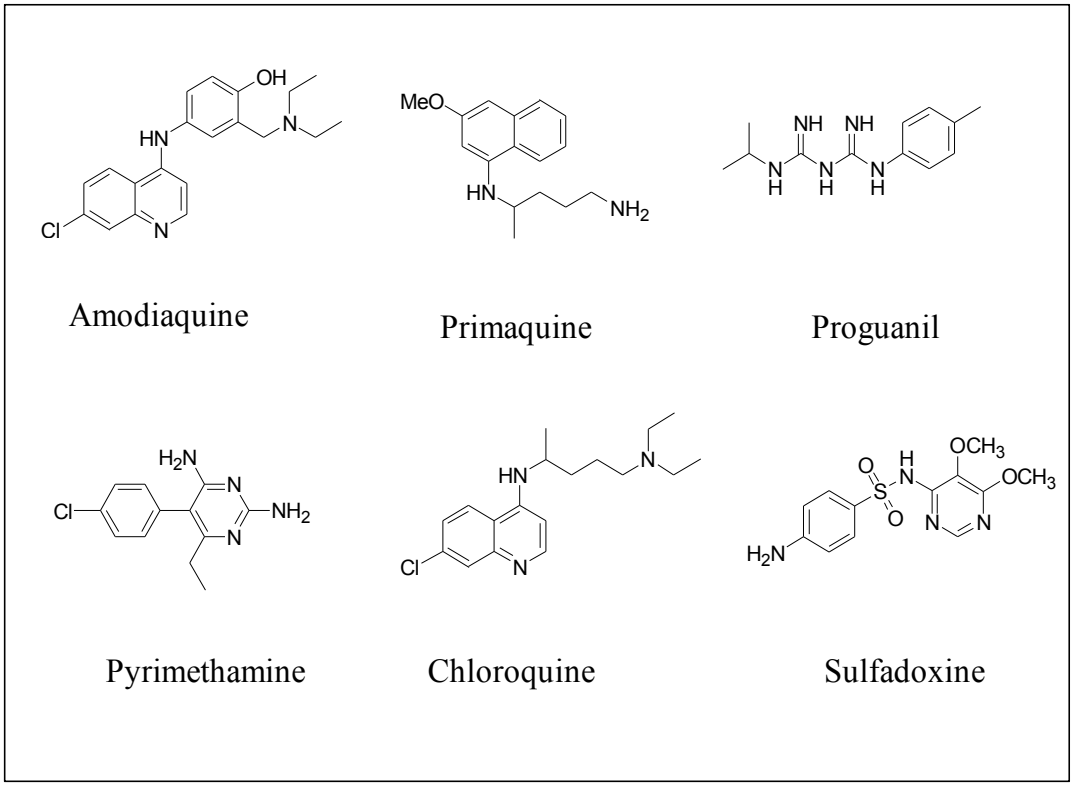

Figure 12. Structures of some antimalarials

Unfortunately, many strains of *P. falciparum* are now resistant to chloroquine and more recently, chloroquine-resistant *vivax* malaria has also been reported.[7] In 1939, a Swiss chemist Paul Hermann Müller discovered DDT (dichlorodiphenyltrichloroethane – Figure 13), which became a widely used insecticide used to control mosquitoes spreading malaria; he was awarded the Nobel Prize in Physiology and Medicine in 1948 for this discovery.[20] By 1957 based on the application of DDT, malaria was eliminated in 37 countries mainly in Europe and the Americas.[21]

However in 1967, some mosquitoes developed resistance to DDT and also it has been suggested that the use of DDT over time has devastating effects on biodiversity, hence it was banned in 1972.[22]

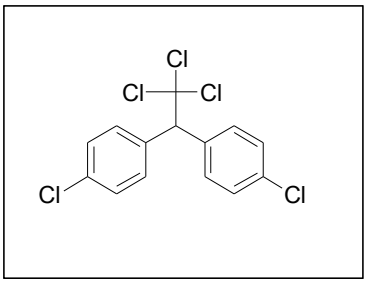

Figure 13. The structure of DDT (dichlorodiphenyltrichloroethane)

During the Vietnam War, there were heavy losses as a result of chloroquine-resistant malaria. So the development of new antimalarial drugs was encouraged by the American military and resulted in the development of mefloquine and halofantrin (Figure 14). Mefloquine was first introduced in 1971; this drug is related structurally to quinine. Unfortunately, widespread resistance has now developed and this, together with undesirable side effects, has resulted in a decline in its use. Halofantrin belongs to a class of compounds not related to quinine and it was introduced in the 1980s, but due to its short half-life of 1 to 2 days, it is not suitable for use as a prophylactic. Unfortunately, resistant forms are increasingly being reported and there is some concern about its side-effects. It is suggested that the use of this drug is not safe in pregnancy and is not advised for women who are breastfeeding.

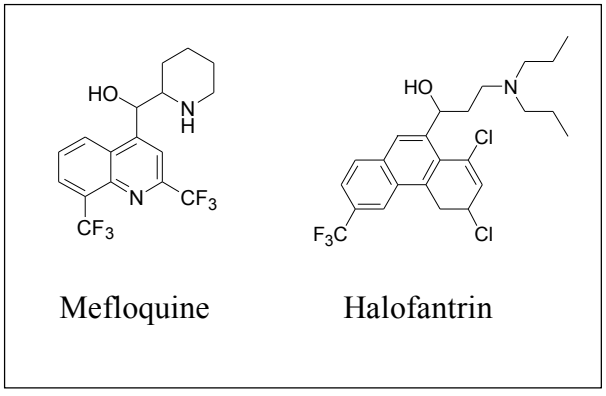

Figure 14. Structures of two antimalarials

A completely different group of drugs was derived from traditional Chinese medicine. The sweet wormwood *Artemisia annua* has been used by Chinese herbalists for more than a thousand years in the treatment of many illnesses, such as skin diseases and malaria. The compound artemisinin (Figure 15) was first isolated from the plant *Artemisia annua by* Chinese military researchers in 1965 and used to treat multi-drug resistant *P. falciparum* strains. In a malaria epidemic in the early 1990's in Vietnam, artemisinin reduced the death rate by 97%. This drug contains two oxygen atoms linked together in what is known as an 'endoperoxide bridge', which reacts with iron atoms to form free radicals.[24] Artemisinin becomes toxic to malaria parasites when it reacts with the high iron content of the parasites, generating free radicals, and leading to damage to the parasite. Later more water soluble artemisinin analogues (Figure 15) were synthesized to treat malaria.

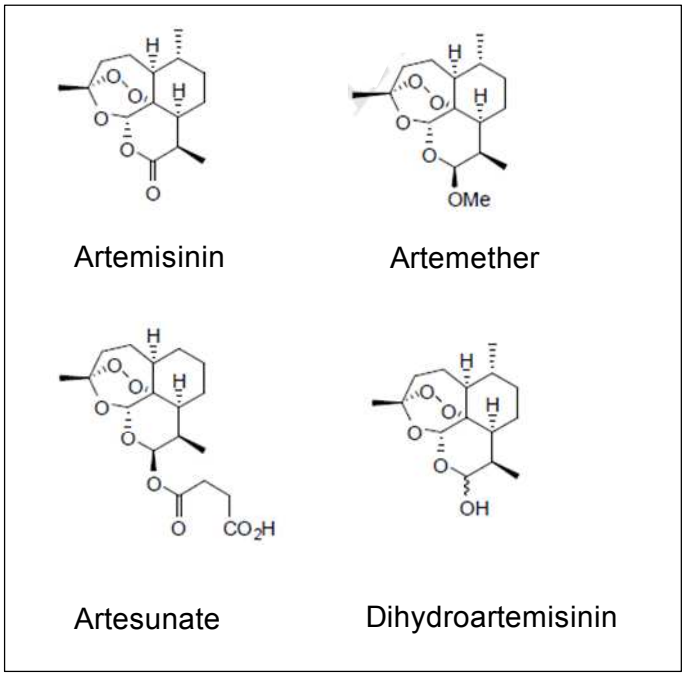

Figure 15. Structures of artemisinin and its analogues

Artemisinin and its derivatives are fast acting, but display short plasma half-lives.[25-27] (Plasma half life is the time it takes for a drug to lose half of its pharmacologic activity). Because of that the use of artemisinin and its derivatives as a monotherapy (a therapy which is taken alone) is clearly discouraged by the World Health Organization (WHO) as there have been signs that malarial parasites are developing resistance to the drug. Therefore, artemisinin combination therapy (ACT) composed of artemisin derivatives such as artesunate and artemether with other drugs like lumefantrine, mefloquine or amodiaquine[23] are recommended by WHO, which results in effective treatment with no resistance.[28,29]

However, these physical combinations suffer from some significant drawbacks related to the different solubility and pharmacokinetics of the individual components. In addition, although the price is approximately $2.20 per adult course, these drugs are still beyond the reach of the world's poorest people.

As a summary, so far chemotherapy of malaria has relied on chemically related drugs belonging to four classes of compounds: 4-aminoquinolines, 8-aminoquinolines, antifolate compounds and artemisinin and its derivatives. The most important drugs can be categorized into 4 groups are shown in Table 1.

Table 1. Four classes of antimalarials

The class of compounds	Antimalarial drugs
4- Aminoquinolines	Chloroquine Quinine Mefloquine Amodiaquine Halofantrin
8- Aminoquinolines	Primaquine
Antifolates	Pyrimethamine Proguanil Chlorcycloguanil Dapsone Sulfadoxine
Artemisinin & Derivatives	Artemisinin Artesunate Artemether Arteether Dihydroartemisinin

Even though several drugs have been used to treat malaria, chloroquine remains the treatment of choice for *P. vivax, P. ovale, P. malariae* and uncomplicated *P. falciparum* malaria in those few geographical areas where this drug can still be relied on. Even in areas of high level resistance such as East Africa, the drug is often the most widely used treatment and still produces certain level of a clinical response although with recrudescence in a majority of patients.

1.7 Mechanism of drug action and resistance

Drug resistance is one of the major factors contributing to the renaissance of malaria and, in order to design and develop new therapies to overcome drug resistance it is important to fully understand the mode of action of the existing antimalarial drugs and the way parasites become resistant to them. In many cases including 4-aminoquinoline derivatives, the mechanisms of action and parasite's resistance are not fully understood.

The hypotheses of the antimalarial action of quinoline drugs include, direct binding to the heme group of hemoglobin,[30,31] unidentified vacuolar phospholipase inhibition[32], inhibition of protein synthesis and/or binding with DNA.[33] However, it is now generally accepted that chloroquine and other quinolines act by interfering with the detoxification of ferriprotoporphyrin IX inside the acidic digestive vacuole of the parasite. (This will be discussed in detail in the following sections). This thesis is focused on CQ derivatives, and therefore, from here on, the discussion will concentrate on the mechanism of action of CQ and possible mechanisms of CQ resistance by the malaria parasites.

1.7.1 Heme aggregation as the target of chloroquine

Hemoglobin degradation and the food vacuole

Malaria parasites spend part of their life cycle inside the erythrocyte of the human host. The parasite ingests the red blood cell cytoplasm of the host via a cytosome, resulting in a double membrane vesicle; the transport vesicle.

The transport vesicle delivers the contents to the acidic digestive vacuole (pH 4.9) where hemoglobin is digested by proteolytic enzymes including plasmepsin I, II, IV, histoaspartic protease (HAP), falcipains 2 and 3 and falcilysin.[34-36] Then the short peptides formed are further degraded to amino acids by aminopeptidases, probably in the parasite's cytoplasm. It is believed that during the blood stage of the parasite 60% - 80% of the hemoglobin present in the red blood cell is digested. Moreover, it is confirmed that amino acids formed during the hemoglobin degradation process are used by the parasite as its food source.[37] In addition it is believed that hemoglobin degradation is also required to make space available in the red blood cell for parasite growth and to maintain the osmotic balance inside the cell. During the hemoglobin degradation process, heme present in hemoglobin is released into the parasite digestive vacuole.[37] Heme actually refers to iron protoporphyrin; Fe(II)PPIX (Figure 16) which is irreversibly and rapidly oxidized by molecular oxygen to H_2O-Fe(III)PPIX.

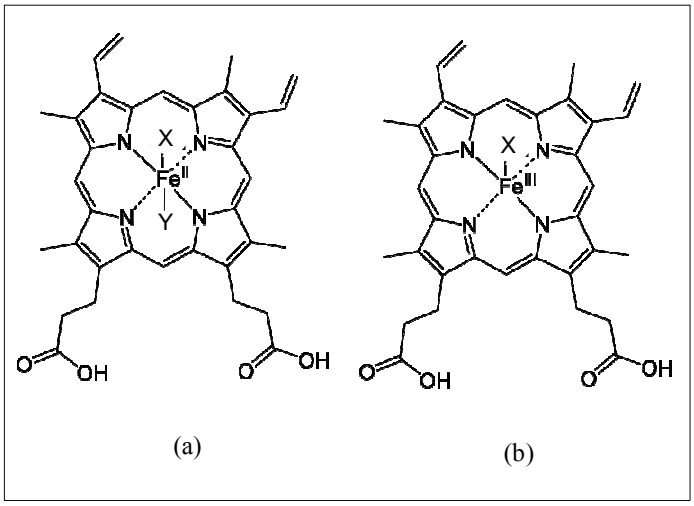

Figure 16. Heme and oxidized heme (a) heme is present in hemoglobin (where Y represents the proximal histidine residue of the protein and X is O_2 in oxyhemoglobin or vacant in deoxyhemoglobin). (b) oxidation of heme produces H_2O-Fe(III)PPIX where X represents H_2O.

Although the detailed mechanism of heme oxidation is not fully understood, it is believed that during heme oxidation superoxide (O_2^-) is generated under acidic pH. Inside the food vacuole of the parasite, O_2^- spontaneously dismutates to O_2 and H_2O_2. Toxic H_2O_2 is eliminated from the site by breaking it down in to O_2 and H_2O by catalase activity.[38] The formed H_2O-Fe(III)PPIX which is in high concentration (0.4 M) inside the food vacuole, is also known to be toxic to the parasite. This has been invoked in lipid peroxidation (known to potentially dissolve in a non-polar environment such as lipid membranes) membrane damage of the parasite and eventually can cause death to the parasite. So the parasite must have some mechanism for disposing of this toxic material in order to survive heme toxicity.

Hemozoin formation as a heme detoxification processs

It is now accepted that malaria parasites overcome heme toxicity by formation of hemozoin or malaria pigment, an inert, highly insoluble and compact crystalline material which is no longer harmful to the parasite. Not only the malaria parasites *P. falciparum*, *P. vivax*, *P. malariae*, *P. ovale*,[39] form hemozoin but also the bird-infecting protozoan *Haemoproteus columbae*[40] and the blood-feeding helminths *Schistosoma manson*[41,42] and *Echinostoma trivolvis*[43] as well as the blood-sucking triatomine insect *Rhodnius prolixus*.[44] Hemozoin formation is not the only route of heme detoxification in some of these organisms but now it is believed that hemozoin formation is the major pathway of disposal of heme in malaria parasites.

According to studies performed by Egan and coworkers[45] H_2O-Fe(III)PPIX and/or HO-Fe(III)PPIX spontaneously form π-π complexes in back to back (or stacked) interaction between two porphyrins to form dimers in aqueous medium. This involves noncovalent interaction of the unligated faces of two five-coordinate H_2O/HO-Fe(III)PPIX molecules, with the axial H_2O/OH– ligands directed outwards (Figure 17). This arrangement is consistent with the crystal structures of related five-coordinate iron (III) porphyrins.[46]

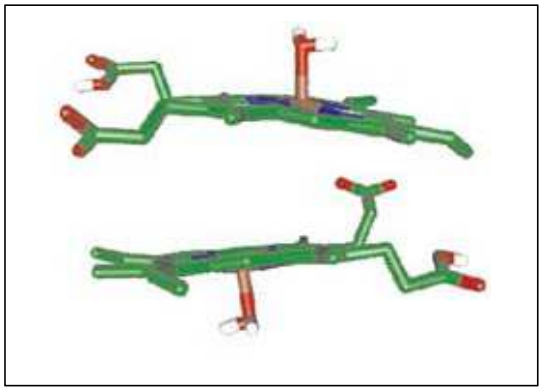

Figure 17. Molecular dynamics performed in water - when the dynamics were performed in a cube of H_2O starting from the β-hematin precursor, the propionate groups quickly moved away from the Fe(III) centres to interact with the solvent molecules . Water molecules are omitted for clarity. **(*Ref: Egan, T.J. et al. FEBS Letters, 2006, 580, 5105–5110*)**

These dimers are delivered by endocytotic transport vesicles to neutral lipid bodies commonly named as lipid nanospheres within the digestive vacuole where the hemozoin is believed to form.[47] Lipid bodies are usually surrounded by a monolayer of a phospholipid, glycolipid or sterol and their origin appears to be the inner membrane of the endocytotic transport vesicles, which transport hemoglobin to the digestive vacuole.

It is still not clear how the hemozoin crystal formation is nucleated but it is suggested that probably a protein would have to act as a nucleation site for crystal growth or it may act as a chaperone to deliver Fe(III)PPIX to lipid bodies. The proposed mechanism of hemozoin formation is illustrated in (Figure 18)

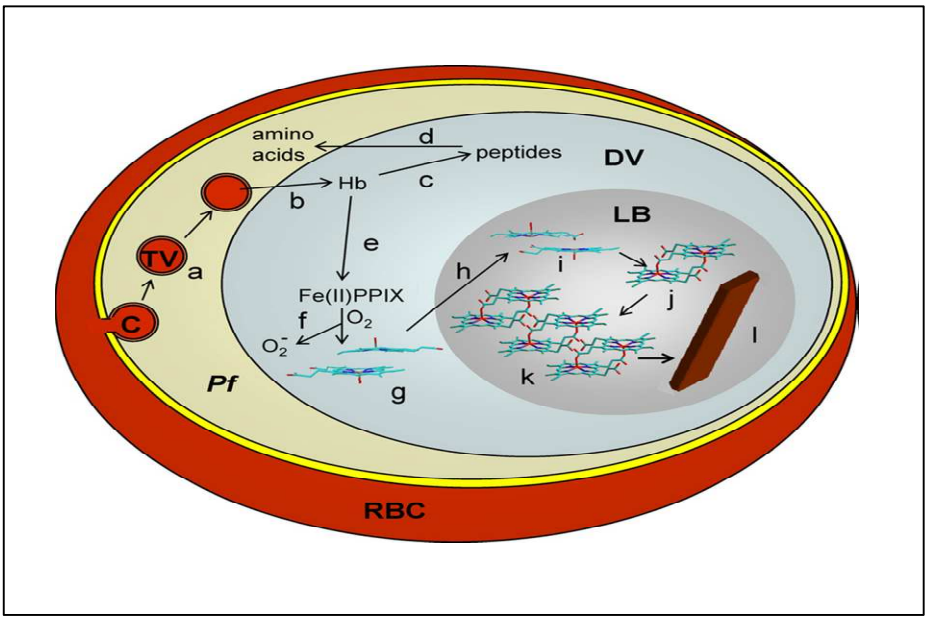

Figure 18. Proposed schematic representation of the processes involved in hemozoin formation in *P. falciparum* based on recent studies. Red blood cell (RBC) cytoplasm is ingested by the parasite (*Pf*) via a cytostome **(C)** and **(a)** transported to the digestive vacuole (DV) by double membrane bound transport vesicles **(TV).** Upon delivery into the DV **(b),** hemoglobin (Hb) is digested by plasmepsins, falcipains and falcilysin to short peptides **(c).** These are exported from the DV **(d)** and finally degraded to amino acids, probably by aminopeptidases. The heme (Fe(II)PPIX) released from hemoglobin **(e)** is oxidized **(f),** presumably by molecular dioxygen, generating Fe(III)PPIX and superoxide anion. In aqueous solution Fe(III)PPIX dimerizes probably to form a π–π dimer **(g)** which is delivered **(h)** to a lipid body (LB) dubbed a lipid nanosphere. Within the low dielectric medium of the lipid nanosphere Fe(III)PPIX forms a "hemozoin precursor" dimer **(i)** which converts to the hemozoin dimer **(j)** by displacement of the axial water ligands of H_2O–Fe(III)PPIX together with formation of the Fe(III)–propionate bonds. In the absence of competing hydrogen bonding by the solvent, these dimers can start to assemble into hemozoin nuclei by hydrogen bonding to each other **(k),** finally assembling the hemozoin crystal **(l) (*Ref: Egan, T.J. Molecular & Biochemical Parasitology, 2008, 157, 127–136*)**

Inside the lipid bodies, H_2O-Fe(III)PPIX forms the initial hemozoin dimer by displacement of an axial water ligand and formation of the Fe(III)-propionate bond with the adjacent monomer (Figure 19).[48] Then these dimers interact via hydrogen bonds between the protonated propionate groups to form hemozoin crystals. In simple words, hemozoin consists of centrosymmetric dimers linked by hydrogen bonds (Figure 20) and its crystal structure was solved by X-ray powder diffraction pattern in 2000 by Pagola et.al.[49]

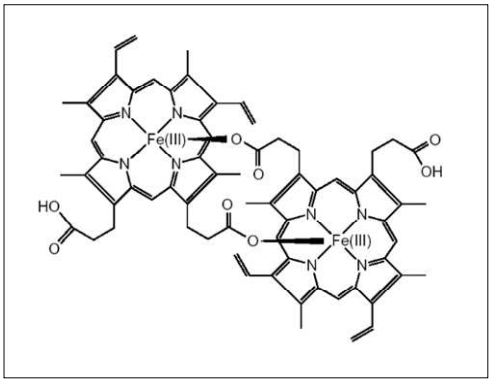

Figure 19. The basic unit of hemozoin; Fe(III)PPIX dimers, an iron-oxygen coordinate bond links the central iron of one Fe(III)PPIX to the oxygen of the carboxylate side-chain of the adjacent Fe(III)PPIX.

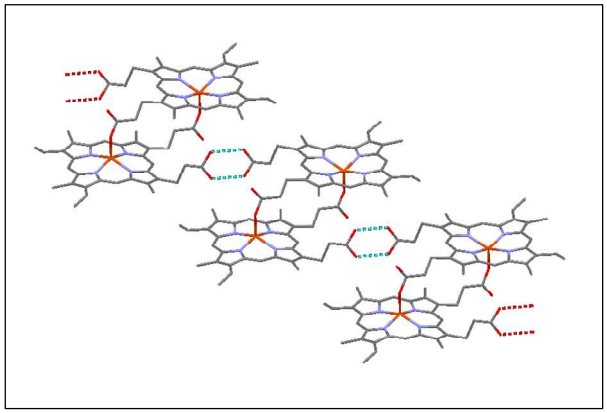

Figure 20. Hemozoin is a cyclic dimer of Fe(III)protoporphyrin IX, with the deprotonated propionate group of each porphyrin coordinated to the Fe(III) centre of the other.(as red lines). The dimers interact via hydrogen bonds (dotted lines) between the protonated propionate groups. **(*Ref: en.wikipedia.org/wiki/Hemozoin*)**

The crystals of hemozoin can be seen in transmission electron micrographs and the crystal has been described as lath-like in shape (long narrow strip).[50] According to the X-ray powder diffraction pattern of hemozoin, the crystal belongs to a centrosymmetric space group (Figure 21) and are close to one micron in length and several hundred nanometers wide making them almost macroscopic objects (see Figure 22).

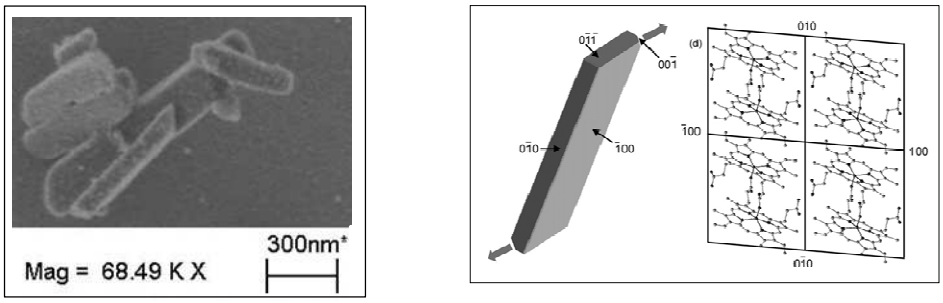

(a) **(b)**

Figure 21. Crystal of hemozoin.

(a) Transmission electron micrograph of crystals of hemozoin isolated from the malaria parasite magnified 68,490 times, **(b)** a sketch of a hemozoin crystal illustrating the crystal faces identified by Buller et al. which can be related to the structure of the unit cell. The fastest growing faces are indicated by thick grey arrows. ***(Ref: Egan, T.J. Molecular & Biochemical Parasitology, 2008, 157, 127–136)***

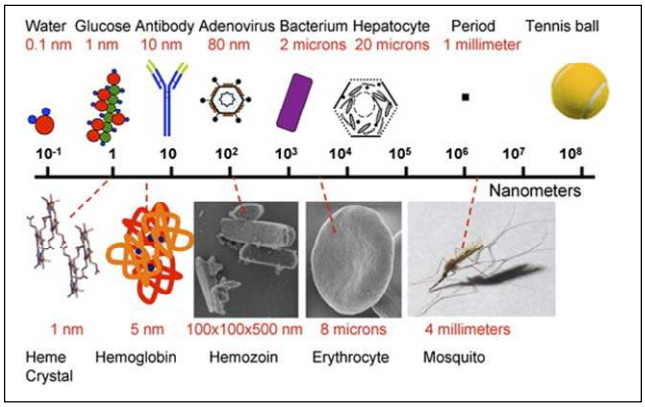

Figure 22. Relative size of hemozoin crystals - nanometer scale bar illustrating the relative size of objects ranging from 0.1nm with a water molecule (far left) to a 100 mm tennis ball (far right). ***(Pisciotta, J. M. Parasitology International, 2008, 57, 89-96)***

Although according to early literature, people argue that the site of hemozoin formation is the cytoplasm of the food vacuole of the parasite, it is now confirmed that hemozoin formation occurs in the neutral lipid bodies; nanospheres within the digestive vacuole of the parasite.[47] It is believed that previously published TEM images of parasite removed all evidence of neutral lipid nanospheres by the ethanol processing. The idea of lipid bodies as a site of hemozoin formation is further supported by insights from molecular dynamics simulations[48] which suggest that the lipid environment promotes interaction of the propionate group with the Fe(III) center, which drives water off the axial position and promotes the hydrogen bonding required for hemozoin crystal formation. **All these studies suggested that a lipid - aqueous interface inside the lipid bodies is the key site for the formation of hemozoin crystals.**

Apart from enzymes for digesting hemoglobin, no special catalysts are now thought to be required for hemozoin formation, but in early literature it was proposed that hemozoin formation is catalysed by an enzyme which they dubbed "heme polymerase".[51] In 1995 Dorn et.al. suggested that hemozoin formation is autocatalytic[52] and Bendrat et. al.[53] proposed that lipids promote β-hematin formation, the synthetic analog of hemozoin. In 1996 Sullivan et. al. argued that the histidine-rich protein II (HRP II), a protein found in the malaria parasite *P. falciparum* also promotes hemozoin formation. So at that time it was believed that hemozoin formation was dependent on either histidine-rich protein or lipids. However, in 2001 Papalexis et.al. showed that HRP II is mainly localized in the red cell cytoplasm[54] and his idea was further supported by Akompong et.al. They suggested that 97% of HRP II is exported from the parasite to the red blood cell cytoplasm.

According to these findings, the role of HRP II[55] in the process of hemozoin appears to be questionable because only 3% of HRP II present in the food vacuole is not enough to account for hemozoin formation. In 2004, Jackson et.al. demonstrated the presence of lipid particles closely associated with the food vacuole of the parasite by using a combination of fluorescence microscopy and transmission electron microscopy.[56] Those lipids contain mono- and di- acylglycerols and were found to facilitate β-hematin formation. In 2005, for the first time, Coppens and Vielemeyer published an electron micrograph image that showed hemozoin fully encapsulated within a neutral lipid body in the food vacuole of the *P. falciparum*[57] and this was also further confirmed by Pisciotta et.al in 2007 (Figure 23).[58]

Not only in malaria parasites, but also in *S. mansoni*, hemozoin formation takes place in lipid droplets within the gut of the worm. In any case, the hemozoin is seen to be in direct contact with the lipid but no protein associated with lipid bodies. In contrast to the declining evidence for involvement of HRP II in the formation of malaria pigment, the evidence for the role of lipids has been growing.

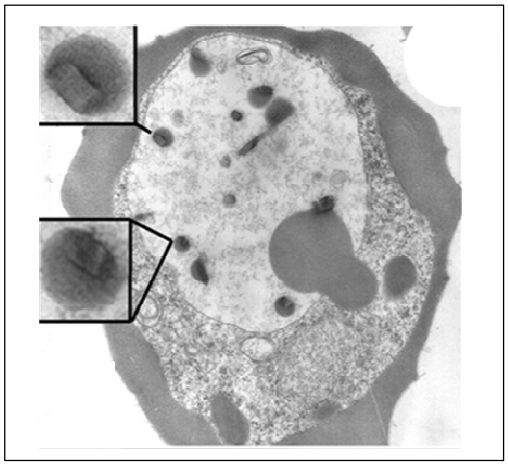

Figure 23. Hemozoin is present within neutral lipid nanospheres. TEM of early trophozoite stages highlights five to six small heme crystals surrounded by neutral lipid spheres inside digestive vacuoles. (***Ref: Pisciotta, J. Biochem. J. 2007, 402, 197–204)***

Relevant to these studies, in 2006 Egan et.al. carried out biomimetic studies on β-hematin formation and provided mechanistic details about the role of lipids in hemozoin formation,[59] using organic solvents (octanol and pentanol) and model lipid monomyristoylglycerol (MMG) to mimic the lipid environment. They investigated the role of the lipid-water interface for the formation of hemozoin and showed that these interfaces brought about β-hematin formation within 5 min. Interestingly, none of the aqueous or organic solvents alone showed any β-hematin formation within 30 min. Although some argued that a protein present in small quantities could act as a nucleation site of hemozoin and its possible role to deliver Fe(III)PPIX to lipid bodies, strong evidence to support this idea is still not available. Recently Dewal Jani et.al[60] reported the identification and characterization of a novel Plasmodium Heme Detoxification Protein (HDP), a parasite enzyme that is extremely active in converting heme into hemozoin and that was detected in close proximity of hemozoin, within the food vacuole (Figure 24).

According to their studies, HDP (18 nm particles) is secreted into the cytosol of infected erythrocytes before any hemozoin could be observed inside the parasite and the transport vesicles deliver both HDP and hemoglobin to the food vacuole. They have further proposed that HDP may be involved in the process of hemozoin formation and suggested that it could be a malaria drug target.

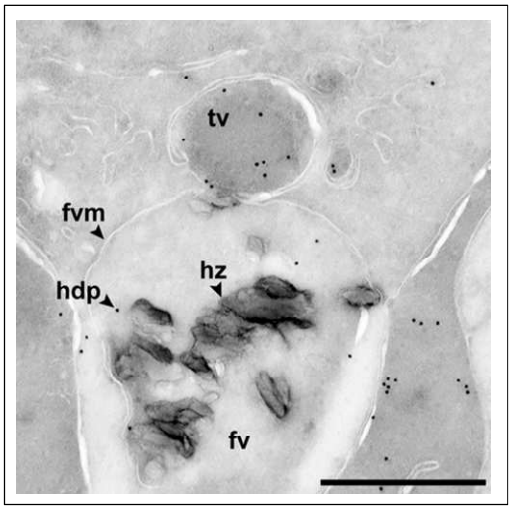

Figure 24. Transport vesicle **(tv)** delivering a heme detoxification protein (hdp) to a malaria food vacuole **(fv)** containing crystals of hemozoin **(hz).** Scale bar is 0.5 μm.[60]

Nevertheless, a wealth of evidence has recently led to the conclusion that hemozoin formation occurs in close association with lipids and it takes place spontaneously and rapidly at water/lipid interfaces within the digestive vacuole, without any need for specific proteins.

In summary, parasite factors responsible for hemozoin formation are subject of debate. Although some have argued that hemozoin formation is an autocatalytic process, others believe that lipids could be the primary mediators of hemozoin formation. In addition to those two ideas, some authors suggested that histidine rich protein or HDP could catalyze the process. It is possible that either one of these or all may be factors that contribute to the formation of hemozoin inside the acidic food vacuole of the parasite. Nevertheless, the extensive data available in support of the direct heme aggregation at water-lipid interfaces without involvement of a protein seems be important for the heme detoxification process.

1.7.2 Mechanism of action of chloroquine

Since the time of its introduction in the 1940s, chloroquine (CQ) remained the main treatment for malaria for 5 decades until the spread of resistant organisms, beginning from South America and Southeast Asia. However, CQ has saved more lives than any other drug in history. The mechanism of action of quinoline antimalarials such as CQ is not fully understood, but it is believed that hemozoin formation is the principal target of many quinoline based antimalarial agents. CQ in particular, is able to penetrate infected RBCs and accumulate within the food vacuole of the parasite through pH trapping due to the weak basicity of the drug.

pH trapping is essential for drug activity by ensuring that CQ is concentrated at the acidic site, the digestive vacuole. CQ needs to cross three membranes (RBC, parasite cell and the food vacuole) in its unprotonated neutral form and at the low pH of the food vacuole it becomes doubly charged and trapped inside the vacuole, where the accumulated chloroquine ions then associate with Fe(III)PPIX. Complex formation between CQ and ferriprotoporphyrin IX (Fe(III)PPIX) was first reported in the 1960's by Cohen et.al.[65] They presented spectrophotometric evidence that Fe(III)PPPIX can bind to CQ *in vitro*. In 1980, Fitch and co-workers proposed that Fe(III)PPIX is the molecular target of 4-aminoquinolines, such as CQ and quinoline methanol antimalarials.[50] Interestingly, in 1996 D. Sullivan et.al. examined the association of ^{3}H chloroquine with hemozoin in culture and *in vitro* and they observed CQ accumulation and its association with hemozoin crystals in the FV of the parasite by electron microscopic autoradiography (Figure 25).[61] According to that picture the signal was almost exclusively over hemozoin crystals (hemozoin associated radioactivity).

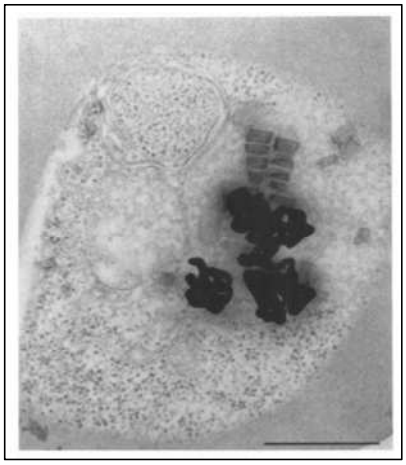

Figure 25. ^{3}H Chloroquine is located over the hemozoin pigment crystals situated in the digestive vacuole. (Bar = 0.5 μm.)[61]

Hemozoin is chemically and structurally identical to its synthetic analog β-hematin, and this substance can be readily synthesized under different conditions.[62,63] Numerous studies have shown that CQ and related antimalarial compounds inhibit β-hematin formation under various conditions.[63,64] These studies also provide considerable evidence that inhibition of hemozoin formation is the mechanism of antimalarial action of CQ and other 4-aminoquinolines by strong π-π molecular interactions between the planar quinoline moiety and the porphyrin ring of monomeric heme units (Figure 26), which prevents the formation of malaria pigments. As a result, toxic monomeric heme accumulates inside the vacuole, lyses the membranes and leads to parasite death. Some believe that the complex CQ-Fe(III)PPIX itself is toxic to the parasite.[66]

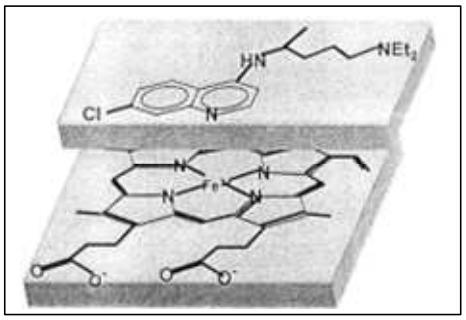

Figure 26. CQ forms the stacked π-π complex with Fe(III)PPIX[69]

Recent studies on hematin-quinoline interactions have provided insight into the structural requirements for these drugs to interact with Fe(III)PPIX and the structure-function relationship of 4-aminoquinolines on the activity of inhibition of hemozoin formation[68] (Figure 27).

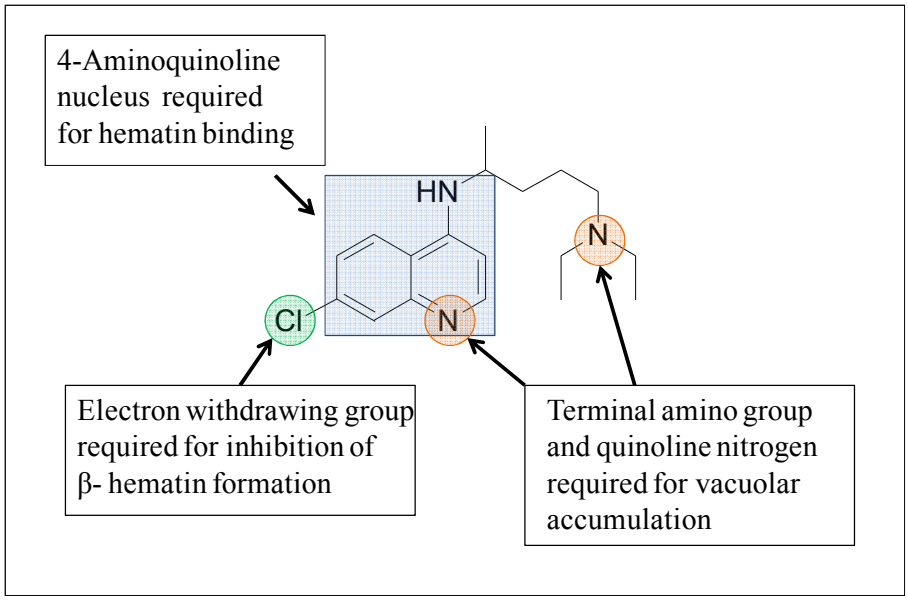

Figure 27. Recently proposed structure-activity relationship of chloroquine[67]

According to these studies, the 4-aminoquinoline nucleus in CQ is required to bind with Fe(III)PPIX to prevent heme detoxification in the parasite; the electron withdrawing ability of the chloro group at the seven position of CQ seems to be required for the inhibition of β-hematin formation and to maintain the pK_a value of the drug. The weak basic properties of the CQ due to the terminal amino group and the quinoline ring nitrogen are required for the drug accumulation in the acidic food vacuole of the parasite, where hemozoin formation is known to take place.[67]

Unfortunately, the success of CQ as chemotherapeutic agent for the treatment of malaria has declined owing to emergence of resistant *Plasmodium* parasitic species, especially resistant strains of *P. falciparum.*

1.7.3 The mechanism of chloroquine resistance

Parasites can become resistant to a particular drug due to several reasons. The use of a single drug over a long period of time may lead to a selection, and the administration of drugs with low quality may also contribute to the emergence of resistance. In most cases drug resistance mechanisms are poorly understood. In particular, CQ resistance began from 2 epicentres – Colombia (South America) and Thailand (South East Asia) in the early part of the 1960s. Since then, resistance has been spreading worldwide and reached the Indian state of Assam in 1973. In general, some of the resistance mechanisms include mutations in target gene, increased production of target, decreased drug accumulation (increase drug efflux from the parasite) and drug inactivation.[70]

The resistance mechanism of parasites to 4-aminoquinoline drugs is still not completely understood but microarray studies have suggested that genetic polymorphisms in some strains are linked to drug resistance.

The modifications observed are mutations in genes that encode transport proteins localized in the parasite digestive vacuole membrane. Two transporters are mainly involved in quinoline drug resistance such as PfCRT (*Plasmodium falciparum* chloroquine resistance transporter) and Pgh1(P-glycoprotein homologue 1). Especially relevant is the case of the pfcrt gene, which encodes the synthesis of the 48.6-kDa protein PfCRT,[71,72a] localized at the membrane of the food vacuole and believed to function as a transmembrane transporter (or channel). Fifteen amino acid mutations at positions 72, 74, 75, 76, 97, 144, 148, 160, 194, 220, 271, 326, 333, 356, and 371 have been identified in *pf*crt of CQR parasites from various regions[72b] and among these, K76T (threonine to lysine substitution at residue 76) mutation is present in all CQR strains, regardless of the geographic origin.[72c] For an example, the most heavily studied mutant (CQR-associated) *Pf*CRT molecule is the Dd2 isoform and this resistant strain harbors seven point mutations including K76T mutation relative to a common allele associated with CQ-sensitive (CQS) parasites, the HB3 allele.[72d]

As mentioned earlier, the critical mutation of PfCRT in CQR isolate involves the change of a charged amino acid, lysine, facing the vacuolar side of the transmembrane protein to uncharged threonine at the residue 76 (Figure 28).

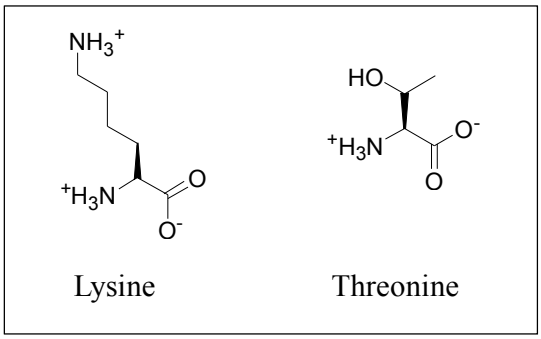

Figure 28. Structure of two important amino acids in PfCRT

As shown in Fig 29, in the wild type or CQ sensitive (CQS) strains, (due to the positively charged lysine at the residue 76 of PfCRT (K76)), there is repulsion between the doubly protonated CQ and this protein. This prevents the interaction of CQ with the transporter; hence it remains inside the digestive vacuole and is responsible for the inhibition of hemozoin formation.

In contrast to CQS strains, in all CQR strains, (due to the uncharged threonine instead of positively charged lysine at residue 76), CQ^{2+} can interact with PfCRT (K76T) and be extruded by it, thus lowering the CQ concentration inside the FV and thereby reducing its activity. There is experimental evidence to show that CQ binds to PfCRT (Figure 30).[73]

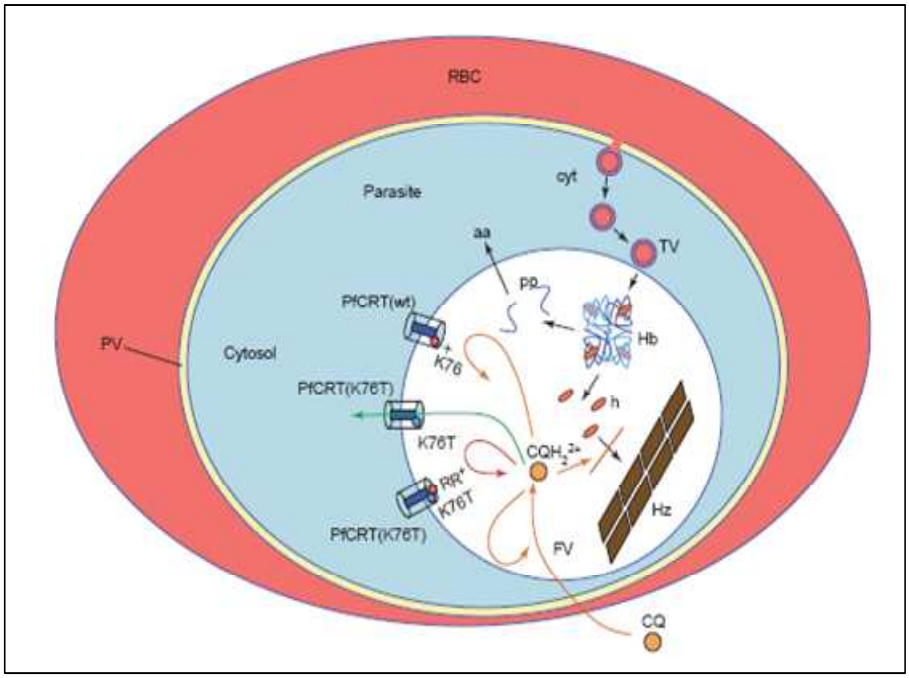

Figure 29. A schematic diagram showing a red blood cell (RBC) parasitized by a *P. falciparum* parasite. A charged form of CQ cannot exit via the wild-type PfCRT transporter [PfCRT(wt)] because of the positively charged K76 residue (orange arrow). In the CQ-resistant mutant [PfCRT(K76T)], the neutral threonine residue permits exit of the drug down its electrochemical gradient (green arrow). One possibility is that the association of a protonated, positively charged resistance reverser (RR^+), such as primaquine, with the mutant PfCRT could prevent exit of CQ (red arrow) ***(*Ref*: Kats, L. M.; Black, C. G.; Proellocks, N. L.; Coppel, R.L. Trends in Parasitology, 2006, 22, 236)***

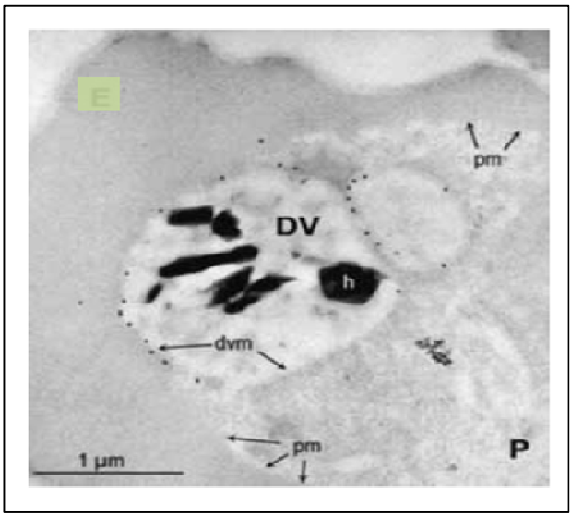

Figure 30. Localization of PfCRT in the food vacuole membrane by immuno-electron microscopy. Gold-tagged antibodies that bind to anti-PfCRT antibodies (small dots) are seen almost exclusively in the FV (marked as DV) membrane.
Abbreviations: E = erythrocyte, P = parasite, pm = plasma membrane, dvm = FV membrane. ***(Ref:Cooper, R.A.; Ferdig, M.T.; Ursos, L.M, Molecular Pharmacology 2002, 61, 35-42)***

How to overcome CQ resistance?

One way to recover the activity of CQ is by using of a protonated positively charged CQ-resistance reverser such as verapamil (Figure 31). It has been proposed that the resistance-reversing effect of verapamil is due to hydrophobic binding to the mutated PfCRT protein, and replacement of the positive charge at residue 76, which repels the CQ (4-aminoquinoline) cations. This hinders the efflux of CQ by mutual repulsion of positive charges and by partialy blocking the channel. So resistance-reversing agents lower the IC_{50} of CQ in CQ-resistant parasites to a value comparable to that in CQ-sensitive parasites. This substance is not itself active against the resistant strains of the parasite at the concentration at which it restores activity and it does not alter activity against CQ-sensitive parasites.[74]

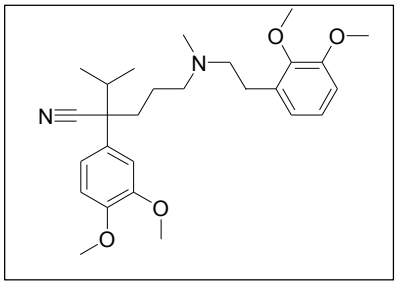

Figure 31. The strucuture of verapamil

Warhurst and co-workers have shown that the ability of a compound to be extruded by PfCRT decreases with increasing lipophilicity.[75] They have proposed that more hydrophobic compounds such as amodiaquine are likely to bind to the hydrophobic (due to uncharged threonine) mutated PfCRT channel lining and stay inside the vacuole. The positive charges repel further access of 4-aminoquinoline to the channel, hence increasing the drug accumulation inside the vacuole, thereby overcoming resistance. A higher antiplasmodial activity of highly lipophilic compounds may also be related to the fact that, since hemozoin crystals grow at water/lipid interfaces in lipid nanospheres within the food vacuole, increasingly lipophilic drugs would accumulate better near water/lipid interfaces and should consequently be more efficient at inhibiting aggregation.

Although continuing efforts towards a vaccine for malaria are producing interesting results, such a preventive solution is not envisaged in the near future.[76] Therefore the need for chemotherapeutic approaches in the control of these pathogens is necessary, especially for novel agents capable overcoming resistance.

The main focus of this project is the synthesis of new metal-CQ derivatives with antimalarial activity particulary against resistant strains of *P. falciparum.*

1.8 Metal complexes as chemotherapeutic agents

Biomedical inorganic chemistry ("Elemental Medicine") is an important area of chemistry. It offers potentials for the design of novel therapeutic and diagnostic agents for the treatment and understanding of diseases. It is known that many organic compounds used in medicine do not have a metal-independent mode of action; some are activated or biotransformed by metal ions, including metallo-enzymes. Others also may have a direct or indirect effect on metal ion metabolism.

Precious metals have been used for medicinal purposes for at least 3500 years. Records show that gold was included in a variety of medicines in Arabia and China. Although metals have been used for medicinal purposes since ancient times, the success of cisplatin in the treatment of cancer[77] has stimulated the recent search for novel metal-based chemotherapies for other diseases. Cisplatin is a truly remarkable drug. Since the discovery of its antitumor properties in 1965, it has been used to treat more than 70% of all types of cancer patients.

As cisplatin has been such a successful drug, many researchers used this molecule as a starting point to design improved therapies and some new generation Pt based anticancer agents are shown in Figure 32.[78]

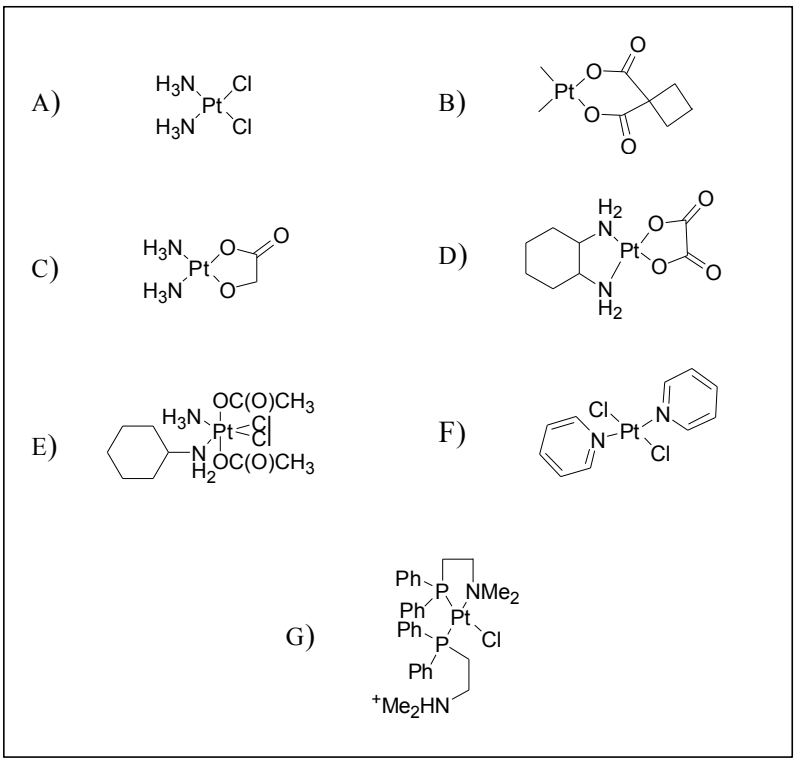

Figure 32. Selected platinum-based anticancer compounds
(A) cisplatin. Second generation anticancer drugs (B) carboplatin, (C) nedaplatin (D) oxaliplatin; and novel complexes with interesting clinical properties such as the orally administered (E) satraplatin and complexes designed to overcome cisplatin resistance (F) *trans*-dipyridine dichloroplatinum and (G) a platinum amino phosphine complex.

The target of cisplatin and related drugs is DNA and the mechanism of action involves the formation of irreversible 1,2-intrastrand d(GpG) cross-linked Pt-DNA adducts, which cause significant distortion of the helical structure, resulting in inhibition of DNA replication and transcription.[77,79] Due to the high toxicity, side effects and drug resistance of cisplatin and Pt based drugs new inorganic anticancer therapies are being developed. Among different metals, ruthenium displays chemical properties that make it an excellent candidate for rational anti-cancer drug design.[80]

Ru(II) complexes show similar ligand exchange kinetics to those of Pt(II), but a much lower toxicity, possibly due to its ability to mimic iron in binding to plasma proteins, which leads to selective transport of Ru into tumor cells.[81] Also, the preferred

octahedral coordination geometry of Ru(II) and Ru(III) allows different modes of DNA binding from the square-planar Pt(II) compounds. NAMI, $Na[trans\text{-}Ru^{III}(Im)(Me_2SO)Cl_4]$ (Im = imidazole) (Fig. 33), is the first Ru complex to enter clinical trials.[82,83] This relatively non-toxic compound shows marked efficacy against metastases. The Ru(III) center in this drug is required to be reduced to Ru(II) for activity, and cellular uptake appears to be mediated by transferrin. The activity of NAMI does not appear to involve DNA binding.

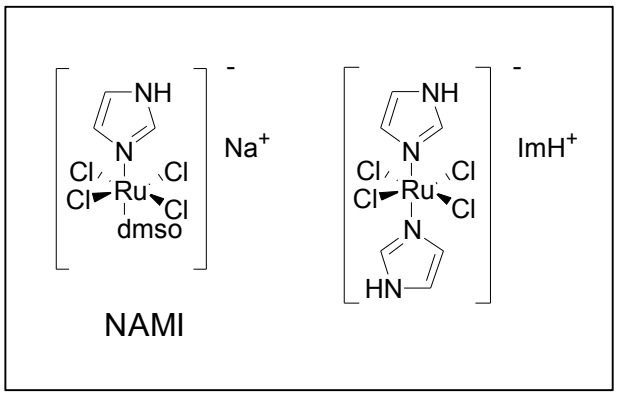

Figure 33. The structures of two ruthenium complexes for chemotherapy of cancer

Sadler and coworkers have evaluated the cytotoxicity of ionic, water soluble Ru(II) complexes containing N-donor and π-arene ligands,[84] potentially useful for the treatment of cancer. Some of these complexes are shown in Figure 34. The arene ligand not only provides a lipophilic site to the complex but also stabilizes the ruthenium atom in the oxidation state (II). Some of these complexes display anti-tumor activity *in vitro* and *in vivo* with IC_{50} values comparable to carboplatin against ovarian cancer cells, and DNA seems to be the main target of action.

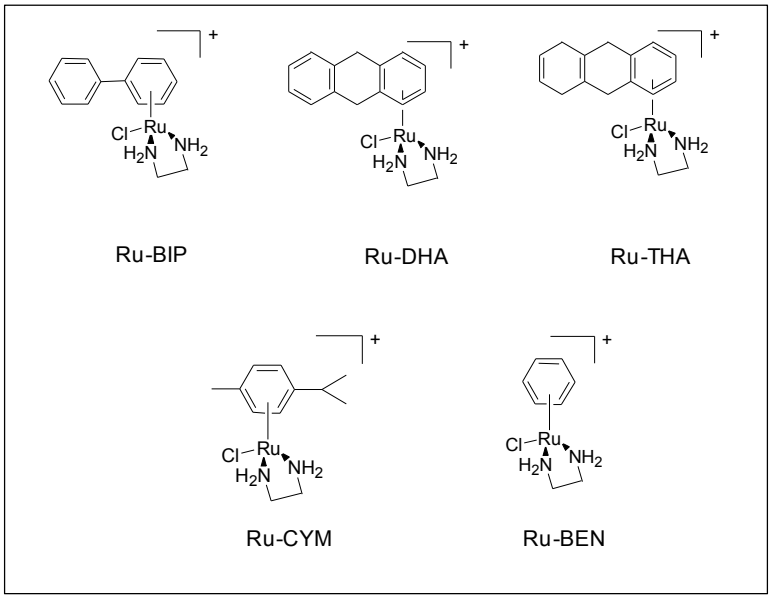

Figure 34. Structures of ruthenium complexes with anticancer properties synthesized by Sadler et.al.[84]

In addition to metal based chemotherapeutic agents for cancer, there are inorganic chemotherapeutic agents to treat other diseases. One example is gold complexes as antiarthritic drugs (Figure 35).[85]

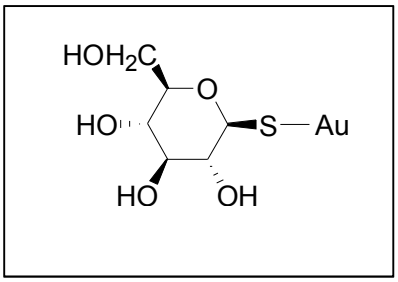

Figure 35. Gold antiarthritic drug; solganol

In addition, silver and its compounds have been long used as antimicrobial agents. A common example is the silver sulfadiazine which is used clinically as an antimicrobial and antifungal agent (Figure 36).[85]

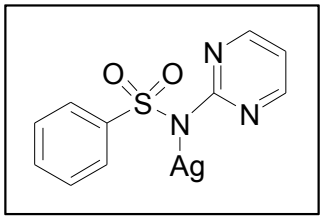

Figure 36. The structure of silver sulfadiazine

Some therapeutic or diagnostic applications of metal complexes are summarized in Table 2.[78]

Table 2. Metals with biomedicinal applications.[78]

Metal	Applications
Arsenic	Syphilis, ulcers, parasitic disease, acute promyelocytic leukaemia
Aluminium	Antacid, dermatology, hyperphosphataemia
Antimony	Leishmaniasis
Barium	Diagnostic agents
Bismuth	Gastrointestinal disorders, syphilis, angina, adenotonsillectomy
Copper	Diagnostic and imaging agents, radiopharmaceuticals, photodynamic therapy, Menkes disease
Chromium	Diagnostic agent, diabetes
Calcium	Hyperphosphataemia
Cobalt	Diagnostic and imaging agents, photodynamic therapy
Iron	Photodynamic therapy, hypotensive, hyperphosphatamia
Gadolinium	Diagnostic and imaging agents
Gallium	Diagnostic and imaging agents, cancer
Germanium	Cancer
Gold	Rheumatoid arthritis, bronchial asthma, malaria, bacterial infections, cancer, viral infections including AIDS
Holmium	Radiopharmaceuticals
Indium	Diagnostic and imaging agents
Lead	Ulcer treatment
Lithium	Manic depressive psychoses and viral infections including AIDS
Magnesium	Antacid, laxative, hyperparathyroidism
Manganese	Photodynamic therapy
Mercury	Diuretic, microbial infections, dermatology (syphilis), heart failure
Molybdenum	Menkes disease
Palladium	Photodynamic therapy, cancer, HIV
Platinum	Cancer, photodynamic therapy, microbial infections, viral infections including AIDS
Rhodium	Leishmaniasis, radiotherapy, bacterial infections
Ruthenium	Malaria, cancer, Chagas' disease, bacterial infections, septic shock, HIV
Rhenium	Diagnostic and imaging agents, radiotherapy

Metal	Applications
Silver	Microbial infections, fungal infections, dermatology, diagnosis and imaging agents
Strontium, Radium, Plutonium, Samarium	Radiopharmaceuticals
Tin	Radiopharmaceuticals, photodynamic therapy
Thallium	Diagnostic and imaging agents
Technetium	Diagnostic and imaging agents
Vanadium	Insulin mimics
Yttrium	Diagnostic and imaging agents, radio-immunotherapy
Zinc	Photodynamic therapy, Menkes disease, dermatology, HIV

The most important issue in the treatment of diseases today is the widespread emergence of resistance to commonly used organic drugs. There are two major approaches in drug design to overcome this problem. One of the approaches would be the synthesis of new drugs by modifying the molecular structure of existing compounds with known activity in order to overcome resistance, while maintaining the same target. The second approach would be developing new families of drugs based on understanding of both pathogen biology and the chosen molecular target. One way of modifying the activity of organic drugs for which resistance has emerged is to incorporate a metal ion into the molecular structure of the organic drug. The concept of metal drug synergism[86,87] is of great use in this type of drug design.

Metal drug synergism

Two beneficial effects result from the coordination of an organic drug to a metal ion (Figure 37). The first is the enhancement of the activity of the drug due to stabilization by complexation, which results in longer residence times in the organism, allowing the drug to reach its biological target more efficiently. The second effect is a decrease in the toxicity associated with metal ions, due to the fact that binding to the organic drug makes the metal less available for undesirable side reactions while in transit to the site of therapeutic action. The organic compound may serve as a carrier for the metal to the point of action, while the metal-containing fragment can in turn improve transport and delivery of the organic drug to its own target.

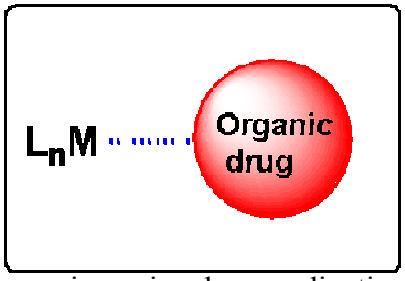

Figure 37. Metal-drug synergism arises by coordination of metal to an organic drug.

In 1975, it was found that substituting the aromatic groups in the antibiotic penicillin and cephalosporine with ferrocenyl moieties produced compounds with enhanced antibacterial activity compared to the starting materials, especially to the strains of *Staphlococcus aureus* resistace to penicillin-type antibiotics (Figure 38).[78]

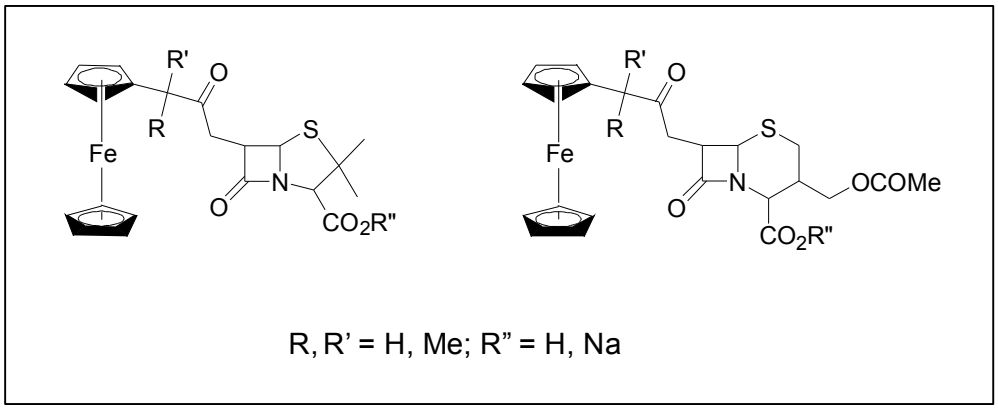

Figure 38. Organomettalic complexes of known organic antiproliferation agents designed to overcome drug resistance; **(a)** ferrocenyl-penicillin derivatives, **(b)** ferrocenyl-cephalosporin derivatives[78]

Another example to show metal-drug synergism is ferrocifen (Figure 39); a treatment for breast cancer, a hormone related disease. Ferrocifen has improved antiestrogenic properties and increased cytotoxicity compared to the common organic drug tamoxifen. In ferrocifen, the phenyl group of tamoxifen is replaced by the iron-containing ferrocenyl moiety.

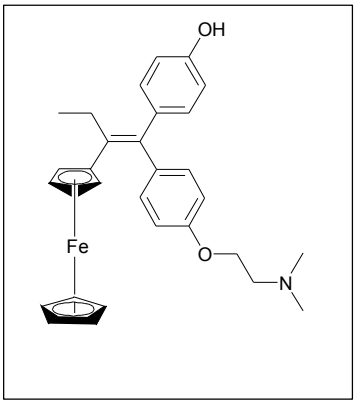

Figure 39. The structure of ferrocifen

The concept of metal – drug synergism has also been used in the design and synthesis of antiparasitic drugs especially against resistant strains.

Metal compounds as antiparasitic agents

New advances in the treatment of parasitic tropical diseases have been largely neglected, despite the fact that such diseases have been identified among the most important world health problems. The use of metal compounds as antiparasitic agents[86,87] dates back to 1906 with the observation of the activity of "ruthenium red" (Figure 40) against *Trypanosoma brucei*, a parasite responsible for "sleeping sickness" prevalent in Africa.

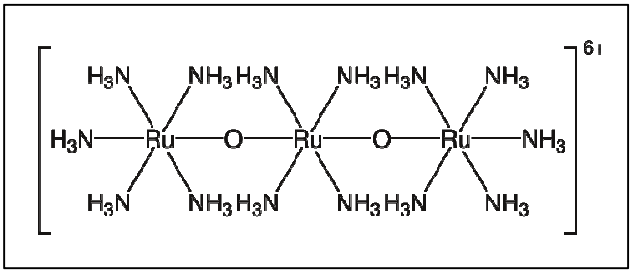

Figure 40. The strucuture of ruthenium red

Since then, there were several attempts to synthesize metal compounds for parasitic diseases. Dr. Sanchez-Delgado and his co-workers successfully applied the concept of metal-drug synergism by demonstrating that the activity of clotrimazole (CTZ) and ketoconazole (KTZ) against *T. cruzi*, the causative agent of Chagas' disease (American trypanosomiasis), is markedly enhanced by complexation to Ru (Figure 41), while the toxicity of the parent drugs is lowered.[88-92]

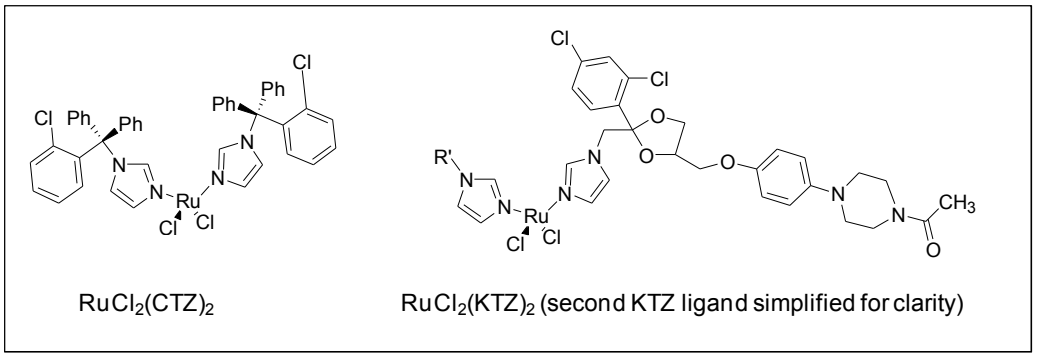

Figure 41. Two ruthenium complexes show improved activity over their organic drug

More directly related to this thesis, the same group has shown in early studies that the concept of metal-drug synergism can be adapted to produce novel metal-based antimalarials, by attaching chloroquine to metal containing fragments.[93,94] Some of the metals used in this study were Ru(II), Au(I) and Rh(I) (Figure 42) and in some cases a notable activity against resistant strains was observed.

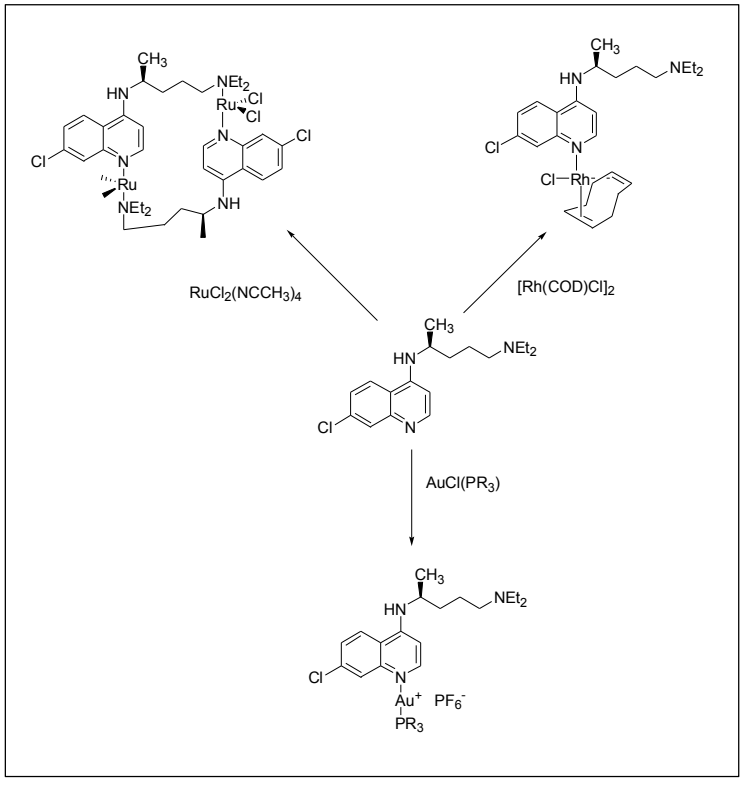

Figure 42. Examples of the syntheses and structures of metal-chloroquine complexes[93,94]

As shown by the examples presented in Table 3, the complexes $[RuCl_2(CQ)]_2$ and $[Au(PPh_3)(CQ)]PF_6$ are more active than chloroquine diphosphate against two moderately CQ-resistant strains of *P. falciparum* (FcB1 and FcB2). Also, *in vivo* tests using the rodent malaria parasite, *P. berghei* (Figure 43) showed the higher efficacy of $[RuCl_2(CQ)]_2$ and $[Au(CQ)(PPh_3)]PF_6$, as compared to chloroquine diphosphate.[93,94]

Table 3. Effect of chloroquine diphosphate and two metal-cloroquine complexes on the *in vitro* growth of chloroquine-resistant strains *of P. falciparum*[93,94]

Compound	IC_{50} (nM)[a]	
	FcB1	FcB2
CQDP	47.0	110.0
$RuCl_2(CQ)_2$	11.0	47.0
$[Au(PPh_3)(CQ)]PF_6$	5.1	23.0

[a] IC_{50} = 50% inhibitory concentration of the drug

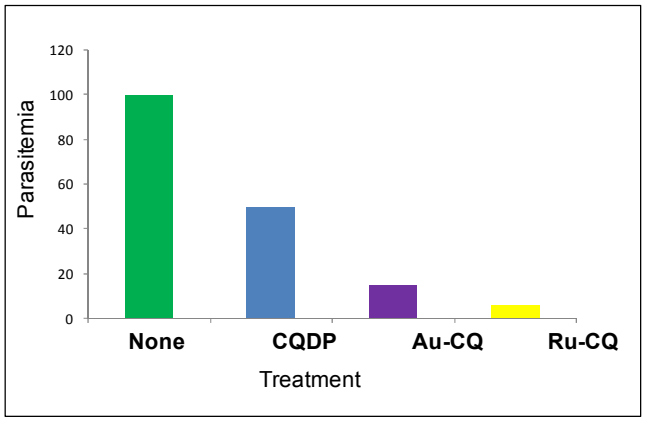

Figure 43. Effect of chloroquine diphosphate and metal-chloroquine complexes on *P. berghei* parasitemia in mice treated with 1 mg of CQ equivalents per Kg of body weight.[93,94]

One limitation in the use of these complexes is their low solubility in water; more soluble compounds with improved antimalarial potential would be welcome and the new design of cationic π-arene-Ru-CQ envisaged in this thesis appears as a promising alternative for new treatments of malaria, especially for the resistant strains. Although the mechanism of antimalarial action of metal complexes remains largely unknown, the transport properties, stability and heme aggregation inhibition ability of our new π-arene-Ru-CQ complexes will provide some insight to establish the mechanism of drug action and this will be presented in this thesis.

Further support for the metal-based approach to anti-malarial drugs comes from the work of Brocard and Biot.[95] In this case iron is introduced into the structure of CQ in the form of a ferrocenyl moiety, through a covalent C-C link of one cyclopentadienyl ring to the side chain of CQ. This results in a stable, non-toxic, potent anti-malarial, ferrochloroquine (Figure 44). The *in vitro* activity of this compound is similar to that of chloroquine diphosphate against CQ-sensitive strains of *P. falciparum*, but it is about 30 times higher for resistant strains. They have clearly demonstrated that the presence of both CQ and Fe in the same molecule is related to the ability of the drug to overcome CQ-resistance[96-99] but ferrocene alone shows no antimalarial activity. This drug is now in phase II[100] clinical trial.

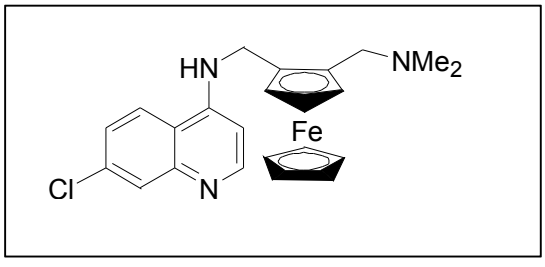

Figure 44 – The structure of ferroquine

In a similar manner to the metallation of chloroquine, a series of iridium, platinum, rhodium, palladium, antimony and osmium complexes of various organic drugs[101-103] has been prepared and evaluated for activity against *L. donovani*, *T. cruzi*, helminth worms and other parasites. Some of these compounds show improved activity against resistant strains.

The mechanisms of biological action and of overcoming resistance have not been studied or understood in detail for metal-CQ complexes. However, when we consider quinoline based drugs for the chemotherapy of malaria, the accepted target is the heme detoxification process. Similar to CQ, metal-based antimalarial agents derived from CQ are expected to maintain heme aggregation as the main target. Their possible mechanism of overcoming CQ resistance will be also discussed in later chapters in this thesis.

1.9 References

1. (a) World Malaria Report 2008, World Health Organization, http://www.who.int/malaria/wmr2008/. (b) Sachs, J.; Malaney, P. *Nature* **2002**, *415*
2. http://www.malariasite.com/MALARIA/History.htm
3. http://www.medicinenet.com/malaria/article.htm
4. http://www.vistamedica.com/main/images/stories/plasmodium_falciparum.jpg
5 http://www.malariasite.com/malaria/AnophelesMosquito.htm
6 http://iictenvis.nic.in/moreaboutmalaria.html
7. http://drugdiscoveryopinion.com/images/mosquito.jpg
8. Targeted delivery of drugs for the treatment of parasitic infections - US Patent 7101842 Description.mht
9. pathport.vbi.vt.edu/.../falciparum.html
10. http://www.malariasite.com/malaria/history_parasite.htm
11. http://www.pathobio.sdu.edu.cn/sdjsc/webteaching/Course/webteach/Protozoan/malaria-20parasites/world.jpg
12. http://en.wikipedia.org/wiki/Malaria
13. http://upload.wikimedia.org/wikipedia/commons/d/db/Symptoms_of_Malaria.png
14. http://www.malariasite.com/malaria/history_treatment.htm
15. http://www.discoveriesinmedicine.com/Ni-Ra/Quinine.html
16. http://www.rain-tree.com/Plant-Images/Cinchona_pubscens_p3jpg.jpg
17. http://www.homeopathyandmore.com/med_images/CHINA_OFFICINALIS.jpg
18. http://www.revolutionhealth.com/images/multum/Quinine%20200%20mg-GG.jpg
19. http://nobelprize.org/educational/medicine/malaria/readmore/treatment.html
20. http://nobelprize.org/nobel_prizes/medicine/laureates/1948/
21. http://www.appropedia.org/Appropriate_use_of_DDT

22. http://www.apsu.edu/oconnort/GSS2010/GSS2010lect05.htm

23. http://www.quackometer.net/blog/2009/01/artemisinin-and-malaria.html

24. http://www.antiaging-systems.com/PRG-23/artemisinin-wormwood-malaria.htm

25. Ph. J. Rosenthal, Ed. "Antimalarial Chemotherapy: mechanism of action, resistance and new directions in drug discovery", Humana Press, New Jersey, **2001**

26. Hyanes, R. K. *Curr.Top. Med. Chem.* **2006**, *6*, 509-537

27. O'Neill, P. M.; Posner, G. H. J. *Med. Chem.* **2004**, *47*, 2945-2964

28. Ashley, E. A.; White, N. J. *Curr. Opin. Infect. Dis.* **2005**, *18*, 531-536

29. Adjuik, M.; Babiker, A.; Garner, P.; Olliaro, P.; Taylor W.; White, N. *Lancet,* **2004**, *363*, 9-17

30. Egan, T.J.; Marques, H. M. *Coord Chem Rev*, **1999**, *190-192*,493–517

31. Ziegler, J.; Linck, R.; Wrigth, D. W. *Curr Med Chem*, **2001**, *8*,171–189

32. Sullivan, D. J.; *Int. J. Parasitol*, **2002**, *32*, 1645-1653

33. Cohen, S.N.; Yielding, K. L. *Proc Nat Acad. Sci*. **1965**, *54,* 521–527

34. Banerjee, R.; Liu, J.; Beatty, Pelosof, L.; Klemba, M.; Goldberg, D.; E. *Proc. Natl. Acad*. Sci. USA, **2002**, *99*, 990–5

35. Rosenthal, P.J.; Sijwali, P. S.; Singh, A.; Shenai, B. R. *Curr. Pharm. Des*. **2002**, *8*, 1659–72

36. Eggleson, K. K.; Duffin, K. L.; Goldberg, D. E. *J. Biol .Chem*. **1999**, *274* 32411–7.

37. http://www.tulane.edu/~wiser/malaria/fv.html

38. Atamna, H.; Ginsburg, H. *Mol. Biochem. Parasitol*. **1993**, *61*, 231–41

39. Noland, G. S.; Briones, N.; Sullivan, D. J. *Mol. Biochem. Parasitol*. **2003**, *130*, 91– 9

40. Chen, M. M.; Shi, L.; Sullivan, D. J. *Mol. Biochem. Parasitol*. **2001**, *113,* 1–8

41. Oliveira, M.; Avila, J. C. P.; Torres, C. R. *Mol. Biochem. Parasitol*. **2000**, *111*, 217–21

42. Pisciotta, J. M.; Ponder, E. L.; Fried, B.; Sullivan, D. J. *Int. J Parasitol*, **2005**, *35*, 1037–42

43. Oliveira, M. F.; Silva, J. R.; Dansa-Petretski, *Nature*, **1999**, *400*, 517–8.

44. Oliveira, M. F; Gandara, A. C. P.; Braga, C. M. S, *Comp. Biochem. Physiol*, 2007, C146:168–74

45. Katherine, A.; Villiers, Catherine, H.; Kaschula, E.; Egan, T.J.; Helder, M.; Marques, *J. Biol. Inorg. Chem*. 2007, *12*, 101–117

46. Koenig, D. F. *Acta Crystallogr*. **1965**, *18,* 663–673

47. Pisciotta, J. M.; Coppens, I.; *Biochem. J*. **2007**, *402*, 197-204.

48. Egan, T. J.; FEBS *letter*, **2006**, *580*, 5105-5110

49. Pagola, S.; Stephens, P.W.; Bohle, D. S.; Kosar, A.D.; Madsen, S. K. *Nature,* **2000**, *404,* 307–10

50. Solomonov, I.; Osipova, M.; Feldman, Y. *J. Am. Chem. Soc*. **2007**,*129*, 2615–27

51. Slater, A. F. G.; Cerami, A. *Nature*, **1992**, *355,*167–9

52. Dorn, A.; Stoffel, R.; Matile, H.; Bubendorf, A.; Ridley, R.G. *Nature* **1995**, *374*, 269–71

53. Bendrat, K.; Berger, B. J. *Nature*, **1995**, *378*, 138–9

54. Papalexis, V.; Siomos, M. A.; Campanale, N. *Mol. Biochem. Parasitol.* **2001**, *115*, 77–86

55. Akompong, T.; Kadekoppala, M.; Harrison, T. *J. Biol. Chem*, **2002**, *277,* 28923

56. Jackson, K.E.; Klonis, N.; Ferguson, D. J. P.; *Mol. Microbiol*. **2004**, *54*, 109–22

57. Coppens, I.; Vielemeyer, O. *Int. J Parasitol*. **2005**, *35*, 597–615

58. Pisciotta, J. M.; Coppens, I.; Tripathi, A. K. *Biochem. J*. **2007**, *402, 197*–204

59. Egan, T. J.; Chen, J. Y. J.; deVilliers, K. A. et al. *FEBS Lett*. **2006**, *580*, 5105–10

60. Dewal J.; Nagarkatti1, R.; Beatty, W.; Angel, R.; Slebodnick, C.; Andersen, J.; Kumar, S.; Rathore1, D. *PLOS pathogens*, doi:10.1371/journal.ppat.1000053

61. David, J.; Sullivan, J. R.; Ilya, Y.; Gluzman, I.; Russell, D.; Goldberg, D. E. *Proc. Natl. Acad. Sci. USA, **1996**, 93,* 11865 – 11870

62. Bohle, D. S.; Helms, J. B. *Biochem. Biophys. Res. Commun.,* **1993**, *193*, 504-508

63. Egan, T. J.; Ross, D. C. Adams, P. A. *FEBS Lett*. **1994**, *352*, 54-57

64. Egan, T. J. *J. Inor. Biochem*. **2005**, *99*, 1532-1539

65. Cohen, S. N.; Phifer, K. O.; Yielding, K. L.; Nature, **1964**, *202*, 805–806

66. http://en.wikipedia.org/wiki/Chloroquine

67. Egan, T. J.; Hunter, R.; Kaschula, C. H.; Marques, H. M.; Misplon, A.; Walden, J, *J. Med. Chem.* **2000**, *43*, 283

68. Egan. T. J. *Mini Reviews in Medicinal Chemistry*, **2001**, *1*, No. 1, 113-123.

69. Pagola, S. et al. *Nature*, **2000**, 307-310

70. http://www.tulane.edu/~wiser/protozoology/notes/drugs.html

71. a) Fidock, D.A. et al. *Mol. Cell*, **2000**, *6*, 861–871

b) Chen, N.; C.; Wilson, D. W.; Pasay, C.; Bell, D.; Martin, L. W.; Kyle, D.; Cheng, *Antimicrob. Agents Chemother*. **2005**, *49*, 2102-2105.

c) Sidhu, A. B. S.; Verdier-Pinard, D.; Fidock, D.A. *Science*, **2002,** *298*, 210-213.

d) Zhang, H.; Paguio, M.; Roepe, P.D.; *Biochemistry*, **2004**, *43*, 8290-8296.

72. Cooper, R.A. et al. *Mol. Pharmacol*., **2002**, 61, 35–42

73. Zhang, H. et al.; *Biochemistry*, **2004**, *43*, 8290–8296

74. Warhurst, D. C. *Malaria J*. **2003**b, *2*, 31–43

75. Warhurst, D. C.; Craig, J. C.; Adagu, I. S; Meyer, D. J.; Lee, S.Y. **2003**a. *Malaria J. 2*, 26

76. a) Ballou, W. R. Arevalo-Herrera, M.; Carucci, D.; Richie, T. L.; Corradin, G.; Diggs, C. *Am. J.Trop. Med. Hyg.* **2004,** *71* (2 Suppl)**,** 239-247

b) Druilhe, P.; Spertini, F.; Soesoe, D.; Corradin, G.; Mejia, P.; Singh, S.; Audran, R.; Bouzidi, A.; Oeuvray, C.; Roussihon, C. *PLoS Medicine* **2005**, *2*, 1135-1144

77. a) Jakupec, M. A.; Galanski, M.; Keppler, B. K, *Rev. Physiol. Biochem. Pharmacol.* **2003***, 146,* 1-54

b) Lippert, B, Helvetica Chimica Acta, and Weinheim WILEY- VCH: **1999**

78. Claire, S.; Allardyce, Dyson, P. J. *Top Organomet Chem*, **2006**, *17*, 177–210

79. a) Farrell, N.; *Transition Metal Complexes as Drugs and Chemotherapeutic Agents*. R. Ugo and B. R. James, Eds. *Catalysis by Metal Complexes*, Kluwer Academic Publishers: Dordrecht, **1989**, 11

b) N. Farrell. *Polynuclear platinum drugs*, **2004**, *42*, 251-296

c) Farrell, N. *ACS Symp. Ser,* **2005**, *903*, 62-79

80. Clarke, M. J.; *Coord. Chem. Rev.* **2003**, *236*, 209.233

81. Aird, R. E.; Cummings, J.; Ritchie, A. A.; Muir, M.; Morris, R. E.; Chen, H.; Sadler, P. J.; Jodrell, D. I, *British Journal of Cancer*, **2002**, *86*, 1652 – 1657

82. Alessio, E.; Balducci, G.; Lutmn, A.; Mestroni, G.; Calligaris, M.; Attia, W. M. *Inorg. Chim. Acta,* **1993**, *203*, 205-217

83. a) Sava, G.; Capozzi, I.; Clerici, K.; Gagliardi, R.; Alessio, E.; Mestroni, G, *Clin. Exp. Metastasis* **1998**, 371-379

b) Sava, G.; Gagliardi, R.; Bergamo, A.; Alessio, E.; Mestroni, G. *Anticancer Res.* **1999***, 19*, 969-972

c) Alessio, E.; Mestroni, G.; Bergamo, A.; Savva, G. *Curr. Top. Med. Chem* **2004**, *4*, 1525-1535

84. a) Morris, R. E.; Aird, R. E.; Murdoch, P. S.; Chen, H.; Cummings, J.; Hughes, S. Parsons, N. D.; Parkin, A.; Boyd, C.; Jodrell, D. J.; Sadler, P. J. *J. Med. Chem* **2001**, *44*, 3616-3621

b) Aird, R. E.; Cummings, J.; Ritchie, A. A.; Muir, M.; Morris, R. E.; Chen, H.; Sadler, P. J.; Jodrell, D. I. *J. Cancer*, **2002**, *86*, 1652-1657

c) Chen, H.; Parkinson, J. A.; Novakova, O.; Bella, J.; Wang, P.; Dawson, A.; Gould, R.; Parsons, S.; Brabec, V.; Sadler, P. J. *Proc. Nat. Acad. Sci.* **2003**, *100*, 14623-14628

d) Yan, Y. K.; Melchart, M.; Habtemariam, A.; Sadler, P. J. *Chem. Commun.* **2005**, 4764-4776.

85. Guo, Z.; Sadler, P. J. *Angew. Chem. Int. Ed.* **1999**, *38*, 1512 – 1531
86. Sánchez-Delgado, R. A.; Anzellotti, A. *Minirev. Med. Chem.*, **2004**, *4*, 23-30
87. Sánchez-Delgado, R. A.; Anzellotti, A.; Suárez, L. *Metal Ions and their Complexes in Medication* of *Metal Ions in Biological Systems*, Eds. H. Siegel and A. Siegel, Marcel Dekker: New York, 41, **2004**
88. Sánchez-Delgado, R. A.; Lazardi, K.; Rincón, L.; Urbina, J. A.; Hubert, A. J.; Noels, A. N, *J. Med. Chem.*, **1993**, *36*, 2041-2043
89. Sánchez-Delgado, R. A.; Navarro, M.; Lazardi, K.; Atencio, R.; Capparelli, M.; Vargas, F.; Urbina, J. A.; Bouillez, A.; Noels, A. F.; Masi, D. *Inorg. Chimica Acta* **1998**, *275,* 528-540
90. a) Anzellotti, A.; Sánchez-Delgado, R. A, unpublished results.

    b) Anzellotti, A. Estudio de los posibles mecanismos de acción de complejos Ru- azole contra el Trypanosoma cruzi. M.Sc. Thesis, IVIC, **2004**
91. Navarro, M.; Lehmann, T.; Cisneros, E. J.; Fuentes, A.; Sánchez-Delgado, R. A.; Silva, P.; Urbina, J. A. *Polyhedron,* **2000**, *19*, 2319-2325
92. Navarro, M.; Cisneros-Fajardo, E; Lehmann, T. R.; Sánchez-Delgado, R. A.; Atencio, R.; Silva, P.; Lira, R.; Urbina, J. A. *Inorg. Chem.* **2001**, *40***,** 6879-6884.
93. Sánchez-Delgado, R. A.; Navarro, M.; Pérez, H. ; Urbina, J. A, *J. Med. Chem.* **1996**, *39*, 1095-1099
94. Navarro, M.; Pérez, H.;Sánchez-Delgado, R. A. *J. Med. Chem.* **1997**, *40*, 1937- 1939
95. a) Biot, C.; Delhaes, L.; N' Diaye, C. M.; Maciejewski, L. A.; Camus, D.;

Brocard, J. S.; Dive, D. *J. Med. Chem*. **1997**, *40*, 3715-3718

b) Biot, C.; Delhaes, L.; Abessolo, H.; Domarle, O.; Maciejewski, L. A.; Mortuaire, M.; Delcourt, P.; Deloron, P.; Camus, D. ; Dive, D.; Brocard, J. S. *J. Organomet. Chem.* **1999**, *589*, 59-65

96. a) Delhaes, L.; Abessolo, H.; Biot, C.; Berry, L.; Delcourt, P.; Maciejewski, L.; Brocard, J.; Camus, D.; Dive, D, Parasitol. *Res.* **2001**, *87*, 239-244

b) Pierrot, C.; Lafitte, S.; Dive, D.; Fraisse, L.; Brocard, J.; Jamal, K. *Int. J. Parasitol.* **2005**, *35*, 1601-1610

97. Pradines, B.; Fusai, T. ; Daries, W.; Laloge, V. ; Rogier, C.; Millet, P.; Panconi, E.; Kombila, M.; Parzy, D. *J. Antimicrob. Chemother.* **2001**, *48*, 179-184

98. Pradines, B.; Tall, A.; Rogier, C.; Spiegel, A.; Mosnier, J. ; Marrama, L.; Fusai, T.; Millet, P.; Panconi, E.; Trape, J. F.; Parzy, D. *Trop. Med. Int. Health.* **2002**, *7*, 265-270

99. Blackie, M. A. L.; Beagley, P.; Chibale, K.; Clarkson, C.; Moss, J. R.; Smith, P. J. *J. Organomet. Chem.* **2003**, *688*, 144-152

100. Henry, M.; Briolant, S.; Fontaine, A. et al. *Antimicrob. Agents Chemother*. **2008**, *52*, 2755-2759

101. Loiseau, P.M.; Craciunescu, D. G.; Doadriovillarejo, J. C.; Certadfombona, G.; Gayral, P, **1992**, *Tropical medicine and parasitology, 43*, 110

102. Zinsstag, J.; Brun, R.; Craciunescu, D.G.; Iglesias, E. P.; **1991**, *Tropical medicine and parasitology*, *42*, 41

103. Mesa Valle, C.M.; Moraleda, Lindez, V.; Craciunescu, D.; Alonso, M.; Osuna, A. **1993**, *Arzneimittel Forsch/Drug Res, 43*, 1010

Chapter 2

Synthesis, Characterization and Antimalarial Activity of New (π-Arene)-Ruthenium-Chloroquine Complexes

1 Introduction

A new molecular design that should result in improved stability and antimalarial activity has been devised based on the knowledge gained from previous experiments[1] from our own group, together with the recently published work by other researchers in related subjects. Scheme 1 summarizes our molecular design, based on Ru(II) forming coordinate bonds to CQ through one of the basic nitrogen atoms. The possible role of each fragment of the arene-ruthenium-CQ complex is indicated below:

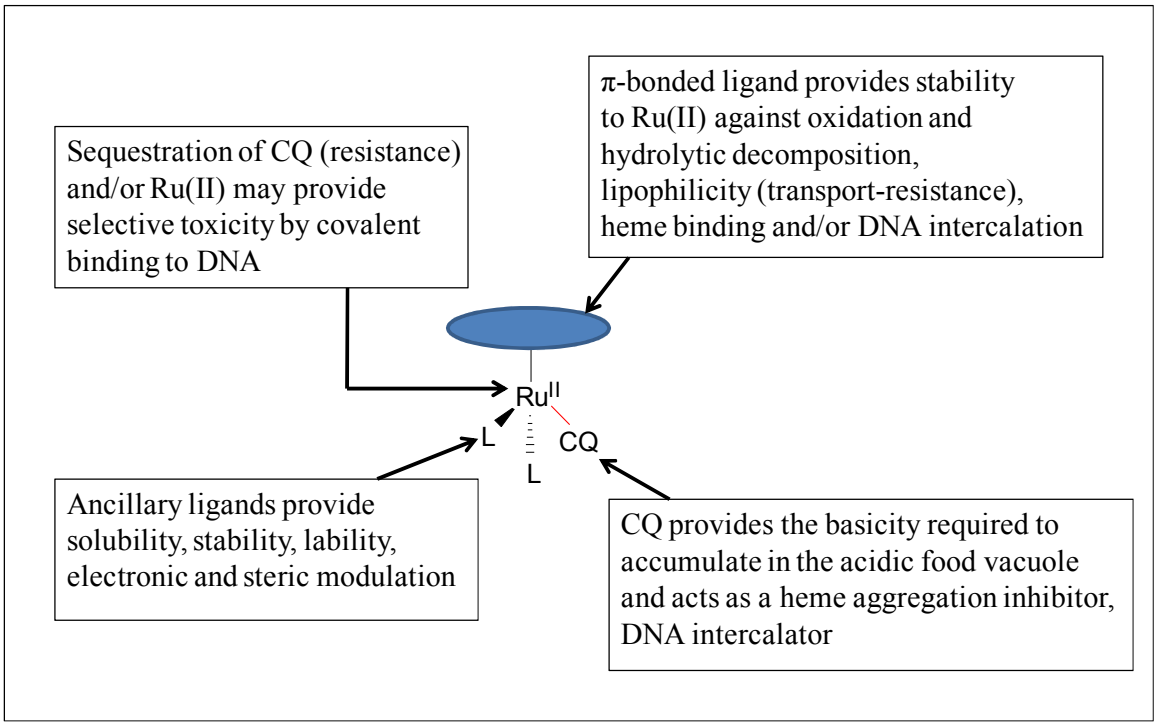

Scheme 1. Coordinative molecular design

1. The central metal atom is **Ru(II).** This metal is known to be biologically active, and of low toxicity, particularly in the +2 oxidation state.[2] Ru (II) is expected to contribute to the desired biological properties in the following ways:

   - Sequestering chloroquine in a form "invisible" to *Plasmodium* parasites, as the main pathway to overcome resistance.

- It may provide selective toxicity through DNA binding.

2. The new complexes will contain a **π-bonded ligand (Ar)** and its role in the biological action would be:

- Stabilizing Ru(II) against oxidation or hydrolytic decomposition.[3-5]
- Providing the lipophilicity necessary (to overcome CQ resistance) for recognition and transport of the complexes through cell membranes.[6]
- Engaging in π-π interactions with heme, thereby promoting a secondary mode of aggregation inhibition, in order to enhance the standard action of chloroquine.

3. **Chloroquine** will be coordinated to ruthenium. The various possible binding modes of CQ to the metal ion in these complexes are discussed in the results and discussion section. Two major roles can be ascribed to CQ in this molecular design:

- To provide the basicity required for the complexes to accumulate in the acidic food vacuole of *Plasmodium* parasites.
- To act as a heme aggregation inhibitor, the fundamental mechanism of anti-malarial action contemplated in this proposal. In line with our previous results for other metal-CQ complexes,[7,8] a marked enhancement of the activity of coordinated chloroquine is expected with respect to free chloroquine, especially against resistant parasites.
- The new molecular design provides improved water solubility and transport properties and a multifunctional mode of action, which should result in more active compounds.

4. The complexes contain **ancillary ligands** that complete the coordination sphere. This is a key feature of our design and they will have following main functions:

- To provide water-solubility.
- To provide the necessary balance of stability and lability of the active species.
- To allow the modulation of the electron density of the complexes, of importance in determining the donor-acceptor behavior and therefore the biological properties.

2.2 Specific aims

The long-term object of this project is to discover new leads toward ruthenium -based antimalarial agents capable of reducing or overcoming resistance.

The central hypothesis of this project is that combining CQ, π-bonded ligands and ruthenium in a single molecule will produce modifications of the physicochemical properties of CQ leading to a better activity against resistant strains, through enhanced heme aggregation inhibition activity (HAIA)

This hypothesis is based on the following observations:

1. ***Ru complexes are a powerful alternative in anti-malarial drug design***

The antimalarial activity of CQ is enhanced by complexation to Ru, particularly against CQ-resistant strains of *P. falciparum*.[7,8] Among other metal-CQ complexes, $[RuCl_2(CQ)]_2$ shows improved antimalarial activity *in vivo* (Figure 1).

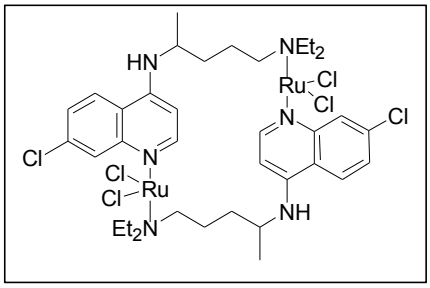

Fig 1. The structure of $[RuCl_2(CQ)]_2$

2. ***Ruthenium has some properties which make its compounds suited to biological applications***[9]

Ru has similar ligand exchange kinetics to those of Pt(II) complexes. Ligand exchange ability is an important factor for biological activity because most drugs undergo interactions with macromolecules such as proteins.

Another property of ruthenium that makes it suitable for medicinal application is that it has range of oxidation states, Ru(II), Ru(III) and Ru(IV), which are accessible under physiological conditions; among those, Ru(III) is more biologically inert than the other two states.

Also the redox potential of ruthenium complexes can be easily modified by varying the ligands. Ruthenium has the ability to mimic iron in binding to many biomolecules such as serum transferrin and albumin, two important proteins that are used by mammals to solubilize and transport iron. This results in a low toxicity of ruthenium.

3. ***Although the CQ resistance strains are widespread, CQ is still the most common treatment for malaria against CQ-sensitive strains.***

Work by Dr. Sanchez-Delgado et.al.[7,8] and Brocard et.al.[10-13] have shown the possibility to overcome CQ resistance by modifying the CQ skeleton by metals.

4. ***Π-arene ligands enhance the stability and improve the delivery of cytotoxic Ru agents.***

Arene ligands stabilize Ru(II) and provide a hydrophobic face that may enhance recognition and transport through cell membranes. Sadler et.al[14] pointed out that organometallic complexes of the type [arene-(en)-Ru(II)-X]$^{+}$, (en = ethylenediamine) containing arene ligands inhibit the growth of the human ovarian cancer cell lines. In this

case the arene ligand not only provides a lipophilic site to the complex but also stabilizes the ruthenium atom in the oxidation state (II).

5. ***Our group has shown that the complex $[RuCl_2(CQ)]_2$ (Figure 1) displays modified physicochemical properties of CQ, which lead to better activity against CQ resistant malaria through enhanced heme aggregation inhibitory activity (HAIA).***[1]

The mechanism of antimalarial action of $[RuCl_2(CQ)]_2$,which was previously reported to be active *in vitro* against CQ-resistant strains of *P. falciparum* and *in vivo* against *P. berghei*[7], has been investigated by a variety of techniques.

We have concluded that as in the case of CQ, heme aggregation is the principal target of the ruthenium-CQ complex. The higher heme aggregation inhibition activity of Ru-CQ complex as compared to that of CQDP at the interface of octanol-water, has provided evidence to strengthen the idea that heme aggregation takes place at water-lipid interfaces under physiologically relevant conditions.[3]

Since the combination of ruthenium and CQ results in a higher lipophilic character compared to CQ, we suggested that the enhanced antimalarial activity of complex both *in vitro and in vivo* may also be related to its greater lipophilicity, in line with previous reports indicating a lowered ability of the mutated transmembrane transporter PfCRT to promote the efflux of highly lipophilic drugs.[15,16]

Also, the concentration of highly lipophilic drugs must be higher near the lipid-water interfaces where heme aggregation is known to take place.[3]

Although the complex $[RuCl_2(CQ)]_2$ displays high antimalarial activity and has provided some insights into the principal mechanism of action, there are few possibilities

to modify its simple structure. Hence we conceived the new molecular design in Scheme 1 in order to improve the physicochemical properties relevant to antimalarial potential. Based on these considerations, the primary focus of the first part of this thesis is the synthesis of new ruthenium complexes containing CQ and π-bonded arene ligands. The new molecules are synthesiszed with a dual purpose:

1. **Targeting anti-malarial action through heme aggregation inhibition together with a metal-mediated reduction of the emergence of resistance and**
2. **Understanding the correlation between the physicochemical properties of the new ruthenium complexes and their antimalarial activity.**

In line with our hypothesis, the following specific aims have been established:

1. Synthesis and characterization of new arene-ruthenium-CQ complexes.
2. Evaluation of the *in vitro* heme aggregation inhibition activity and DNA binding ability of the new complexes as a measure of their antimalarial potential and as mechanistic probes.
3. Studies of their physiochemical properties relevant to their antimalarial potential.
4. Evaluation of their antiplasmodial activity (Dr. J. Schrevel et.al. at the National Museum of Natural History, Paris)

2.3 Experimental Section

2.3.1 Techniques reagents and solvents

All manipulations were carried out under N_2 using common Schlenk techniques in order to avoid undesirable oxidation processes during the preparation of the complexes. Solvents (analytical grade, Aldrich) were dried and degassed immediately prior to use by means of an Innovative Technology solvent purification unit; ruthenium trichloride hydrate (Pressure Chemicals, Inc.), chloroquine diphosphate, and other reagents (Aldrich) were used as received. Calf thymus DNA, hemin, buffers and solvents were purchased from Sigma-Aldrich. Elemental analyses were performed by Atlantic Microlab, Norcross, Georgia. FTIR spectra were measured on a Thermoelectron NICOLET 380 FTIR spectrometer. Conductivity values were obtained using 1 mM solutions of the complexes in water or other appropriate solvents at various time intervals using an Oaklon pH/Conductivity meter. NMR spectra were obtained using an AVANCE Bruker 400 instrument. UV spectra were obtained with an Agilent 8453 diode - array spectrophotometer equipped with a HP 89090 Peltier temperature control accessory.

2.3.2 Chloroquine base

CQ was obtained by a modified version of a published procedure.[17] Concentrated ammonia solution (20 mL) was added to chloroquine diphosphate (CQDP) (20 g, 38.9 mmol) followed by two extractions with chloroform (200 mL). Removal of the solvent yielded an oil to which acetonitrile (30 mL) was added. The solution was evaporated to dryness to yield a white powder, which was washed with acetonitrile (5 mL) and diethyl ether (5 mL) and dried under vacuum. The atom numbering for chloroquine is shown in Figure 2.

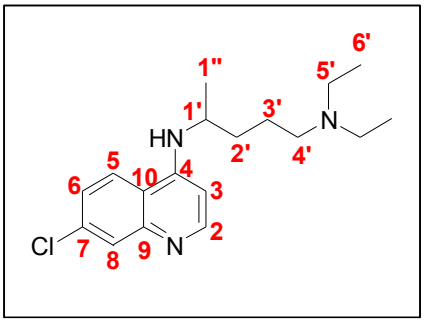

Figure 2. The structure of chloroquine (CQ)

2.3.3 Synthesis of starting materials

The synthesis of the starting materials $[Ru^{II}(\eta^6\text{-}p\text{-cymene})Cl_2]_2$ and $[Ru^{II}(\eta^6\text{-benzene})Cl_2]_2$ was performed by dehydrogenation of α-phellandrene or 1,3-cyclohexadiene by ruthenium trichloride hydrate, respectively, according to the general method published by Bennett (Figure 3).[18] For instance, for $[Ru^{II}(\eta^6\text{-}p\text{-cymene})Cl_2]_2$, a solution of $RuCl_3.3H_2O$ in ethanol was treated with α-phellandrene and heated under reflux for 4 h under inert atmosphere. The solution was cooled to room temperature, and the product was filtered off and dried *in vacuo*. The analogous benzene material was obtained by a similar procedure, using cyclohexadiene.

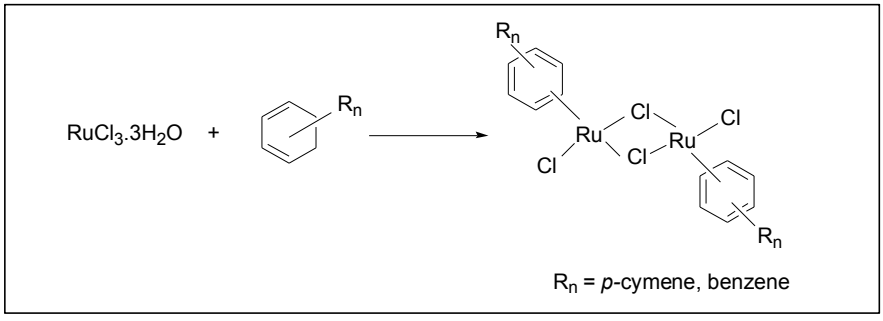

Figure 3. Preparation of starting materials

2.3.4 Synthesis of complexes

2.3.4.1 [$Ru^{II}(\eta^6$- *p*-cymene)Cl_2(CQ)] (1)

[$Ru^{II}(\eta^6$-*p*-cymene)$Cl_2]_2$ (612 mg, 1 mmol) and chloroquine base (640 mg, 2 mmol) were stirred in acetone (30 mL) under N_2 for 4 h at room temperature. The orange suspension was evaporated to dryness to yield an orange solid, which was dissolved in water. The yellow aqueous solution was filtered through Celite and evaporated to dryness to yield a solid that was dried under vacuum. Yield 96%.

^{1}H NMR (400 MHz, D_2O) δ 8.25 (d, J = 6.73 Hz, 1H), 8.09 (d, J = 9.11 Hz, 1H), 7.75 (d, J = 2.05 Hz, 1H), 7.51 (dd, J = 2.08 Hz, J' = 9.09 Hz, 1H), 6.72 (d, J = 6.85 Hz, 1H), 5.32 (d, J = 6.21 Hz, 2H), 5.13 (d, J = 6.21 Hz, 2H), 4.00 (m, 1H), 3.12 (m, 6H), 2.62 (m, 1H), 2.03 (s, 3H), 1.76 (br, 4H), 1.33 (d, J = 6.48 Hz, 3H), 1.18 (d, J = 6.93 Hz, 6H), 1.16 (t, J = 7.29 Hz, 6H). ^{13}C NMR (100 MHz, D_2O) δ 153.87 C(4), 144.42 C(2), 140.22 C(9), 136.01 C(7), 126.60 C(6), 123.69 C(5), 120.59 C(8), 115.37 C(10), 98.76 C(3), 98.49 C(F), 92.74 C(G), 76.47 C(E), 75.94 C(D), 51.45 C(4′), 49.14 C(1′), 47.48 C(5′), 32.05 C(2′), 30.51 C(C), 21.93 C(6′), 20.42 C(3′), 18.98 C(1″), 17.67 C(B), 8.33 C(A). Anal. Calcd for $C_{28}H_{40}N_3Cl_3Ru.H_2O$: C, 52.17; H, 6.52; N, 6.52. Found: C, 52.48; H, 6.48; N, 6.64.

2.3.4.2 [$Ru^{II}(\eta^6$-benzene)Cl_2(CQ)] (2)

[$Ru^{II}(\eta^6$-benzene)$Cl_2]_2$ (250 mg, 0.5 mmol) was suspended in acetonitrile (30 mL) under N_2. The mixture was stirred at room temperature until all the solid dissolved to form a dark-brown solution. Chloroquine base (320 mg, 1.0 mmol) was then added and the resulting solution was stirred at room temperature for 20 h. A dark beige-green solid formed which was filtered off and dried under vacuum.

The product was purified by stirring the solid in 20 mL of acetone for 1 h after which it was filtered off and dried under reduced pressure.Yield 70%.

^{1}H NMR (400 MHz, MeOD) δ 8.33 (d, 1H, J = 8.80 Hz), 8.26 (d, 1H, J = 6.40 Hz), 7.71 (d, 1H, J = 2.00 Hz), 7.43 (dd, 1H, J = 8.90 Hz, J' = 2.00 Hz), 6.68 (d, 1H, J = 6.40 Hz), 5.38 (s, 6H), 3.94 (m, 1H), 3.07 (m, 6H), 1.76 (m, 4H), 1.29 (d, 3H, J = 6.40 Hz), 1.18 (t, 6H, J = 7.20 Hz). ^{13}C NMR (100 MHz, MeOD) δ 153.30 C(4), 146.79 C(2), 143.59 C(9), 137.36 C(7), 125.94 C(6), 124.24 C(5), 122.52 C(8), 116.55 C(10), 98.67 C(3), 77.30 C(A), 51.61 C(4′), 48.88 C(1′), 45.88 C(5′), 32.39 C(2′), 20.81 C(3′), 18.77 C(1″), 7.82 C(6′). Anal. Calcd for $C_{24}H_{32}N_3Cl_3Ru$: C, 50.58; H, 5.66; N, 7.37.Found: C, 50.51; H, 5.84; N, 7.55.

2.3.4.3 $[Ru^{II}(\eta^6$-*p*-cymene)$(H_2O)_2(CQ)][BF_4]_2$ (3)

$[Ru^{II}(\eta^6$-*p*-cymene)$Cl_2]_2$ (400 mg, 0.653 mmol) and $AgBF_4$ (509 mg, 2.614 mmol) were stirred in acetone (40 mL) for about 2 h at 55 ^{0}C under nitrogen. After cooling to room temperature, the solution was filtered through celite to remove the white precipitate of AgCl. Then chloroquine (418 mg, 1.307 mmol) was added to the filtrate. The mixture was stirred at 55 ^{0}C for 20 h and then cooled to room temperature. The resulting reddish brown colored solution was concentrated and hexane (3 mL) was added until the solution became turbid. Then the solution was dried under vacuum to obtain a brown solid.

Finally the solid was washed by stirring the solid in a large volume of pentane overnight. Pentane was filtered off under nitrogen and the resulting brownish yellow colored solid was dried under vacuum. Yield 96%.

^{1}H NMR (400 MHz, MeOD) δ 8.25 (d, 1H), 8.23 (d, 1H), 7.71 (s, 1H), 7.46 (dd, J = 9.03 Hz, J' = 7.45 Hz, 1H), 6.71 (d, J = 6.17 Hz, 1H), 5.31 (d, J = 5.25 Hz, 2H), 5.11 (d, J = 5.27 Hz, 2H), 3.95 (m , 1H), 3.10 (m, 4H), 3.06 (m, 2H),

2.68 (m, 1H), 2.09 (s, 3H), 1.74 (m, 2H), 1.71 (m, 2H), 1.30 (d , J = 6.08 Hz, 3H), 1.19 (d, 6H), 1.15 (t, 6H). ^{13}C NMR (100 MHz, MeOD) δ 153.34 C(4), 146.62 C(2), 143.29 C(9), 137.44 C(7), 126.02 C(6), 123.91 C(5), 122.31 C(8), 116.42 C(10), 98.67 C(3), 51.55 C(4'), 48.77 C(1'), 47.19 C(5'), 32.26 C(2'), 20.66 C(3'), 18.67 C (1"), 7.81 C(6'). Anal. Calcd for $C_{28}H_{42}N_3ClORuB_2F_8$ C, 45.08; H, 5.63; N, 5.63. Found: C, 45.09; H, 5.88; N, 5.52.

2.3.4.4 [Ru^{II}(η^6-*p*-cymene)(η^6-CQDP)][BF$_4$]$_2$ (4)

[Ru^{II}(η^6-*p*-cymene)Cl$_2$]$_2$ (300 mg, 0.490 mmol) was dissolved in warm deionized water (40 mL, 55 °C); $AgBF_4$ (382 mg, 1.96 mmol) and chloroquine diphosphate (506 mg, 0.98 mmol) was added under nitrogen. The mixture was stirred for 20 h at 55°C and then filtered through celite to yield an orange solution. The solvent was evaporated and the final product was dried under vacuum for 20 h. Yield 78%.

^{1}H NMR (400 Mhz, D_2O) δ 8.18 (d, J = 7.24 Hz, 1H), 8.13 (d, J = 9.11 Hz, 1H), 7.76 (d, J = 1.94 Hz, 1H), 7.54 (dd, J = 9.12 Hz, J' = 1.97 Hz, 1H), 6.74 (d, 7.30 Hz, 1H), 5.84 (d, J = 6.30 Hz, 2H), 5.62 (d, J = 6.22 Hz, 2H), 4.03 (m, 1H), 3.06 (m, 6H), 2.78 (m, 1H), 2.13 (s, 3H), 1.71 (m, 4H), 1.28 (d, J = 6.47 Hz, 3H), 1.24 (d, J = 6.94 Hz, 6H), 1.12 (td, J = 7.15 Hz, J' = 1.91 Hz, 6H).

^{13}C NMR (100 MHz, D_2O) δ 155.63 C(4), 142.26 C(2), 139.38 C(7), 138.36 C(9), 127.40 C(6), 124.17 C(5), 119.25 C(8), 115.43 C(10), 99.73 C(F), 98.52 C(3), 96.07 C(G), 79.03 C(E), 76.24 C(D), 51.28 C(5′), 49.51 C(1′), 47.43 C(4′), 30.72 C(C), 21.28 C(A), 31.98 C(2′), 20.30 C(3′), 17.70 C(1′′), 17.70 C(B), 8.19 C(6′).

Anal. Calcd for$C_{28}H_{46}N_3ClO_8P_2RuB_2F_8.2H_2O$ C, 34.96; H, 5.20; N, 4.37. Found: C, 35.04; H, 4.94; N, 4.37.

2.3.5 DFT calculations

All calculations reported in this study were carried out by use of the *Gaussian 03* program package.[19] All molecular structures, frequencies, and normal-mode composition were computed using the B3LYP density functional in combination with a LANL2DZ effective core potential (ECPs) for ruthenium[20] and moderate 6-31G(d) basis sets for all remaining atoms. Computed frequencies of all structures are positive, indicating that the structures are at real minima of their ground-state potential energy surfaces. The relative energies of structural isomers were estimated based on full optimizations employing both gas-phase model and the polarizable continuum model (PCM)[21] to mimic electrostatic effects of aqueous solutions. Previous studies[22] have demonstrated that B3LYP calculation is effective in reproducing experimental structures for transition metal complexes.

2.3.6. Conductivity measurements

For conductivity measurements, a 1 mM solution of each complex in de-ionized water was prepared. The conductivity was measured using an Oaklon pH/Conductivity meter.

2.3.7 Biological activity evaluation *in vitro*

The antimalarial activity of new ruthenium-CQ complexes against CQ-sensitive and CQ-resistant *P. falciparum* was evaluated by Prof. J. Schrevel at the National Museum of Natural History, Paris. The following strains of *P. falciparum* were employed in this study: FcB1(Colombia), PFB (Brazil), F32 (Tanzania), W2 (Indonesia), Dd2 (SE. Asia), K1 (SE. Asia), and 3D7 (origin unknown). In our routine culture conditions, that is in the

absence of chloroquine pressure, FcB1, PFB, 3D7, and F32 were chloroquine-sensitive (IC_{50} < 100 nM), whereas W2, Dd2, and K1 were chloroquine-resistant (IC_{50}> 100 nM).

Cultures were grown in complete medium consisting of RPMI 1640 (Life Technologies Inc.) supplemented with 11 mM glucose, 27.5 mM $NaHCO_3$, 100 UI/mL penicillin, 100 μg/mL streptomycin, and 8-10% heat-inactivated human serum, following the procedure of Trager and Jensen.[23] Parasites were grown at 37 °C in human A+ (FcB1, PFB, F32) or O+ (W2, Dd2, K1, 3D7) redblood cells at a 2% hematocrit and a 2-6% parasitemia, under a 3% CO_2, 6% O_2, and 91% N_2 atmosphere. W2, Dd2, K1, and 3D7 parasites were synchronized by sorbitol[24] treatment. According to their respective solubility in H_2O, 1 mM stock solutions of the Ru complexes **1**- **4** were prepared in either H_2O or 10% DMSO (Ru-complex **3**). Further dilutions were in complete culture medium. The complexes were tested for their inhibitory effect toward the *P. falciparum* intraerythrocytic development. Increasing concentrations of the complexes and chloroquine (100 μL/well, top concentration 50 μM) were distributed in a 96 well microplate; DMSO (0.2% vol/vol, top concentration) was distributed for control.

Then, for the FcB1, PFB, and F32 strains, 100 μL from an asynchronous culture at a 1.0% parasitaemia and a 4.0% hematocrit in complete medium was added per well. Parasites were allowed to grow at 37 °C for 24 h in a candle jar; then 0.5 μCi of 3H-hypoxanthine was added per well, and the culture was incubated for an additional 24 h period. For the K1, Dd2, 3D7,and W2 strains, 100 μL from a culture containing >90% rings (age 0-20 h postinvasion) at a 0.5-1.0% parasitaemia and a 3.0% hematocrit in complete medium was added per well along with 1.0 μCi of 3H-hypoxanthine. Parasites were grown for 42 h at 37 °C in a candle jar. Plates were freeze-thawed and parasites

were harvested on filters. Dried filters were moistened in scintillation liquid mixture (OptiScint, Hisafe) and counted in a 1450 Microbeta counter (Wallac, PerkinElmer). Percentage growth inhibition was calculated from the parasite-associated radioactivity. 100% ^{3}H-hypoxanthine incorporation was determined from a control grown in the absence of Ru complexes. IC_{50} values were determined according to the method reported by Desjardins et al.[25]

2.4 Results and Discussion

2.4.1 Synthesis of complexes

2.4.1.1 Introduction

According to our molecular design, we proposed several target compounds, with the generic structures shown in Scheme 2:

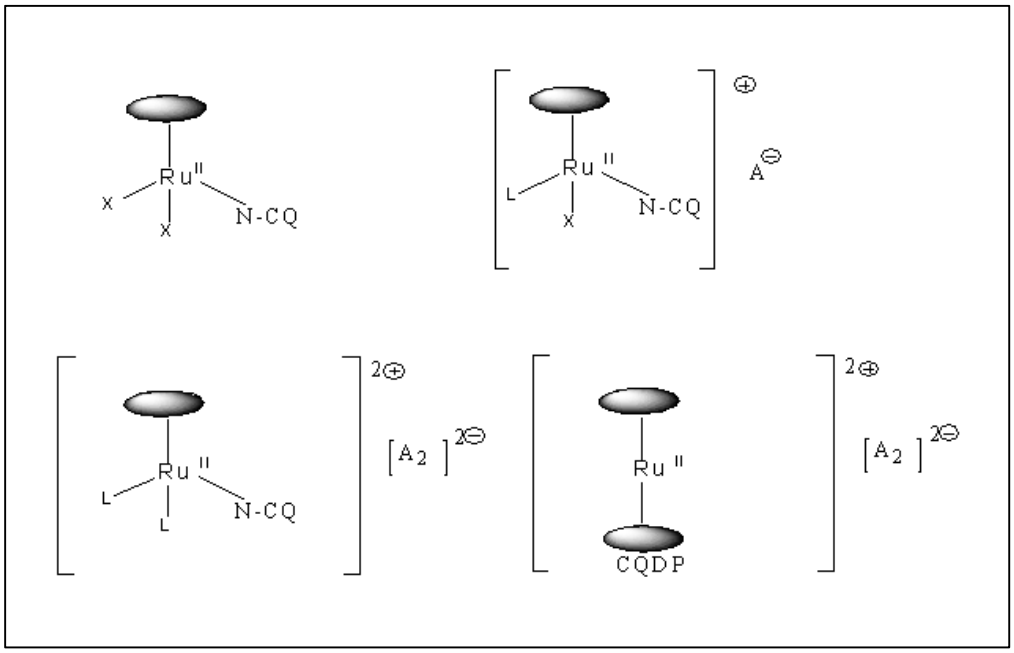

Scheme 2. Proposed target compounds (a), (b), (c) and (d)

All complexes consist of an arene ligand, ruthenium in the +2 oxidation state, ancillary ligands and chloroquine. *p*-Cymene and benzene were selected as the arene ligands present in the new complexes. Neutral (a), monocationic (b) and dicationic (c) compounds featuring N-bonded chloroquine and a tetracationic compound with π – bonded chloroquine diphosphate (d) were envisaged in order to evaluate the influence of the arene ligand, the binding mode of ruthenium to chloroquine and the overall charge in the chemical and biological properties of the complexes.

2.4.1.2 Synthesis of neutral compounds

2.4.1.2.1 $[Ru^{II}(\eta^6\text{-}p\text{-cymene})Cl_2CQ]$ (1)

Upon reaction of $[Ru^{II}(\eta^6\text{-}p\text{-cymene})Cl_2]_2$ with chloroquine in acetone, the chloride bridge splits and the complete reaction (96% yield) results in 2 equivalents of the neutral dichloro compound $[Ru^{II}(\eta^6\text{-}p\text{-cymene})Cl_2(CQ)]$; **(1)** (Scheme 3). The complex was purified according to the methods described in the experimental section. Elemental analysis and NMR data discussed in detail in section 2.4.2 confirm this formulation.

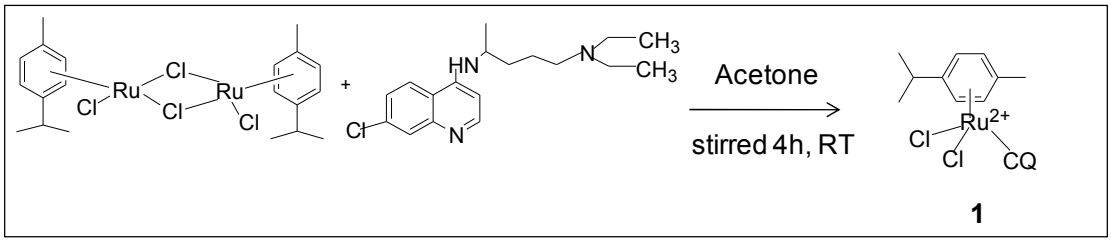

Scheme 3. Synthesis of compound **1**

Conductivity measurements indicate that **1** remains neutral in chloroform solution (non-conducting) but it rapidly exchanges one chloride ligand with a solvent molecule in polar solvents to reach conductivities of 47 μScm^2Mol^{-1} in methanol and 100.5 μScm^2Mol^{-1} in water; these are values typical of a 1:1 electrolyte (Scheme 4). The conductivity values do not vary over a period of 24 h. In aqueous solution, the only Ru-containing species present within 1 min of dissolution is thus the monocationic derivative $[Ru^{II}(\eta^6\text{-}p\text{-cymene})Cl(H_2O)(CQ)]^+$ (**1′**) as the chloride salt and no NMR spectral changes consistent with recoordination of chloride are observed upon addition of up to 2 equiv of sodium chloride. Aqueous solutions of **1′** are stable over prolonged periods of time in the air, something important in relation to possible biological applications.

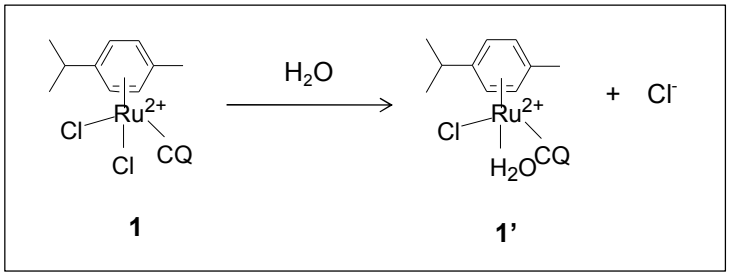

Scheme 4. Solvolysis of compound **1** in water

2.4.1.2.2 [$Ru^{II}(\eta^6$-benzene)Cl_2CQ] (2)

Upon reaction of $[Ru^{II}(\eta^6$-benzene$)Cl_2]_2$ with chloroquine in acetonitrile, the chloride bridge splits and this results in 2 equivalents of the neutral dichloro(benzene) complex $[Ru^{II}(\eta^6$-benzene$)Cl_2(CQ)]$ (70 % yield) (Scheme 5). Elemental analysis and NMR data (see section 2.4.2) confirm this formulation.

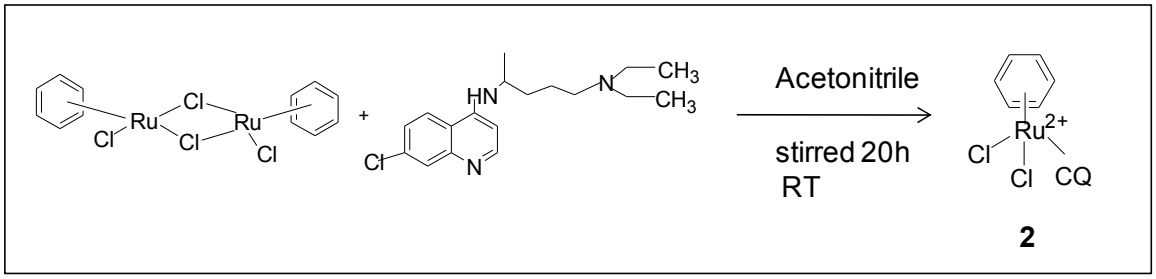

Scheme 5. Synthesis of compound **2**

The conductivity of a freshly prepared 1 mM solution of $[(Ru^{II}$-η^6-benzene$)Cl_2(CQ)]$ in de-ionized water was 104 μScm^2Mol^{-1}, a value typical of a 1:1 electrolyte. This suggests that in an aqueous medium, the complex rapidly loses one chloride, becomes aquated and thereby forms a mono cationic complex **2'** (Scheme 6):

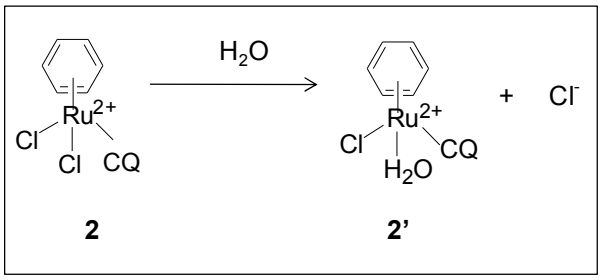

Scheme 6. Solvolysis of compound **2** in water

2.4.1.3 Synthesis of di - and tetra- cationic compounds

2.4.1.3.1 $[Ru^{II}(\eta^6\text{-}p\text{-cymene})(H_2O)_2(CQ)][BF_4]_2$ (3)

In order to synthesize dicationic compounds, four chlorine atoms must be removed from $[Ru^{II}(\eta^6\text{-}p\text{-cymene})Cl_2]_2$. The starting material, $[Ru^{II}(\eta^6\text{-}p\text{-cymene})Cl_2]_2$ was treated with 4 eq of the chloride abstracting agent $AgBF_4$ in acetone in order to obtain the labile intermediate $[Ru^{II}(\eta^6\text{-}p\text{-cymene})(Solv)_3][BF_4]_2$ which was subsequently reacted with CQ to obtain the desired pure dicationic compound (Scheme 7) in 96% yield according to the procedure described in the experimental section. Elemental analysis and NMR data (section 2.4.2) confirm this formulation. This compound is stable as a solid and in aqueous or methanol solutions.

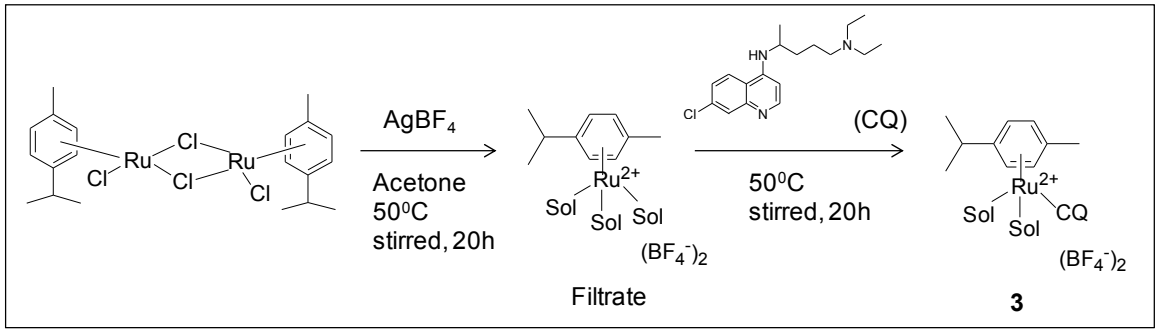

Scheme 7. Synthesis of compound **3**

The conductivity of a freshly prepared 1 mM solution of $[Ru^{II}(\eta^6\text{-}p\text{-cymene})(H_2O)_2(CQ)][BF_4]_2$ in de-ionized water was 232 μScm^2Mol^{-1}, a value within a range typical of three ions in solution.

2.4.1.3.2 $[Ru^{II}(\eta^6\text{-}p\text{-cymene})(\eta^6\text{-CQDP})][BF_4]_2$ (4)

Another feature of interest in connection with biological properties is to compare complexes containing chloroquine base with those containing chloroquine diphosphate, which is the form in which this drug is administered. In structural terms, when the two nitrogen atoms are protonated, N-coordination of chloroquine to ruthenium is no longer possible and binding through the aromatic rings of the ligand will be favored. In order to obtain dicationic π-bonded "sandwich" compounds a different approach was developed. This involves the abstraction of the four chlorides in $[Ru^{II}(\eta^6\text{-}p\text{-cymene})Cl_2]_2$ by use of 4 eq of $AgBF_4$ in the presence of 2 eq of chloroquinediphosphate (CQDP) in water.

Upon chloride removal, the labile intermediate $[Ru^{II}(\eta^6\text{-}p\text{-cymene})(H_2O)_3]^{2+}$ was quickly stabilized by replacing the coordinated water molecules by CQDP, which acts as a 6-electron donor, in a π – fashion (Scheme 8). The desired compound was isolated and purified according to the procedure described in the experimental section (78% yield). Elemental analysis and NMR data (section 2.4.2 below) confirm this formulation.

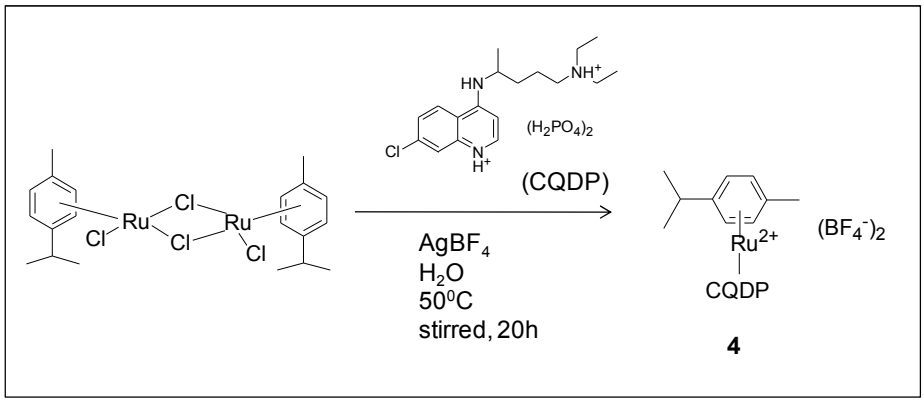

Scheme 8. Synthesis of compound **4**

The conductivity of a freshly prepared 1 mM solution of [Ru^{II} (η^6-*p*-*c*ymene)(η^6-CQDP)] $[BF_4]_2$ in de-ionized water was 522 μScm^2Mol^{-1}, a value that corresponds to five ions in solution, which supports the proposed dicationic sandwich structure **4**.

The syntheses of new arene- ruthenium-CQ complexes achieved in the first phase of the project are summarized in Scheme 9.

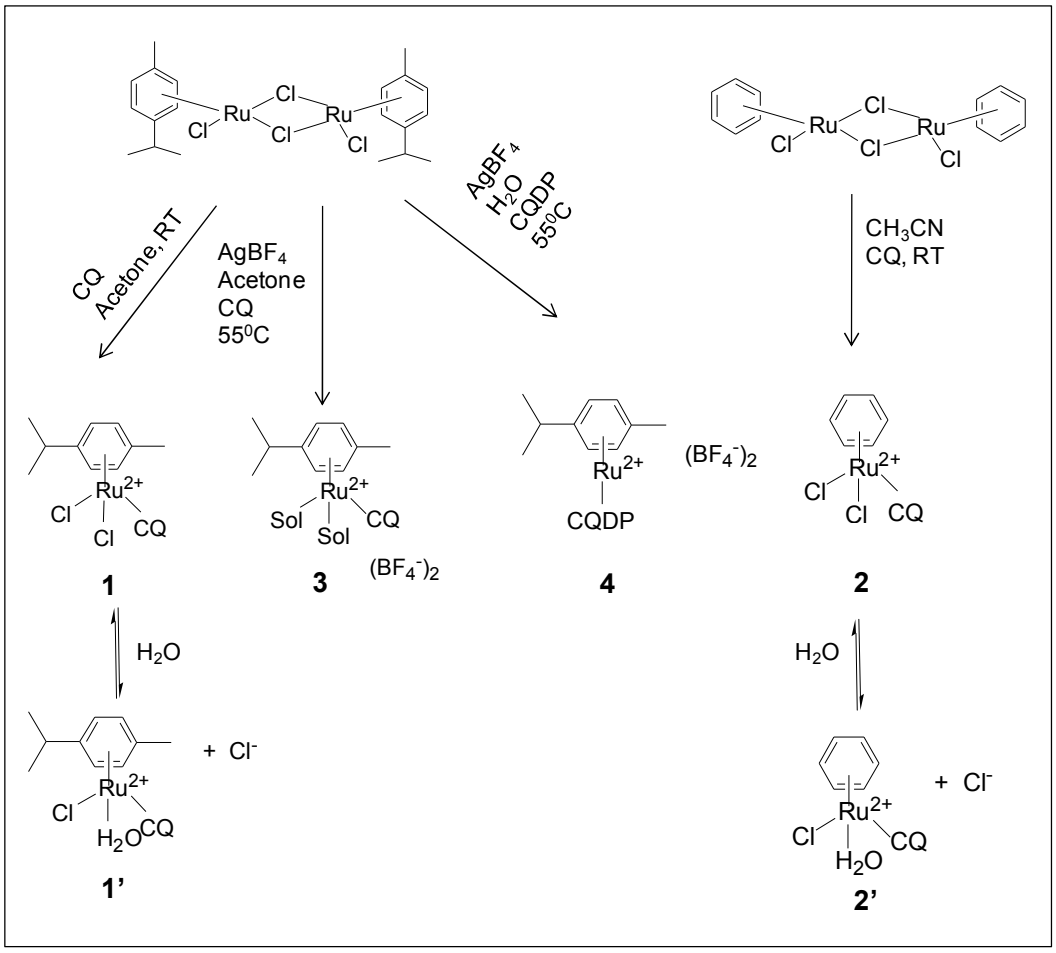

Scheme 9. Synthesis of compounds **1**, **2**, **3** and **4**

2.4.2 Spectroscopic characterization of new compounds

All complexes have been characterized by NMR spectroscopy. All resonances for free chloroquine, and for the new complexes were unequivocally identified by 1D (^{1}H and ^{13}C NMR), and 2D COSY (Correlated SpectroscopY- H/H correlation), HSQC (Heteronuclear Single Quantum Correlation - C/H correlation about 1 bond), and HMBC (Heteronuclear Multiple Bond Correlation - C/H correlation about 2-3 bonds) experiments. The integral ratios for the π-arene and chloroquine protons confirm the formulations proposed above (Scheme 9).

As an example, the characterization of compound **1** by the use of 1D and 2D NMR is described in detail as follows. The full COSY spectrum of compound **1** is shown in Figure 4.

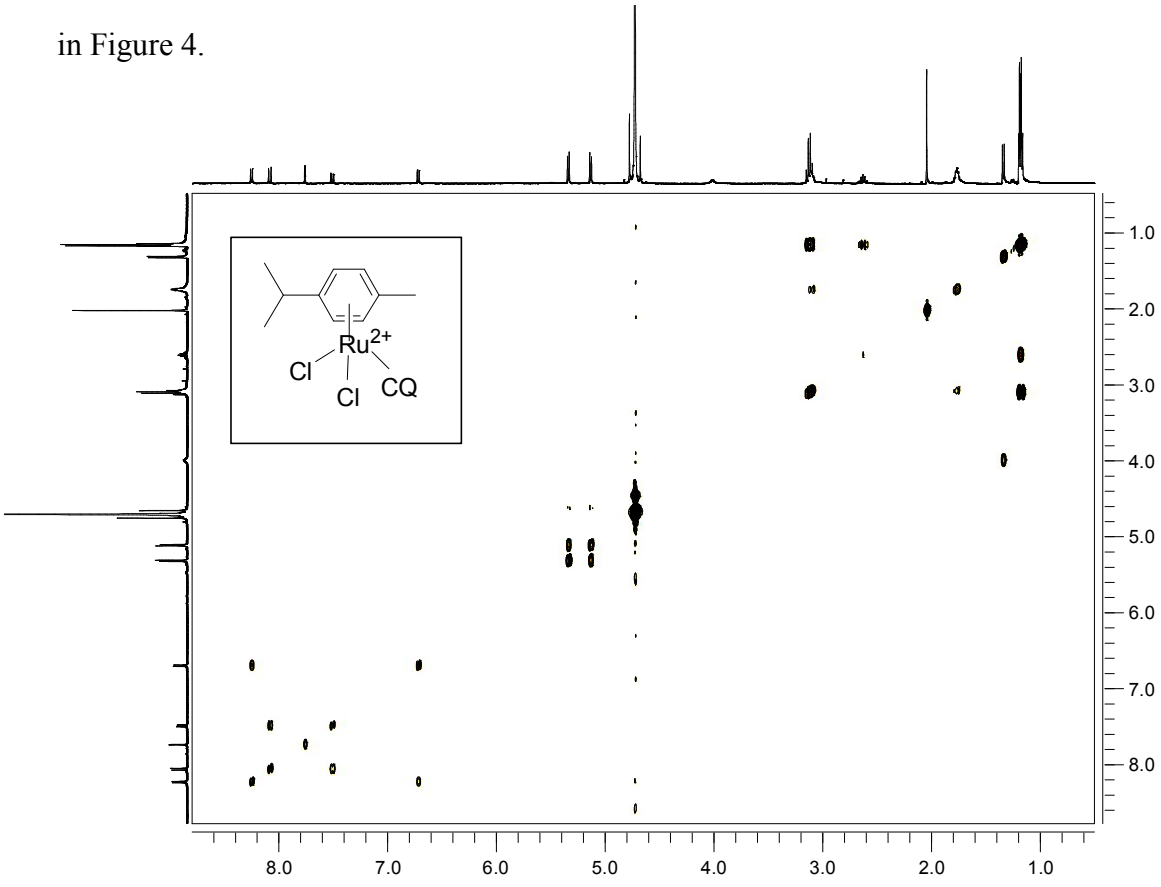

Figure 4. COSY of compound **1** in D_2O

^{1}H-^{1}H COSY is a useful method for determining which proton signals arise from neighboring protons (usually up to three bonds or occasionally four bonds away). Correlations appear when there is spin-spin coupling between two protons, but where there is no coupling, no correlation is expected to appear. The COSY spectrum shown above contains a diagonal and cross peaks. The signals of the proton spectrum appear along the diagonal whereas cross peaks indicate couplings between two neighboring proton nuclei.

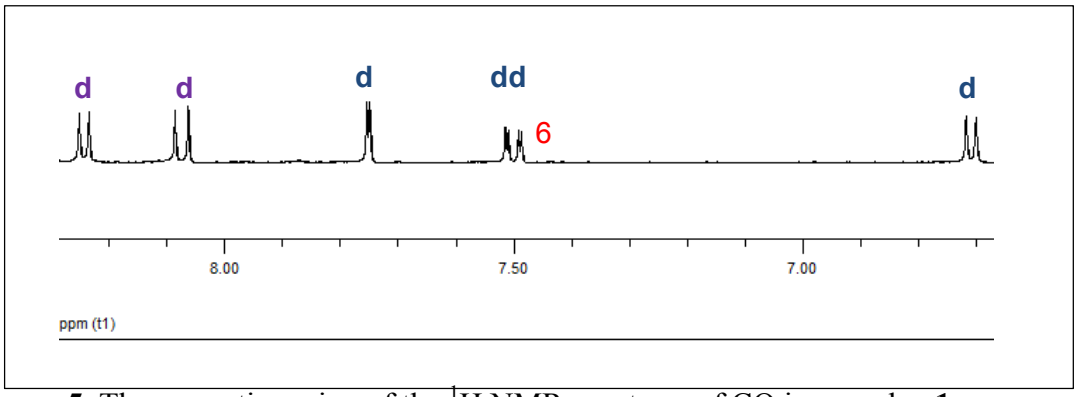

Figure 5. The aromatic region of the ^{1}H NMR spectrum of CQ in complex **1**

When we consider the prediction of proton signals in the aromatic region of CQ in complex **1**, the signal due to H6 should be a dd (it should couple with H5 and H8), hence it can be easily recognized in the proton spectrum because there is only one dd in the aromatic region of the proton spectrum. The rest of the proton signals in the aromatic region can be assigned by the COSY experiment as follows. The section of COSY spectrum, responsible for the signals of the aromatic region of CQ in complex **1** is shown in Figure 6.

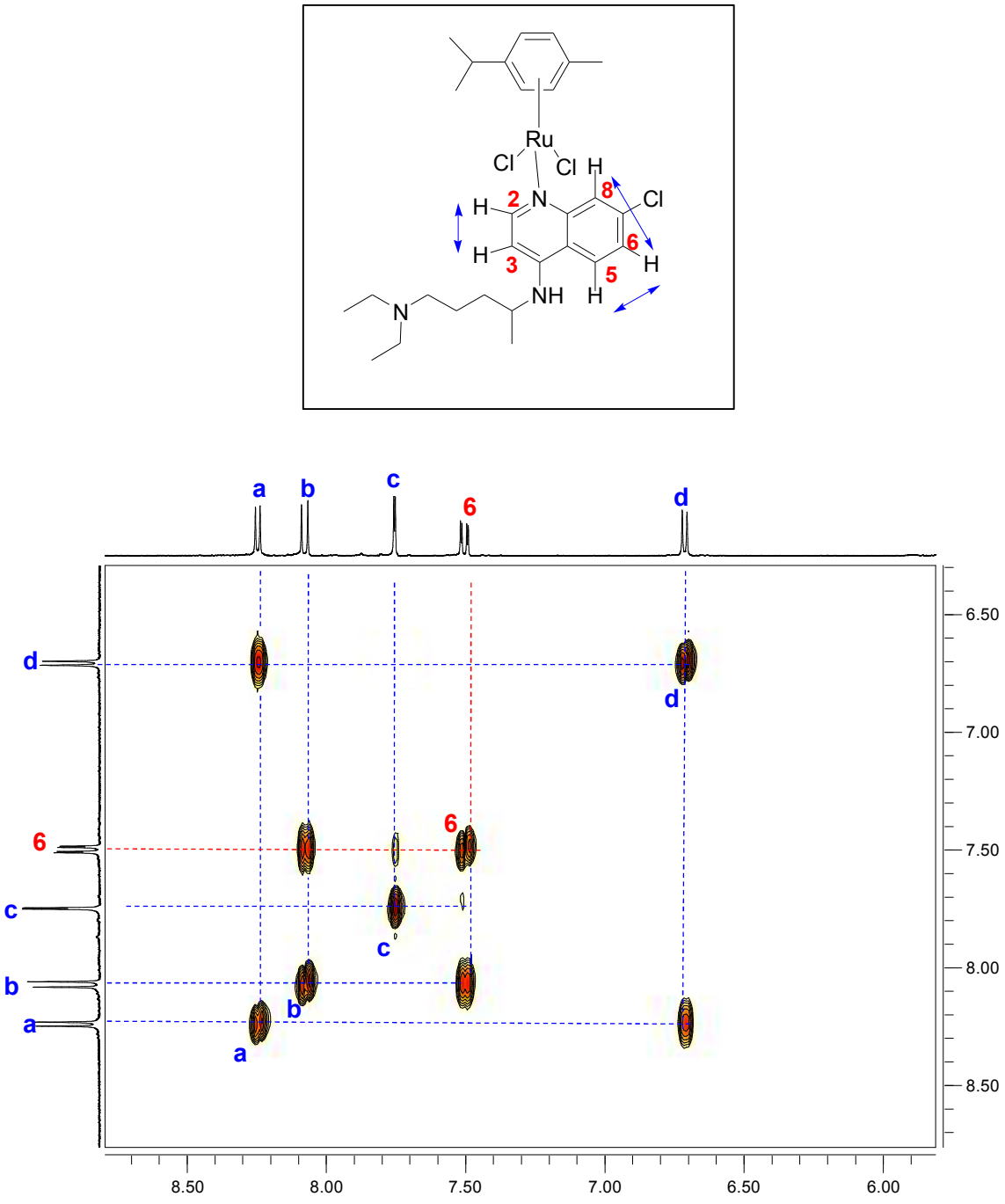

Figure 6. The COSY of the aromatic region of CQ in complex **1** in D_2O

The signal for H6 appears at 7.51 and it must correlate with H5 (3 bond correlation) and more weakly with H8 (a long range 4 bond correlation). According to the COSY, H6 correlates with two protons; **c** and **b**. It is important to keep in mind that the larger the coupling constant, the more intense are the off-diagonal contours whereas the smaller the coupling constant, the weaker the off- diagonal contours. Hence the most intense cross peak (corresponds to the coupling of **b** and H6) is assigned as H5 and the much weaker cross peak with smaller coupling constant between H6 and **c** due to long-range coupling is assigned to H8.

Peaks **a** and **d** corresponds to H2 and H3. Among H2 and H3 signals, H2 should appear more downfield, because the carbon attached to the H2 proton is connected to the electronegative N atom. Hence the most downfield signal **a** is assigned as H2 and the apparent cross-peak (corresponds to coupling between H2 and **d**) is labeled as H3. Other proton signals are also unequivocally assigned in complex **1** and the fully labeled proton NMR spectrum in D_2O is represented in Figure 7.

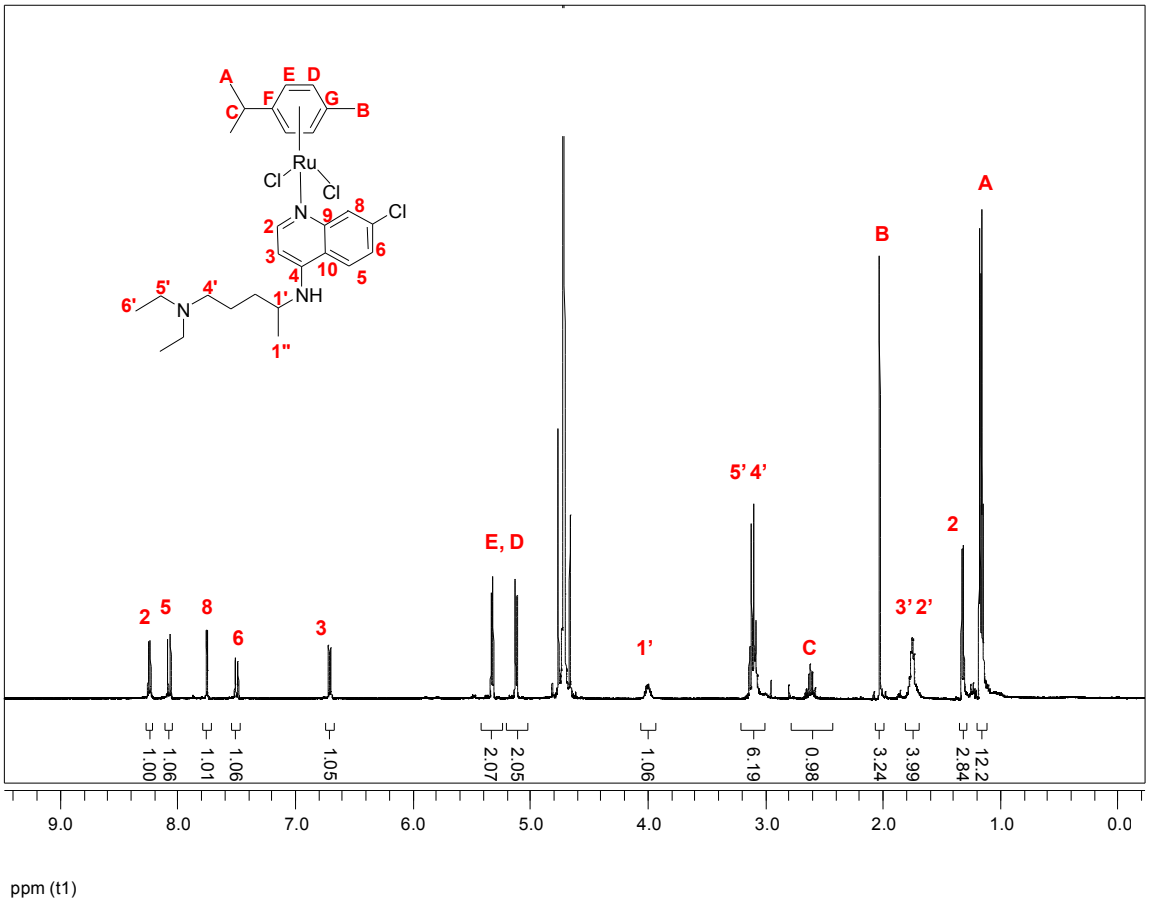

Figure 7. ^{1}H NMR of complex **1** in D_2O with signal assignment

The carbons directly attached to protons in complex **1** were predominantly assigned by the use of HSQC. Peaks occur where the chemical shift of a ^{1}H and the chemical shift of the attached ^{13}C atoms intersect. Since the proton signals of H(2), H(5), H(8), H(6), H(3), H(D), H(E), H(1'), H(5'), H(4'), H(C), H(B), H(3'), H(2'), H(1"), H(A) and H(6) were identified by the use of COSY, the corresponding carbon directly attached to these protons were easily identified from HSQC (Figure 8) as follows: **a** corresponds to C2, **b** corresponds to C6, **c** corresponds to C5, etc.

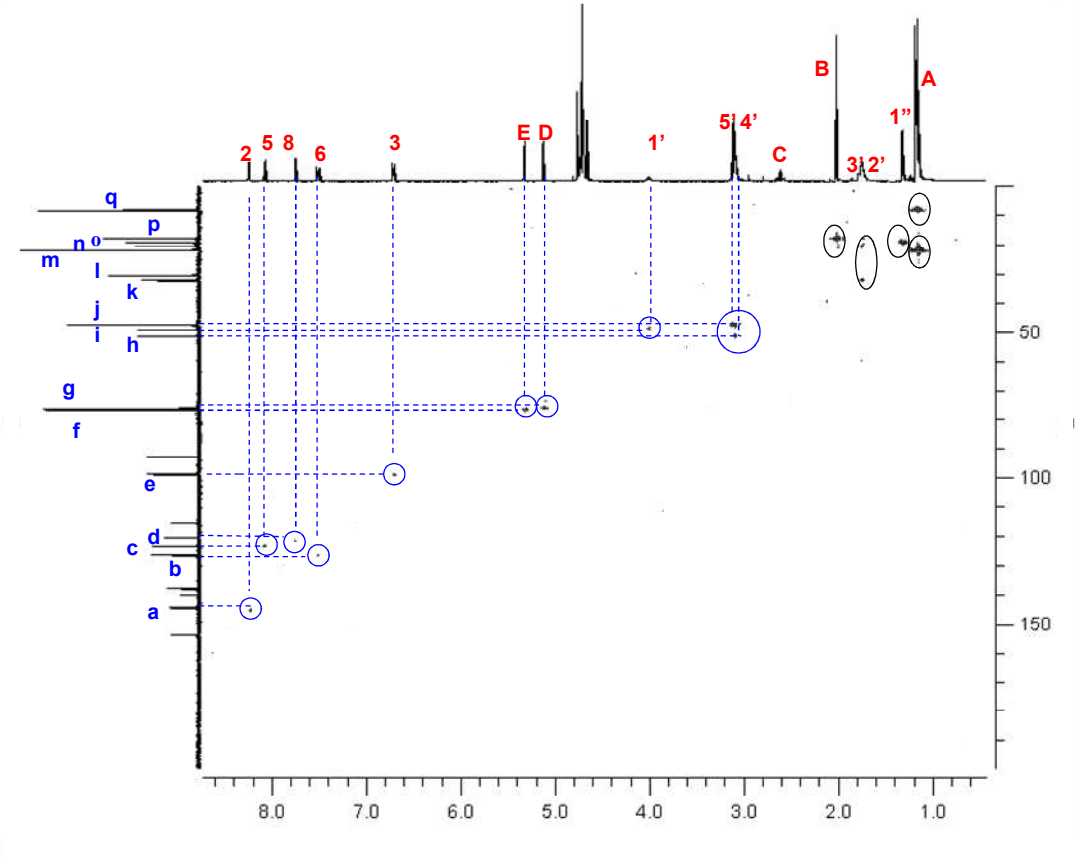

Figure 8. HSQC of complex **1** in D_2O with signal assignments for carbon directly attached to protons (primary, secondary and tertiary carbons of the complex **1**).

Quaternary carbons not attached to any protons, are not assigned using HSQC. Another NMR technique, HMBC was used to get the information about carbons that are near (but not directly bonded to) different protons (carbons which are two and three bonds away from the proton). The full HMBC spectrum of complex **1** is shown in Figure 9 and it is mainly used to identify the quaternary carbons as well as to confirm other carbon signal assignments.

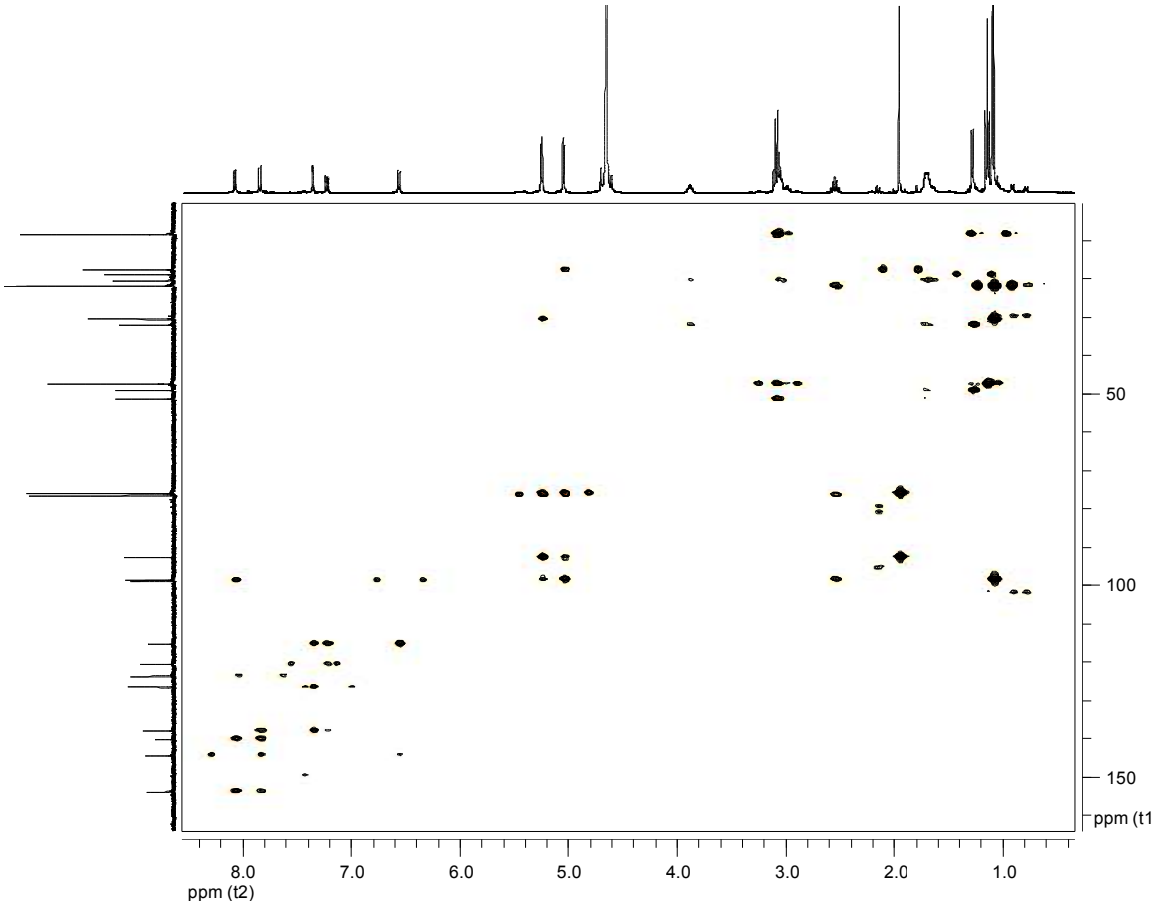

Figure 9. HMBC of complex **1** in D_2O

For simplicity, a part of the HMBC spectrum, particularly the aromatic region of CQ of complex **1** is shown in Figure 10.

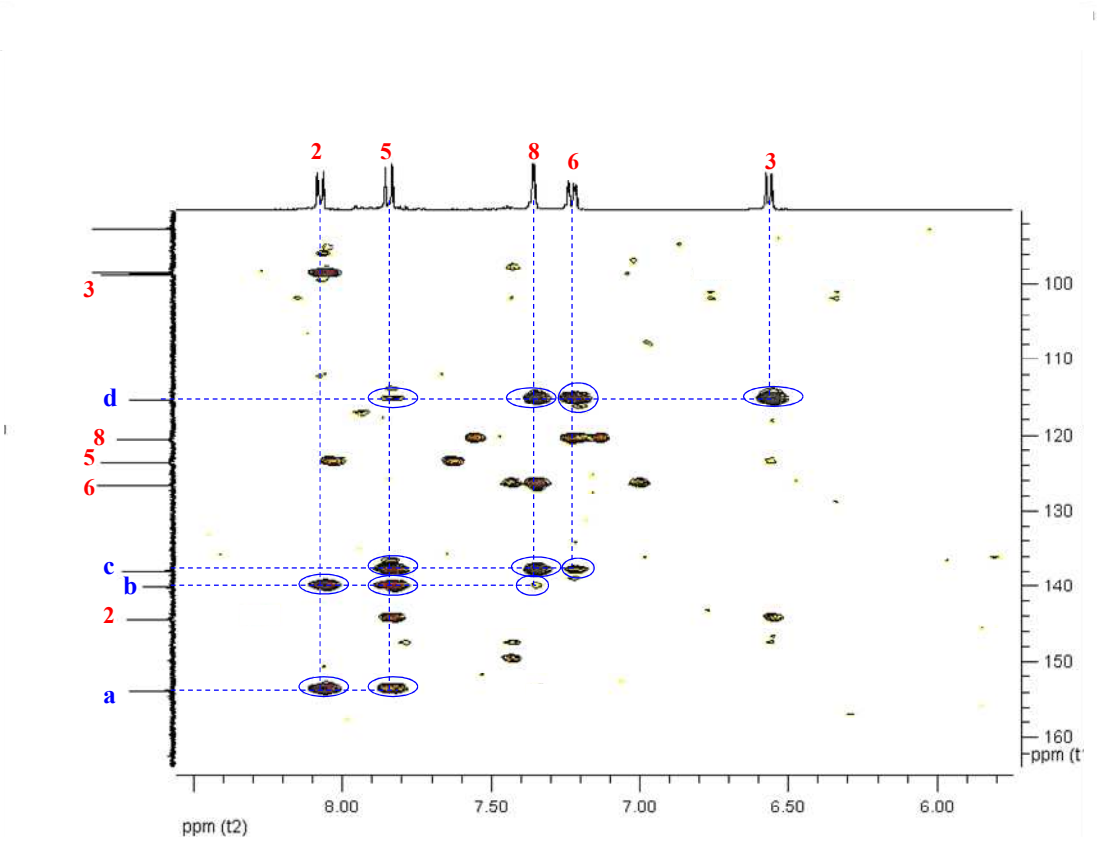

Figure 10. HMBC of the aromatic region of CQ of complex **1** in D_2O

Carbons which are directly attached to proton/protons are identified by the use of HSQC as described earlier and labeled in red. The peak labeled as **d** correlates with H5, H8, H6 and H3. This indicates that **d** is either 2 or 3 bonds away from H5, H8, H6 and H3. So **d** should correspond to C10, because this carbon is 2 bonds away from H5 and 3 bonds away from H8, H6 and H3. When considering the signal assignment of **c**, it correlates with three proton peaks; H5, H8 and H6. This indicates that the signal **c** must be C7, because H8 and H6 are situated two bonds away from C7 while H5 is situated 3 bonds away from C7.

In a similar way the other carbon nuclei **b** and **a** are identified as C9 and C4, respectively because **b** correlates with H2, H5 and H8 where as **a** does not have any correlation with H8, although it has cross peaks with H2 and H5. All other quaternary carbons of complex **1** are successfully identified using this technique and the fully labeled ^{13}C NMR spectrum of complex is shown in Figure 11.

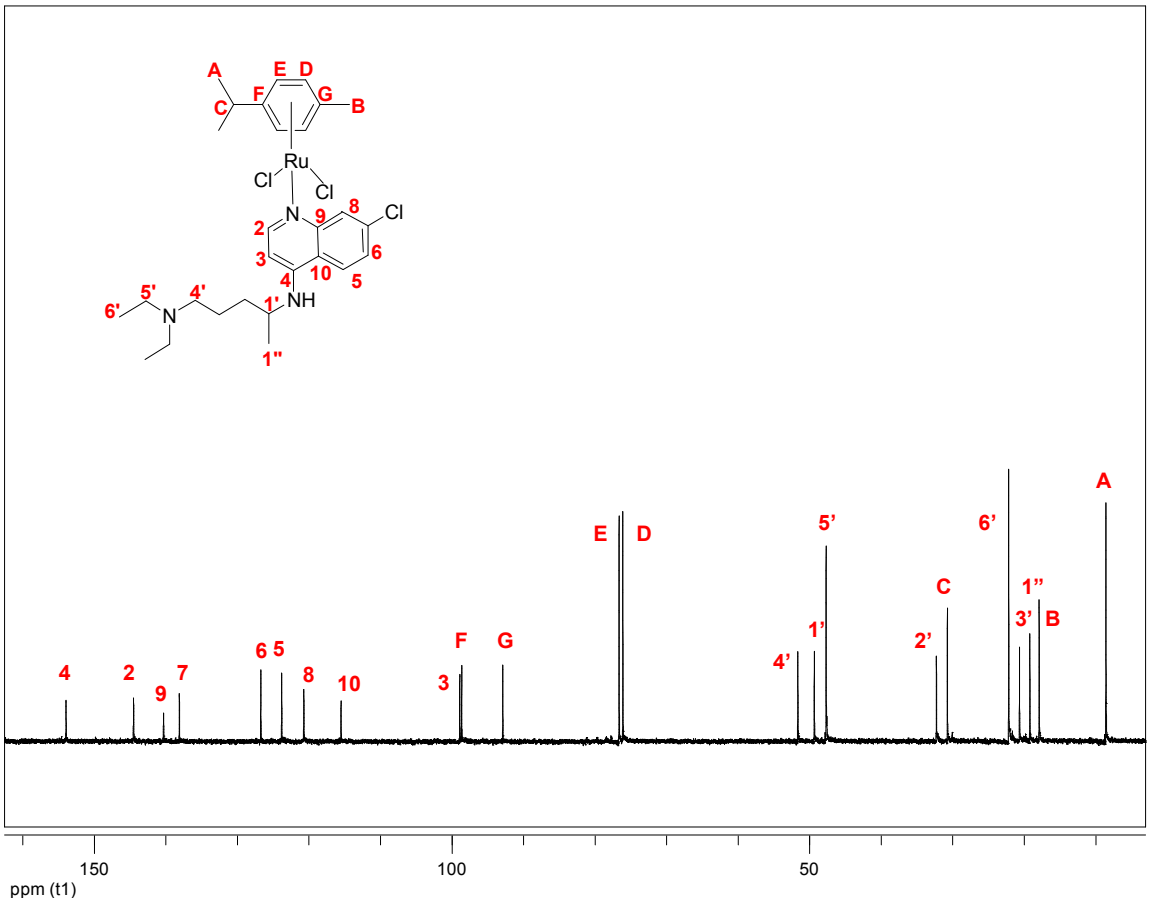

Figure 11. ^{13}C NMR of complex **1** in D_2O with signal assignment

Fully labeled spectra for all other complexes are contained in the Appendix.

2.4.3 Bonding mode of chloroquine in Ru complexes

Chloroquine has several potential sites that can accommodate the binding of a metal. The coordination mode of chloroquine is very likely to affect its physicochemical and biological properties and therefore it is important to establish the precise mode of bonding in the new Ru-CQ complexes. In particular, basicity and lipophilicity are key properties for the accumulation of the drug in the acidic food vacuole of malaria parasites; the quinoline and diethylamino nitrogen atoms are the most basic sites of this molecule and therefore they are the most likely sites for metal binding. Binding of Ru to the NH group in the side chain is unlikely due to steric hindrance at that position and reduced basicity of that nitrogen because of electron delocalization.

Scheme 10 summarizes the possible coordination modes of CQ and CQDP to Ru(η^6-arene) fragments. Examples of CQ binding to metals through the nitrogen atom of the quinoline ring (A)[26] or the one in side chain (B)[27] are known. In the case of CQDP, those two nitrogen atoms are protonated and therefore coordination to Ru must involve π-bonding to either the carbocyclic (C) or the heterocyclic (D) ring of the quinoline moiety; to our knowledge, there are no previous examples of complexes containing π-bonded CQDP ligands.

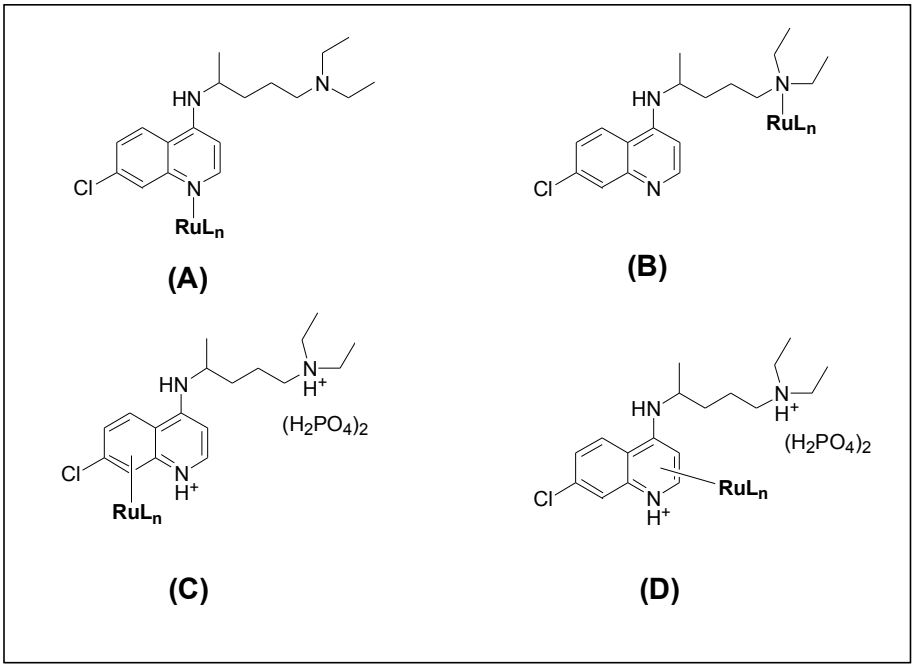

Scheme 10 – Possible coordination modes of CQ (A and B) and CQDP (C and D) to Ru(η^6-arene) fragments.

In any one of the possible binding modes, coordination to the metal will have an important effect on the basicity and lipophilicity of CQ and it clearly represents a major structural modification of the organic drug. Although the mechanisms of CQ-resistance are not entirely clear, it is generally accepted that drugs with increased lipophilicity are more efficient in overcoming resistance[28] and that the mutated protein responsible for resistance is highly structure specific.[1,29] It is, therefore, important to ascertain the coordination mode of CQ to Ru in each new complex to understand how such structural variations are reflected in different biological properties.

2.4.3.1 NMR studies

Since the new Ru-CQ complexes can only be isolated as amorphous powders, they were not amenable to X-ray diffraction studies and therefore we rely on a combination of NMR experiments and DFT calculations, together with FTIR data to determine the binding mode of CQ to Ru in our new complexes.

It was previously suggested that the largest variations in chemical shifts ($\Delta\delta$) of the chloroquine protons and carbons (with respect to those of free CQ) are generally observed for the protons/ carbons located in the vicinity of the N-atom attached to the metal[13] and this may therefore serve as a diagnostic tool for determining binding preferences of bioactive ligands. Selected NMR data ($^{1}H/^{13}C$) for complexes **1**, **2**, **3** and **4** are contained in Table 1. $\Delta\delta$ represents the displacement of each signal in the complex with respect to the corresponding one in free CQ.

Table 1. Selected NMR data for the complexes; **1** in $CDCl_3$; **2, 3** and **4** MeOD. Δδ represents the displacement of the signal in the complex with respect to the corresponding one in free CQ. Numbers in bold are the largest observed Δδ values for each complex.

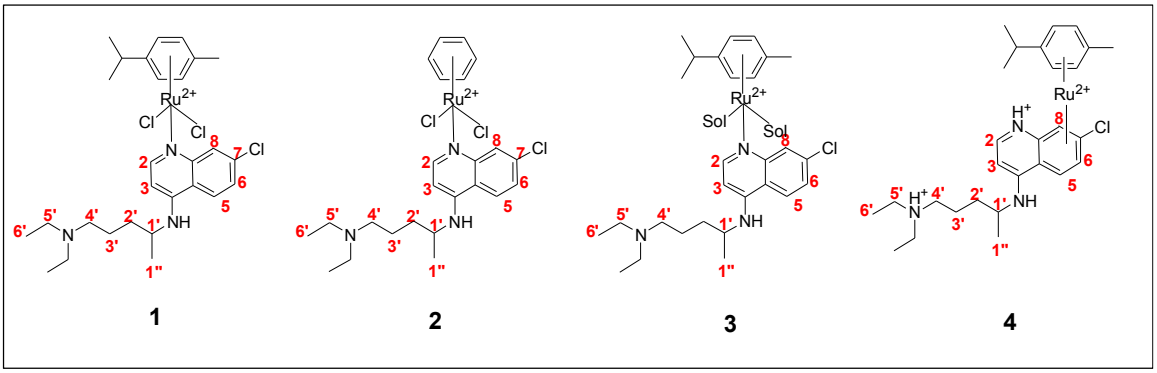

	1		**2**		**3**		**4**	
H/C	^{1}H Δδ ppm	^{13}C Δδ ppm	^{1}H Δδ Ppm	^{13}C Δδ ppm	^{1}H Δδ ppm	^{13}C Δδ ppm	^{1}H Δδ ppm	^{13}C Δδ ppm
6'	0.02	2.64	0.36	2.04	0.25	2.07	0.07	0.99
1"	0.09	1.12	0.15	0.27	0.07	0.39	0.05	0.03
2'	0.14	2.57	0.23	1.39	0.06	1.53	0.09	1.01
3'	0.07	2.43	0.35	1.92	0.22	2.09	0.09	1.09
4'	0.10	1.13	**0.75**	0.61	**0.69**	2.44	0.07	0.87
5'	0.13	0.73	**0.76**	0.58	**0.67**	0.88	0.07	1.04
1'	0.15	0.26	0.31	0.6	0.23	3.46	0.13	0.96
3	0.20	0.85	0.32	0.17	0.15	0.18	0.14	0.90
6	0.23	0.54	0.24	1.50	0.23	1.59	**0.33**	**1.34**
5	0.20	1.71	0.35	1.17	0.15	0.85	**0.32**	**1.27**
8	**0.97**	0.05	0.14	**3.77**	0.04	**3.96**	**0.42**	**1.58**
2	**0.48**	**4.26**	0.13	**4.28**	0.01	**4.45**	0.15	1.07

The complexes **1**, **2** and **3** contain CQ, whereas complex **4** contains CQDP. Since the two possible binding modes of ruthenium to CQ are the nitrogen atoms on the quinoline ring and on the side chain, it is important to investigate the proton and carbon chemical shift variation of H(2), H(8), C(2), C(8) and H(4'), H(5'), C(4') and C(5') signals of the complexes 1-3 compared to those signals of free CQ. As suggested

previously,[13] if the largest variations in chemical shifts ($\Delta\delta$) of the chloroquine protons and carbons of the metal-CQ complex (with respect to those of free CQ) are observed for the protons/ carbons located in the vicinity of the quinoline N-atom, the metal is likely bound to the nitrogen in the quinoline ring. If the largest variations in chemical shifts ($\Delta\delta$) are observed for the protons and carbons at H(4'), H(5') and C(4'), C(5') respectively, compared to those of free CQ, the binding mode of ruthenium to CQ will be likely through the tertiary N atom at the side chain.

In the case of complex **4**, the possible binding modes of ruthenium to CQDP are through the carbocyclic ring or the heterocyclic ring. Therefore, it is important to investigate the carbon and proton chemical shift variations of metal-CQDP complex (with respect to those of free CQDP) located in the carbocyclic ring and heterocyclic ring. The signals of interest are protons and carbons at positions 2 and 3 in the heterocyclic ring and those at 8, 5, and 6 in the carbocyclic ring.

The data in Table 4 show that for complex **1,** the largest shifts with respect to free CQ are observed for H(8) ($\Delta\delta$ 0.97) and H(2) ($\Delta\delta$ 0.48), located in the vicinity of the quinoline N atom. On the other hand, for the protons in the vicinity of the side chain N atom, the $\Delta\delta$ values H(4')($\Delta\delta$ 0.10) and H(5') ($\Delta\delta$ 0.13) are much lower. Similarly, C(2) experienced a larger shift ($\Delta\delta$ 4.26) than C(4') ($\Delta\delta$ 1.13) and C(5') ($\Delta\delta$ 0.73). These data indicate that CQ binds to Ru in complex **1** through the N atom of the quinoline ring (A), and not through the N atom on the side chain (B).

When considering the selected NMR data for complex **2,** the largest shifts with respect to free CQ are observed for H(4') ($\Delta\delta$ 0.75) and H(5') ($\Delta\delta$ 0.76), located in the vicinity of the diethylamino group and not for H(2)($\Delta\delta$ 0.13) and H(8) ($\Delta\delta$ 0.14) as in

complex **1**. In contrast, C(2) (Δδ 4.28) and C(8) (Δδ 3.77) experienced a larger shift than C(4') (Δδ 0.61)and C(5') (Δδ 0.58). This indicates that according to the ^{13}C NMR data, CQ seems to bind to Ru through the unsubstituted N(1) atom on the quinoline ring but according to the ^{1}H NMR data CQ could be binding to Ru through the tertiary N in the side chain. Similarly, the results observed for complex **3** lead to ambiguities in the assignment of the coordination site.

For complex **4** the largest shifts with respect to CQDP are observed for H(8) (Δδ 0.42), H(5) (Δδ 0.32), and H(6) (Δδ 0.33), located at the carbocyclic ring. Consistent with the proton data, C(8) (Δδ 01.58), C(5) (Δδ 1.27) and C(6) (Δδ 1.34) experienced a somewhat larger shift than the carbon atoms in the heterocyclic ring C(2) (Δδ 1.07) and C(3) (Δδ 0.90). This indicates that CQDP binds to Ru through the carbocyclic ring(C) and not through the heterocyclic ring (D).

Although both carbon and proton spectra provided consistent results for complexes **1** and **4,** some inconsistencies have been observed in the corresponding spectra for complexes **2** and **3**. This may probably be arising due to the protonation of side chain N, in a polar solvent like MeOD, which would also cause variations in the chemical shifts. These observations suggest that variations in chemical shifts alone may lead to ambiguities. Further NMR experiments were needed in order to get a clear idea about the binding mode of CQ to Ru in our new complexes. .

2.4.3.2 Proton relaxation studies

T_1 relaxation measures the rate at which the spin system comes into thermal equilibrium with the other degrees of freedom and it involves interactions of the nucleus being observed with its immediate surroundings,[30] therefore, T_1 magnitudes are very

sensitive to electronic and structural perturbations, such as the one caused by coordination of an organometallic fragment to the molecule under study. A particularly marked variation in T_1 values with respect to the free ligand (ΔT_1) is thus expected for protons located in the vicinity of the Ru-N bond. Selected proton relaxation time measurements (T_1) for the complexes **1**, **2**, **3** and **4** are contained in Table 2.

Table 2. Selected proton relaxation time measurements (T_1) for the complexes **1** in $CDCl_3$ and **2**, **3** and **4** in MeOD. ΔT_1 represents the variation of the proton relaxation time of CQ/CQDP in the complexes with respect to the corresponding one in free CQ/CQDP. (Numbers in bold are the largest ΔT_1 values observed for each complex)

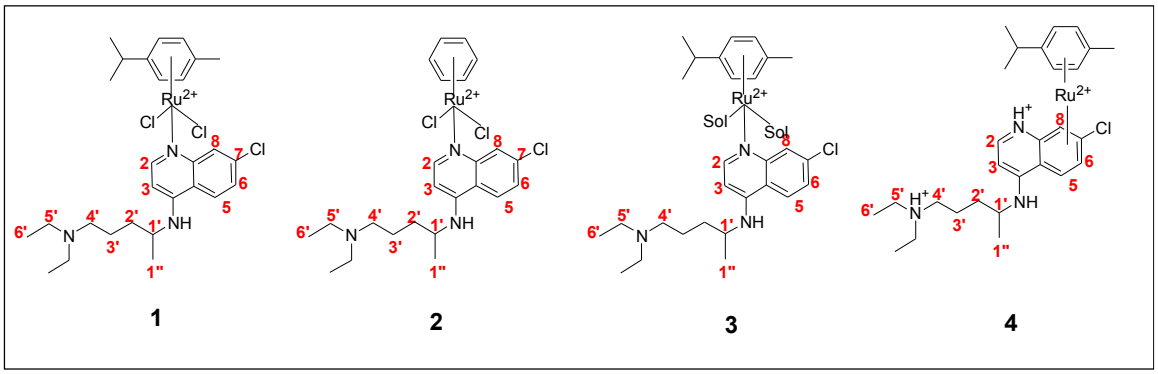

	1	2	3	4
H	ΔT_1 ms	ΔT_1 ms	ΔT_1 ms	ΔT_1 ms
6'	0.448	0.093	0.338	0.273
1"	0.322	0.019	0.091	0.035
2'	0.324	0.019	0.092	0.011
3'	0.324	0.019	0.092	0.011
4'	0.391	0.012	0.154	0.127
5'	0.381	0.012	0.154	0.127
3	0.668	0.012	0.137	0.001
6	1.321	0.105	0.722	**0.382**
5	0.348	0.380	0.876	**0.401**
8	**3.672**	**1.985**	**3.712**	**1.249**
2	**1.586**	**0.478**	**1.352**	**0.492**

These data show that the largest T_1 variations with respect to free CQ for complex **1** are observed for H(8) (ΔT_1, 3.672) and H(2) (ΔT_1, 1.586), located in the vicinity of N(1) (quinoline N), consistent with the results we obtained from ^1H and ^{13}C NMR. This supports the proposal that coordination occurs at the quinoline nitrogen site (A). More importantly, as pointed out above, when we studied the proton and carbon NMR chemical shift variations ($\Delta\delta$), for complexes **2** and **3,** some ambiguities were observed.

However, the largest T_1 variation with respect to free CQ was observed for proton H(2) (ΔT_1, 0.478 for complex **2** and ΔT_1, 1.352 for complex **3**) and H8 (ΔT_1, 1.985 for complex **2** and ΔT_1, 3.712 for complex **3**). These data agree in both cases with Ru being bound to CQ through the quinoline ring N, which is consistent with the results obtained from ^{13}C NMR.

Also, when we consider the ΔT_1 data for complex **4**, the largest T_1 variation with respect to CQDP are observed for H(8) (ΔT_1, 1.249), H(2) (ΔT_1, 0.492.), H(5) (ΔT_1, 0.402), and H(6) (ΔT_1, 0.382) located in the carbocyclic ring, which is consistent with the results we obtained from ^1H and ^{13}C NMR . Thus T_1 data further supports that the binding mode of CQDP to Ru is through the carbocyclic ring (C).

In conclusion, the set of NMR experiments performed shows that ΔT_1 measurements and to a lesser extent, ^{13}C $\Delta\delta$ values, provide a much better means than ^1H $\Delta\delta$ values for assigning the coordination site of a ligand with multiple possible binding modes. T_1 measurements are thus a very valuable technique for structural assignment in those cases where X-ray structures are not available. Based on the experimental data presented so far, the structures proposed for the new complexes are summarized in Scheme 11.

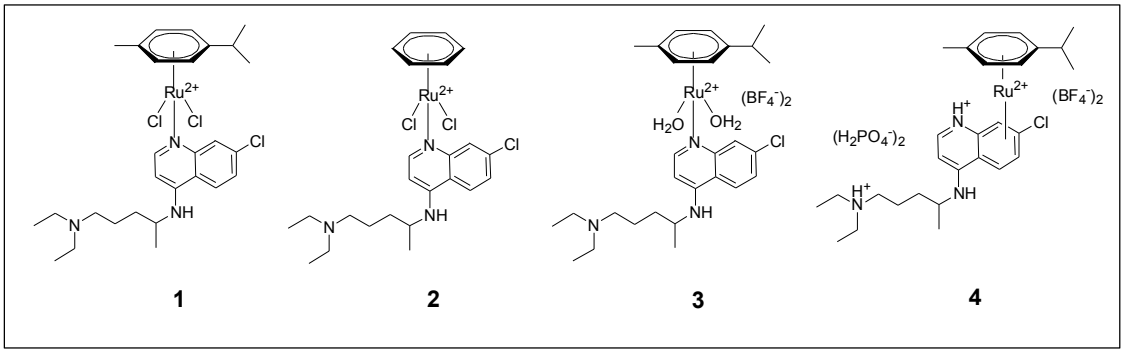

Scheme 11. The structures proposed for the new complexes

2.4.3.3 Computational studies

Further evidence in support of our structural proposals was obtained from DFT calculations on total energies of the different possible coordination isomers of our complexes, to see which structures are thermodynamically favored. The main points of interest are:

(i) Whether chloroquine binds to ruthenium through the nitrogen atom of the quinoline (A) or of the diethylamino group in the side chain (B).

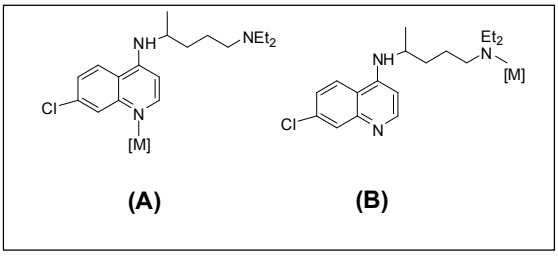

(ii) Whether π-bonding of chloroquine diphosphate to ruthenium through the aromatic rings is energetically reasonable and, if so, which of the two rings should be favored?

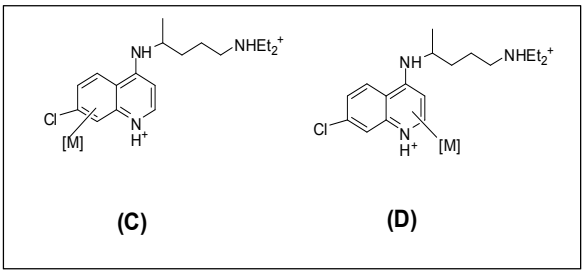

2.4.3.3.1 Energy Calculations

The structures of complexes **1**-**3** in both isomeric forms (A) and (B), and of **4** in isomeric forms (C) and (D) were fully optimized in the gas phase (optimized structures and total energies for all the complexes can be found in the Appendix). While gas phase predictions are appropriate for many purposes, they are inadequate for describing the characteristics of the molecules in solution. Indeed properties of molecules can differ considerably between the gas phase and solution phase. Moreover, since the Ru-CQ complexes need to be dissolved in water for biological testing, we have also carried out the energy calculations using water as a solvent in order to compare their stability in aqueous medium. The Self-Consistent Reaction Field (SCRF) method and Tomasi's Polarized Continuum Model (PCM) were used to simulate the aqueous environment and to assess the relative energies of these structures in aqueous solution.

$[Ru^{II}(\eta^6\text{-}p\text{-cymene})Cl(H_2O)(CQ)]^+$ (1')

Figure 12 shows the optimized structures for **1'** in its two isomeric forms (A) and (B)

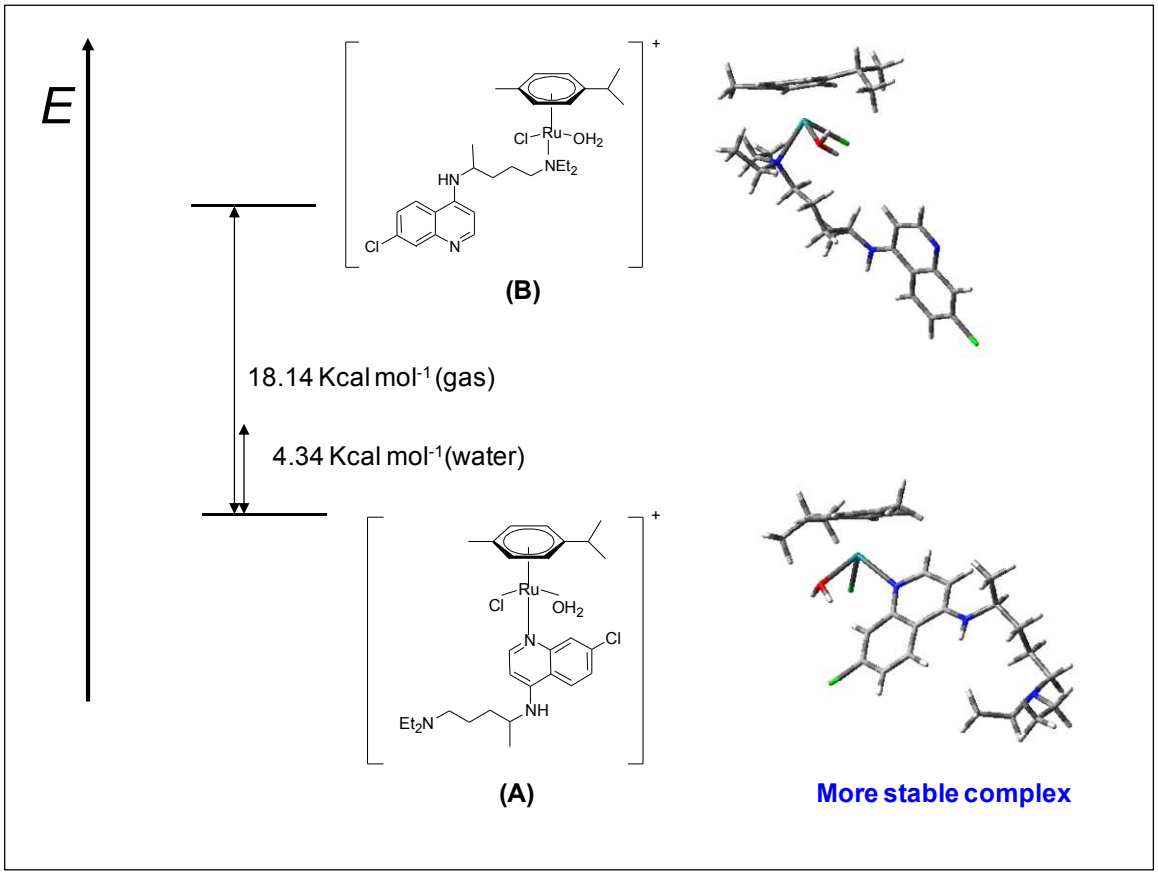

Figure 12. Optimized structures and the energy differences between isomeric forms of complex $[Ru^{II}(\eta^6\text{-}p\text{-cymene})Cl(H_2O)(CQ)]^+$ **(1')** both in the gas phase and in water

According to the calculated energy values for the possible structures of the complex $[Ru^{II}(\eta^6\text{-}p\text{-cymene})Cl(H_2O)(CQ)]^+$, structure (A) having the quinoline nitrogen atom as the binding site for Ru is 18.14 kcal/mol more stable in the gas phase than structure (B), having the side chain nitrogen as the binding site for Ru. Structure (A) is also 4.34 kcal/mol more stable in water than structure (B). The reduction in energy difference between two complexes in water may be due to the stabilization of both complexes by solvation.

$[Ru^{II}(\eta^6\text{-benzene})Cl(H_2O)(CQ)]^+$ (2')

Figure 13 shows the optimized structures for **2'** in its two isomeric forms (A) and (B)

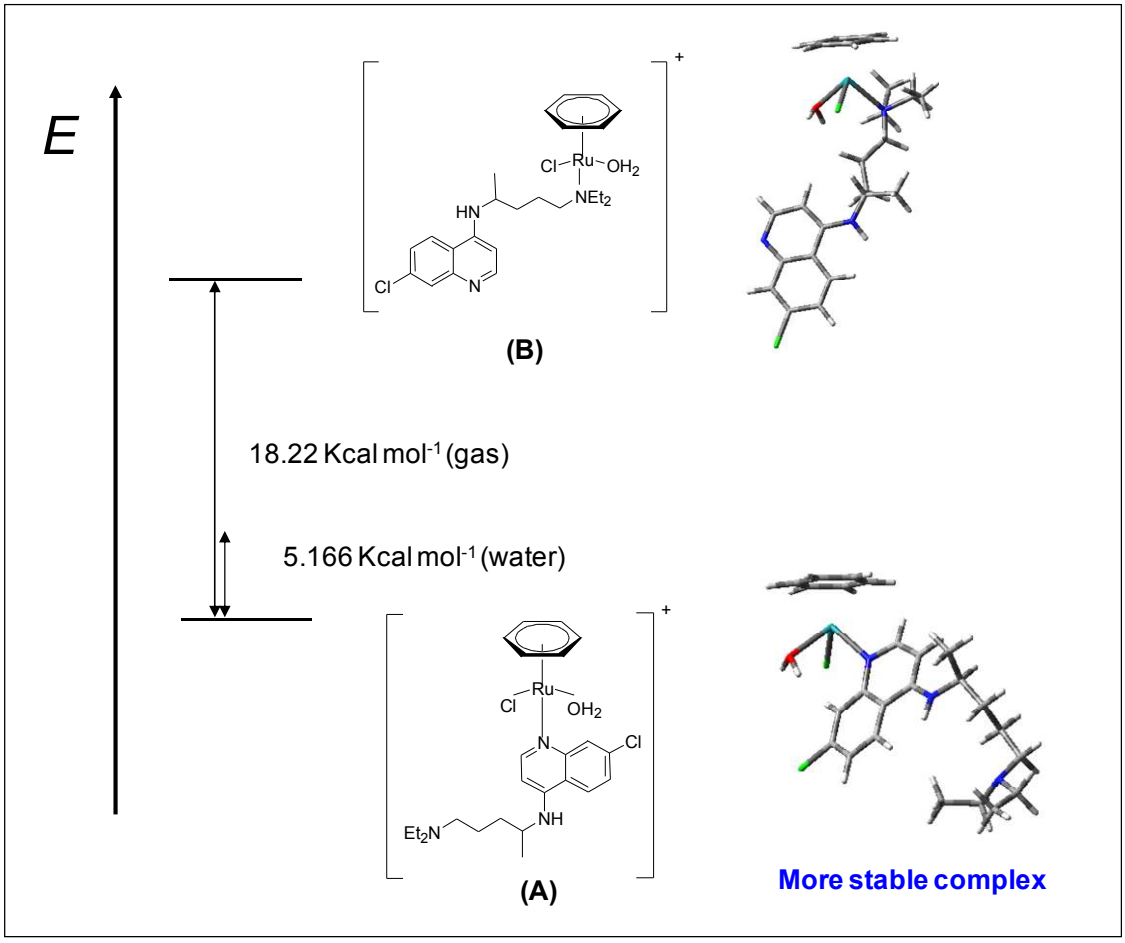

Figure 13. Optimized structures and the energy differences between isomeric forms of complex $[Ru^{II}(\eta^6\text{-benzene})Cl(H_2O)(CQ)]^+$ **(2')** both in the gas phase and in water.

For the benzene analog, the energy differences between the two possible complexes clearly show that structure (A) having the quinoline nitrogen atom as the binding site for Ru is energetically more stable both in the gas phase and in solution, as compared to structure (B) having the side chain nitrogen atom as the binding site for Ru.

$[Ru^{II}(\eta^6\text{-}p\text{-cymene})\ (H_2O)_2(CQ)]^{+2}$ (3)

The two possible structures for complex **3**, (A and B) are shown in Figure 14.

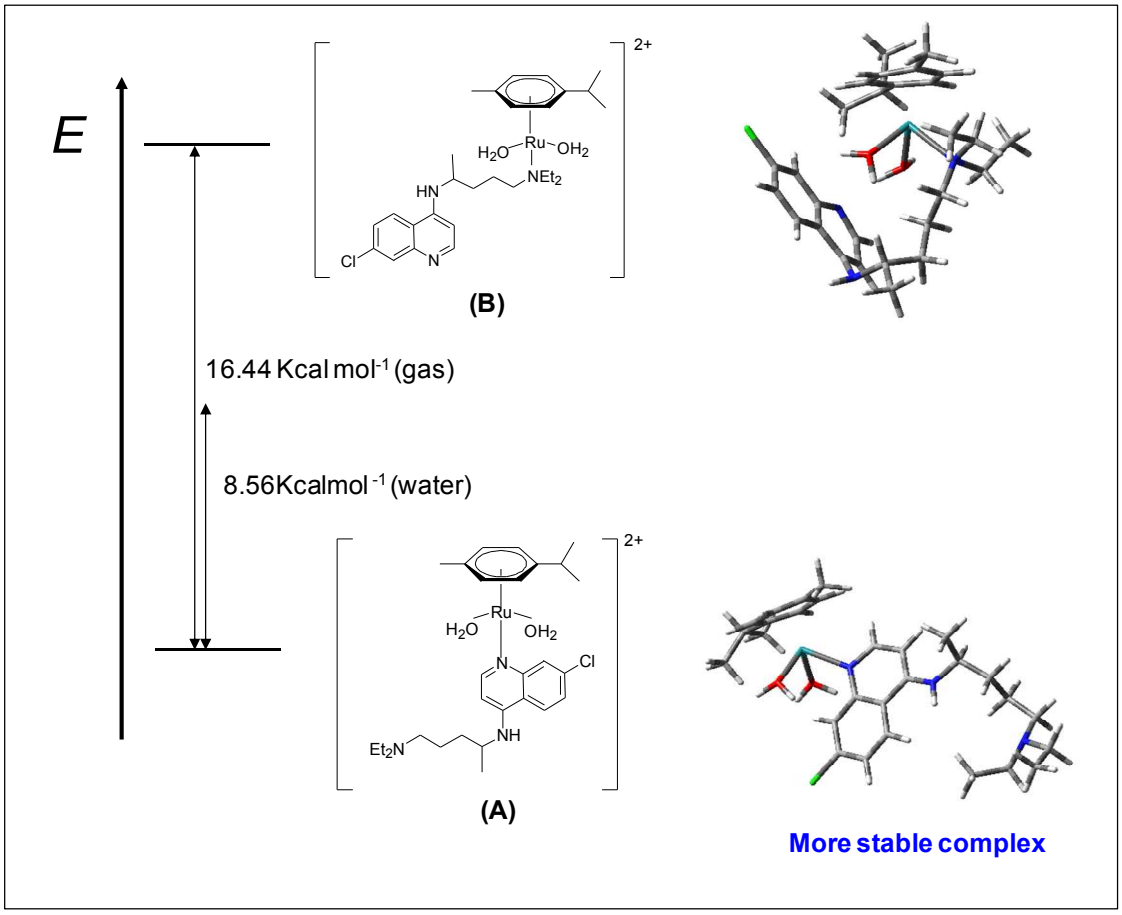

Figure 14. Optimized structures and the energy differences between isomeric forms of complex $[Ru^{II}(\eta^6\text{- }p\text{-cymene})(H_2O)_2(CQ)]^{+2}$ **(3)** both in the gas phase and in water.

According to the energy differences obtained from the calculations for the two possible structures of the dicationic complex $[Ru^{II}(\eta^6\text{-}p\text{-cymene})(H_2O)_2(CQ)]^{+2}$, the energetically most stable structure is again (A) having the quinoline nitrogen atom as the binding site to Ru, with respect to the other possibility (B).

In conclusion, these DFT energy calculations consistently indicate that the preferred mode of coordination of chloroquine to ruthenium in complexes **1'**, **2'** and **3** is

through the quinoline nitrogen atom, both in the gas phase and in aqueous solution. This is in good agreement with our conclusions based on NMR data, providing a higher level of confidence on our structural assignments.

$[Ru^{II}\ (\eta^6\text{-}p\text{-cymene})\ (\eta^6\text{-CQDP})]^{+2}$ (4)

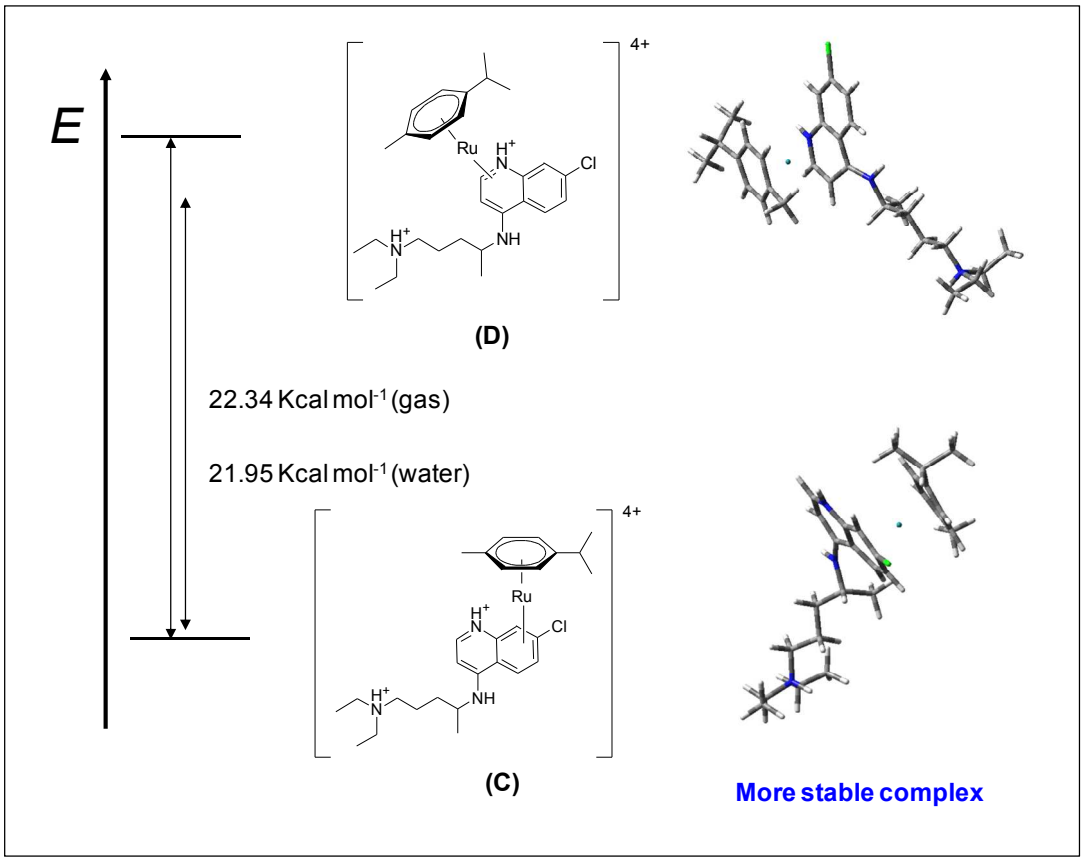

Figure 15. Optimized structures and the energy differences between isomeric forms of complex $[Ru^{II}(\eta^6\text{-}p\text{-cymene})\ (\eta^6\text{-CQDP})]^{+2}$ **(4)** both in the gas phase and in water.

In the case of the 'sandwich' compound $[Ru^{II}(\eta^6\text{-}p\text{-cymene})(\ \eta^6\text{-CQDP})]^{+2}$ (**4**), the most stable structure is found when Ru binds through the carbocyclic ring (C) rather than the heterocyclic ring (D) of cloroquine diphosphate. This may be due to the relative electron deficiency of the heterocyclic ring compared to the carbocyclic ring. The results of these calculations are also in good agreement with NMR data.

Table 3 summarizes the relative energies (in kcal/mol) of the two possible CQ-binding modes for each complex in the gas phase and in aqueous solution.

Table 3. calculated ΔE values for the complexes at the B3LYP level of theory.

Complex	ΔE in gas phase (kcal/mol)	ΔE in water (kcal/mol)
$[Ru^{II}(\eta^6\text{-}p\text{-cymene})Cl(H_2O)(CQ)]^+$	-18.14	-4.34
$[Ru^{II}(\eta^6\text{-benzene})Cl(H_2O)(CQ)]^+$	-18.22	-5.66
$[Ru^{II}(\eta^6\text{-}p\text{-cymene})((H_2O)_2(CQ)]^{+2}$	-16.44	-8.56
$[Ru^{II}(\eta^6\text{-}p\text{-cymene})(\eta^6\text{-CQDP})]^{+2}$	-22.34	-21.95

For the first three complexes, ΔE = Energy of the optimized structure having Ru to quinoline N as a binding mode – energy of the optimized structure with Ru-side chain N as a binding mode. For the last compound, $[Ru^{II}(\eta^6\text{-}p\text{-cymene})(\eta^6\text{-CQDP})]^{+2}$, ΔE = Energy of the complex having π-bonding of CQDP to Ru through the carbocyclic ring - Energy of the complex having π-bonding of CQDP to Ru through the heterocyclic ring.

2.4.3.3.2 IR simulations

One further piece of evidence that was obtained from DFT calculations is the prediction of IR spectral data for the various possible structures under consideration, which may be, in turn, compared with experimental spectra.

In order to simulate the corresponding IR spectrum using Density Functional Theory (DFT) with the standard B3LYP/6-31G* method and basis set combinations frequency calculations were carried out in the gas phase for the possible isomers of each compounds. In each case the focus was on the FTIR spectra measured in the 1500-1700cm^{-1} region, in comparison with the simulated IR spectra for the two possible structures of each complex.

$[Ru^{II}(\eta^6\text{-}p\text{-cymene})Cl_2(CQ)]$ (1)

The FTIR spectral signature of **1** measured in the 1500-1700 cm^{-1} region, compared with computed IR spectra for both isomers **1**(A) and **1**(B) are shown in Figure 16. Experimental and computed frequencies, their relative IR intensities, and vibrational assignments based on the normal-mode analysis of computed harmonic force field are listed in Table 4.

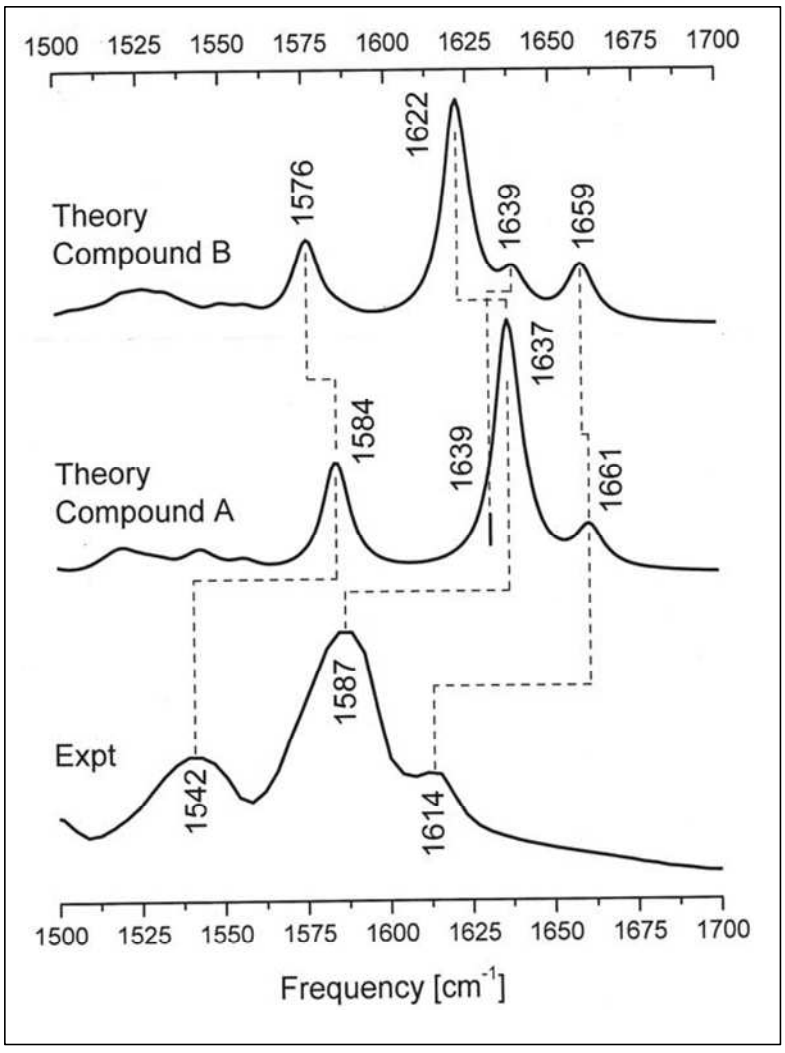

Figure 16. IR spectra for **1**. Spectra (A) and (B) are DFT simulated for the two isomers of **1**. The bottom spectrum is an experimental measurement.

Table 4. Experimental and calculated frequencies (cm^{-1}) and relative intensities (%) of IR bands for model compounds for complex **1.**

1 (exptl)	Isomer **1(A)** (calcd)	Isomer **1(B)** (calcd)	Assignment
1542 (m)	1584 (44%)	1576 (37%)	NH rock
	1631 (1%)	1639 (18%)	NH rock + C=N strech (N-ring)
1587 (s)	1637 (100%)	1622 (100%)	C=C stretch + C-H bend (N-ring)
1614 (m)	1661 (16%)	1659 (25%)	C=C stretch + CH bend (C-ring)

Computed spectra are systematically up shifted compared to experimental signals by about 3% (40-50 cm^{-1}), which is generally expected for computed vibrational bands because they are subject to systematic errors due to basis set truncation, incomplete treatment of electron correlation, and a harmonic approximation. The errors are commonly corrected by applying empirical or semi-empirical scaling factors; nevertheless, even without scaling of computed frequencies, definite assignments of experimental bands are easily achieved in this case.

The most intense band in the region measured at 1587 cm^{-1} is assigned to quinoline ring deformation with C=C stretch and C-H bending mostly localized on the heterocyclic ring and is computed at 1637 cm^{-1} for isomer (A) and at 1622 cm^{-1} for isomer (B). The other two bands observed in the region are assigned to an NH rock (at 1542 cm^{-1}) and another quinoline ring deformation involving C=C stretch and C-H bending, localized on the carbocyclic ring (at 1614 cm^{-1}). These two bands are also successfully predicted for both isomers of **1**.

The band predicted by DFT calculations at 1631 cm^{-1} for isomer (A) and at 1639 cm^{-1} for isomer (B), is of particular interest for our discussion of spectral assignment and isomer recognition. The band is assigned to an NH rock mixed with the C=C stretch of

the quinoline ring and is predicted to be moderately IR intense and detectable only for isomer (B) while down shifted by about 8 cm^{-1} and with virtually undetectable intensity for isomer (A). Thus, the IR spectra of **1** supported by computational analysis, and assignments of vibrational bands are suggestive again that isomer (A), in which CQ binds to Ru through the nitrogen atom of the quinoline moiety, is the most favorable form of the complex.

$[Ru^{II}(\eta^6\text{-benzene})Cl_2(CQ)]$ (2)

IR bands were analyzed in a similar way as described in the previous example in order to ascertain the binding mode of CQ to Ru in the complex $[Ru^{II}(\eta^6\text{-benzene})Cl_2(CQ)]$ **(2)**. The selected experimental and computed frequencies, their relative IR intensities, and vibrational assignments are listed in Table 5. The most intense band in the region measured at 1587 cm^{-1} is computed at 1639 cm^{-1} for isomer (A) and at 1622 cm^{-1} for isomer (B). In addition to the band at 1587 cm^{-1} there are two other prominent bands at 1545 $cm^{-1}$and 1612 cm^{-1} which are responsible for NH rock and quinoline ring deformation involving C=C stretch and C-H bending respectively. These two characteristics bands predicted for isomer A at 1586 cm^{-1} and 1662 cm^{-1} of compound **2** and those for isomer (B) at 1576 cm^{-1} and 1659 cm^{-1} respectively. A band at 1639 cm^{-1} which is assigned to an NH rock mixed with the *C*=C stretch of the quinoline ring was only detectable for isomer (B) while down shifted by about 7 cm^{-1} and with undetectable intensity for isomer (A). This may be due to the restriction of vibration of atoms in the quinoline ring when Ru is bound to quinoline N. This strongly suggests that the binding mode of CQ to Ru in complex $[Ru^{II}(\eta^6\text{-benzene})Cl_2(CQ)]$ **(2)** is through the

quinoline ring nitrogen and not through the side chain nitrogen, in agreement with our energy calculations and NMR data.

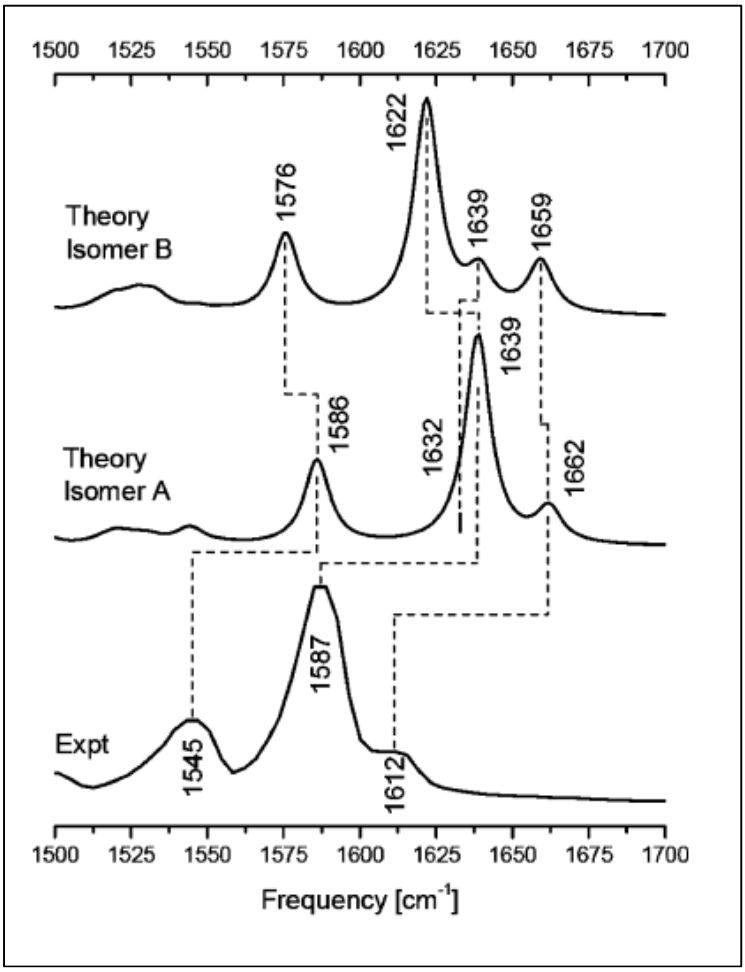

Figure 17. IR spectra for **2**. Spectra (A) and (B) are DFT simulated for the two isomers of complex **2**. The bottom spectrum is an experimental measurement.

Table 5. Experimental and calculated frequencies (cm^{-1}) and relative intensities (%) of IR bands for model compounds for complex **2.**

2 (exptl)	Isomer **2(A)** (calcd)	Isomer **2(B)** (calcd)	Assignment
1545 (m)	1586 (41%)	1576 (38%)	NH rock
	1632 (1%)	1639 (18%)	NH rock + C=N strech (N-ring)
1587 (s)	1639 (100%)	1622 (100%)	C=C stretch + C-H bend (N-ring)
1612 (m)	1662 (16%)	1659 (24%)	C=C stretch + CH bend (C-ring)

$[Ru^{II}(\eta^6\text{-}p\text{-cymene})(H_2O)_2(CQ)]^{+2}$(3) and

$[Ru^{II}(\eta^6\text{-}p\text{-ymene})(CQDP)]^{+2}$ (4)

Similar studies were attempted for compounds **3** and **4** but these cases proved to be much more complex and a clear analysis could not be achieved. Full IR spectra for all complexes are contained in Appendix.

It is important to note that although each of the individual techniques used in this study may leave some ambiguities in the assignment of a bonding mode for some of the complexes, perusal of the combined experimental and theoretical data at hand leads to a very coherent picture that allows us to confidently propose the structures depicted in Scheme 12 for the new Ru-CQ complexes.

For 16 electron $Ru(\eta^6\text{-arene})X_2$ fragments, CQ coordination through the quinoline ring nitrogen atom is preferred, whereas the highly unsaturated $Ru(\eta^6\text{-arene})$ moiety, 12 electron fragment, binds to CQ through an η^6-interaction at the carbocyclic ring; this is the first example of η^6-bonding of CQ to a transition metal, but a similar preference has been previously observed in Ru^{II} complexes of quinoline.[31] Another point of interest is that our proposed assignments correspond to molecular structures in solution, which are the ones responsible for the biological properties studied.

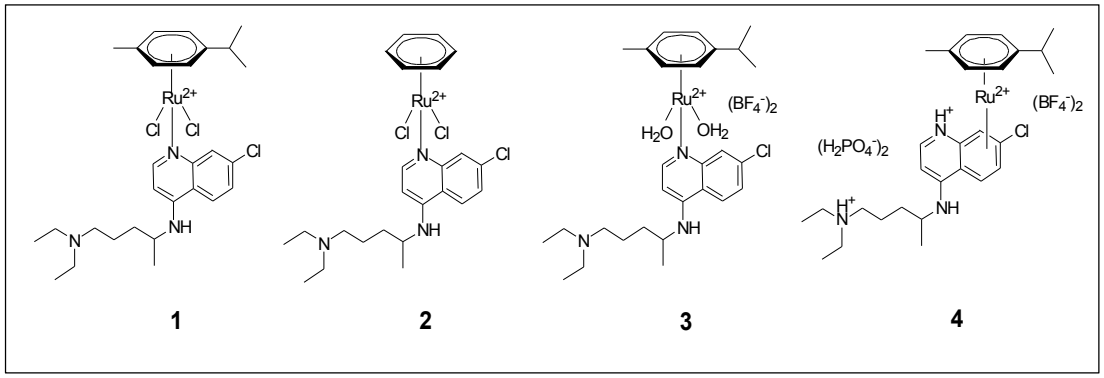

Scheme 12. Structural assignments for **1-4.**

2.4.4 Antimalarial activity evaluation *in vitro*

The antiplasmodial activity of the new Ru-CQ complexes were evaluated against CQ-sensitive and CQ-resistant *P. falciparum*, in collaboration with Prof. Joseph Schrevel of the National Museum of Natural History in Paris. The most relevant results are summarized in Table 6.[32] Values in parentheses, in red, represent the relative activity compared to CQDP for which an activity of 1.0 was assigned.

Table 6. Antimalarial Activity of New Ru-CQ Complexes against *P. falciparum*;

Strain	IC50 (nM) (relative activity)				
	CQDP	**1**	**2**	**3**	**4**
FcB1	45.6 ± 4.5 **(1.0)**	120 ± 4.0 **(0.3)**	81.6 ± 1.2 **(0.5)**	96.5 ± 6.0 **(0.4)**	65 - 70 **(0.6)**
PFB	58.3 ± 8.5 **(1.0)**	109.0 ± 15.1 **(0.5)**	79.0 ± 4.9 **(0.7)**	122.6 ± 15.2 **(0.5)**	
F32	8.2 ± 1.3 **(1.0)**	11.5 ± 1.8 **(0.7)**	13.2 ± 0.2 **(0.6)**	22.5 ± 0.4 **(0.4)**	
3D7	39.5 ± 7.0 **(1.0)**	19.6 ± 3.4 **(2.0)**	17.9 ± 1.5 **(2.2)**	19.5 ± 2.1 **(2.0)**	19.3 ± 2.8 **(2.0)**
Dd2	1184 ± 188 **(1.0)**	483 ± 110 **(2.5)**	442 ± 30 **(2.7)**	234 ± 41 **(5.0)**	557 ± 49 **(2.1)**
K1	1883 ± 165 **(1.0)**	600 ± 87 **(3.1)**	508 ± 84 **(3.7)**	353 ± 61 **(5.3)**	529 ± 97 **(3.6)**
W2	2155 **(1.0)**	1667 **(1.3)**	1619 **(1.3)**	906 **(2.4)**	2549 **(0.8)**

IC_{50} = 50% Inhibitory Concentration (nM).
Relative activity = IC_{50}(CQDP)/IC_{50}(complex)

The activity of complexes **1**, **2**, **3**, and **4** was evaluated *in vitro* against four CQ-sensitive strains (FcB1, 3D7, PFB, and F32) and three CQ-resistant strains (W2, Dd2, and K1) of *P. falciparum*. According to the data obtained (Table 6), all of the compounds tested exhibit activity against malaria parasites.[32]

In the case of the CQ sensitive strains FcB1, PFB, and F32, the activities displayed by the Ru-CQ complexes are in general somewhat lower than the one observed for the standard drug CQDP, except in the case of the 3D7 strain, for which the metal derivatives are about twice as active as CQDP.

Nevertheless, the medically relevant problem is not in parasites that can be treated with the standard drug chloroquine, but in the resistant ones, Dd2, K1, and W2. In this case we note that the potency of all Ru-CQ complexes is consistently higher than that of CQDP, with the single exception of **4** which is of slightly lower activity than CQDP against the highly resistant W2 strain. The highest activities were observed for the dicationic N-bonded complex **3**, reaching values around 5 times better than CQDP for the Dd2 and K1 strains and 2.4 times better for the highly resistant W2. *It is therefore clear that the combination of Ru(II) and chloroquine in a single molecule enhances the activity against CQ resistant strains as postulated in our central hypothesis.*

2.5 Conclusion

We have successfully synthesized a series of complexes with the formulas $[Ru^{II}(\eta^6\text{-}p\text{-cymene})Cl_2(CQ)]$, $[Ru^{II}(\eta^6\text{-benzene})Cl_2(CQ)]$, $[Ru^{II}(\eta^6\text{-}p\text{-cymene})(H_2O)_2(CQ)][BF_4]_2$ and $[Ru^{II}(\eta^6\text{-}p\text{-}c\text{ymene})(CQDP)][BF_4]_2$. Through the use of 1D/2D NMR spectroscopy and proton relaxation (T_1) experiments, the binding mode of Ru(II) to CQ was determined for each complex. Further support for our structural assignments was obtained through DFT calculations on total energies and IR simulations.

All new complexes were active against CQ-resistant (Dd2, K1, and W2) and CQ-sensitive (FcB1, PFB, F32 and 3D7) malaria parasites (*P. falciparum*); importantly, the potency of these complexes against resistant parasites is consistently higher than that of the standard drug chloroquine diphosphate.

2.6 References

1. Martinez, A.; Rajapakse, C. S. K.; Naoulou, B.; Kopkalli, Y.; Davenport, L.; Sanchez-Delgado, R. A. *J. Biol. Inorg. Chem*., **2008**, *13*, 703–712
2. Clarke, M. J. *Coord. Chem. Rev,* **2003**, *236*, 209. 233
3. Egan, T. J.; Chen, J.Y.; J. de Villiers, K. A.; Mabotha, T. E.; Naidoo, K. J.; Ncokazi, K. K.; Langford, S. J.; McNaughton, D.; Pandiancherri, S.; Word, B. R. **2006**, *FEBS Lett. 580,* 5105–5110
4. Cotton, F. A.; Wilkinson, G.; Murillo, C. A.; Bochmann, M. *Advanced Inorganic Chemistry*, (6th Ed.), **1999**, John Wiley and Sons: New York Ch. 16
5. Wilkinson, G.; Stone, F. G. A.; Abel, E. W. *Comprehensive Organometallic Chemistry*, **1982**, Pergamon Press: Oxford and Abel, E. W.; Stone, F. G. A.; Wilkinson, G, **1995**, *Comprehensive Organometallic Chemistry II*, Pergamon Press: Oxford
6. a) Chen, H.; Parkinson, J. A.; Parsons, S.; Coxall, R. A.; Gould, R.; Sadler, P. J.; *J. Am. Chem. Soc.* **2002**, *124*, 3064-3082

   b) Chen, H.; Parkinson, J. A.; Morris, R.; Sadler, P. J. *J. Am. Chem. Soc.* **2003**, *125*, 173-186

   c) Novakova, O.; Chen, H.; Vrana, O.; Rodger, A.; Sadler, P. J.; Brabec, V. *Biochemistry*, **2003**, *42*, 11544-11554
7. Sánchez-Delgado, R. A.; Navarro, M.; Pérez, H.; Urbina, J. A. *J. Med. Chem.* **1996**, *39*, 1095-1099
8. Navarro, M.; Pérez, H.;Sánchez-Delgado, R. A. *J. Med. Chem.* **1997**, *40*, 1937-1939

9. Dayson, P. J.; Allardyce, C. S. *Platinum Metals Rev*. **2001**, *45*, 62-69

10. **a)** Delhaes, L.; Abessolo, H.; Biot, C.; Berry, L.; Delcourt, P.; Maciejewski, L.; Brocard, J.; Camus, D.; Dive, D. Parasitol. Res. **2001**, *87*, 239-244

b) Pierrot, C.; Lafitte, S.; Dive, D.; Fraisse, L.; Brocard, J.; Jamal, K. *Int. J. Parasitol.* **2005**, *35*, 1601-1610

11. Pradines, B.; Fusai, T. ; Daries, W.; Laloge, V. ; Rogier, C.; Millet, P.; Panconi, E.; Kombila, M.; Parzy, D. *J. Antimicrob. Chemother.* **2001**, *48*, 179-184

12. Pradines, B.; Tall, A.; Rogier, C.; Spiegel, A.; Mosnier, J. ; Marrama, L.; Fusai, T.; Millet, P.; Panconi, E.; Trape, J. F.; Parzy, D. *Trop. Med. Int. Health.* **2002**, *7*, 265-270

13. Blackie, M. A. L.; Beagley, P.; Chibale, K.; Clarkson, C.; Moss, J. R.; Smith, P. J. *J. Organomet. Chem.* **2003**, *688*, 144-152

14. **a)** Morris, R. E.; Aird, R. E.; Murdoch, P. S.; Chen, H.; Cummings, J.; Hughes, S. Parsons, N. D.; Parkin, A.; Boyd, C.; Jodrell, D. J.; Sadler, P. J. *J. Med. Chem* **2001**, *44*, 3616-3621

b) Aird, R. E.; Cummings, J.; Ritchie, A. A.; Muir, M.; Morris, R. E.; Chen, H.; Sadler, P. J.; Jodrell, D. I. *J. Cancer*, **2002**, *86*, 1652-1657

c) Chen, H.; Parkinson, J. A.; Novakova, O.; Bella, J.; Wang, P.; Dawson, A.; Gould, R.; Parsons, S.; Brabec, V.; Sadler, P. J. *Proc. Nat. Acad. Sci.*, **2003**, *100*, 14623-14628

d) Yan, Y. K.; Melchart, M.; Habtemariam, A.; Sadler, P. J. *Chem. Commun.* **2005**, 4764-4776

15. Wolf, A.; Shimer, G. H.; Meehan, T. **1987**, *Biochemistry*, 26, 6392–6396

16. Warhurst, D. C.; Craig, J. C.; Adagu, I.S.; Meyer, D. J.; Lee, S.Y. *Malaria J* **2003**, *2*, 26–30

17. Sanchez-Delgado, R. A.; Navarro, M.; Perez, H.; Urbina, J. A. *J. Med.Chem.* **1996**, *39*, 1095–1099

18. a) Bennet, M. A.; Coord. *Chem. Rev.* **1997**, *166*, 225-254

b) Bennet, M. A.; Huang, T.N.; Matheson, T. W.; Smith, A. K. *Inorg. Synth.* **1882**, *25*, 74-78

19. Frisch, M. J.; Trucks, G. W.; Schlegel, H. B.; Scuseria, G. E.; Robb, M. A.; Cheeseman, J. R.; Montgomery, J. J. A.; Vreven, T.; Kudin,K. N.; Burant, J. C.; Millam, J. M.; Iyengar, S. S.; Tomasi, J.; Barone,V.; Mennucci, B.; Cossi, M.; Scalmani, G.; Rega, N.; Petersson, G. A.;Nakatsuji, H.; Hada, M.; Ehara, M.; Toyota, K.; Fukuda, R.; Hasegawa,J.; Ishida, M.; Nakajima, T.; Honda, Y.; Kitao, O.; Nakai, H.; Klene,M.; Li, X.; Knox, J. E.; Hratchian, H. P.; Cross, J. B.; Bakken, V.;Adamo, C.; Jaramillo, J.; Gomperts, R.; Stratmann, R. E.; Yazyev,O.; Austin, A. J.; Cammi, R.; Pomelli, C.; Ochterski, J. W.; Ayala,P. Y.; Morokuma, K.; Voth, G. A.; Salvador, P.; Dannenberg, J. J.;Zakrzewski, V. G.; Dapprich, S.; Daniels, A. D.; Strain, M. C.; Farkas,O.; Malick, D. K.; Rabuck, A. D.; Raghavachari, K.; Foresman, J. B.;ORitiz, J. V.; Cui, Q.; Baboul, A. G.; Clifford, S.; Cioslowski, J.;Stefanov, B. B.; Liu, G.; Liashenko, A.; Piskorz, P.; Komaromi, I.;Martin, R. L.; Fox, D.J.; Keith, T.; Al-Laham, M. A.; Peng, C. Y.;Nanayakkara, A.; Challacombe, M.; Gill, P. M.W.; Johnson, B.; Chen,W.; Wong, M. W.; Gonza´lez, C.; Pople, J. A. *Gaussian 03*, Rev. C.02; Gaussian, Inc.: Wallingford, CT, **2004**

20. Hay, P. J.; Wadt, W. R. *J. Chem. Phys.* **1985**, *82*, 270–283

21. Cossi, M.; Scalmani, G.; Rega, N.; Barone, V. *J. Chem. Phys.* **2002**, *117*, 43–54

22. Pisciotta, J. M.; Ponder, E. L.; Fried, B.; Sullivan, D. J, *Int. J Parasitol*, **2005**, *35*, 1037–42

23. Trager, W; Jensen, J. B. *Science* **1976**, *193*, 673–675

24. Pasvol, G.; Wilson, R. J.; Smalley, M. E.; Brown, J. *Ann. Trop. Med.Parasitol.* **1978**, *72*, 87–88

25. Desjardins, R. E.; Canfield, C. J.; Haynes, J. D.; Chulay, J. D. *Antimicrob. Agents Chemother.* **1979**, *16*, 710–718

26. Sanchez-Delgado, R. A.; Navarro, M.; Perez, H.; Urbina, J. A. *J. Med. Chem.* **1996**, *39*, 1095–1099

27. Navarro, M.; Pekerar, S.; Perez, H. *Polyhedron,* **2007**, *26*, 2420–2424

28. Van Schalkwyk, D. A.; Egan, T. J. *Drug Res. Updates* **2006**, *9*, 211–226

29. *Antimalarial Chemotherapy: Mechanism ofAction, Resistance and New Directions in Drug Discovery*; Rosenthal, Ph. J., Ed.; Humana Press: NJ, **2001**

30. a) Hore, P. J. *Nuclear Magnetic Resonance*; Oxford University Press:New York; **1995**.

    b) Pople, J. A.; Schneider, W. G.; Bernstein, H. J. *High-Resolution Nuclear Magnetic Resonance*; McGraw-Hill: NewYork, **1959**

31. a) Fish, R. H.; Fong, R. H.; Tran, A.; Baralt, E. *Organometallics,* **1991**, *10*, 1209–1212

    b) Fish, R. H.; Kim, H. S.; Fong, R. H. *Organometallics* **1991**, *10*, 770–777

32.Rajapakse, C. S. K.; Martinez, A.; Naoulou, B.; Jarzecki, A. A.; Surez, L.; Deregnaucourt, C.; Sinou, V.; Schrvel, J.; Musi, E.; Ambrosini[¶], G.; Schwartz, G.K.; Sanchez-Delgado, R. A. *Inorg. Chem*., **2009**, *48*, 1122-1131

Chapter 3

An Investigation of the Origin of the Enhanced Activity of (π-Arene)-Ruthenium-Chloroquine Complexes against CQ-Resistant *Plasmodium falciparum*

Heme Aggregation as the Main Target of Action

3.1 Introduction

It is important to investigate the factors that determine the improved antimalarial activity of the new Ru-CQ complexes against CQ resistant strains, as well as the mechanism of action of ruthenium complexes.

As previously explained, CQ enters the red blood cell, resides in the parasite cell and enters the digestive vacuole by simple diffusion. Since CQ is a weak base, it becomes protonated (to CQ^{2+}), as the digestive vacuole is known to be acidic (pH 4.8); chloroquine then cannot leave by diffusion through the vacuole membrane. Next CQ interacts with heme molecules to prevent heme aggregation, thus leading to toxic heme buildup. Heme and/or the heme-chloroquine complex is highly toxic to the cell and disrupts membrane function, resulting in cell lysis and, ultimately in parasite cell death.

Based on the studies on a variety of 4-aminoquinoline analogues of CQ a possible structure-activity relationship for this class of compounds was proposed in the literature[1] (Chapter1, Figure 27). The 4-aminoquinoline nucleus appears to be essential for strong complex formation with Fe(III)PPIX, while the 7-chloro group is required for inhibition of β-hematin formation. The tertiary amino group in the side chain and the quinoline N, both of which are basic, appear to be important for drug accumulation in the acidic parasitic food vacuole through pH trapping. Thus, a number of physicochemical properties of the CQ molecule, including association with Fe(III)PPIX, strength of inhibition of heme aggregation, pK_a, and lipophilicity, are related to its biological activity.

Although chloroquine remained the main treatment for malaria for 5 decades the effectiveness of chloroquine against the parasite has declined as resistant strains of the

parasite evolved. CQ-resistant cells extrude chloroquine at 40 times the rate of CQ-sensitive cells.[2]

The CQ resistance mechanism is still not completely understood, but it is believed that this is due to critical mutations in the p*f*crt gene which encodes the PfCRT (*Plasmodium falciparum* Chloroquine Resistance Transporter) transmembrane transporter that pumps the protonated CQ from the food vacuole.

Our concept for overcoming resistance in malaria was to synthesize new arene-Ru-CQ complexes (Figure 1), which represents a major modification of the structure of CQ, but is expected to maintain the same target as CQ - the heme aggregation process.

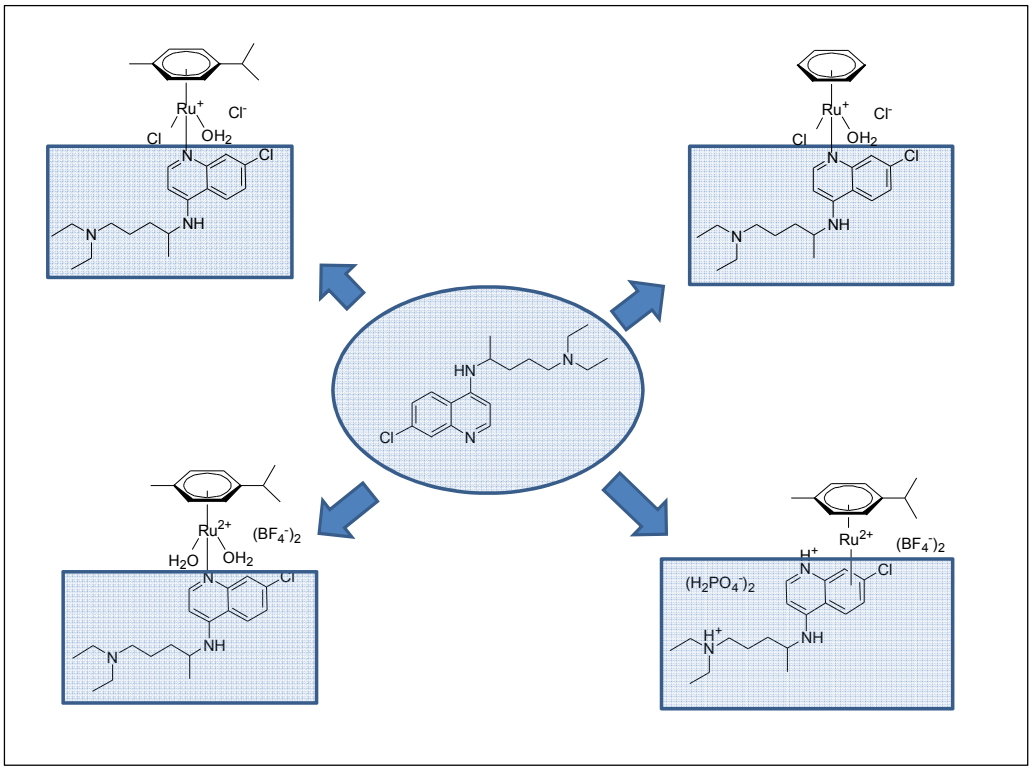

Figure 1. New arene-Ru-CQ complexes were synthesized by modifying the CQ/CQDP structure

The new complexes **1-4** modify the CQ/CQDP structure by incorporation of a Ru-arene fragment in different ways as shown in Figure 1. In complexes **1-3** the Ru-

containing fragment is N-bonded to the quinoline moiety of CQ, whereas in complex **4** ruthenium is π bonded to CQDP. The results obtained from the biological tests confirm the validity of our concept in that having Ru and CQ in the same molecule may lead to enhanced antimalarial activity, particularly against the resistant strains. Introducing a metal-containing fragment into the structure of CQ produces a dramatic modification in terms of the electronic structure and the physicochemical properties of the molecule and makes a number of alternative chemical and biochemical pathways available as part of a potential mechanism of antimalarial action. Metal–DNA binding, for instance, is a common phenomenon that could lead to new or additional pathways of antimalarial action. Also, the basicity of the molecule as well as its hydrophilicity/lipophilicity characteristics are strongly modified by a metal–ligand fragment and this may result in improvements in the efficacy of the metal-based drug with respect to the parental organic compound, as demonstrated in the case of the iron-containing ferroquine.[3] Moreover, recognition of CQ by the parasite may be seriously impaired by the presence of the transition-metal containing moiety, possibly leading to a reduction of the emergence of resistance.

In the following section, we describe our studies on some physicochemical characteristics of metal complexes and the evaluation of its heme aggregation inhibition activity in comparison with CQDP, in order to ascertain the principal mechanism of action against CQ resistant strains.

3.2 Experimental Section

3.2.1 Determination of pK_a

For the determination of pK_a values, a 1 mM solution of each compound in deionized water was titrated by following pH changes at room temperature (23.0 ± 2.0^0C) using 0.03 M NaOH (10-µL additions). Titration plots were generated and the pK_a values were obtained from the maxima of the first derivative plots (dpH/dV) versus V, where V represents the volume of the titrant added.

3.2.2 Determination of partition coefficients

The distribution of each complex between *n*-octanol and water was studied by use of the stir-flask method.[4-6] A mixture of 10 mL *n*-octanol and 10 mL of water (each saturated in the other) was stirred for 30 min at the desired temperature after the right amount of the sample to be analyzed (approximately 0.7 mmol) had been added. The pH was adjusted to the desired value by addition of a 0.1 M solution of H_3PO_4 (10–20 µL). Once the equilibrium had been reached, the organic and aqueous phases were separated and centrifuged. Finally, the concentration of drug in each phase was measured spectrophotometrically to determine values of D = [drug](in octanol)/[drug] (in water). Experiments were carried out in triplicate.

3.2.3 Interaction of complexes with hematin

The binding constants for binding of hematin with chloroquine diphosphate (CQDP) and all the ruthenium complexes were determined by spectrophotometric titration according to literature methods[7,8] In short, hemin (3.5 mg) was dissolved in dimethyl sulfoxide (DMSO) (15 mL) to obtain a stock solution. A 4 µM working solution

of hemin was freshly prepared by diluting the stock solution in a buffer consisting of 40% v/v DMSO and 20 mM 2-(N-morpholino)ethanesulfonic acid buffer (pH 4.97). This mixture was titrated with a 1.0 mM solution of each drug in the same buffer at 25 ^{0}C by monitoring the absorbance of the Soret band (402 nm). Blank measurements were performed at the same wavelength by titration of 40% v/v buffer with the solution of each complex to correct for the absorbance of the drugs.

The data were fitted to the equation $A = (A_0 + A_\infty K[C])/(1 + K[C])$ for a 1:1 complexation model using nonlinear least squares fitting, strictly following the procedure of Egan et al.[7] A_0 is the absorbance of hemin before addition of the drug, A_∞ is the absorbance for the drug–hemin adducts at saturation, A is the absorbance at each point of the titration, and K is the conditional association constant.

3.2.4 Heme aggregation inhibition activity (HAIA)

3.2.4.1 HAIA in acidic buffer

The ability of each complex to inhibit heme aggregation was quantified using a modification of the method reported by Parapini et al.[9] In short, triplicate samples at different drug-to-hemin molar ratios, containing 1 mL of an 8 mM solution of hemin in DMSO, 1 mL of drug in deionized water (or 20% DMSO/ 80% water for less soluble complexes), and 2 mL of 8 M acetate buffer (pH 4.9) were prepared (solutions of each compound in water were of appropriate concentrations to achieve drug-to-hemin molar ratios in the range 0 – 2). The mixtures were incubated for 24 h at 37^{0}C to allow for complete reaction and then centrifuged for 20 min. The soluble fraction was separated from each sample and the remaining β-hematin pellet was washed with 4 mL of DMSO, centrifuged again, and finally the pellet of pure β-hematin was dissolved in NaOH (0.1M)

for spectrophotometric quantification. Control experiments using no drug or CQDP were carried out under analogous conditions.

3.2.4.2 HAIA at a water/*n*-octanol interface

Inhibition of heme aggregation near the interface of aqueous buffer/*n*-octanol mixtures was studied following the method previously described by us.[10] To establish a baseline for the aggregation process, hemin was dissolved in 0.1 M NaOH solution to generate hematin and acetone was added until the acetone-to-water ratio was 4:6; the final solution contained 15 mg hematin/mL. A sample of this solution (200 μL) was carefully introduced close to the interface between *n*-octanol (2 mL) and aqueous acetate buffer (8 M; 5mL pH 4.9) in a cylindrical vial with an internal diameter of 2.5 cm. The mixture was incubated at 37^0C for 60 min and at the end of the incubation period it was stirred to ensure the transfer of all solid particles to the aqueous layer. The product (β-hematin) was isolated by centrifugation. The pellet was collected and washed with DMSO (4 mL), centrifuged again for 20 min, washed with 2 mL of ethanol, and finally dissolved in 25 mL of 0.1 M NaOH for spectrophotometric quantification at 386 nm.

For the aggregation inhibition activity measurements, the appropriate amount of each drug (23 mM in water) to yield drug-to-hemin concentration ratios in the range 1–6 was added to the acetate buffer/*n*-octanol mixture; after stirring for 30 min to equilibrate the drug between the two phases, the hematin solution was added close to the interface and the procedure was followed as described above. All experiments were performed in triplicate.

3.3 Results and Discussion

3.3.1 Interaction of complexes with hematin

Recent studies continue to support the hypothesis that quinoline antimalarial drugs[1] exert their antimalarial effect by binding to hematin, which leads to inhibition of hemozoin formation and death of the parasite by hematin poisoning. There is strong evidence[10] that this inhibition involves direct interaction between the drug and the Fe(III)PPIX. In order to test our hypothesis that the most likely target of biological action for complexes **1-4** is the heme aggregation process, as a first step we studied the interaction of our new complexes with hematin by spectrophotometric titration in aqueous DMSO at pH 4.97, which simulates the conditions within the acidic food vacuole of the parasite. Fe(III)PPIX is maintained in a monomeric, unaggregated state in aqueous DMSO containing a minimum of 40% DMSO.[12] The Soret band of hematin at 402 nm was monitored as a function of drug concentration. Blank measurements were performed at the same wavelength by titrating the buffer with a solution of CQDP or with each drug in order to correct for any absorbance of the drug. Figure 2 shows the results of a titration for CQDP, while Figure 3 shows the corresponding data for complexes **1-4**.

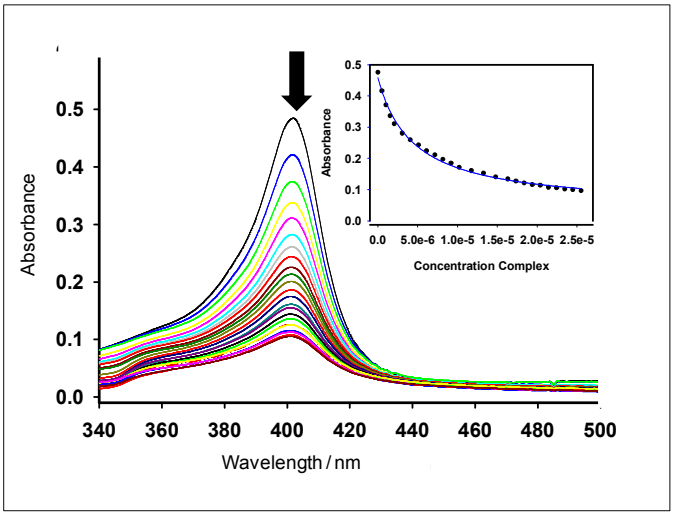

Figure 2. Variation in absorbance of Fe(III)PPIX at 402 nm as a function of CQDP concentration

As the concentration of drug is increased, the absorbance of Soret band is decreased, indicating that there is an interaction between the drug and the porphyrin unit of the hematin.

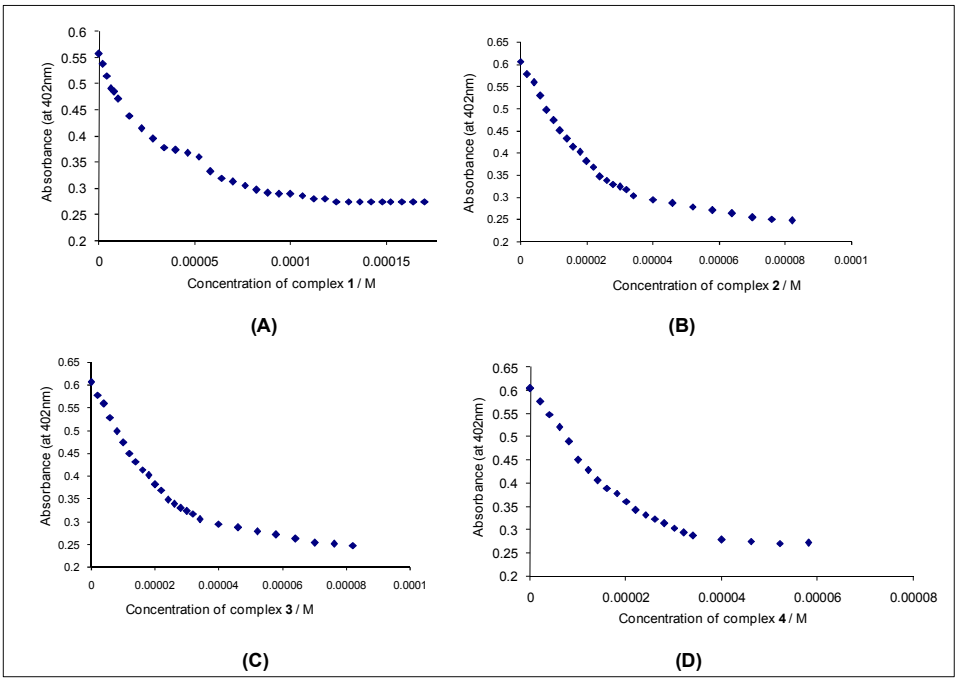

Figure 3. Variation in absorbance of Fe(III)PPIX at 402 nm as a function of drug concentration (A) compound **1**, (B) compound **2**, (C) compound **3**, (D) compound **4**

Biot et al.[14] have previously described the interaction of Fe(III)PPIX with CQ; several possibilities were considered but a simple 1:1 association model fits their data adequately except at very low drug to hematin ratios. Following that procedure and fitting data, for a 1:1 association model (with omission of the first few data points), we obtained values of log K (K= binding constant), which are summarized in Table 1.

Table 1. Binding constants for the interaction of Ru-CQ complexes with hemin at pH 4.97 from spectrophotometric titration experiments

Compound	Log K
CQDP	4.82 ± 0.02
[Ru (η^6-*p*-cymene)(CQ)Cl_2] – **1**	4.57 ± 0.08
[Ru (η^6-benzene)(CQ)Cl_2] – **2**	4.67 ± 0.03
[Ru (η^6-*p*-cymene)(CQ)$(H_2O)_2$]$(BF_4)_2$] - **3**	4.52 ± 0.16
[Ru (η^6-*p*-cymene)(η^6-CQDP)]$(BF_4)_2$ - **4**	4.71 ± 0.03

The log K value of 4.82 ± 0.02 obtained for CQDP under our experimental conditions (pH 4.97) is in excellent agreement with the value of 4.8 previously reported by Egan et al.[15] at pH 5.6. A similar association constant was reported by Biot et al.[14] for the metal complex ferroquine (log K = 4.95 ± 0.05) at pH 7.5. More important for our discussion is the fact that under our experimental conditions the values for the association constants of the Ru–CQ complexes are in the same order as the value for CQDP and are very similar to each other, indicating that the metal–CQ derivatives **1–4** interact with hematin in a similar way and to a comparable extent as CQDP under these conditions. The mode of bonding between CQ and Fe(III)PPIX is believed to be π-π complexation between the porphyrin of Fe(III)PPIX and the quinoline moety of CQ (Chapter1, Figure 26). Since the binding affinity of complexes **1-4** to hemin is similar to the affinity of CQ,

we can conclude that the mode of interaction of new Ru-CQ complexes with hemin is most probably through π-π intercalations.

These results suggest that the binding affinity to hemin by itself is not the reason for the improved activity of complexes **1-4** against CQ resistant strains. In order to further investigate the cause for the improved antimalarial activity of complexes **1-4**, their heme aggregation inhibition activity was evaluated.

3.3.2 Heme aggregation inhibition activity (HAIA) in acetate buffer

Various methods have been proposed to mimic, *in vitro,* the heme polymerization process leading to the formation of the malaria pigment and to study the inhibition thereof.[14] Assays differ mostly in the reaction conditions, and the method used to identify and quantify the reaction products. Among the published procedures, we first followed the β-hematin inhibition activity (BHIA) assay developed by Parapini et. al.[16] (with some modifications) in order to measure the ability of new arene-Ru-CQ complexes to inhibit the formation of β-hematin.

β-hematin is the synthetic analog of hemozoin (malaria pigment) and it is chemically, spectroscopically and crystallographically identical to native hemozoin.[17,18] According to powder diffraction data, the Fe(III)PPIX molecules are linked into dimers through reciprocal iron carboxylate bonds to one of the propionic side chains of each porphyrin (Figure 4), and the dimers form chains linked by hydrogen bonds in the crystal.

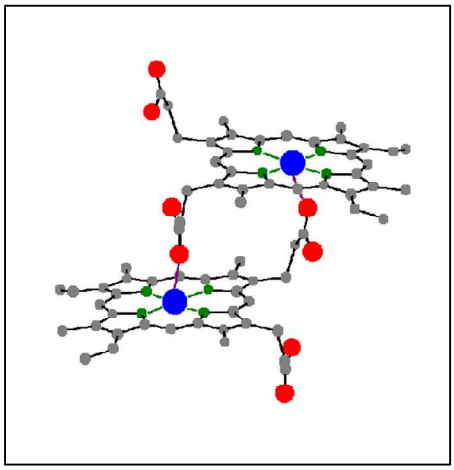

Figure 4. Basic unit of β-hematin

Both hemozoin and its synthetic analog β-hematin can be easily identified by IR spectrophotometry. The IR spectra contain two intense characteristic bands at 1662 cm^{-1} due to the C=O stretching frequency and at 1209 cm^{-1} due to the C-O stretching frequency when the carbxylate oxygens are bound to the Fe(III) in Fe(III)PPIX (Figure 5). These bands are absent in the spectra of hemin or hematin.

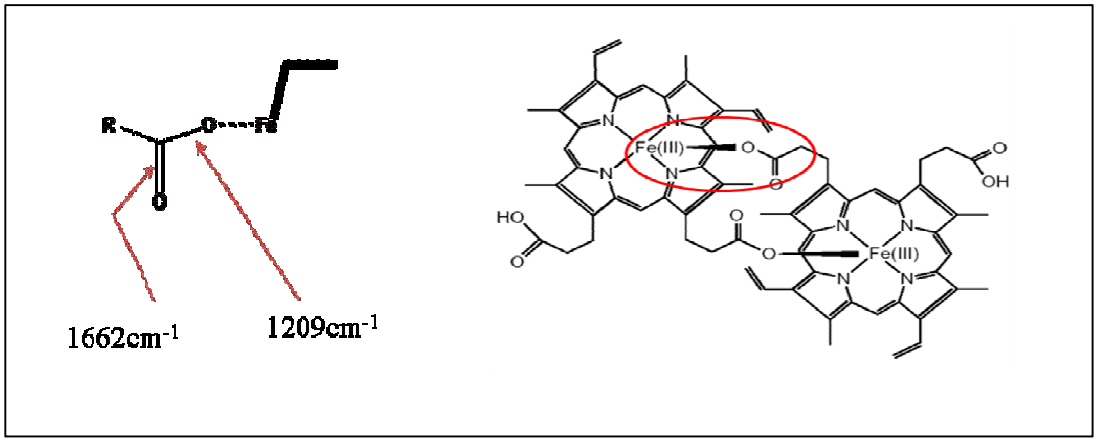

Figure 5. Sharp bands at 1662 cm^{-1} and 1209 cm^{-1}; characteristic bands due to β-hematin

The ability of complexes **1-4** as well as CQDP to inhibit heme aggregation was quantified after 24 h incubation under strictly comparable conditions, starting from commercial hemin in acetate buffer (pH 5) (see the experimental section).

First, formation of β-hematin was confirmed under our experimental conditions by carrying out the assay without adding any drug and measuring the IR spectrum of the resulting material (Figure 6). Two intense bands at 1662 cm^{-1} and 1208 cm^{-1} confirmed the formation of β-hematin under our experimental conditions.

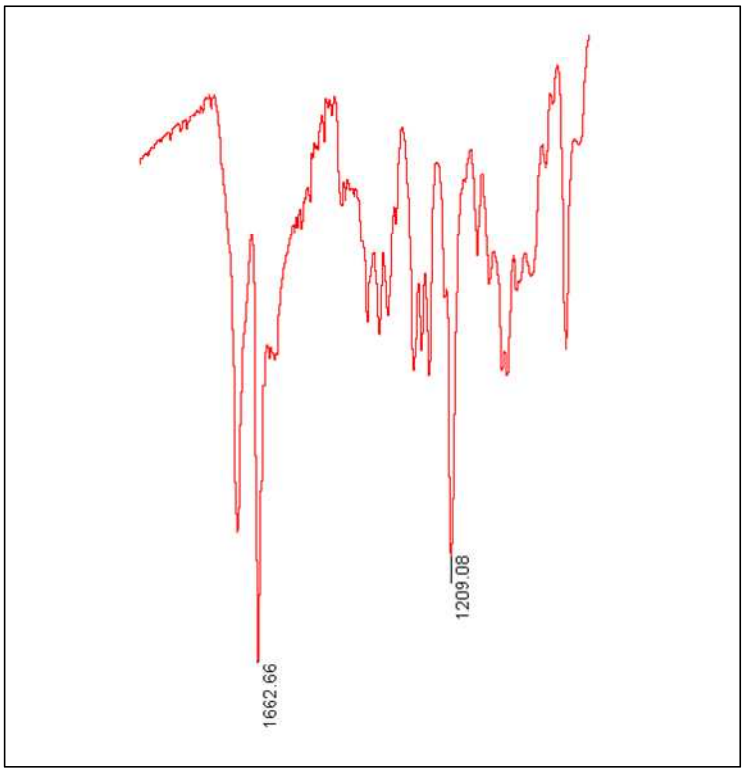

Figure 6. IR spectrum of β-hematin

In order to measure the heme aggregation inhibition ability of the Ru-CQ complexes, the assays were repeated using appropriate concentrations of complexes **1-4**

and of CQDP to achieve drug-to-hemin molar ratios in the range 0–2. The β-hematin formed in the presence of different concentrations of drug was dissolved in NaOH (0.1 M) for spectrophotometric quantification. Here we measured the absorbance of hematin (386 nm), which is formed from the hydrolysis of β-hematin under basic conditions. The results of these experiments for CQDP and the new Ru-CQ complexes are shown in Figure 7.

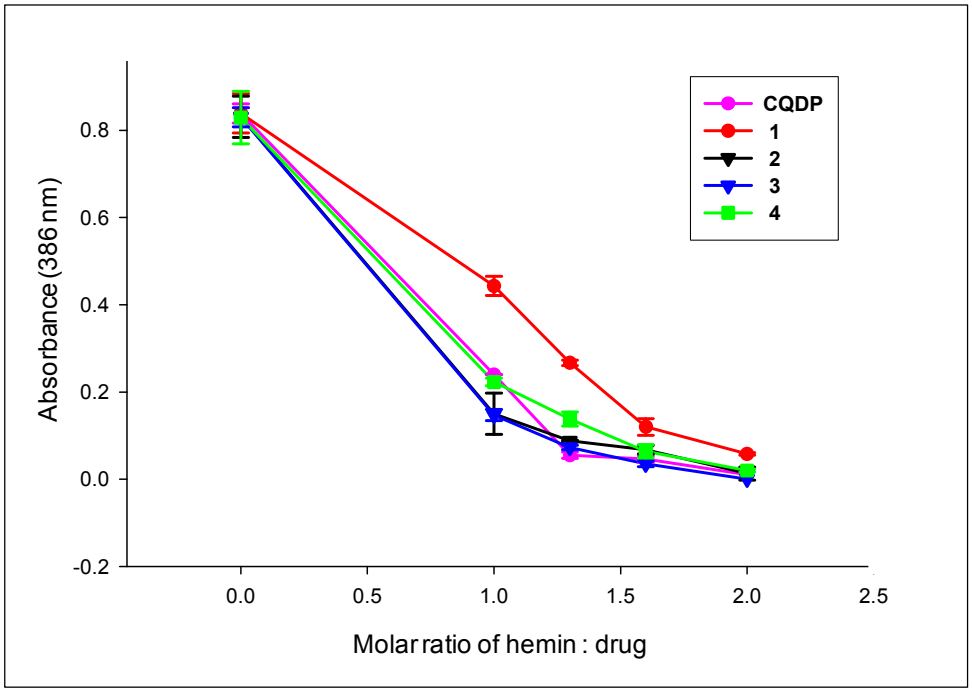

Figure 7. β-hematin recovered from assay at different concentrations of CQDP and new compounds.

In general, as the hemin:drug ratio increases, β-hematin formation is decreased indicating that complexes **1-4** inhibit the heme aggreagation process, but complex **1** appears as somewhat less active than CQDP in this assay while complexes **2–4** display an activity very similar to that of CQDP and to each other. HAI_{50} values are shown in Table 2, where HAI_{50} is the drug to hemin ratio required to inhibit 50% of heme

aggregation against a control experiment in the absence of drugs. Values in *parentheses* are relative activities with respect to CQDP. According to these results, the new arene-Ru-CQ complexes show somewhat lower or similar HAI_{50} values with respect to that of CQDP. These heme aggregation inhibition data, obtained using the standard literature assay in acetate buffer, do not agree with the improved antiplasmodial activity observed in the biological tests of complexes **1-4** (Chapter 2, Table 6)**,** with respect to CQDP.

Table 2. HAI_{50} values obtained from BHIA assay in acetate buffer (pH = 4.9) of compounds **1-4** and CQDP. Values in parentheses are the relative activity with respect to CQDP

Compound	HAI_{50} at acetate buffer
CQDP	0.69 **(1.0)**
[Ru(η^6-*p*-cymene)(CQ)Cl_2] – **1**	0.96 **(0.7)**
[Ru(η^6-benzene)(CQ)Cl_2] – **2**	0.67 **(1.0)**
[Ru(η^6-*p*-cymene)(CQ)$(H_2O)_2$]$(BF_4)_2$] - **3**	0.65 **(1.1)**
[Ru(η^6-*p*-cymene)(μ6-CQDP)]$(BF_4)_2$ - **4**	0.67 **(1.0)**

.3.3.3 HAIA at an acetate buffer/*n*-octanol interface

As mentioned in the introduction section, Egan and coworkers have demonstrated that under acidic physiologically more realistic conditions β-hematin rapidly and spontaneously forms at alcohol/water or lipid /water interfaces.[19] According to them, the aggregation takes place in aqueous buffers when the entire sample of Fe(III)PPIX is introduced directly into an acidic aqueous environment at the beginning of the reaction. This might result in immediate precipitation of amorphous Fe(III)PPIX. They have pointed out that if this occurs, the solid can convert to β-hematin only slowly probably by dissolution and re-precipitation. They further argued that since Fe(III)PPIX is released in

a continuous process *in vivo,* and large quantities of amorphous Fe(III)PPIX are not observed in hemozoin forming organisms, use of an aqueous model to mimic heme aggregation is unrealistic.

They also presented molecular dynamic simulations (MD) to provide further insight into the mechanism of hemozoin formation and the role of lipids in the process. When the simulation was carried out in vacuum, two H_2O-Fe(III)PPIX intermolecularly interacted with each other through the propionate group of one Fe(III)PPIX linked with the Fe(III) center of the other (Figure 8). They also suggest that the β-hematin formation process is a ligand exchange process with bond formation from the propionate O to Fe(III) and displacement of water from the opposite face of each porphyrin. Then the β-hematin dimers were found to form H bonds between the protonated propionic acid groups to form the crystal.

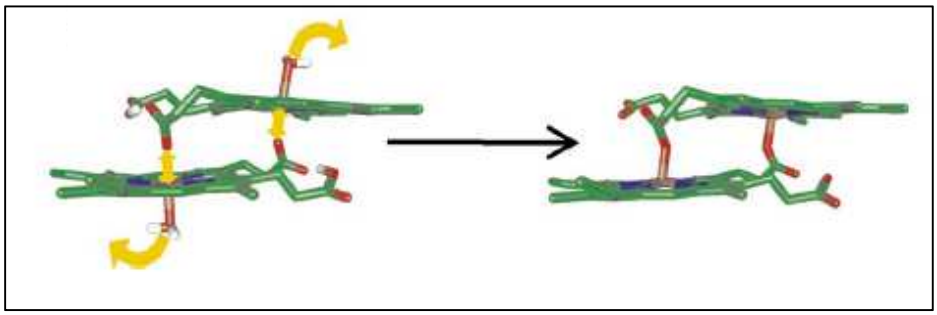

Figure 8. Molecular dynamics simulation of the interaction of two H_2O–Fe(III)PPIX molecules (the protonation state expected at FV pH). In vacuum, these two molecules rapidly form the β-haematin precursor. Bond formation of the propionate groups with Fe (III) and release of H_2O is all that is required to convert this precursor to the β-hematin dimer **(*Egan,T.J.; et al, FEBS Letters, 2006, 580, 5105–5110*).**

Interestingly when MD simulations were carried out in water, the propionate groups of the β-hematin precursor moved away from the Fe(III) centers to interact with water

molecules, probably because of competitive hydrogen bonding between water and the propionic groups (Figure 9).

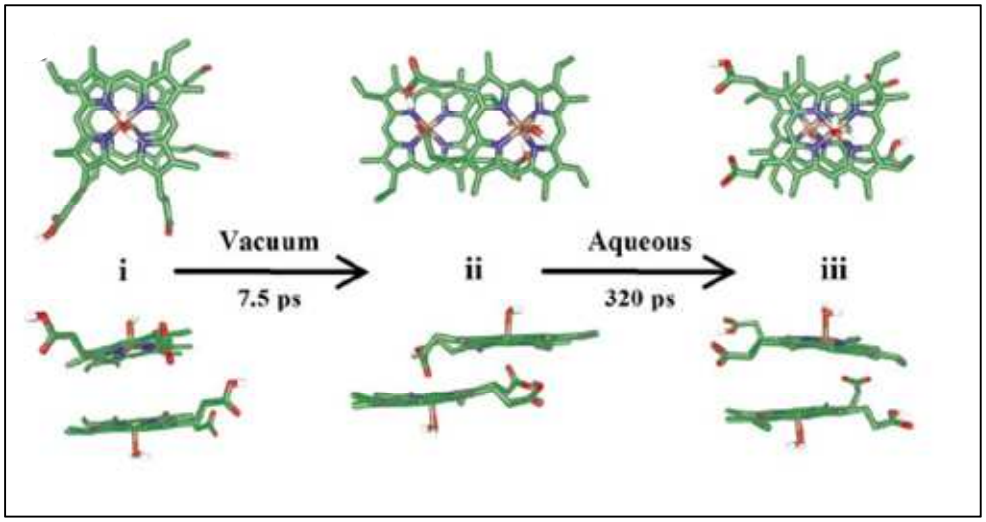

Figure 9. Molecular dynamics simulation of the interaction of two H_2O–Fe(III)PPIX molecules **(i),** In vacuum two molecules rapidly form the β-hematin precursor **(ii)**. When the dynamics were performed in a cube of H_2O starting from the β-haematin precursor, the propionate groups quickly moved away from the Fe(III) centers to interact with the solvent molecules **(iii)(*Egan, T.J.; et al., FEBS Letters,2006, 580, 5105–5110).***

From these findings they have concluded that β-hematin formation in aqueous media is unlikely. Their simulation further provided evidence that as a hydrophobic Fe(III)PPIX dimer enters a lipid layer, competitive hydrogen bonding by water molecules weakens. With all these evidence they have proposed that hemozoin formation takes place near a lipid/water interface *in vivo*.

To model such interfaces they used different alcohol/water mixtures and found that an octanol/water interface is a suitable model. Octanol has recently been shown to have lipid like qualities at the aqueous interface.[19] This is because the OH groups of octanol hydrogen bond with water molecules, resulting in a polar region and a non polar region where the alkyl chains are partially aligned, resembling half of the bilayer of a

lipid membrane.[20] They also showed experimentally that β-hematin forms quickly (30 min) at such interfaces. It thus seemed logical that if heme aggregation takes place preferentially at a water/lipid interface, the inhibition of heme aggregation by a drug should be best measured at such an interface. On this basis, a new method was developed by Dr. Alberto Martinez in our research group, to evaluate the heme aggregation activity of new drugs, and consequently predict their antimalarial behavior.[21] Using this new method (Figure 10) (details in experimental section), we have evaluated the activity of complexes **1-4**.

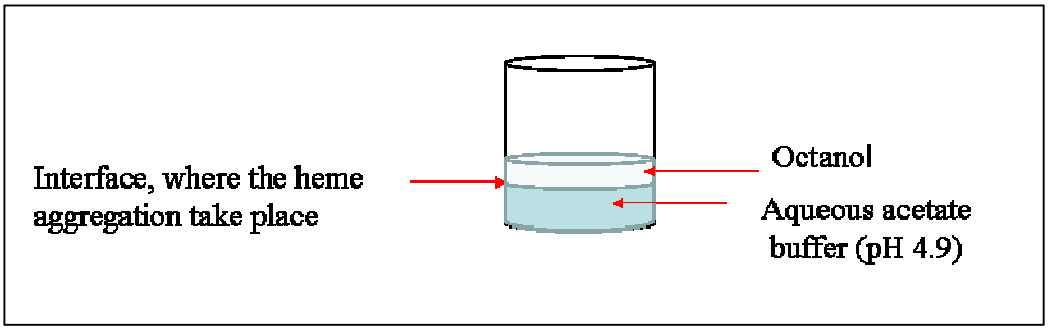

Figure 10. Experimental set-up for carrying out heme aggregation at water/octanol interface

HAI_{50} values for compounds **1-4** as well as of CQDP are contained in Table 3. Values in parentheses are the relative activity with respect to CQDP. These results predict all complexes to be significantly more potent than CQDP for inhibiting heme aggregation at the interface, in agreement with the higher antimalarial activities observed (Chapter2, Table 6).

Complex **1**, which appeared as the least active compound in aqueous buffer, displays the highest activity at the interface, twice as active as CQDP. Although no significant differences were observed in the activity of complexes **2–4** in the

experiments performed in an aqueous medium, the values measured at the interface for the four compounds follow a clear trend: **1 > 3 > 4 > 2 > CQDP**, in qualitative agreement with antimalarial results.

Table 3. HAI_{50} values obtained by carrying out heme aggregation inhibition assay at aqueous acetate buffer (pH = 4.9)/octanol interface of compounds **1-4** and CQDP. Values in parentheses are the relative activity with respect to CQDP.

Compound	HAI_{50} at interface
CQDP	2.92 **(1.0)**
[Ru(η^6-*p*-cymene)(CQ)Cl_2] – **1**	1.47 **(2.0)**
[Ru(η^6-benzene)(CQ)Cl_2] – **2**	2.42 **(1.2)**
[Ru(η^6-*p*-cymene)(CQ)$(H_2O)_2$]$(BF_4)_2$] - **3**	1.73 **(1.7)**
[Ru(η^6-*p*-cymene)(μ6-CQDP)]$(BF_4)_2$ - **4**	2.15 **(1.4)**

These findings provide further evidence to support the idea of Egan[19] that β-hematin formation in aqueous media is unlikely, and that process favorably takes place near water/lipid interfaces. From these findings, we can conclude that measuring HAIA of potential drugs near water/*n*-octanol interfaces is a better predictor of antimalarial potency than the standard tests in aqueous acidic buffer. Also, our results further suggest that heme aggregation is one of the principal targets of our new ruthenium – CQ complexes.

3.3.4 Determination of distribution coefficient (*D*)

In the absence of special transport mechanisms, the accumulation of weak bases like CQ can be described using its physicochemical behavior based on the partitioning theory.[22] This involves the influence of pK_a and lipophilicity of the CQ/drug.[23] In order to investigate the reasons for the new Ru-CQ complexes **1-4** showing improved heme

aggregation inhibition activity at water/octanol interfaces, we have measured some of their physicochemical properties, namely the basicity and the hydrophilic/lipophilc character.

First, to probe the influence of the lipophilicity of each complex on the heme aggregation and antimalarial activity of new Ru-CQ complexes, distribution coefficients were measured in water/*n*-octanol mixtures at two pH values (4.9 and 6.6) that can be related to vacuolar and cytosolic conditions of the parasite, respectively. Distribution coefficients (*D*) were calculated according to the following equation.

$$D = [\text{drug}](\text{in octanol})/[\text{drug}] (\text{in water}).$$

The corresponding *D* (pH) values are shown in Table 4. The greater the *D*, the higher the lipophilicity. We note that at the vacuolar pH (4.9) the Ru–CQ complexes are generally more lipophilic than CQDP, with the exception of complex **4**, which is highly hydrophilic. The general lipophilicity trend extracted from the data at, pH 4.9 is **1 > 3 > 2 > CQDP > 4**. On the other hand, at pH 6.6 only complex **4** accumulates preferentially in the aqueous phase (D < 1), while the other Ru–CQ complexes are less lipophilic than CQDP; the lipophilicity trend in this case is **CQDP > 3 > 1 > 2 >> 4**. In summary, at vacuolar pH (4.9) complexes **1-3** display a higher lipophilic character than CQDP and therefore they should accumulate better at the water/octanol interface. Correlation between HAIA at water/*n*-octanol interface/antiplasmodial activity and the lipophilicity will be discussed in detail in section 3.3.6.

Table 4. *D* (4.9) and *D* (6.6) values for CQDP and complexes **1-4**

Compound	*D* (4.9)	*D* (6.6)
CQDP	0.15 ± 0.01	6.61 ± 0.64
[Ru (μ^6-*p*-cymene)(CQ)Cl_2] – **1**	0.41 ± 0.08	3.29 ± 0.34
[Ru (μ^6-benzene)(CQ)Cl_2] – **2**	0.19 ± 0.02	1.27 ± 0.06
[Ru (μ^6-p-cymene)(CQ)$(H_2O)_2$]$(BF_4)_2$ – **3**	0.31 ± 0.01	4.76 ± 0.06
[Ru (μ^6-*p*-cymene)(μ6-CQDP)]$(BF_4)_2$ - **4**	0.038 ± 0.008	0.66 ± 0.02

3.3.5 Determination of pK_a values

Drugs targeting heme aggregation must accumulate inside the acidic food vacuole of the parasite. Lipophilic CQ is believed to cross membranes in its unprotonated form by passive diffusion and then accumulate after protonation in the food vacuole of the parasite due to pH trapping (Figure 11) but resistant parasites have developed a mechanism for extruding CQ from the food vacuole.

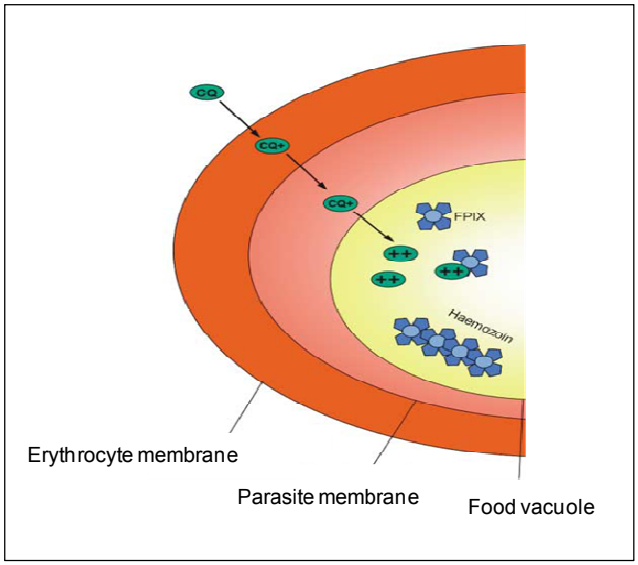

Figure 11. Schematic diagram to show transport of CQ through membranes in its unprotonated form and accumulation inside the acidic food vacuole as a diprotonated form, responsible for the inhibition of heme aggregation ***(Johnson, D.; et.al., Molecular cell, 2004, 15, 867-877)***.

With these considerations in mind, the basicity of each complex becomes an important additional feature to consider. Since any effective drug must have sufficient basicity to accumulate inside the acidic food vacuole of the parasite, pK_a values were measured by pH titration following the procedure described in experimental section. Then the pK_a values were obtained from the maxima of the first derivative plots (dpH/dV) versus V; (volume of the titrant added). (See Figure 12 as an example for a weak base such as CQ)

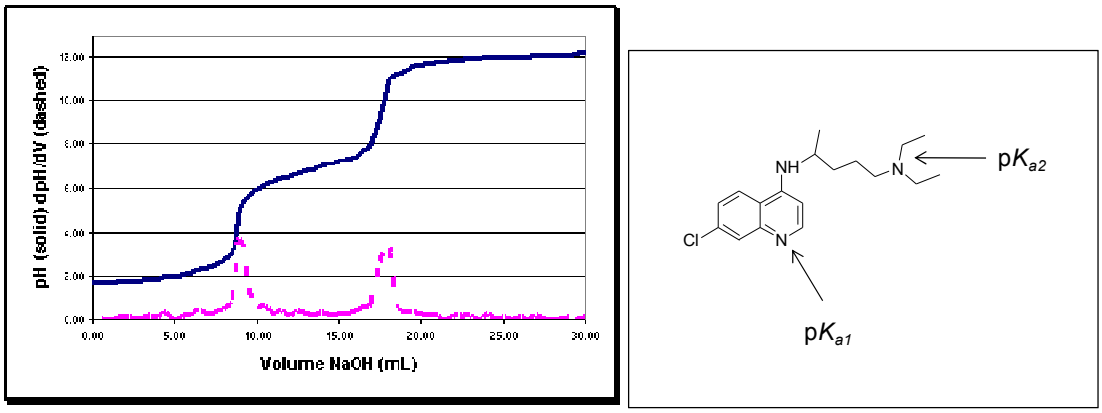

Figure 12. Schematic pH titration curve of diprotic acid with strong base.
(blue – pH Vs Volume of NaOH; pink – dpH/dV Vs volume of NaOH)[13]

Since CQ has three nitrogen atoms, three pK values could be measured, but we are mainly concerned with the pK_a's of the quinoline and tertiary side chain N due to their higher basicity over NH. pK_{a1} corresponds to the basicity of the quinoline N and pK_{a2} corresponds to that of tertiary side chain N. pK_a values for complexes **1-4** and CQDP are contained in Table 5 and our values of pK_{a1} and pK_{a2} of 9.69 and 8.12 for CQDP are similar to previously reported values.[14]

For the metal complexes, we first note that in the π-bonded Ru–CQDP complex **4** the basicity is only modestly reduced with respect to free CQDP (pK_{a1} and pK_{a2} of 9.31 and 7.91). On the other hand, in complexes **1–3**, the quinoline nitrogen is blocked by coordination to ruthenium and therefore only pK_{a2} values are measured, and they indicate a considerably lowered basicity with respect to pK_{a1} of CQDP, following the trend **1 < 2 < < 3**. So, it is clear that the incorporation of the arene-Ru fragment modified the basic properties of CQ in an important manner, by blocking the quinoline nitrogen in complexes **1-3**. In the absence of special transport mechanisms, complexes **1-4** as weaker bases would be expected to accumulate in the food vacuole less than CQ, which may be detrimental to the antimalarial potency, however, these effects must be considered in conjunction with lipophilicity characteristics.

Table 5. pK_a values of complexes **1–4**

Compound	pK_{a1}	pK_{a2}
CQDP	9.69	8.12
[Ru(η^6-*p*-cymene)(CQ)Cl_2] – **1**	-	7.91
[Ru(η^6-benzene)(CQ)Cl_2] – **2**	-	7.99
[Ru(η^6-*p*-cymene)(CQ)$(H_2O)_2$]$(BF_4)_2$ – **3**	-	8.92
[Ru(η^6-*p*-cymene)(μ6-CQDP)]$(BF_4)_2$ - **4**	9.31	7.91

Therefore, another parameter of interest for our discussion is the Vacuolar Accumulation Ratio (VAR), which is normally calculated from a simple model of drug accumulation based on the weak base characteristics of the drug and Henderson-Hasselbach considerations. Here VARs were calculated by following the form of Henderson-Hasselbach equation as described by Biot et al.[24]

$$VAR = 10\ [\log D(6.6) - \log D(4.9)]$$

D (6.6) corresponds to the distribution coefficient of the drug at cytosolic pH whereas *D*(4.9) corresponds to that of at vacuolar pH. VAR aids the understanding of the extent of drug accumulation inside the acidic food vacuole of the parasite and corresponding values for complexes **1-4** and CQDP are included in Table 6.

Table 6. VAR values calculated for complexes **1-4**

Compound	VAR
CQDP	44
[Ru(η^6-*p*-cymene)(CQ)Cl_2] – **1**	8
[Ru(η^6-benzene)(CQ)Cl_2] – **2**	7
[Ru(η^6-*p*-cymene)(CQ)$(H_2O)_2$]$(BF_4)_2$] - **3**	15
[Ru(η^6-*p*-cymene)(μ6-CQDP)]$(BF_4)_2$ - **4**	17

In general, the higher the VAR value, the greater the predicted accumulation of the drug within the acidic food vacuole. According to these results, VAR for complexes **1-4** are lower than that for CQDP; this indicates that the complexes will tend to accumulate inside the food vacuole to a lesser extent than CQ in the absence of other effects. However, it is important to keep in mind that VAR values do not say anything about the extent of drug retention inside the food vacuole, which is governed by the action of the PfCRT protein. The correlation between basicity and VAR of complexes with antiplasmodial activity of new Ru-CQ complexes will be discussed in section 3.3.6.

The results obtained so far agree with the idea that our new ruthenium-chloroquine complexes share the main target of action with CQ, heme aggregation, and some physicochemical properties, such as lipophilicity and basicity contribute to their activity.

3.3.6 Structure - activity correlations

Our approach for overcoming CQ resistance is to maintain the main target of CQ (heme aggregation) but to introduce important modifications to the structure of the drug by complexation to a metal containing fragment, as in complexes **1-4**. It is important to relate the study on structural and physicochemical properties of the new metallodrugs with their antiplasmodial activity, particularly against CQ-resistant strains of *P. falciparum* in order to provide a possible explanation for their improved antimalarial activity.

3.3.6.1 Lipophilicity and basicity versus HAIA

First we discuss the relationship between the drug lipophilicity, as measured by aqueous buffer (pH 4.9)/ *n*-octanol partition coefficients (*D*), and the HAIA measured both in aqueous buffer (pH 4.9) and aqueous buffer (pH 4.9)/ *n*-octanol interface.

As can be observed in Figure 13A, the lipophilicity of drugs **1-4** does not display any correlation with HAI_{50} obtained when the assays were carried out in aqueous medium, following standard literature procedures.[9]

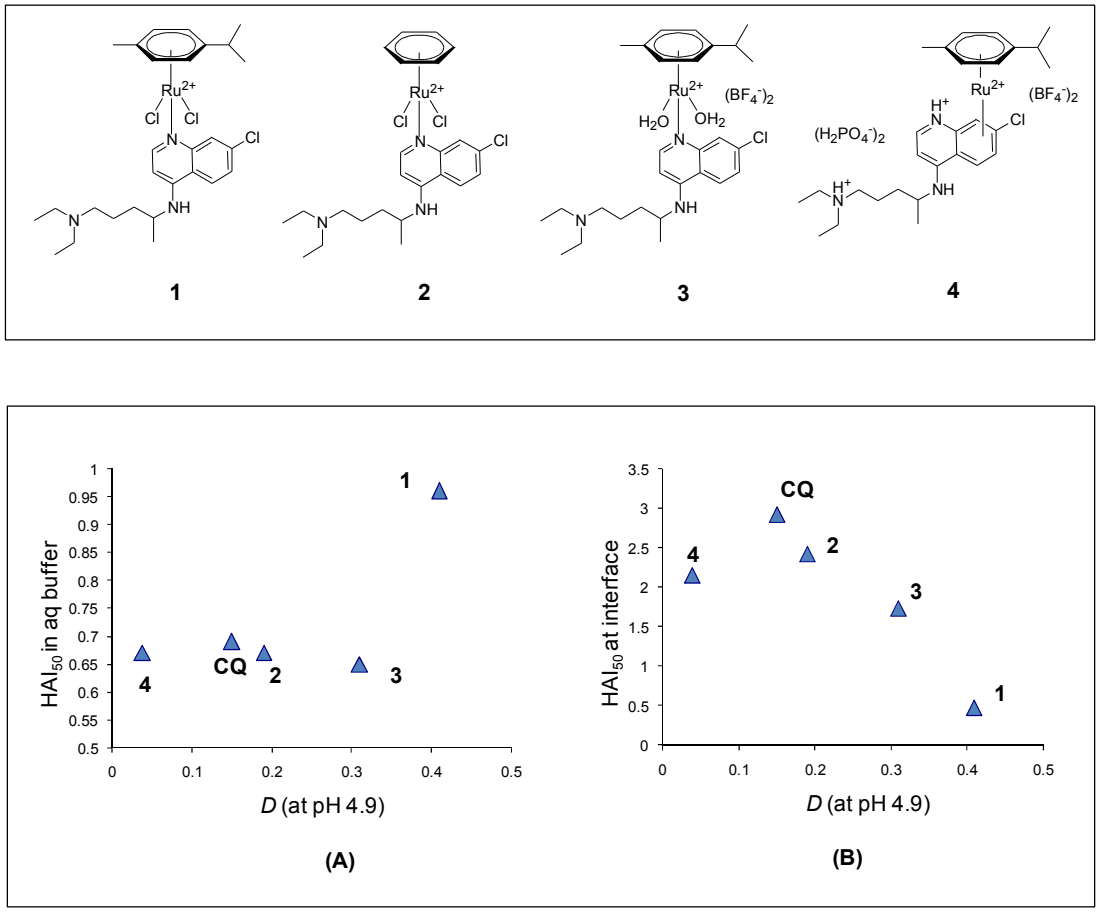

Figure 13 - Correlation between partition coefficients and heme aggregation inhibition activity for chloroquine diphosphate and complexes **1–4** (A) in aqueous acetate buffer (pH 4.9) and (B) at an aqueous acetate buffer (pH 4.9)/*n*-octanol interface

On the other hand, the data for CQ and complexes **1-4** measured at the aqueous acetate buffer (pH 4.9)/*n*-octanol interface (Figure 13B), following the method developed in our laboratory, clearly show that the HAI_{50} values of the structurally related complexes **1–3** decreases smoothly as the lipophilicity increases; this is reasonable, since the effective concentration of increasingly lipophilic compounds will be higher near the interface, where the aggregation process is believed to take place.

Complex **4**, on the other hand, does not fall within the correlation, most likely due to the fact that the structure of **4**, containing a diprotonated π-bonded CQDP ligand and a high overall charge of +4, is very different from the structures of all the other complexes under study, which are monocationic or dicationic and contain neutral CQ bonded to ruthenium through the nitrogen atom of the quinoline ring. In the case of compound **4** other factors besides lipophilicity must be contributing to the higher activity of the complex in relation to that of free CQ, but the data available do not allow a full interpretation of this fact.

Also, as demonstrated in section 2.4.9, the metal complexes display a considerably lower basicity than CQ owing to the fact that the most basic site, the quinoline nitrogen atom, is blocked by ruthenium and cannot be protonated. Nevertheless, their HAIA is consistently higher than that of CQDP at the interface (Table 9); this implies that at a water/*n*-octanol interface at pH 4.9, lipophilicity is a dominant factor over basicity in determining HAIA.

3.3.6.2 HAIA versus antiplasmodial activity against CQ-resistant strains

As described in the previous section, lipophilicity trends of the structurally related compounds correlate well with HAIA values measured at water/*n*-octanol interfaces. It is important to establish whether the HAIA values measured using our method adequately model and correlate well with antimalarial potency of the Ru–CQ compounds.

A comparison of HAI_{50} values measured at the water/*n*-octanol interface with the IC_{50} obtained from the antimalarial activity experiments on CQ-resistant strains of *P. falciparum* is presented in Table 7. Values in parentheses in red represent the relative activity compared to CQDP for which an activity of 1.0 was assigned.

Table 7. HAI_{50} values measured at the water/*n*-octanol interface with the IC_{50} obtained from the antimalarial activity experiments on CQ-resistant strains of *P. falciparum*

Compound	HAI $_{50}$ at at interface	IC_{50} (nM)		
		Dd2	K1	W2
CQDP	2.92 **(1.0)**	1184 ± 188 **(1.0)**	1883 ± 165 **(1.0)**	2155 **(1.0)**
1	1.47 **(2.0)**	483 ± 110 **(2.5)**	600 ± 87 **(3.1)**	1667 **(1.3)**
2	2.42 **(1.2)**	442 ± 30 **(2.7)**	508 ± 84 **(3.7)**	1619 **(1.3)**
3	1.73 **(1.7)**	234 ± 41 **(5.0)**	353 ± 61 **(5.3)**	906 **(2.4)**

The IC_{50} values measured for the activities of the structurally related complexes **1–3** against the CQ-resistant strains Dd2, W2, and K1 (Chapter 2, Table 15) demonstrate that the metal complexes are consistently more active than CQ, in agreement with the HAIA measurements near water/*n*-octanol interfaces. It is interesting to consider the possible factors governing this good qualitative correlation.

Careful examination of the IC_{50} vs. lipophilicity (at pH 4.9) data in Figure 14 reveals that the enhanced lipophilicity of structurally related complexes are mainly responsible for the improved antimalarial activity against CQ-resistant parasites.

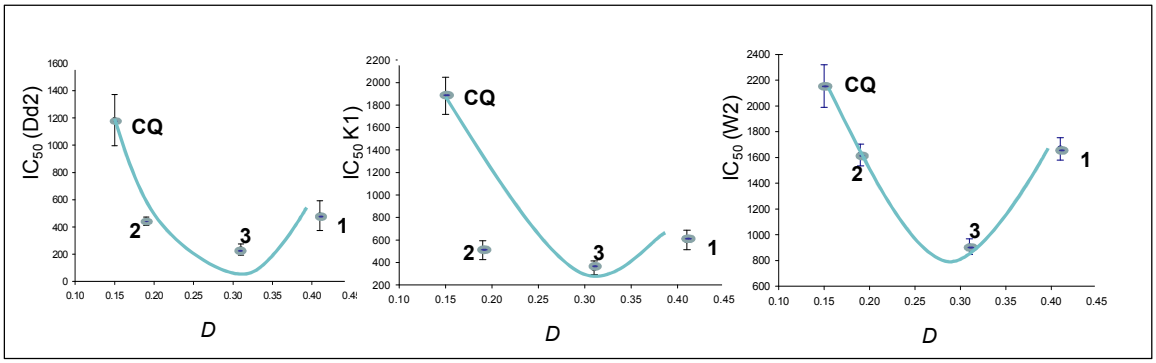

Figure 14. Correlation between lipophilicity and antiplasmodial activity against CQ-resistant strains of *P. falciparum* Dd2 (left), K1 (center), and W2 (right) for complexes **1–3** (values for *D* from Table 4; values for IC_{50} from Chapter 2, Table 6)

These findings are in line with recent work indicating that heme aggregation takes place preferentially at water/lipid interfaces[25,26] and with earlier reports relating increased

lipophilicity of drugs with a lower tendency for them to be excreted from the food vacuole of resistant parasites.[27-29] We can argue that if a given lipophilic drug is not expelled by the transmembrane transporter PfCRT, it remains inside the vacuole near water/lipid interfaces. Thus it should display an enhanced HAIA, which translates into a higher antimalarial activity against resistant strains.

Although the antiplasmodial activities do not correlate linearly with lipophilicity (lipophilicity trend = **1 > 3 > 2 > CQDP)**, they consistently follow the order **3 > 2 > 1 > CQDP**, going through a maximum potency corresponding to complex **3** for three different CQ-resistant strains of *P. falciparum* (Figure 14). This deviation from linearity means that other factors like basicity may come into play in determining antimalarial activity.

In resistant strains, most of the CQ would be effectively expelled from the food vacuole by PfCRT despite its higher basicity and, therefore, its effective concentration is lowered. The weaker bases, Ru-CQ complexes, on the other hand, are probably not expelled from the food vacuole due to their modified molecular structures and their enhanced lipophilicity. In consequence, the net effective concentrations of the metallodrugs would be higher than that of CQ and this explains the higher activity of all the complexes relative to CQ. Once the Ru–CQ combinations overcome the resistance mechanism, the relative basicity of the different complexes on vacuolar drug accumulation may become dominant. In agreement with this hypothesis, compound **3** has the highest basicity (basicity trend = **3 > 2 > 1 > CQDP)** and highest VAR (VAR = **3 > 2 > 1 > CQDP)** values for the set of compounds **1-3**, and it displays the highest antiplasmodial activity. Thus we can conclude that the basicity and VAR differences

observed for complexes **1–3** may account for the deviations from linearity observed in the correlation trends between lipophilicity/HAI_{50} at the interface and antimalarial activity against chloroquine resistant strains. It is important to note at this point that calculated values have been shown to deviate strongly from experimentally determined values.[29] We therefore place more weight for our interpretations on the direct relations we find between the antimalarial potency against resistant parasites and the experimentally determined lipophilicity, basicity and HAI_{50} values measured at water/*n*-octanol interfaces. This point is discussed in more detail in Chapter 5.

3.3.6.3 HAIA versus antiplasmodial activity against CQ-sensitive strains

A comparison of HAI_{50} values measured at the water/*n*-octanol interface with the IC_{50} obtained from the antimalarial activity experiments on CQ-sensitive strains of *P. falciparum* is presented in Table 8. Values in parentheses in red represent the relative activity compared to CQDP for which an activity of 1.0 was assigned.

Table 8 - HAI_{50} values measured at the water/*n*-octanol interface with the IC_{50} obtained from the antimalarial activity experiments on CQ-sensitive strains of *P. falciparum*

Compound	HAI_{50} at at interface	IC_{50} (nM)		
		FcB1	PFB	F32
CQDP	2.92 **(1.0)**	45.6 ± 4.5 **(1.0)**	58.3 ± 8.5 **(1.0)**	8.2 ± 1.3 **(1.0)**
1	1.47 **(2.0)**	120.0 ± 4.0 **(0.3)**	109.0± 15.1 **(0.5)**	11.5 ± 1.8 **(0.7)**
2	2.42 **(1.2)**	81.6 ± 1.2 **(0.5)**	79.0 ± 4.9**(0.7)**	13.2 ± 0.2 **(0.6)**
3	1.73 **(1.7)**	96.5 ± 6.0 **(0.4)**	122.6 ± 15.2 **(0.5)**	22.5 ± 0.4 **(0.4)**

For the CQ-sensitive strains of *P. falciparum* FCB1, PFB, and F32, the activities of the Ru–CQ complexes are generally lower than those of CQ, in disagreement with the higher HAI_{50} values measured at the water/*n*-octanol interface. Also, a curious inverse correlation between the lipophilicity of the complexes and their antimalarial activity is

observed (Figure 15); the activity of complexes **1–3** actually decreases with increasing lipophilicity.

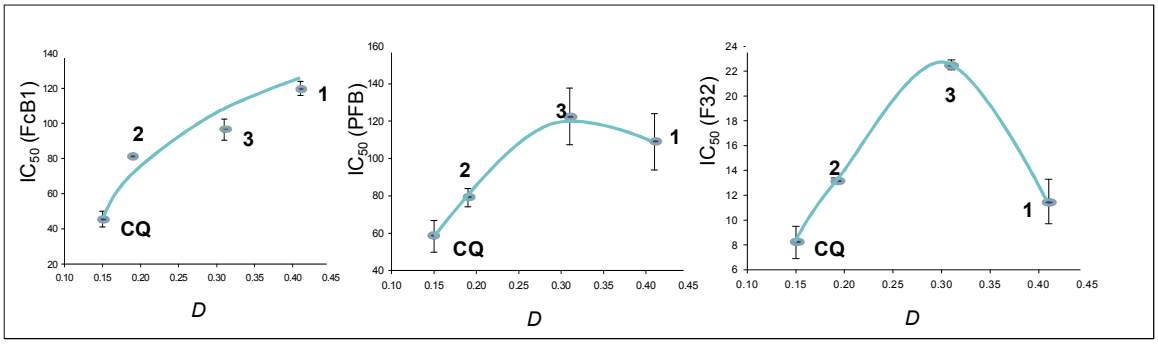

Figure 15. Correlation between lipophilicity and antiplasmodial activity against CQ-sensitive strains of *P. falciparum* FCB1(left), PFB (center), and F32 (right) for complexes **1–3** (values for *D* from Table 4; values for IC_{50} from Chapter 2, Table 6)

Nevertheless, the lower activity values of complexes **1-3** compared to those of CQDP against CQ-sensitive strains are in agreement with the lower basicity of the complexes, as compared with CQ, when resistance mechanisms are not operative. Due to lower basicity, the concentration of complexes **1-4** inside the acidic food vacuole must be lower than that of CQ and this translates into the lower activity of ruthenium–CQ complexes against CQ sensitive strains. No correlations could be established in the case of the 3D7 strain, or for complex **4**.

3.4 Conclusion

We have measured the water/*n*-octanol partition coefficients, p*K*a values, heme binding constants, and heme aggregation inhibition activity in water and at water/*n*-octanol interfaces of new ruthenium-(π-arene)-CQ complexes, in order to understand their improved biological activity. Some interesting tendencies emerge from our data as follows.

The heme aggregation inhibition activity of complexes **1-4** is significantly higher than that of CQDP at the interface of *n*-octanol/aqueous acetate buffer mixtures at pH 4.9, and together with HAI_{50} values correlate well with the antiplasmodial activity against CQ resistant strains of *P. falciparum*. This suggests that heme aggregation is the principal target of the ruthenium–CQ complexes and measuring HAIA of potential drugs near water/*n*-octanol interfaces is a better predictor of antimalarial potency than the standard tests in aqueous acidic buffer especially against CQ-resistant strains.

We further conclude that the enhanced antimalarial activity of new ruthenium – CQ complexes against CQ -resistant strains of *P. falciparum* is related to a delicate balance of effects related to the lipophilicity, the basicity, and structural details of the compounds studied, where the lipophilicity and the structural features appear to play the most prominent roles.[30]

3.5 References

1. http://en.wikipedia.org/wiki/Chloroquine
2. Egan, T. J.; Hunter, R.; Kaschula, C. H.; Marques, H.M.; Misplon, A.; Walden, J, *J. Med. Chem.* **2000**, *43*, 283
3. Biot, C.; Taramelli, D.; Forfar-Bares, I.; Maciejewski, L. A.; Boyce, M.; Nowogrocki, G.; Brocard, J. S.; Basilico, N.; Olliaro, P.; Egan, T. J. **2005**, *Mol Pharm*. *2*, 185–193
4. OECD guidelines for testing of chemicals, **1995**, no 107, OECD, Paris
5. Danielsson, L. G.; Zhang, Y. H. *Trends Anal Chem,* **1996**, *15*, 188–196
6. Rappel, C.; Galanski, M.; Yasemi, A.; Habala, L. ; Keppler, B.; *Electrophoresis,* **2005**, 26, 878–884
7. Egan, T. J.; Mavuso, W. W.; Ross, D.; Marques, H. *J. Inorg. Biochem.* **1997**, 68, 137– 145
8. Biot, C.; Taramelli, D.; Forfar-Bares, I.; Maciejewski, L. A. ; Boyce, M.; Nowogrocki, G.; Brocard, J. S.; Basilico, N.; Olliaro, P.; Egan, T. J. *Mol Pharm.* **2005**, 2, 185–193
9. Parapini, S.; Basilico, N.; Pasini, E.; Egan, T. J.; Olliaro, P.; Taramelli, D.; Monti, D. Exp. Parasitol. **2000**, *96*, 249–256
10. Martinez, A.; Rajapakse, C. S. K.; Naoulou, B.; Kopkalli, Y.; Davenport, L.; Sanchez-Delgado, R. A. *J. Biol. Inorg. Chem*., **2008**, *13*, 703–712
11. Egan, T. J.; Ross, D. C.;Adams P.A.; *FEBS Leet*. **1994**, *352*, 54
12. Collier, G. S,; Pratt, J. M.; De Wet, C. R.; Biochem. **1979**, *179*, 281
13 http://science.csustan.edu/CHEM1112_4/Diprotic/

14. Biot, C.; Taramelli, D.; Forfar-Bares, I.; Maciejewski, L. A.; Boyce, M.; Nowogrocki, G.; Brocard, J. S.; Basilico, N.; Olliaro, P.; Egan, T. J. **2005**, *Mol Pharm. 2*, 185–193

15. Egan, T. J.; Mavuso, W. W.; Ross, D.; Marques, H. *J. Inorg. Biochem.* **1997**, 68, 137– 145

16. Parapini, S.; Basilico, N.; Pasini, E.; Egan, T. J.; Olliaro, P.; Taramelli, D.; Monti, D. **2000**, *Exp Parasitol*. *96*, 249–256

17. Pagola, S.; Stephens, P. W.; Bohle, D. S.; Kosar, A.D.; Madsen, S. K, *Nature,* **2000**, *404,* 307–10

18. Bohle et.al. **1997**, *Biol. Chem. 272*, 713-716

19. Egan, T. J.; Chen, de Villiers, K. A.; Mabotha, T. E.; Naidoo, K. J.; Ncokazi, K. K.; Langford, S. J.; McNaughton, D.; Pandiancherri, S.; Word, B. R. **2006**, *FEBS Lett. 580*, 5105–5110

20. Benjamin, I. **2004**, *Chem. Phys. Lett*. *393*, 453–456

21. Martinez, A.; Rajapakse, C. S. K.; Naoulou, B.; Kopkalli, Y.; Davenport, L.; Sanchez-Delgado, R. A. *J. Biol. Inorg. Chem*., **2008**, *13*, 703–712

22. Gulyaeva, N.; Zaslavsy, A., **2002**, *Eur. J. Pharm. Sci*., *17*, 81-93

23. Ursos, L. M. B.; Roepe, P. D. **2002**, *Med. Res. Rev. 22*, 465-491

24. Biot, C.; Chavain, N.; Dubar, F.; Pradines, B.; Trivelli, X.; Brocard, J.; Forfar, I.; Dive, D.; **2008**, doi:10.1016/j.jorganchem.2008.09.33

25. http://www.vistamedica.com/main/images/stories/plasmodium_falciparum.jpg.

26. Targeted delivery of drugs for the treatment of parasitic infections - US Patent 7101842 Description.mht

27. Ph. J. Rosenthal, Ed. “Antimalarial Chemotherapy: mechanism of action, resistance and new directions in drug discovery”, Humana Press, New Jersey, 2001

28. Hyanes, R. K. *Curr.Top. Med. Chem.* **2006**, *6*, 509-537

29. O’Neill, P. M.; Posner, G. H. J. *Med. Chem.* **2004**, *47*, 2945-2964

30. Martinez, A.; Rajapakse, C. S. K.; Naoulou, B.; Jalloh, D.; Dautriche, C. Sanchez-Delgado, R.A.; *J. Biol. Inorg. Chem*., **2009**, *14*, 863–871

Chapter 4

DNA as a Potential Target in the Antimalarial Action

4.1 Introduction

DNA has two main functions, namely transcription and replication. Transcription and replication are vital to cell survival and proliferation as well as for smooth functioning of all body processes. DNA starts transcribing or replicating when it receives a signal, which is often in the form of a regulatory protein binding to a particular region of the DNA. If the binding specificity and strength of this regulatory protein can be mimicked by a small molecule, then DNA function can be artificially modulated, inhibited, or activated by binding this molecule instead of the protein. Thus, this synthetic molecule can act as a drug when inhibition of DNA function is required to cure or control a disease. DNA inhibition would restrict protein synthesis, or replication, and could induce cell death. The interaction of metal complexes with DNA has recently received much attention because this interaction indicates that the complex may have potential biological and pharmaceutical activity. The activity of the drug depends on the mode and affinity of the molecule for DNA.

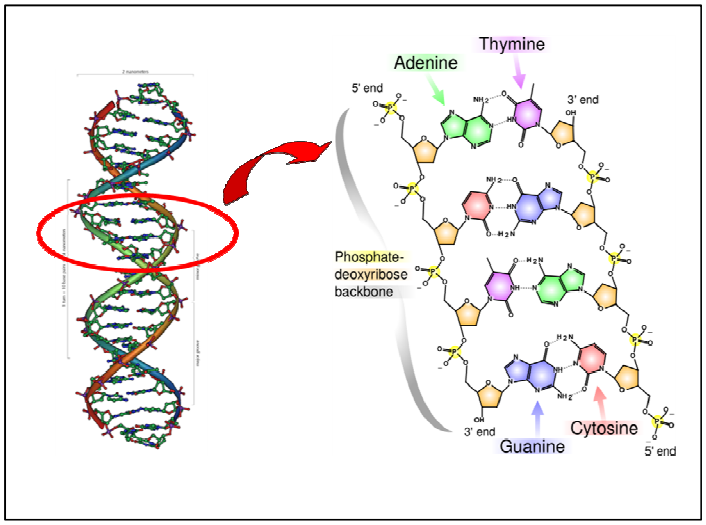

Figure 1. DNA double helix
(*Ref* : http://www.frontiers-in-genetics.org/en/pictures/dna_3.gif)

Metal complexes are known to interact with DNA both covalently as well as non-covalently.[1] Covalent binding in DNA is irreversible and leads to complete inhibition of DNA processing and consequently, cell death. Cisplatin (cis-diamminedichloroplatinum) (Figure 2A) is a well-known covalent binder used as an anticancer drug that acts by making an intra strand cross-link with the nitrogens on the DNA bases (Figure 2B).

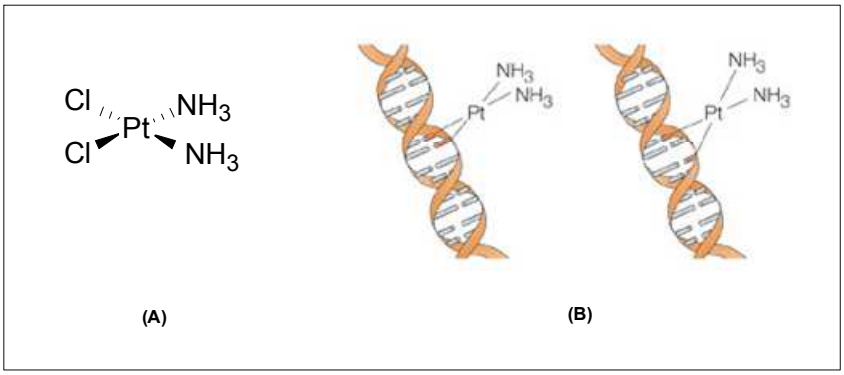

Figure 2. (A) cisplatin, (B) DNA adduct formation with cisplatin (covalent binding) leaving two amino groups coordinated on the platinum atom

Non-covalently bound drugs mostly fall under three classes, external binding, groove binding and intercalation. $[Ru(bpy)_3]^{2+}$ is an example of an external binder (Figure 3). This association is electrostatic in nature. Cations such as Mg^{2+} usually interact in this way also.

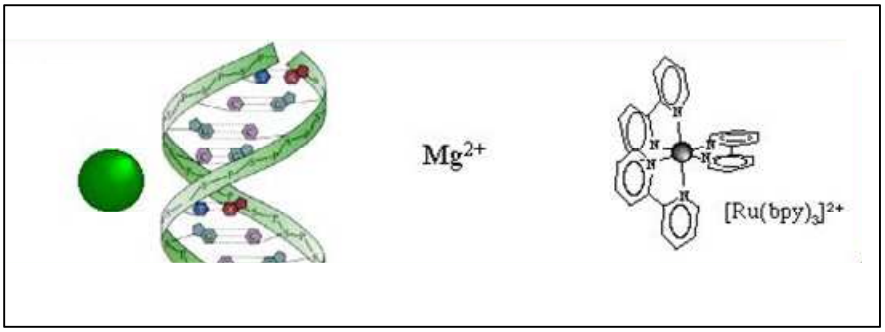

Figure 3. Schematic diagram to show external binding[2] (e.g.- Mg^{2+} and $[Ru(bpy)_3]^{2+}$)

A second non covalent binding mode is groove binding (Figure 4). Groove binding drugs are usually semi-circular shaped, which complements the shape of the groove and facilitates binding by promoting Van der Waals interactions. Additionally, these drugs can form hydrogen bonds to bases. This type of binding stabilizes the DNA. The antibiotic netropsin as well as a ruthenium complex $[Ru(TMP)_3]^{2+}$ (TMP = 3,4,7,8-tetramethyl phenanthroline) are two examples for model groove-binders.

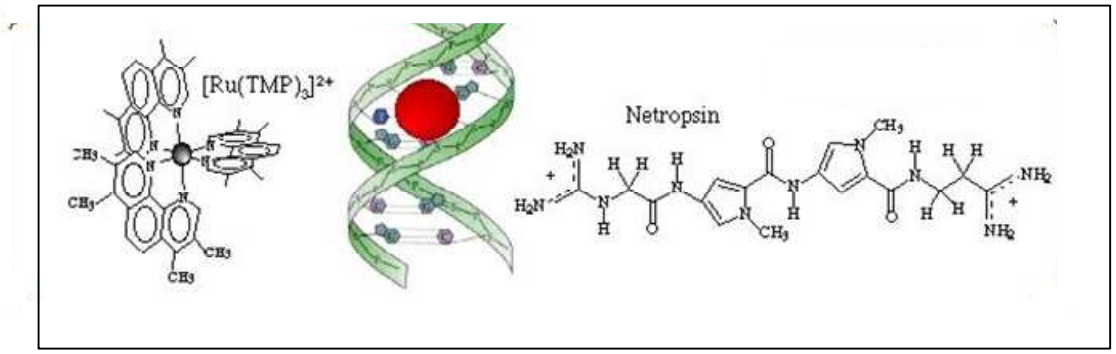

Figure 4. Schematic diagram to show groove binding[2] of a complex with DNA

Intercalators contain planar heterocyclic groups which stack between adjacent DNA base pairs by π-π stacking interactions between the drug and DNA bases (Figure 5). Intercalators introduce strong structural perturbations in DNA. Ethidium bromide and $[Ru(Phen)_2PHEHAT]^{2+}$ are two common DNA intercalators.

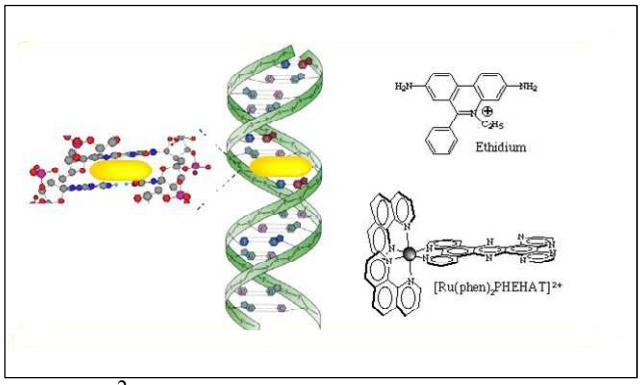

Figure 5. Intercalation[2] of a planar ligand of the complex between stacked DNA base pairs

As mentioned earlier, platinum complexes owe their antitumor activity to strong covalent interactions with the nucleobases of DNA. DNA is also likely the target of many octahedral ruthenium (III) and (II) compounds that exhibit antitumor properties, such as [arene-ruthenium(II)(en)X][PF_6] complexes (Figure 6) and *cis* and *trans* $RuCl_2$(dimethylsulfoxide)$_4$ (Figure 7).[3] Among these, a deeper investigation on the mechanism of arene-ruthenium(II) complexes shows that the phosphate groups in the nucleotides are the initial binding site, leading to subsequent covalent binding of ruthenium to the base. In addition, the arene group of these complexes may act as an intercalator as well as a minor groove binder to double helical DNA.[4]

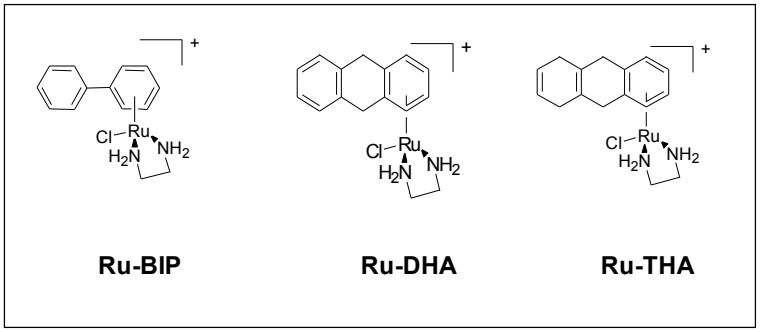

Figure 6. Structures of [arene-ruthenium (II) XYZ] family of complexes[4]

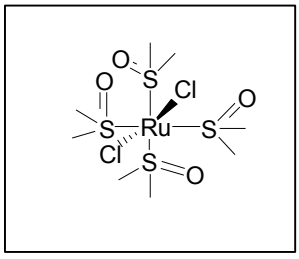

Figure 7. Structure of *trans*- [Ru(II)(dmso)$_4$$Cl_2$]

Also of interest in our work, it is well known that CQDP is able to bind to DNA through intercalation of the quinoline ring along with electrostatic interactions of the ionic side chain and the phosphate groups of DNA.[5-7]

DNA binding was considered the major mechanism of antimalarial action of CQ for many years.[8] There have been some attempts to revive this hypothesis in recent times[9,10] and acridine-based related antimalarials are thought to exert their action predominantly or partially via DNA interactions.[11-13] In complexes **1-4**, introduction of a ruthenium containing fragment into the structure of CQ produces a dramatic modification in terms of the electronic structure and the physicochemical properties of the molecule and makes DNA binding in principle, available as part of a potential secondary mechanism of antimalarial action. Metal–DNA binding is a common phenomenon and the modification of CQ by attachment to a metal-containing fragment could reopen the possibility of DNA as a major or secondary target of therapeutic action. In order to investigate this possibility, the DNA binding ability of the new metal derivatives **1-4** was investigated and compared with that of CQDP.

4.2 Experimental Section

4.2.1 Interaction of complexes with CT DNA

4.2.1.1 UV spectroscopic titration

The binding constants for complex–calf thymus DNA interactions were determined by absorption titration at room temperature through the stepwise addition of a CT DNA solution (10 μL, 1.56 mM) to a cell containing each complex (2 mL, 25 μM), both in 10 mM phosphate buffer containing 50 mM $NaClO_4$ (pH 7.2).

Absorption was recorded at 330 and 343 nm and the titration was terminated when the intensity at those wavelengths did not change significantly upon further addition of DNA. An excellent fit for two binding constants, K_{b1} and K_{b2}, was obtained by using the Scatchard equation r/Cf = K(n-r) for ligand–macromolecule interactions with non-cooperative binding sites,[14,15] where r is the number of moles of ruthenium complex bound to 1 mol of CT DNA (C_b/C_{DNA}), n is the number of equivalent binding sites, and K is the affinity of the complex for those sites. Concentrations of free (C_f) and bound (C_b) complexes were calculated from $C_f = C(1 - \alpha)$ and $C_b = C - C_f$, respectively, where C is the total ruthenium concentration. The fraction of bound complex (α) was calculated from $\alpha = (A_f - A)/(A_f - A_b)$, where A_f and A_b are the absorbances of free and fully bound complex at the selected wavelengths, and A is the absorbance at any given point during the titration. The plots of r/C_f versus r give the binding constants K_b as the slopes of the graphs.

4.2.1.2 Thermal denaturation experiments

Melting curves were recorded in media containing 50 mM $NaClO_4$ and 5 mM Tris-HCl buffer (pH 7.29). The absorbance at 260 nm was monitored for solutions of CT

DNA (2.5 mM) before and after incubation with a solution of the drug under study (1 mM in Tris-HCl buffer) for 1 h at room temperature. The temperature was increased by 0.5 ^{0}C min^{-1} between 65 and 82 ^{0}C and by 3 ^{0}C min^{-1} between 25 and 65 ^{0}C and between 82 and 97 ^{0}C.

4.2.1.3 Viscosity experiments

Viscosity experiments were carried using an Ostwald viscometer, immersed in a thermostated water-bath maintained at a constant temperature of 25 ^{0}C. The DNA concentration was kept constant in all samples (500 μM), but the complex concentration increased from 50 μM to 1 mM. The flow time was measured with a digital chronometer and each sample was measured three times and an average flow time was used. Data are presented as $(n/n_0)^{1/3}$ versus the ratio [complex]/[DNA] , where n is the viscosity of CT-DNA in the presence of complex , and n_0 is the viscosity of CT-DNA alone. Viscosity values were calculated from the observed flow time of DNA-containing solutions, corrected for the flow time of buffer alone (t_0) $n = t-t_0$

4.3 Results and Discussion

4.3.1 Spectrophotometric titration

Absorbance (UV-Visible) titration is a powerful technique to detect and quantify DNA-drug interactions. Absorbance values for each new compound (and CQDP as control) were recorded at 330 and 343 nm, with stepwise addition of CT DNA to a cuvette containing a solution of each drug; the titration was terminated when the intensity of those bands did not change significantly upon further addition of DNA. The absorbance bands under study are due to the $\pi \rightarrow \pi^*$ transition of the aromatic rings of CQ. As shown in Figure 8 the intensity of the bands at 330 and 343 nm in complex **4** decreases with increasing addition of CT DNA, clearly indicating that an interaction is taking place. Similar behavior was observed when a CQDP control solution or solutions of complexes **1-3** were titrated with CT DNA.

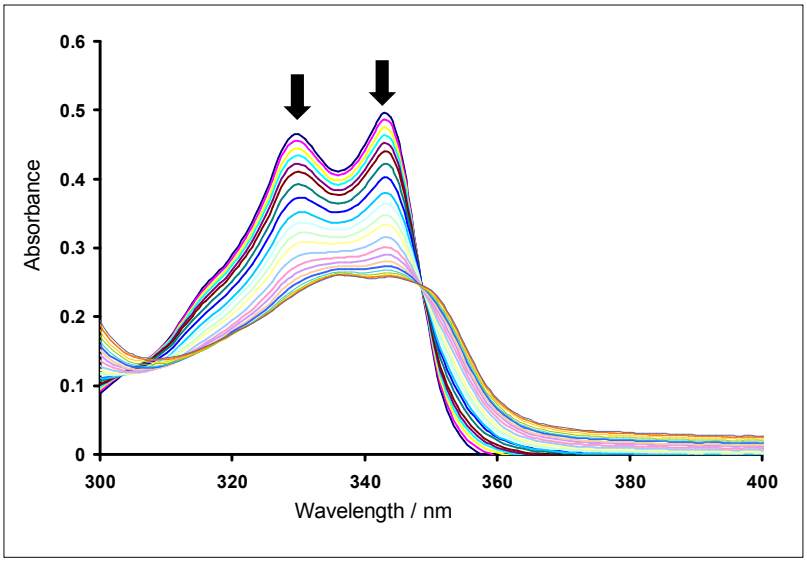

Figure 8. Spectrophotometric titration of metal-CQDP complex **4** with CT DNA in 5 mM Tris/HCl, 50 mM $NaClO_4$ buffer, pH = 7.39

There are several ways to linearize binding data, including the methods of Lineweaver-Burke and Eadie-Hofstee. However, a widely used method is to create a Scatchard plot (Figure 9).[16] The Scatchard equation can be written as $r/C_f = K(n-r)$ for ligand -macromolecule interactions with non-cooperative binding sites, where *r* is the number of moles of ligand bound to 1 mol of CT DNA , *n* is the number of equivalent binding sites, and *K* is the affinity of the ligand for those sites. C_f is the concentration of free ligand. The plot of r/C_f vs. r gives the binding constants K_b as the slopes of the graphs.

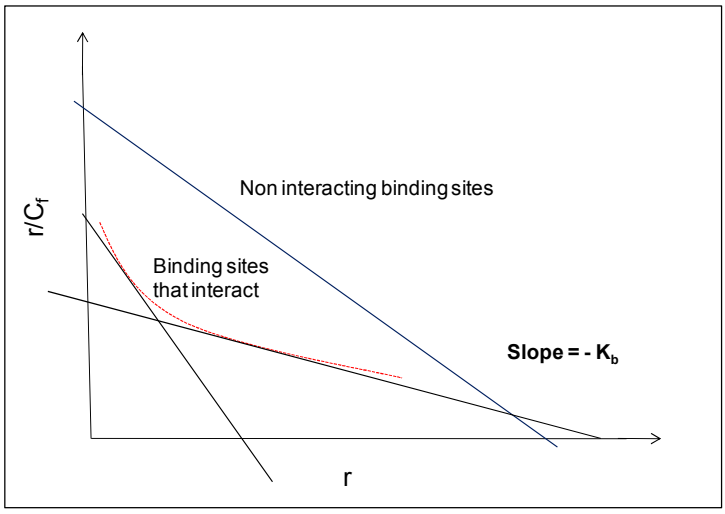

Figure 9. Scatchard plot; two types of Scatchard plots are illustrated, the upper blue line represents binding to a macromolecule with noninteractive sites, the lower red dashed line represents binding of ligand molecules to binding sites that interact.[16]

In many macromolecules such as DNA and proteins, the binding of the first ligand to the macromolecule can change the affinity for the second ligand. This can lead to cooperative binding,[16] an important regulatory mechanism in biochemistry.

Also there are examples of non cooperative association in which the binding of a ligand molecule at one site of the macromolecule is independent of the binding of the

second ligand molecule at another site. Whether binding is cooperative or not can be determined from the shape of the Scatchard curves. If the sites do show cooperative binding, the plot is nonlinear as shown by the red dashed line in Figure 9. This curve can be used to determine the number of types of binding sites. The dashed line in Figure 9 can be resolved into two lines, indicating that two types of binding sites are present on a macromolecule. The binding constant K_b for each type of binding site may be estimated by resolving the smooth curve into straight lines as shown in Figure 9. When there is a non interacting binding, the plot is linear (solid blue line).

In our case, as shown in Figure 10, two binding affinities can be calculated from the Scatchard plot, from the changes at 343 nm for complex **4,** corresponding to two major binding interactions with cooperative effects.[17-20] The same treatment at 330 nm gives two independent affinities that can be averaged with those at 343 nm to obtain two binding constant values (K_{b1} and K_{b2}). A Similar treatment was carried out for data obtained from spectrophotometric titrations for the other arene-ruthenium (II)-CQ complexes **1-3** as well as for CQDP and the corresponding values for the two binding constants (K_{b1} and $K_{b2)}$ at the two wavelengths are contained in Table 1.

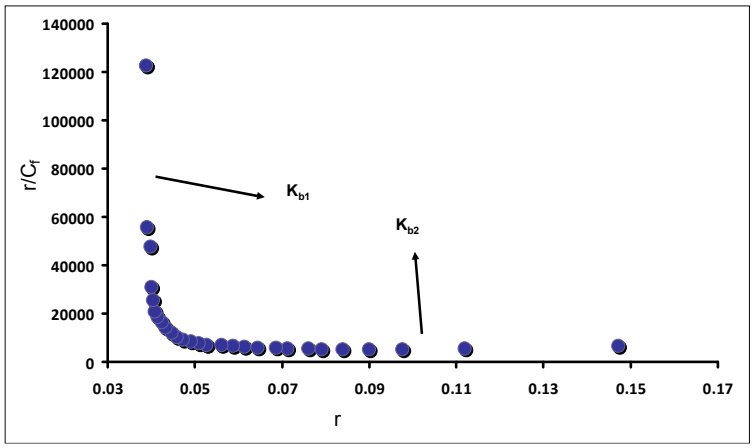

Figure 10. Scatchard plot of data for complex **4** at 343 nm used to calculate K_{b1} and K_{b2}

Table 1. Binding affinities of complexes **1-4** calculated by absorbance titrations at 25^0C in 5 mM Tris/HCl, 50 mM $NaClO_4$ buffer at 7.39

Compound	K_{b1} (x 10^7 M^{-1})[a]	K_{b2} (x 10^5 M^{-1})[a]
CQDP	1.07 ± 0.050	1.23 ± 0.680
[Ru (η^6-*p*-cymene)(CQ)Cl_2] – **1**	0.75 ± 0.040	2.09 ± 0.890
[Ru (η^6-benzene)(CQ)Cl_2] – **2**	2.07 ± 0.070	3.24 ± 0.730
[Ru (η^6-p-cymene)(CQ)$(H_2O)_2$]$(BF_4)_2$ – **3**	0.13 ± 0.001	0.38 ± 0.470
[Ru (η^6-*p*-cymene)(μ^6-CQDP)]$(BF_4)_2$ - **4**	2.10 ± 0.680	3.15 ± 0.120

[a] – Average of values calculated at 330 and 343 nm

K_{b1} and K_{b2} for CQDP are 1.07 x 10^7 M^{-1} and 1.23 x 10^5 M^{-1}, respectively, and the corresponding values obtained for metal-chloroquine complexes are within the same range. From these data we can conclude that the interaction of complexes **1-4** with CT DNA is essentially analogous to that of free CQ. It has been known for some time that CQ binds to DNA[21-27] involving at least two kinds of interaction, one of electrostatic nature between the positively charged diethylammonium side chain and negatively charged phosphate residues in the nucleic acid,[28-30] and a second one, involving intercalation between nucleobases. As seen by the results in Table 1, the binding ability of the new ruthenium-chloroquine complexes is very similar to that of CQDP. This suggests that the most probable binding mode for Ru-CQ complexes is intercalation of the quinoline ring of CQ, coupled with electrostatic interactions of the protonated side chain of chloroquine with the phosphate groups of the DNA.

In order to obtain further evidence for this proposal, a series of other complementary techniques, such as thermal denaturation experiments and viscosity measurements, were employed.

4.3.2 Thermal denaturation experiments

The DNA melting technique is a sensitive and easy tool to detect even slight DNA conformational changes. DNA melting temperature is the temperature at which a DNA double helix dissociates into single strands. The melting temperature (T_m) is normally defined as the temperature at which 50% of the DNA molecules have denatured into random coils. The melting temperature depends on both the length of the molecule, and the specific nucleotide sequence composition of that molecule.

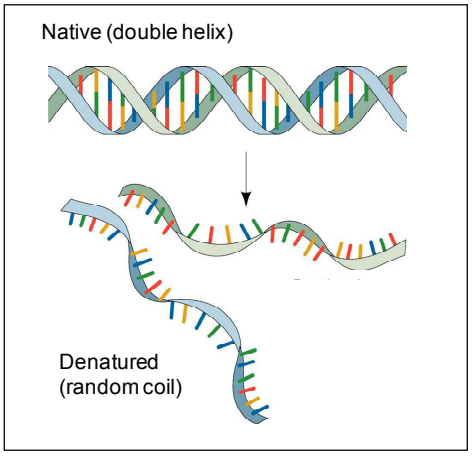

Figure 11. Thermal denaturation of DNA (*Ref*: www.siumed.edu/.../nucleic_acids.html)

It is well known that the covalent interaction of a compound with the double helix destabilizes the DNA (Figure 12) and this lowers the melting temperature, relative to that of DNA itself. Cisplatin and other covalently bonded drugs force DNA to bend and unwind, weakening hydrogen bonds and the stacking interactions between bases.[21] This DNA bending also results in an increase of phosphate repulsions, thereby destabilizing the DNA.

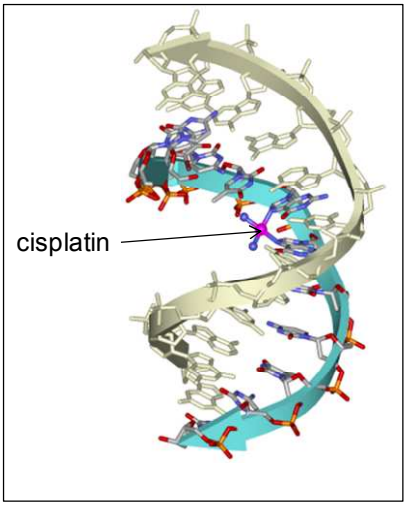

Figure 12. Covalent binder bends the DNA double helix[31]

Intercalation or electrostatic interactions (Figure 13), on the other hand, induce an increase of the $T_{m,}$ because this type of binding stabilizes the DNA.[32] Intercalating drugs increase the distance between phosphates thereby minimizing electrostatic repulsions. Favorable stacking interactions between bases and the intercalator stabilize the double helix. This results in a higher T_m value.

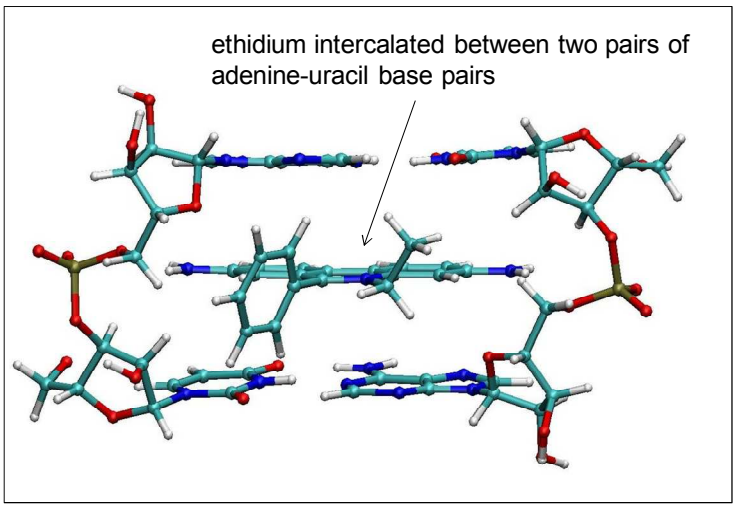

Figure 13. Intercalator bound to double strand DNA[33]

In order to probe the mode of binding of ruthenium-chloroquine complexes with DNA, thermal denaturation experiments were carried out. Solutions of CQDP and of each complex (**1-4**) were incubated with DNA for one hour at 25^0C and the melting curves were recorded by measuring the absorbance at 260 nm as the solution was heated. The melting curve of free DNA is shown in Figure 14A and the corresponding melting curves for metal-CQ complexes are shown in Figure 15. As the temperature increases, the absorbance is increased smoothly and reached a maximum absorbance value where all DNA are melted. The melting temperature can be easily obtained from the first derivative of the melting curve.

Table 2 shows the variation of the melting temperatures of DNA (ΔT_m) after incubation with CQDP, complexes **1-4** and $[Ru^{II}(\eta^6\text{-}p\text{-cymen})(en)Cl]PF_6$, a known covalent binder, as a reference.

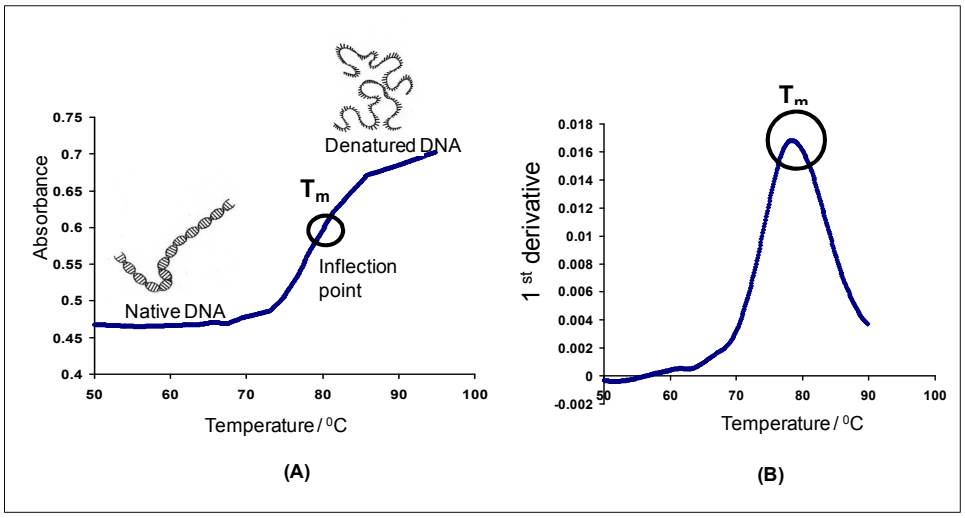

Figure 14. Schematic diagram of (A) melting curve for free DNA, (B) first derivative of a melting curve.

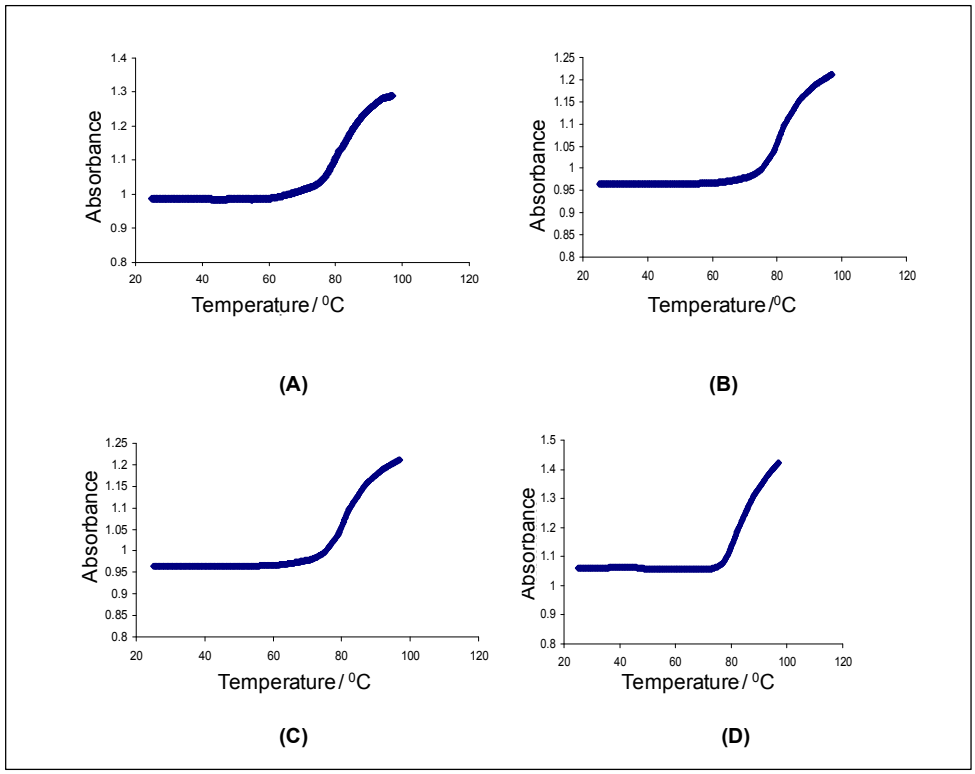

Figure 15. Melting curve of DNA modified by (A) complex **1**; (B) complex **2**; (C) complex **3**; (D) complex **4**.

ΔT values > 0, are indicative of intercalation of the complexes into DNA, while ΔT values < 0 indicate covalent binding of complexes to DNA.

Table 2. Change in the T_m of CT-DNA, when incubated with 0.5 equivalents of each complex for 1h at 25^0C in 5mM Tris/HCl buffer, pH = 7.39.

Complex	ΔT_m (^{0}C) / 1h incubation
CQDP	+ 3.0
1	+ 4.0
2	+ 3.5
3	+ 2.9
4	+ 2.8
[Ru(η^6-*p*-cymene)(en)Cl](PF$_6$)	- 0.6

The results obtained from our thermal denaturation experiments led us to two main conclusions: 1) a covalent interaction between ruthenium and the nucleobases seems not to take place since the ΔT values are positive and similar to that of CQDP. It is accepted that a covalent interaction would commonly destabilize the DNA and thus should result in negative ΔT values such as in the case of cisplatin and $[Ru^{II}(\eta^6$-arene)(en)Cl]PF_6. 2) Most probably complexes **1-4** interact with DNA through electrostatic interactions and intercalation, as has been previously described for free CQDP. This indicates that the attachment of the metal-containing fragment to CQ in complexes **1-4** does not alter the DNA binding properties of CQ to any significant extent.

4.3.3 Viscosity measurements

In order to further support our model for the interaction between the complexes and DNA, viscosity measurements were carried out according to the procedure described in the experimental section. It is well known that if a complex covalently binds to DNA as cisplatin does, it bends the DNA helix, and results in the decrease of the effective length of the helix; as a consequence there is a decrease in the viscosity of the solution. Intercalation (insertion of a ligand) to DNA base pairs, on the other hand, induces a lengthening of the DNA double helix, which produces an increase in the viscosity of the DNA solution.

Varying concentrations of complexes **1-4**, as well as of CQDP, were mixed with CT-DNA to determine the effect of concentration on the flow-time of the DNA solution at 25^0C. The results were plotted as dictated by the theory of Cohen and Eisenberg: $(n/n^0)^{1/3}$ vs [Ru]/[DNA].[34] (n is the viscosity of CT-DNA in the presence of complex, n^0 is the viscosity of CT-DNA). As shown in Figure 16, an increase in the viscosity of

the DNA solutions was observed upon incremental addition of all the ruthenium-CQ complexes and of CQDP, providing further evidence for an intercalation interaction between the new metallodrugs and DNA.

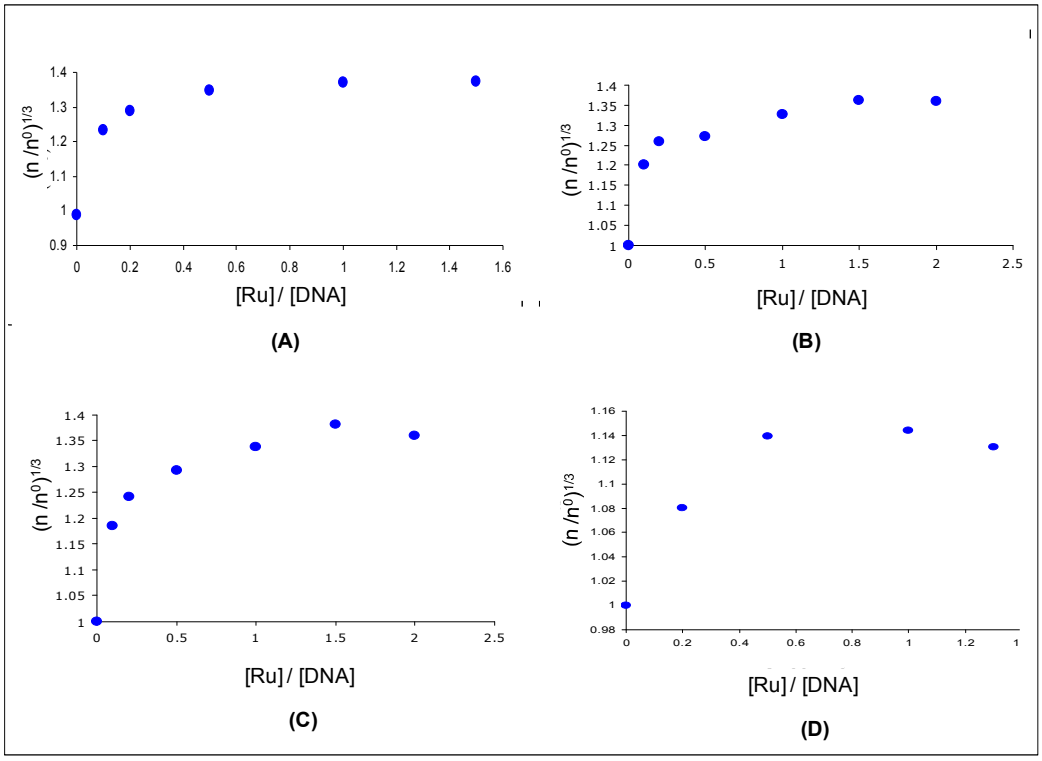

Figure 16. Viscosity curve of (A) CQDP, (B) complex **1**, (C) complex **3**, (D) complex **4**

4.3.4 Structure - activity correlations

DNA binding ability versus antiplasmodial activity

Our results indicate that in spite of the presence of a transition metal in the molecular structure, complexes **1-4** bind to DNA most likely through intercalation and electrostatic interactions of the coordinated CQ moiety, very similarly to the mode of binding of free CQ to DNA. Since all drugs bind to DNA as CQ, we can conclude that the increased potency does not arise from DNA structural changes.

4.4 Conclusion

The attachment of the metal-containing fragment to CQ in complexes **1-4** does not alter the DNA binding properties of CQ to any significant extent and therefore we conclude that the interactions that take place between complexes and DNA do not represent an important component of the mechanism of antimalarial action or of the mechanism of overcoming CQ resistance.[35]

4.5 References

1. http://www.scfbio-iitd.res.in/doc/preddicta.pdf
2. Turro, N.; Barton, J.; Tomalia, D. *Acc. Chem. Res.*, **1991**, *24*, 332-340
3. Gallori, E.; Vettori, C.; Alessio, E.; González-Vilchez, F.; Vilaplana, R.; Orioli, P.; Casini, A.; Messori, L.; *Arch. Biochem. Biophys*, **2000**, 376(1), 156-162
4. Novakova, O.; Chen, H.; Vrana, O.; Rodger, A.; Sadler, P. J.; Brabec, V. *Biochemistry,* **2003,** *42,* 11544-11554
5. Kurnick, N. B.; Radcliffe, I. E., *J. Lab. Clin. Med*., **1962**, *60*, 669-688
6. Cohen, S. N.; Yielding, K. L. *J. Biol. Chem*. **1965**, *240*, 3123-3131
7. Cohen, S. N.; Yielding, K. L., *Proc. Natl. Acad. Sci.*, **1965**, *54*, 521-527
8. Cohen, S. N.; Yielding, K. L. *Proc Nat Acad Sci*, 1965, *54*, 521–527
9. Meshnick, S. R. *Parasitol Today*, **1990**, *6*, 77–79
10. Li, G.D. *Med Hypotheses*, **2006**, *67*, 323–326
11. Guetzoyan, L.; Ramiandrasoa, F.; Dorizon, H.; Desprez, C.; Bridoux, A.; Rogier, C.; Pradines, B.; Perre´e-Fauvet, M. *Bioorg Med Chem*, 2007, *15*, 3278–3289
12. Dheyongera, J. P.; Geldenhuys, W. J.; Dekker, T. G.; Matsabisa, M. G.; Van der Schyf, C. J. *Bioorg Med Chem*, 2005, *13*, 1653–1659
13. Van Miert, S.; Jonckers, T.; Cimanga, K.; Maes, L.; Maes, B.; Lemie`re, G.; Dommisse, R.; Vlietinck, A.; Pieters, L. *Exp Parasitol*, **2004**, 108, 163–168
14. McGhee, J. D.; Von Hippel, P. H. *J. Mol. Biol*. **1974**, *86*, 469–489
15. Wei, C.; Jia, G.; Yuan, J.; Feng, Z.; Li, C. *Biochemistry*, **2006**, *45*,6681–6691
16. http://www.curvefit.com/scatchard_plots.htm
17. McGhee, J.D.; Von Hippel, P. H. *J. Mol. Biol*., **1974**, *86*, 469-489

18. Wei, C.; Jia, G.; Yuan, J.; Feng, Z.; Li, C. *Biochemistry*, **2006**, *45*, 6681-6691

19. Boyer, R. *Biochemistry Laboratory: modern theory and techniques*, **2006**, Benjamin Cummings, 253-260

20. Cusumano, M.; Di Pietro, M. L.; Giannetto, A. *Inorg. Chem*., **1999**, *38*, 1754-1758

21. Irvin, J. L.; Irvin, E. M.; Parker, F. S., *Science*, **1949**, *110*, 426-428

22. Kurnick, N. B.; Radcliffe, I. E., *J. Lab. Clin. Med*., **1962**, *60*, 669-688

23. Cohen, S. N.; Yielding, K. L., *J. Biol. Chem*., **1965**, *240*, 3123-3131

24. Cohen, S. N.; Yielding, K. L., *Proc. Natl. Acad. Sci.*, **1965**, *54*, 521-527

25. O'Brien, R. L.; Olenick, J. G.; Hahn, F. E., *Proc. Natl. Acad. Sci.*, **1966**, *55*, 1511-1517

26. Hahn, F. E.; O'Brien, R. L.; Ciak, J.; Allison, J. L.; Olenick, J. G., *Milit. Med.*, **1966**, *131*, 1071-1089

27. Allison, J. L.; O'Brien, R. L.; Hahn, F. E., *Science*, **1965**, *149*, 1111-1113

28. Scaria, P. V.; Craig, J. C.; Shafer, R. H., *Biopolymers*, **1993**, *33*, 887-895

29. Yielding, K.L.; Blodgett, L.W.; Sternglanz, H.; Gaudin, D., *Prog. Mol. Subcell. Biochem.*, **1971**, *2*, 69-90

30. Geroghiou, S., *Photochem. Photobiol*., **1977**, *26*, 59-68

31. Takahara, P.; Rosenzweig, A.C.; Frederick, C. A.; Lippard, S.J. *Nature*, **1995**, 377, 649

32. Novakova, O.; Chen, H.; Vrana, O.; Rodger, A.; Sadler, P.J.; Bravec, V., *Biochemistry*, **2003**, *42*, 11544-115554

33. wpedia.goo.ne.jp/enwiki/DNA_intercalation

34. Satyanarayana, S.; Dabrowiak, J.C.; Chaires, J. B. *Biochemistry*, **1992**, *31*, No. 39

35. Martinez, A.; Rajapakse, C. S. K.; Varela-Ramirez, A.; Lema, C.; Aguilera, R. J.; Sanchez-Delgado, R. A. *J. Inorg. Biochem*, **2010**, In Press

Chapter 05

New Metal-Free 4-Aminoquinoline Derivatives Are Highly Active against Resistant Strains of *Plasmodium falciparum*

5.1 Introduction

The results obtained from the first phase of our project confirmed the validity of our fundamental concept in that having Ru and CQ in the same molecule may lead to enhanced antimalarial activity against CQ-resistant strains. Also, our work led us to a better understanding of the factors that may be influencing the biological potential of the drugs and their ability to overcome resistance.

The new arene-Ru-CQ complexes (Chapter 2, Scheme 12) display Ru–N coordinate bonds; we demonstrated that this molecular design results in increase in the lipophilicity and a modification in the structure of CQ that produces an enhanced heme aggregation inhibition activity at water-lipid interfaces, which in turn translates into higher potency against CQ-resistant malaria parasites. However, Ru-N coordination also causes a reduction in the basicity of CQ, which probably restricts the ability of the drug to accumulate in the acidic food vacuole and consequently limits its antiplasmodial potential. Therefore, new compounds combining the desired basicity and lipophilicity are needed, in order to preferentially accumulate inside the acidic food vacuole to inhibit heme aggregation while at the same time overcoming CQ resistance.

Although there are some inorganic pharmaceuticals available to treat diseases like diabetes[1] and cancer, no metal containing antimalarials have yet reached clinical use. Pharmaceutical companies still largely rely on organic compounds to develop chemotherapeutic agents rather than metal containing compounds, perhaps more because of habit or prejudice than because of valid chemical or pharmacological reasons. Dr. John McNeill expressed this idea when he talked about vanadium compounds to treat

patients with diabetes *"the other challenge is convincing people that this is real and has potential for working in humans. Drug companies are very skeptical about metals."* [2]

Taking these issues into consideration, in the last part of this project we aimed at preparing new metal-free derivatives of 4-aminoquinoline in which lipophilicity is increased, without reducing the basicity of the molecule.

The hypothesis for this part of the thesis is that modifying 4-aminoquinoline by incorporating a lipophilic organic substituent will not reduce the basicity but will result in structural and physicochemical modifications of the molecule that will lead to improved heme aggregation inhibition ability at water-lipid interfaces and by consequence, higher activity against CQ-resistant parasites.

The hypothesis is supported by the work discussed in previous chapters, together with the following observations.

1. ***Although resistant strains are widespread, 4-aminoquinolines are still used as a treatment for malaria especially against some CQ-resistant strains of P. falciparum.***

Amodiaquine (AQ) is a 4-aminoquinoline antimalarial drug having a CQ-related skeleton (Figure 1), with a phenol group present in the side chain of the structure and it has been shown to be effective in treating some CQ-resistant strains of *P. falciparum*.[3]

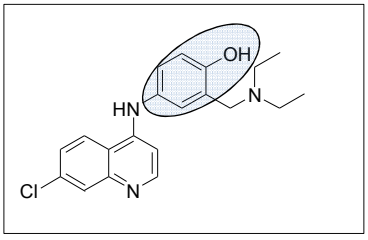

Figure 1. Structure of amodiaquine

For example, the IC_{50} for amodiaquine is 2 nM whereas that for CQ is 15 nM against the CQ-resistant HB3 strain of *P. falciparum* in identical culture conditions.[4] This difference in activity could be due at least in part to the fact that accumulation of amodiaquine is 2- to 3-fold greater than that of CQ in the HB3 isolates, despite the fact that AQ is a weaker base than CQ.[4]

2. Biot and coworkers[7] have shown that incorporation of a lipophilic organoiron moiety to the side chain of CQ results in overcoming CQ resistance.

In the iron-containing drug ferroquine (FQ) (Figure 2A), the metal fragment is incorporated into the side chain of CQ through a C-C link without blocking the basic N atoms. This modification results in high activity and selectivity against CQ-resistant parasites (see Figure 2B) by targeting heme aggregation. The reduced resistance has been ascribed to the presence of the bulky lipophilic organoiron unit.[5]

Since lipophilic compounds are believed to block the PfCRT pore, they proposed that ferroquine may retain the antimalarial properties of CQ while simultaneously blocking PfCRT, like a resistance reversing agent, verapamil. Interestingly, ferroquine is currently in Phase II clinical trials.[6]

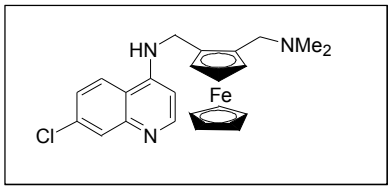

(A)

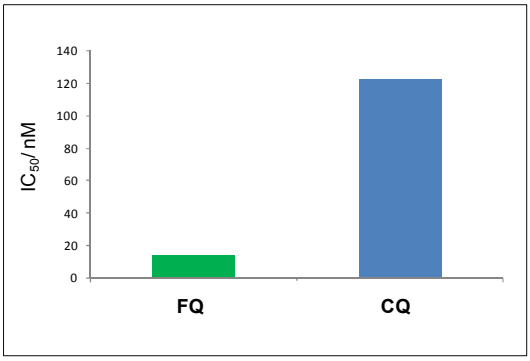

(B)

Figure 2. (A) The structure of ferroquine (FQ), (B) *In vitro* antimalarial activity of CQ and FQ against the Dd2 CQ - resistant strain of *P. falciparum*[5]

Biot's group also made the Ru analogue, ruthenoquine, which displayed very similar antimalarial activity to ferroquine.[5] On the other hand, aminoquinoline drugs other than CQ, such as AQ, are still used as a treatment for some of CQ resistant parasites, but strains resistant to AQ are also reported.[7] ***Consequently, there is a need for other organic compounds based on the aminoquinoline structure, capable of targeting heme aggregation and overcoming CQ resistance.***

The rationale for our molecular design

Our target compounds, generically represented in Scheme 1, represent a promising approach. Two particular advantages must be noted:

(1) Incorporation of an organic moiety to the 4-aminoquinoline structure will increase the lipophilicity without reducing the basicity of the molecule. This modification may provide the necessary lipophilicity for recognition and transport through cell membranes[8] as well as the ability of the drug to overcome PfCRT resistance, while maintaining the drug in the vacuole[9] through pH trapping. The additional ring may engage in π-π interactions with heme, thereby promoting a stronger mode of aggregation inhibition.

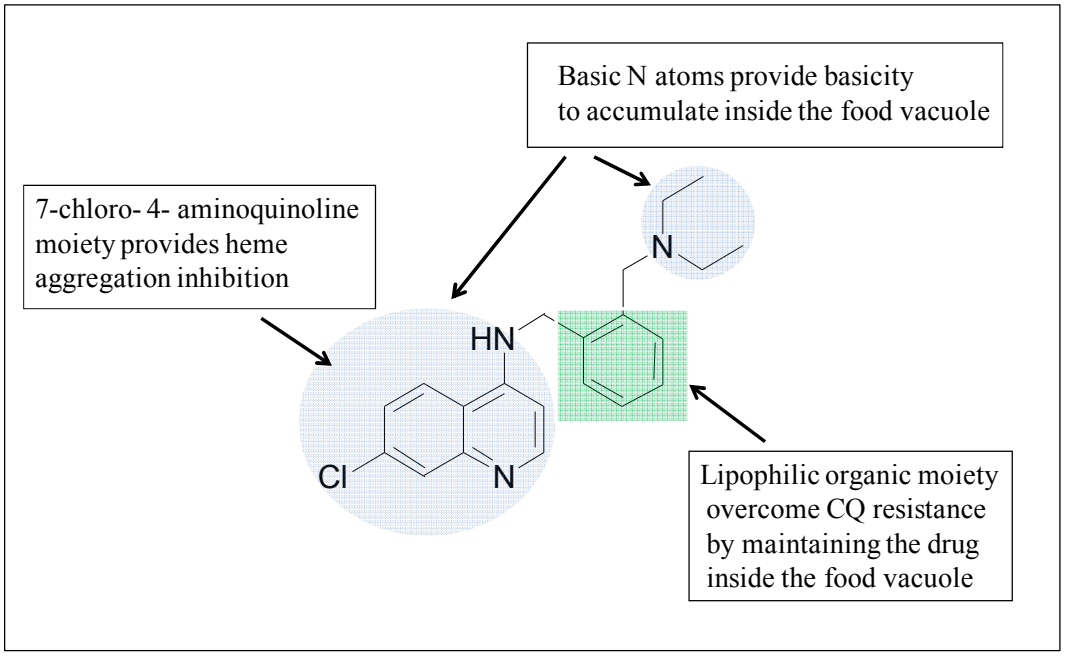

Scheme 1. The rationale for our molecular design

(2) Once synthesized, these new compounds could also serve as ligands for Ru complexes offering the possibility of improved organometallic drugs.

The specific aims we have established for this section of our study are:

1. Synthesis and characterization of new organic derivatives of 4- aminoquinoline not susceptible to resistance by *P. falciparum*.
2. Study of the physicochemical properties relevant to their antimalarial activity: lipophilicity, basicity, binding properties with heme and HAIA at water/*n*-octanol interfaces.
3. Evaluation of their antiplasmodial activity **(**by Prof. J. Schrevel at the National Museum of Natural History, Paris)

Retrosynthesis of new 4-aminoquinoline derivative (4)

Our first new organic 4-aminoquinoline derivative, 7-chloro-N-{(diethylamino) methyl)cyclohexa-1,4-dienyl}quinoline-4-amine **(4)** would be prepared through condensation of 4,7-dichloroquinoline with the desired diene **3**. Diene **3** could be synthesized by Birch reduction of the aromatic diamine **2**. Compound **2** could be readily obtained by nitrile reduction of compound **1**. The commercially available starting material, *ortho*-cyanobenzyl bromide, could be subjected to nucleophilic substitution reaction with diethylamine in order to obtain compound **1**.

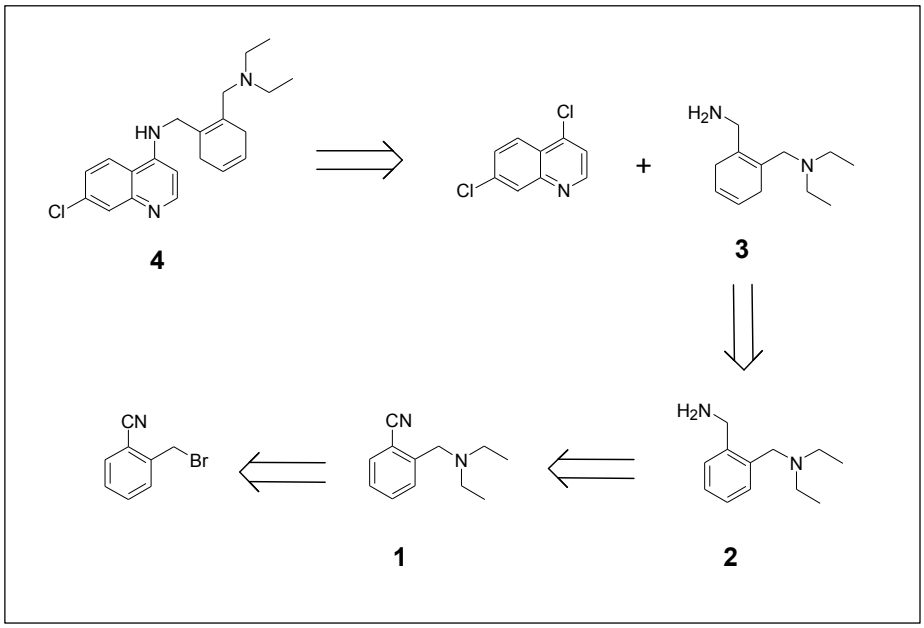

Scheme 2. Proposed retrosynthetic pathway of the new 4-aminoquinoline derivative **4**

Retrosynthesis of new 4-aminoquinoline derivative (5)

Another organic 4-aminoquinoline derivative, (7-chloroquinolin-4-yl)-(2-diethylaminomethylbenzyl)amine **(5)** would be prepared through condensation of 4,7-dichloroquinoline with the desired diamine **2** in the presence of N-methylpyrrolidone

(NMP), K_2CO_3 and triethylamine. Compound **2** could be readily obtained by carrying out a nitrile reduction on compound **1** using $LiAlH_4$. Compound **1** could be synthesized by a nucleophilic substitution reaction on commercially available *o*-cyanobenzyl bromide in the presence of diethylamine.

.

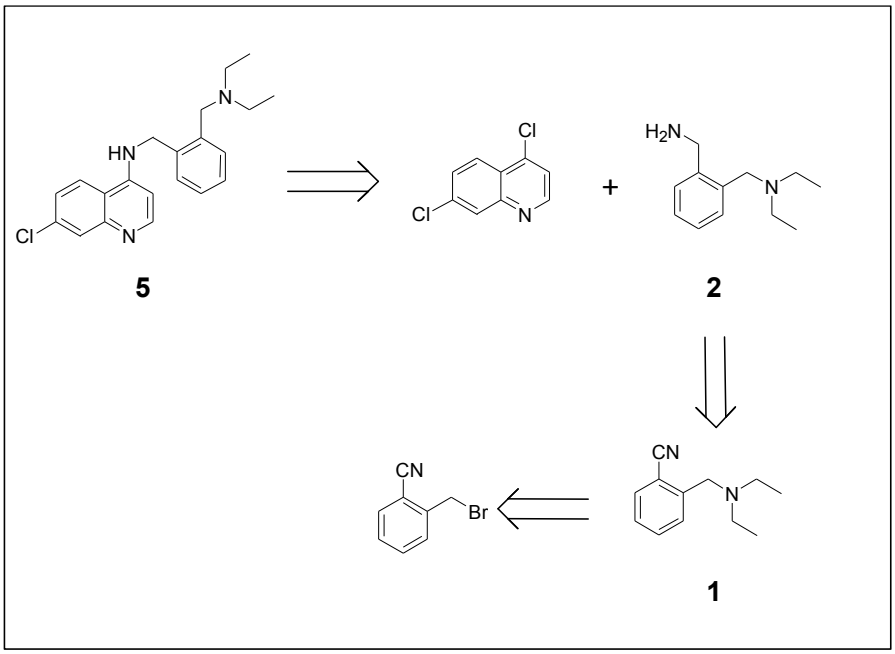

Scheme 3. Proposed retrosynthetic pathway of the new 4-aminoquinoline derivative **5**

5.2 Experimental Section

5.2.1 Reagents and solvents

Solvents (analytical grade, Aldrich) were purified immediately prior to use by means of an Innovative Technology solvent purification unit. *O*-cyanobenzylbromide, chloroquine diphosphate and other reagents (Aldrich) were used as received. Hemin, buffers and solvents were purchased from Sigma-Aldrich. Elemental analyses were performed by Atlantic Microlab, Norcross, Georgia. NMR spectra were obtained using an AVANCE Bruker 400 instrument. UV spectra were obtained with an Agilent 8453 diode-array spectrophotometer equipped with a HP 89090 Peltier temperature control accessory.

5.2.2 Synthesis of compounds

5.2.2.1 Synthesis of (*o*-diethylaminomethyl)benzonitrile (1)

Dropwise addition of 10g (0.05 mol) of *o*-cyanobenzylbromide in 30 mL of ethanol to about 57 mL (0.55 mol) of cold diethylamine was followed by 3 h of stirring at room temperature. The solution became orange and a white precipitate was observed. Twenty mL of 0.1 M Na_2CO_3 aqueous solution was added until the solution became basic to pH paper. At this time the white precipitate was also dissolved. Then the solution was concentrated and extracted into an ether layer. The organic layer was washed with water 3 times to remove ethanol and dried over Na_2SO_4. The dried organic layer was distilled to remove ether and excess diethylamine and the remaining solution was further concentrated under vacuum for 5 minutes. The product was collected as reddish orange colored oil.

Yield= 90%, ^{1}H NMR (400 MHz, $CDCl_3$) δ 7.54 (m, 2H), 7.47 (td, J = 7.52 Hz, J$'$ = 1.43 Hz, 1H), 7.22 (td, J = 6.66 Hz, J$'$ = 0.91Hz), 3.69 (s, 2H), 2.49 (q, J = 7.12 Hz, 4H), 0.98

(t, J = 7.12 Hz, 6H) ,^{13}C NMR (100 MHz, $CDCl_3$) δ 144.70 (C), 132.71 (CH), 132.47 (CH), 129.73 (CH), 117.87 (C), 112.38 (C), 55.69 (CH2), 47.04 (CH2), 11.76 (CH3).

Molecular formula : $C_{12}H_{16}N_2$

ESI-MS $[M+H]^+$ = 189.1313 (cal), 189.1388 (found)

5.2.2.2 Synthesis of *o*-(diethylaminomethyl)benzylamine (2)

O-(diethylaminomethyl)benzonitrile **(1)** (6 g, 32 mmol) in anhydrous diethylether (20 mL) was added dropwise to a suspension of lithium aluminum hydride (2.43 g, 64 mmol) in anhydrous diethyl ether (50 mL, 0 ^{0}C, N_2 atmosphere) within 10 min, allowed to come to room temperature, stirred for 12 h, cooled (ice), treated dropwise with 20% NaOH (17 mL) with cooling, and extracted three times with ether (50 mL each).

The combined organic phases were dried (Na_2SO_4), filtered, and evaporated in vacuo. The product was collected as reddish orange colored oil.

Yield = 79 %, ^{1}H NMR (400 MHz, $CDCl_3$) δ 7.17 (m, 4H), 3.75 (s, 2H), 3.50 (s, 2H), 2.43 (q, J = 7.14Hz, 4H), 1.92 (s, NH_2), 0.962 (t, J = 7.14 Hz, 6H), ^{13}C NMR (100 MHz, $CDCl_3$) 143.68 (C), 137.46 (C), 131.01 (CH), 128.91 (CH), 127.74 (CH), 126.45 (CH), 56.77 (CH2), 46.36 (CH2), 45.05 (CH2), 11.44(CH3).

Molecular formula : $C_{12}H_{20}N_2$, ESI-MS $[M+H]^+$ = 193.1626 (cal), 193.1715 (found)

5.2.2.3 (2-Aminomethyl-cyclohexa-1, 4-dienylmethyl)-diethylamine (3)

A solution of *o*-(diethylaminomethyl)benzylamine **(2)** (1.5 g, 7.8 mmol) in anhydrous ethanol (24 mL) was added to liquid ammonia (25 mL) at –78 ^{0}C . To this mixture was added portion wise Li (540 mg, 10 eq.) over two hours. After quenching with NH_4Cl (1.59 g) in H_2O (7 mL), the solvents were removed, the aqueous suspension

was extracted with CH_2Cl_2, and the organic extracts were dried and concentrated to give the product as a yellow colored oil.

Yield = 89%, ^{1}H NMR (400 MHz, $CDCl_3$) δ 5.72 (m 2H), 3.30 (s, 2H), 3.00 (s, 2H), 2.43 (q, J = 7.12 Hz, 4H), 2.75 (m, 4H), 2.02 (s, NH_2), 1.01 (t, J = 7.23 Hz,6H).

Molecular formula : $C_{12}H_{22}N_2$

ESI-MS $[M+H]^+$ = 195.1783 (cal), 195.1854 (found).

5.2.2.4 Synthesis of 7- chloro -N-((diethylamino)methyl)cyclohexa-1,4-dienyl)quinoline-4-amine (4)

(2-aminomethyl-cyclohexa-1,4-dienylmethyl)-diethylamine **(3)** (951 mg, 4.9 mmol), 4,7-dichloroquinoline (5.0 g, 25 mmol), potassium carbonate (1.0 g, 7.25 mmol), anhydrous triethylamine (5.0 mL, 36 mmol) and anhydrous NMP (7 mL) were placed in a 25 mL round bottomed flask and heated under reflux in an atmosphere of nitrogen for 15 h. The mixture was allowed to cool to room temperature before diluting with ethyl acetate. The product was washed 10 times with brine. Then the product was washed with a large amount of water to remove NMP. The organic layer was dried over sodium sulfate, filtered and the solvent was removed under reduced pressure. The product was purified using two columns and isolated as a white crystalline solid. (Solvent system = ethylacetate: hexane: three drops of Et_3N).

Yield = 50%, ^{1}H NMR (400 MHz,$CDCl_3$) δ 8.45 (d, J = 2.18Hz, 1H), 7.87 (d, J = 2.18 Hz,1H), 7.63 (d, J = 8.95 Hz, 1H), 7.25 (dd, J = 8.92 Hz, J$^{'}$ = 2.12 Hz, 1H), 6.52 (s, NH), 6.36 (d, J = 5.50 Hz, 1H), 5.65 (d, J = 1.24 Hz, 2H), 3.78 (d, J = 4.24 Hz,2H), 2.98 (s, 2H), 2.80 (m, 4H), 2.50 (q, J = 7.11 Hz, 4H), 0.954 (t, J = 7.13 Hz, 6H). ^{13}C NMR (100 MHz,$CDCl_3$) δ 152.12 (CH), 150.49 (C), 149.29 (C), 134.73 (C), 132.19 (C), 129.76 (C),

128.70 (CH), 124.84 (CH), 124.50 (CH), 123.91 (CH), 121.83 (CH), 117.71 (C), 99.00 (CH), 55.08 (CH_2), 46.76 (CH_2), 45.50 (CH_2), 32.33 (CH_2), 31.66 (CH_2), 11.13 (CH_3).

Anal. Calcd for $C_{21}H_{26}N_3Cl$: C, 70.87; H, 7.36; N, 11.81.Found: C, 70.71; H, 7.39; N, 11.70.

ESI-MS $[M+H]^+$ = 356.1815 (cal), 356.1877 (found).

5.2.2.5 Synthesis of (7-chloroquinolin-4-yl)-(2-diethylaminomethylbenzyl)amine (5)

(2-aminomethyl-benzyl)-diethyl-amine **(2)** (0.805 mg, 4.2 mmol), 4-7-dichloroquinoline (5.0 g, 25 mmol), potassium carbonate (1.0 g, 7.25 mmol), anhydrous triethylamine (5.0 mL, 36 mmol) and anhydrous NMP (7 mL) were placed in a 25 mL round bottomed flask and heated under reflux under nitrogen for 15 h. The mixture was allowed to cool to room temperature before diluting with ethyl acetate.

The product was washed 10 times with brine, and then washed with a large amount of water to remove NMP. The organic layer was dried over Na_2SO_4, filtered and the solvent was removed under reduced pressure. The product was purified using a column and it was collected as a yellow crystalline product. (Solvent system ethylacetate: hexane: three drops of Et_3N)

Yield = 50%, ^{1}H NMR (400 MHz, MeOD) δ 8.20 (d, J = 5.59 Hz, 1H), 7.93 (d, J = 8.99 Hz, 1H); 7.68 (d, 1.68 Hz, 1H), 7.29 (dd, J = 9.02, J$^{'}$ = 1.87 Hz, 1H), 7.28 - 7.34 (m, 4H), 6.44 (d, J = 5.62 Hz, 1H), 4.59 (s, 2H), 3.57 (s, 2H), 2.48 (q, J = 7.14 Hz, 4H), 0.935 (t, J = 7.09 Hz, 6H), ^{13}C NMR (100 MHz, $CDCl_3$) δ 152.24 (CH), 150.35 (C), 149.41 (C), 137.37 (C), 132.13 (C), 130.59 (CH), 128.56 (CH), 27.84 (CH), (127.31 (CH), 124.59

(CH), 122.55 (CH), 118.11 (C), 99.16 (CH), 56.31 (CH2), 47.02 (CH2), 46.57 (CH2), 10.48 (CH3).

Anal. Calcd for $C_{21}H_{24}N_3Cl$:C, 71.27; H, 6.84; N, 11.87.Found: C, 71.19; H, 6.85; N, 11.82.

5.2.3 Determination of pK_a values

For the determination of pK_a values, a 1 mM solution of each compound in deionized water was prepared and the appropriate amount of 0.1M HCl (60 - 140 μL) was added to dissolve the compound completely. The determination of pK_a values were carried out by the analogous procedure to that described in Chapter 3 (section 3.2.1).

5.2.4 Determination of partition coefficients

Experiments were carried out by analogous procedure to that described in Chapter 3 (section 3.2.2).

5.2.5 Interaction of compounds with hematin

Experiments were carried out by analogous procedure to that described in Chapter 3 (section 3.2.3).

5.2.6 HAIA at a water/*n*-octanol interface

Experiments were carried out by analogous procedure to that described in Chapter 3 (section 3.2.4.2).

5.2.7 Biological activity evaluation *in vitro*

Experiments were carried out by analogous procedures to those described in Chapter 2 (section 2.3.7).

5.3 Results and Discussion

5.3.1 Synthesis and characterization of new aminoquinoline derivatives 4 and 5

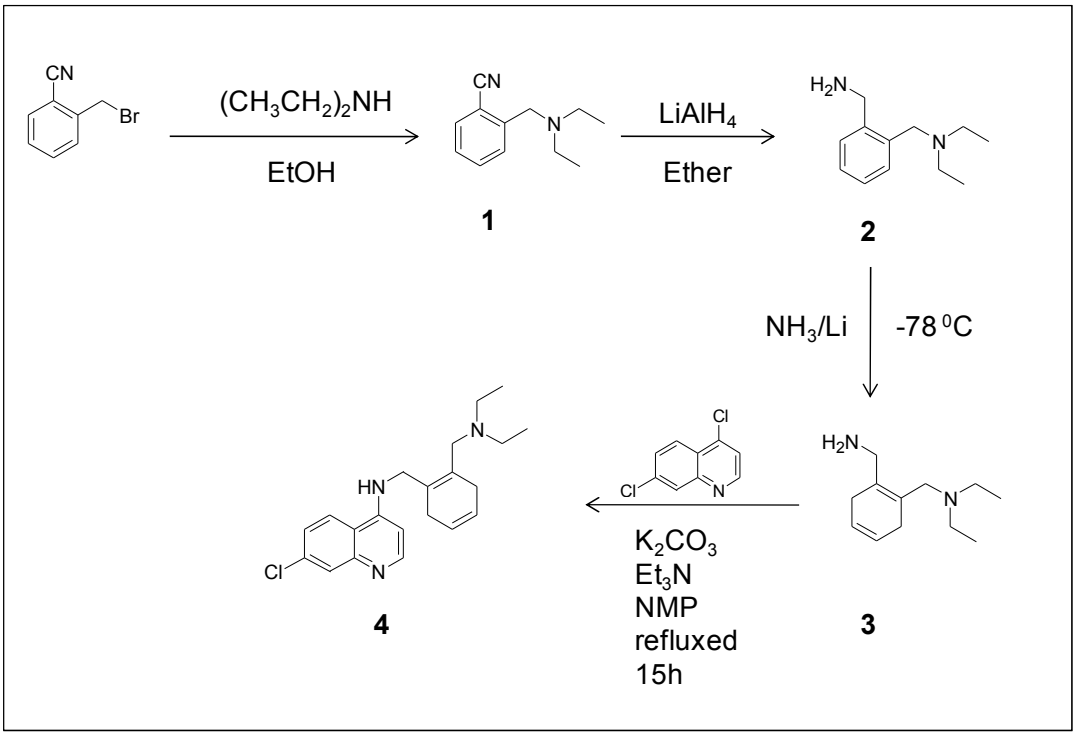

Scheme 4. Preparation of compound **4**

The syntheses were carried out as outlined in Schemes 4 and 5 by following methods analogous to those used to prepare similar compounds, with some modifications. *O*-(diethylaminomethyl)benzylamine **(2)** was synthesized from *o*-cyanobenzyl bromide by a nucleophilic substitution reaction with diethyl amine,[9] followed by lithium aluminum hydride reduction of the nitrile group. Then the benzylamine **2** was subjected to Birch reduction[10] with liquid ammonia and 10 eq of Li at –78 ^{0}C to obtain the corresponding diene **3**. Condensation of **3** with 4,7-dichloroquinoline in N-methyl-2-pyrrolidinone (NMP) produced the new compound (7-chloroquinolin-4-yl)-(2-

diethylaminomethylbenzyl)amine **(4)** which was isolated as a white powder after purification through column chromatography.[11]

Compounds **1-4** were characterized using 1D (^{1}H and ^{13}C NMR) and 2D (COSY, HSQC and HMBC) NMR together with mass spectrometry (see experimental section). The proton and carbon NMR spectra of compound **4** with the signal assignments are shown in Figure 3 and 4 respectively. All other spectra can be found in Appendix.

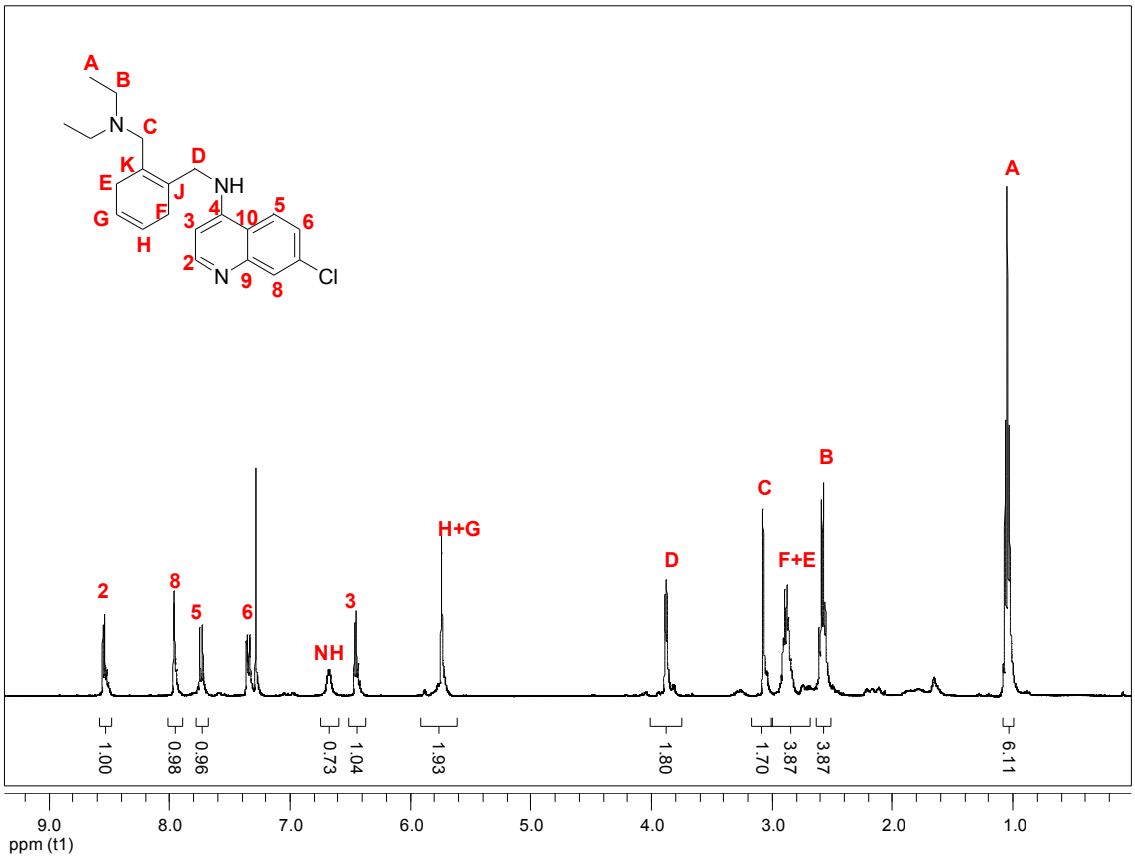

Figure 3. ^{1}H NMR of compound **4** in $CDCl_3$

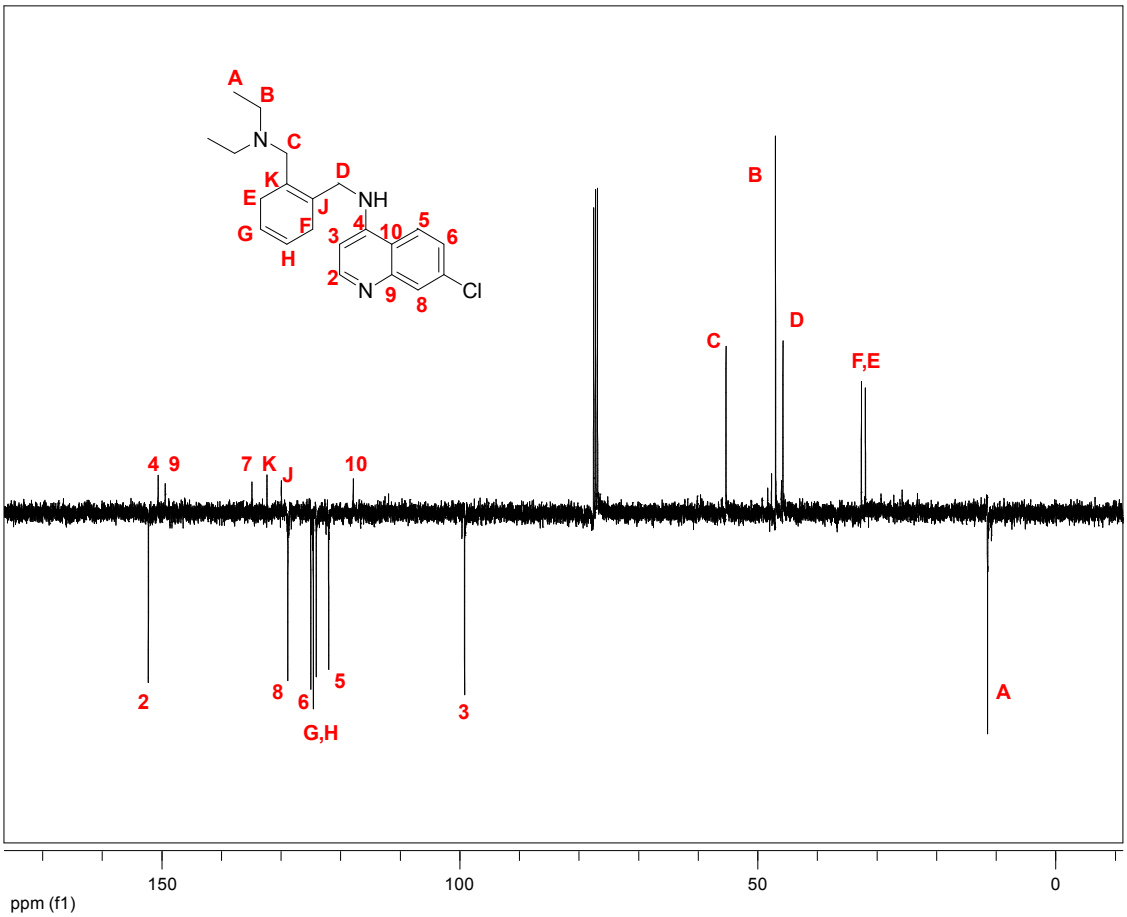

Figure 4. APT (^{13}C) of compound **4** in $CDCl_3$

The new compound **5** was synthesized as follows (Scheme 5).

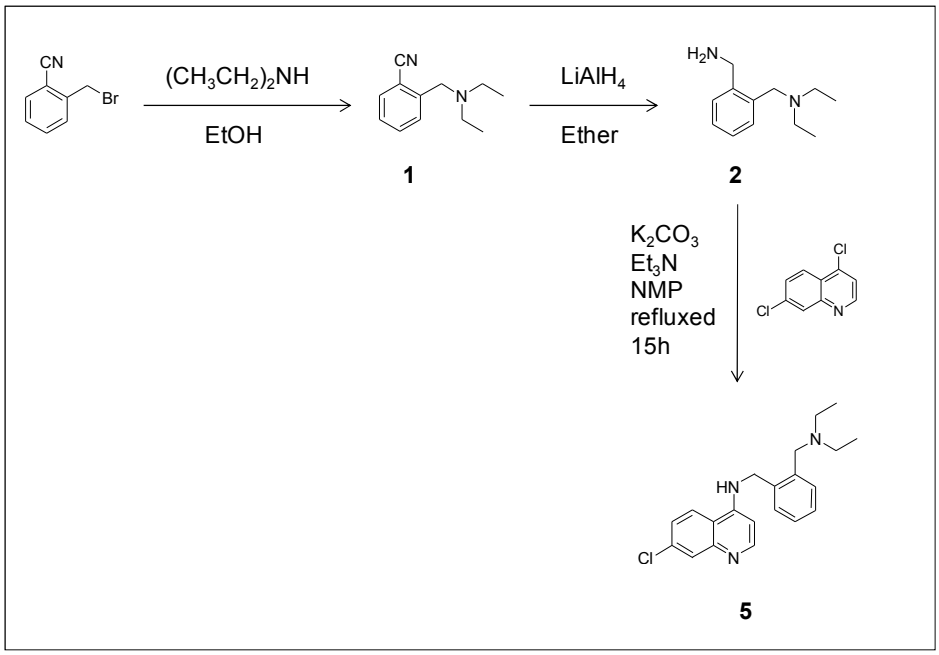

Scheme 5. Preparation of compound **5**

Compound **1** was synthesized by a nucleophlic substitution reaction on commercially available *o*-cyanobenzyl bromide in the presence of diethylamine.[9] Diamine **2** was prepared by carrying out the nitrile group reduction of compound **1** with $LiAlH_4$. Condensation of compound **2** with 4,7-dichloroquinoline in N-methyl-2-pyrrolidinone (NMP) produced (7-chloroquinolin-4-yl)-(2-diethylaminomethylbenzyl)amine **(5)**, which was isolated as a yellow colored crystalline material after purification through column chromatography. Compounds **1**, **2** and **5** were characterized using 1D (^{1}H and ^{13}C NMR) and 2D (COSY, HSQC and HMBC) NMR together with mass spectrometry.

The proton and carbon NMR spectra of compound **5** with the signal assignments are shown in Figure 5 and Figure 6. (All other spectra can be found in Appendix)

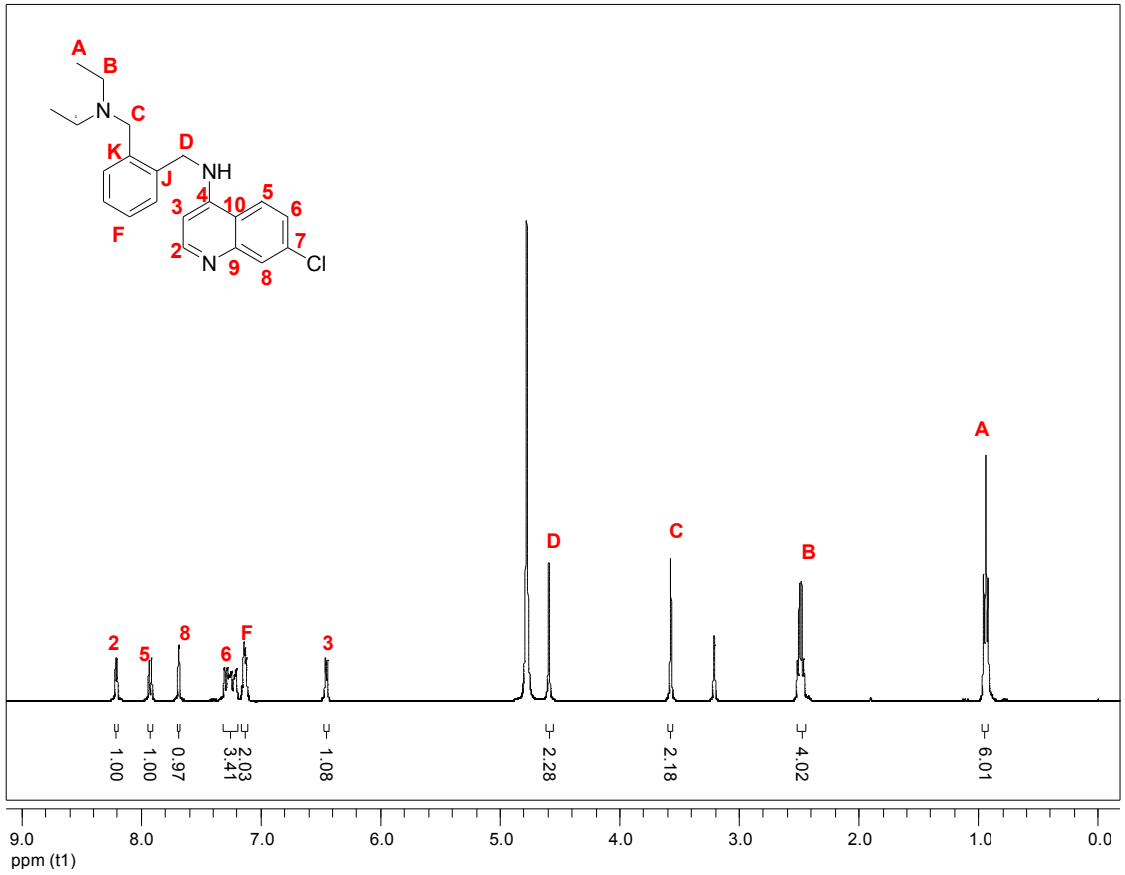

Figure 5. ^{1}H NMR of compound **5** in MeOD

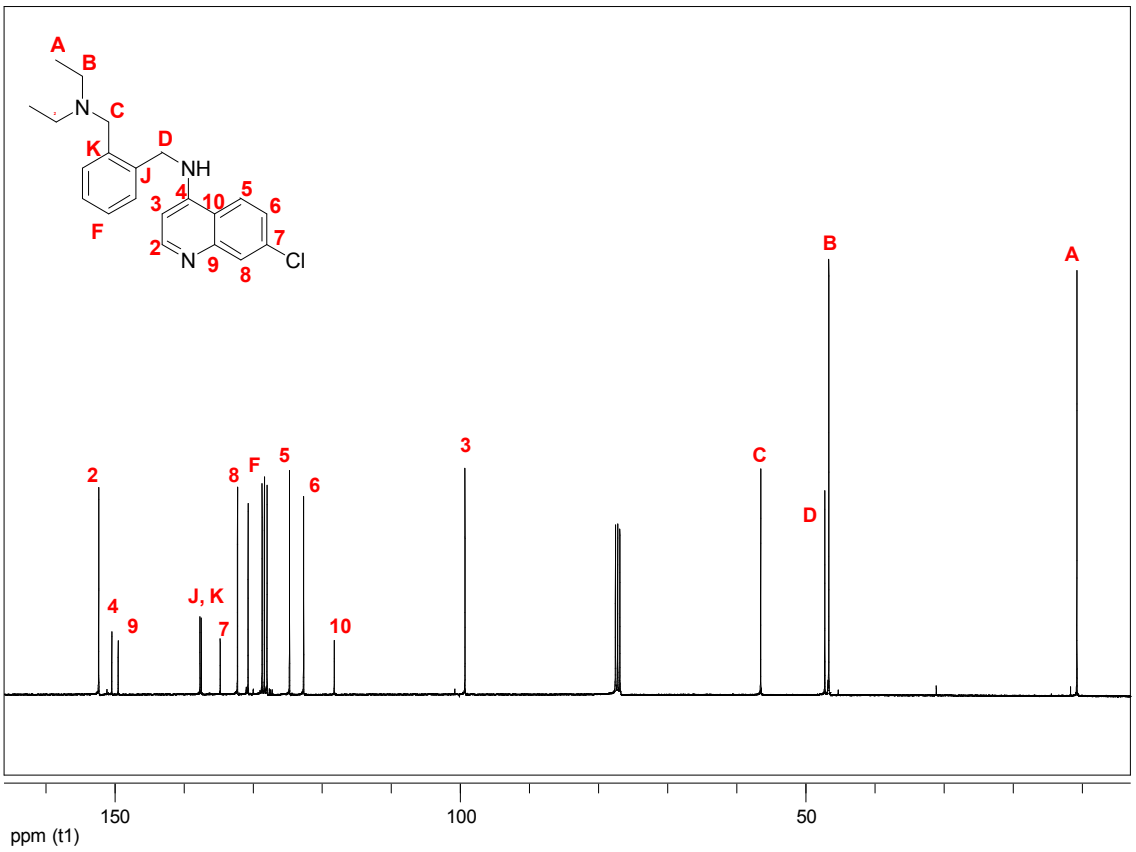

Figure 6. ^{13}C NMR of compound **5** in $CDCl_3$

After we had characterized and tested the antimalarial activity of compounds **4** and **5**, the synthesis and antimalarial properties of a related derivative containing a terminal dimethylamino group instead of diethylamino (Figure 7) was reported.[12]

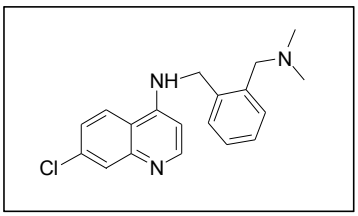

Figure 7. 4-aminoquinoline derivative having dimethyl side chain

5.3.2 Antimalarial activity evaluation *in vitro*

The antiplasmodial activity of the new compounds **4** and **5** was evaluated against a CQ-sensitive strain (D6) and three CQ-resistant strains (K1, K14, and Dd2) of *Plasmodium falciparum* in collaboration with Dr. Joseph Schrevel of the National Museum of Natural History in Paris. The most relevant results are summarized in Table 1. Values in parentheses in red represent the relative activity in each case compared to CQDP for which an activity of 1.0 was assigned.

Table 1. Antimalarial activity of new compounds **4** and **5** against *P. falciparum*

Strain	IC_{50} (nM)		
	CQ	comp **4**	comp **5**
D6	19.1 **(1.0)**	18.18 **(1.05)**	7.23 **(2.6)**
K1	645.47 **(1.0)**	63.74 **(10.1)**	62.8 **(10.3)**
K14	1108.41 **(1.0)**	70.35 **(15.7)**	62.72 **(17.6)**
Dd2	454.1 **(1.0)**	59.02 **(7.7)**	30.82 **(14.7)**

IC_{50} = 50% Inhibitory Concentration (nM)
Relative activity = IC_{50}(CQDP)/IC_{50}(compound)

In the case of the CQ-sensitive strain D6, the activity displayed by the new compound **5** is more than twice that of CQDP, while compound **4** has a comparable activity to CQDP. More importantly, the activities of compounds **4** and **5** against CQ-resistant parasites (Dd2, K1 and K14) are notably higher than that of CQDP. In all cases compound **5** is more active than compound **4**; also, compound **5** is about 18 times more active than CQ against the very resistant strain K14 and compound **4** is about 16 times more active than CQ. Hence, it is clear that the new organic molecules were able to overcome CQ resistance as postulated in our hypothesis. The related compound recently

reported by Chibale et.al. (Figure 7) is also active against CQ-sensitive and CQ-resistant *P.falciparum.*[12]

Once the activity was established, it was important to investigate the factors that determine the improved antimalarial potency of the new compounds **4** and **5,** particularly against CQ- resistant strains, as well as the possible mechanisms of action.

Considering that the principal motif in the new compounds is the 7-chloro-4-aminoquinoline structure, it is reasonable to hypothesize that heme aggregation is retained as the target of action, as has been established for other drugs of this family. Also, our work on Ru-CQ complexes described in the first part of this thesis, led us to conclude that their improved antimalarial activity against CQ-resistant strains is related to a delicate balance of lipophilicity, basicity and structural details, where the lipophilicity and the structural features appear to play the most prominent roles. As a first step toward elucidating the importance of these factors in the activity of the new metal-free drugs we have evaluated some physicochemical properties of compounds **4** and **5**, such as heme binding ability, heme aggregation inhibition activity at water/*n*-octanol interface, pK_a and water-octanol distribution coefficients, and related those features to their antimalarial activity.

5.3.3 Interaction with heme

As described in the first phase of this project, compounds targeting heme aggregation display affinity toward heme. Recent studies on 4-aminoquinoline analogues of CQ also suggested that the 4-aminoquinoline nucleus appears to be essential for complex formation with Fe(III)PPIX.[13] The interaction of compounds **4** and **5** with

monomeric Fe(III)PPIX was studied in 40% aqueous DMSO and 20 mM 2-(N-morpholino)ethanesulfonic acid (MES) buffer (pH = 4.9) at 25^0C.

The absorbance of the Soret band of hematin at 402 nm was monitored as a function of added drug concentration (Figure 8). Then the absorbance data at this wavelength were fitted to a 1:1 association model after corrections for dilution. The calculated values of log K (K = binding constant) for compounds **4**, **5** as well as of CQDP under these experimental conditions are summarized in Table 2.

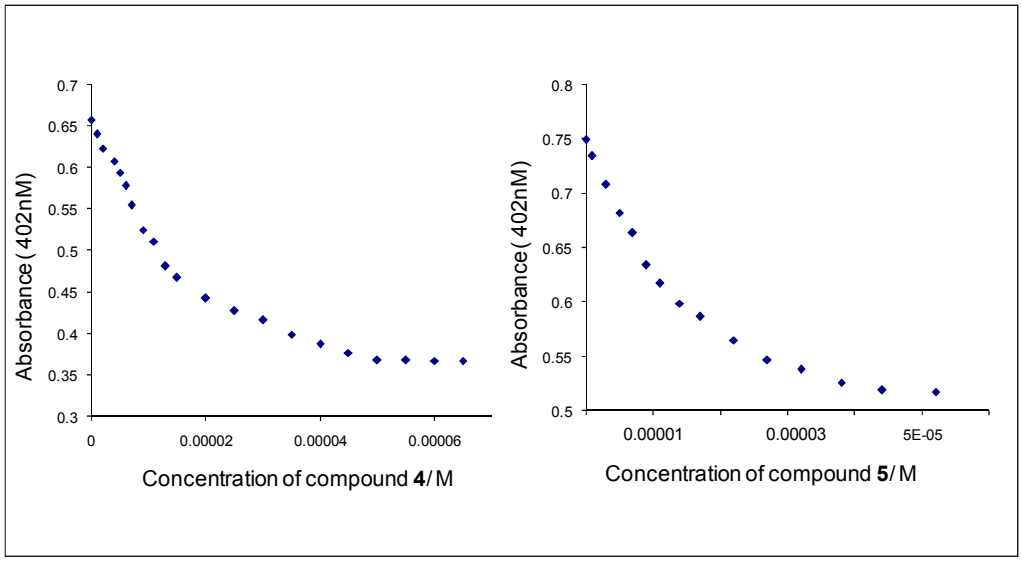

Figure 8. Variation in absorbance of Fe(III)PPIX at 402 nm as a function of added drug concentration; (left) compound **4**, (right) compound **5**

Table 2. Binding constants for the interaction of compounds **4**, **5** and CQDP to hematin at pH 4.9

Compound	log K
CQDP	4.82 ± 0.02
Comp **4**	4.83 ± 0.01
Comp **5**	4.62 ± 0.01

The log K value for the association of CQ with hematin under these experimental conditions (pH 4.9) is 4.82 ± 0.02 and very similar values are observed for compounds **4** and **5** with the value for compound **5** being somewhat lower but within the same range. These results suggest that new compounds have a binding affinity with monomeric hematin, similar to that of CQ; the association most probably takes place through π-π interactions between the porphyrin and the quinoline rings of the compounds, plus electrostatic interactions under acidic conditions (possibly including cation-π interactions).[14] However, these interactions alone cannot be the reason for the improved antimalarial activity of compounds **4** and **5** against CQ resistant strains, since the differences in IC_{50} values are not reflected by the very similar Log K values.

5.3.4 Heme aggregation inhibition activity (HAIA) at water/*n*-octanol interface

The heme aggregation inhibition activity of the new 4-aminoquinoline derivatives **4** and **5** at water/*n*-octanol interfaces was investigated by following the method in chapter 3. HAI_{50} values for compounds **4** and **5** as well as for CQDP are summarized in Table 3. HAI_{50} is the drug to hematin ratio required to inhibit 50% of heme aggregation against a control experiment in the absence of drugs and the values in parentheses are the relative activity of each drug compared to CQDP.

Table 3 - HAI_{50} values obtained by carrying out heme aggregation inhibition assay at aqueous acetate buffer (pH = 4.9)/*n*-octanol interface of compounds **4**, **5** and CQDP. Values in parentheses are the relative activity with respect to CQDP

Compounds	HAI_{50}
CQDP	2.92 ± 0.30 **(1.00)**
Comp **4**	1.54 ± 0.06 **(1.89)**
Comp **5**	0.78 ± 0.01 **(3.74)**

We note that both compounds **4** and **5** have lower HAI_{50} values than the standard drug CQDP; this activity trend **5 > 4 > CQDP** predicts compounds **4** and **5** to be more potent than CQDP. In the case of the CQ-sensitive strain D6 the activity of compound **4** is about the same as that of CQ but **5** is notably more active. More importantly, our data demonstrate that the new compounds are consistently more active than CQ against all the resistant strains, in qualitative agreement with our prediction based on HAI_{50} values. However, as shown in Figure 9, the HAIA of compound **5** is about twice that of compound **4** but the antimalarial activities of **4** and **5** are very similar against the K1 and K14 strains and only in the case of Dd2 a direct correlation (2:1) is found with the HAI_{50} values. Therefore, other factors must be contributing to the antimalarial activity.

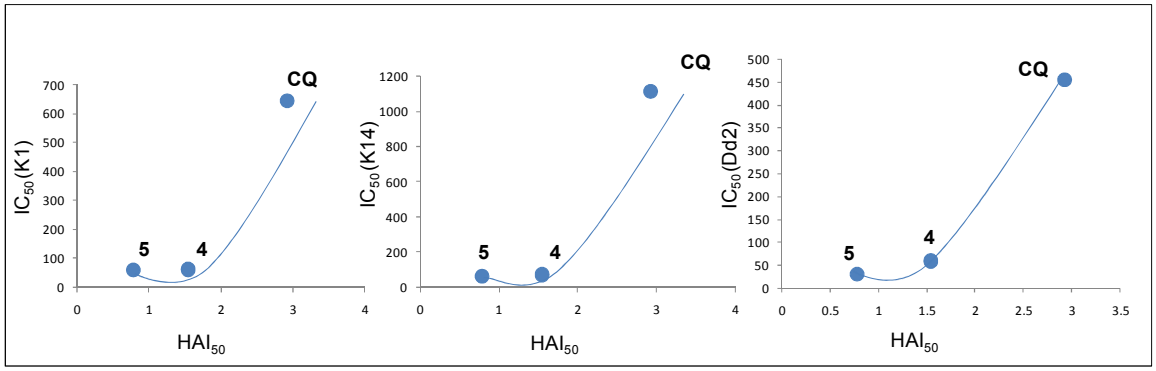

Figure 9. Correlation between HAI_{50} and antiplasmodial activity against CQ-resistant strains of *Plasmodium falciparum* K1 (left), K14 (center), and Dd2 (right) of compounds **4**, **5** and CQ.

In summary, these results indicate that (i) heme aggregation is an important target of antimalarial action for **4** and **5**. (ii) HAI_{50} values measured at water/octanol interface (pH 4.9) qualitatively predict the higher antimalarial activities of **4** and **5** in relation to the standard drug CQDP.

In order to gain a deeper understanding of the origin of the antimalarial properties of the new compounds, the factors governing accumulation of the drugs at the site of action (lipophilicity and basicity) were investigated.

5.3.5 Lipophilicity and antimalarial activity

As mentioned in chapter 3, measuring the distribution coefficients of new potential antimalarial drugs is very important, because it is now believed that heme aggregation preferentially takes place near water/lipid interfaces[15,16] within the acidic food vacuole of the parasite and thus, highly lipophilic drugs are associated with higher accumulation at such interfaces and consequently, higher activities. Also it is known that increased lipophilicity leads to a better ability to overcome CQ resistance.[17-19]

The distribution coefficients for compounds **4** and **5** were determined using the stir-flask method [20-22] at two pH values (4.9 and 6.6) that can be related to vacuolar and cytosolic conditions of the parasite, respectively. The corresponding *D* (pH) values are collected in Table 4.

Table 4. Values of distribution coefficient of new compounds at vacuolar (pH 4.9) and cytosolic pH (pH 6.6)

Compound	*D* (pH 4.9)	*D* (pH 6.6)
CQDP	0.15 ± 0.01	6.61 ± 0.64
4	0.18 ± 0.01	7.17 ± 0.86
5	0.64 ± 0.09	9.21 ± 0.78

The lipophilicity trend at both pH 6.6 and 4.9 is **5 > 4 > CQDP**. Compound **5** has the highest distribution coefficient at vacuolar pH (0.64), 4 times more lipophilic than the standard drug CQDP, whereas compound **4** displays only a moderate increase in lipophilicity with respect to CQDP. These trends are in line with the observed HAI_{50} values (Figure 10); as the lipophilicity of the drug increases, the heme aggregation inhibition activity increases. Among the two new compounds, **5** displays the highest heme aggregation inhibition ability (HAI_{50} = 0.78) and it is the most lipophilic drug (D = 0.64). This can be related to the fact that the effective concentrations of increasingly lipophilic compounds are higher near the interface where heme aggregation takes place and this must result in an improved heme aggregation inhibition activity.

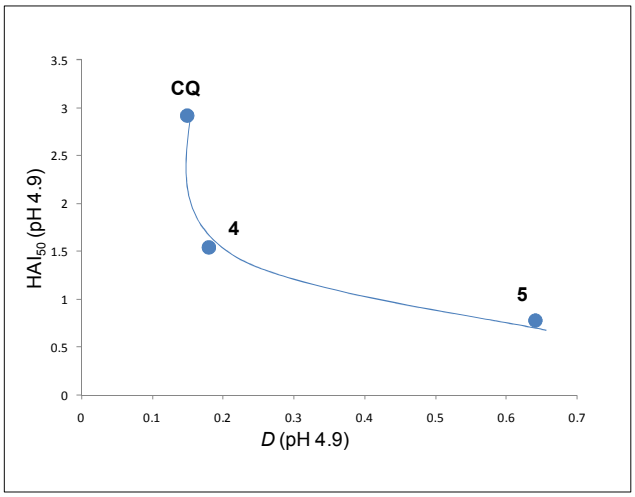

Figure 10. Correlation between partition coefficients and heme aggregation inhibition activity of chloroquine diphosphate and compounds **4** and **5** at an aqueous acetate buffer (pH 4.9)/*n*-octanol interface

This, in turn should be reflected in higher antiplasmodial activity as the lipophilicity of the drug increases. Figure 11 shows the relations between *D* values at pH 4.9 and IC_{50} values for all the malaria strains studied.

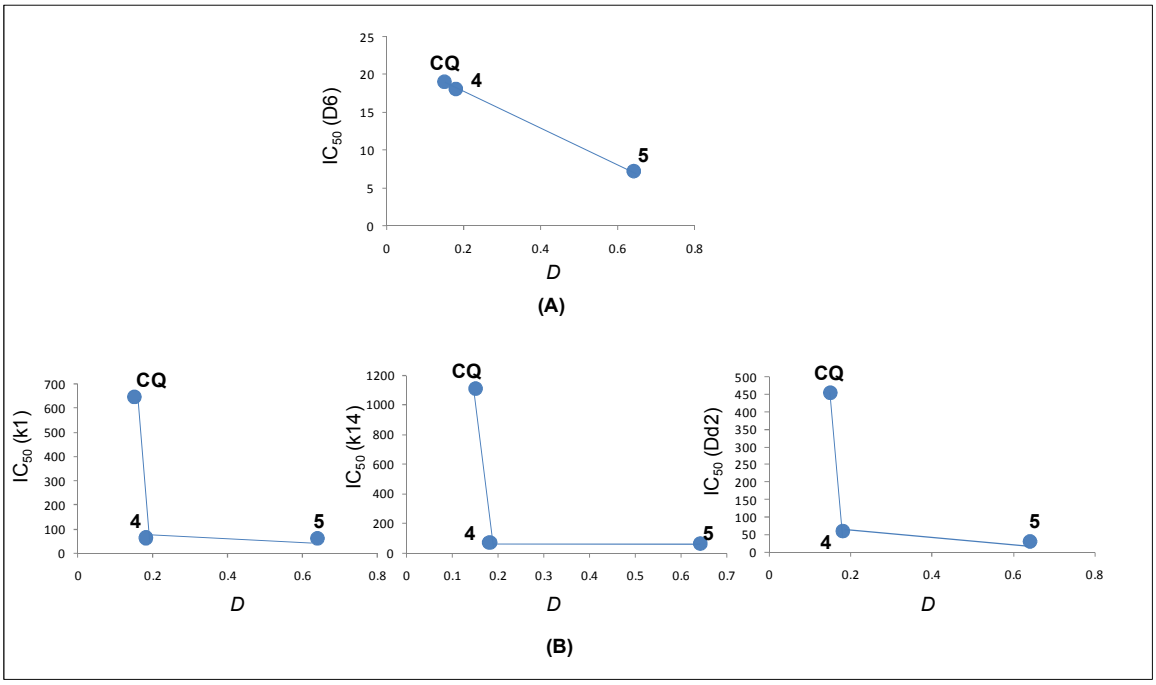

Figure 11. Correlation between lipophilicity and antiplasmodial activity against (A) CQ-sensitive strain D6 and (B) CQ-resistant strains of *P. falciparum* K1 (left), K14 (center), and Dd2 (right) of compounds **4**, **5** and CQ. (Values for *D* from Table 4; values for IC_{50} from table 1)

In the case of the CQ-sensitive parasites D6 a linear correlation is found, whereas for the CQ-resistant strains a more dramatic increase in antiplasmodial potency is achieved upon increasing the lipophilicity. These observations agree with our postulates: (i) Enhanced lipophilicity leads to higher effective drug concentrations near the lipid nanospheres in the food vacuole, where heme aggregation takes place. This explains why both compounds are more active than CQDP against CQ-sensitive and CQ-resistant parasites.

(ii) As previously proposed by Warhurst,[19] the more lipophilic drugs have a greater ability to avoid being extruded by the PfCRT and they are therefore able to overcome resistance.

5.3.6 Basicity and antiplasmodial activity

In addition to lipophilicity, basicity also plays an important role in the accumulation of quinoline-based drugs at the acidic food vacuole of the parasite. In order to explore the effect of basicity on the antimalarial properties of compounds **4** and **5**, the pK_a values were determined from titration plots by following pH changes upon addition of 0.03M NaOH to a 1 mM solution of each compound in distilled water (Figure 12).

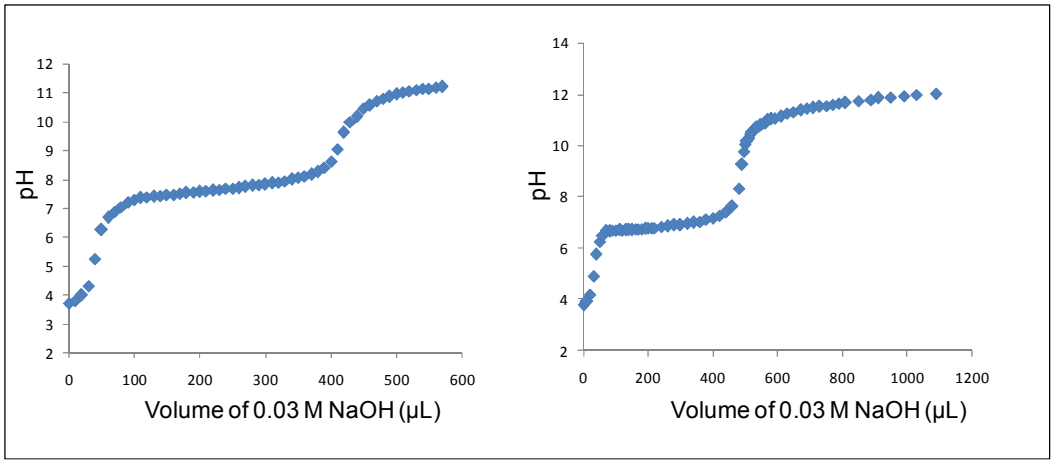

Figure 12. Titration curves for protonated compound (left) **4** and (right) **5** with NaOH.

Since both compounds have three nitrogen atoms, three pK_a values could be measured. pK_{a1} corresponds to the quinoline N atom, while pK_{a2} and pK_{a3} correspond to the tertiary N of the side chain and the NH nitrogen atoms, respectively. The pK_a values of the new compounds and CQDP are summarized in Table 5.

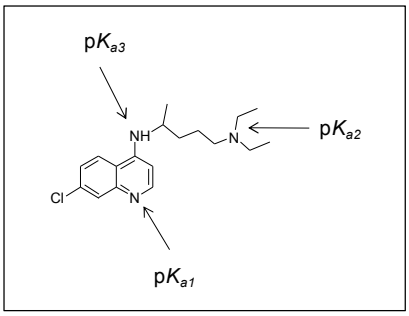

Table 5. pK_a values of compounds **4**, **5** and CQDP

Compound	pK_{a1}	pK_{a2}	pK_{a3}
CQDP	9.69	8.12	5.10
4	10.63	9.31	5.50
5	10.93	9.38	5.15

Both compounds **4** and **5** are more basic than CQDP, following the trend **5 > 4 > CQDP**. These results show that the incorporation of the electron donating fragments, arene or 1,4-cyclohexadiene into 4-aminoquinoline in compounds **5** and **4**, respectively, modified the basicity properties in the desired direction. Therefore the new compounds will tend to accumulate inside the acidic food vacuole to a greater extent than the weaker base CQDP. That should translate into a higher heme aggregation inhibition activity under acidic conditions and, in aggrement with this prediction, the HAI_{50} values measured at aqueous acetate buffer (pH 4.9)/*n*-octanol interface of compounds **4**, **5** together with that for CQ follow a linear correlation with the pK_{a1} values as shown in Figure 13.

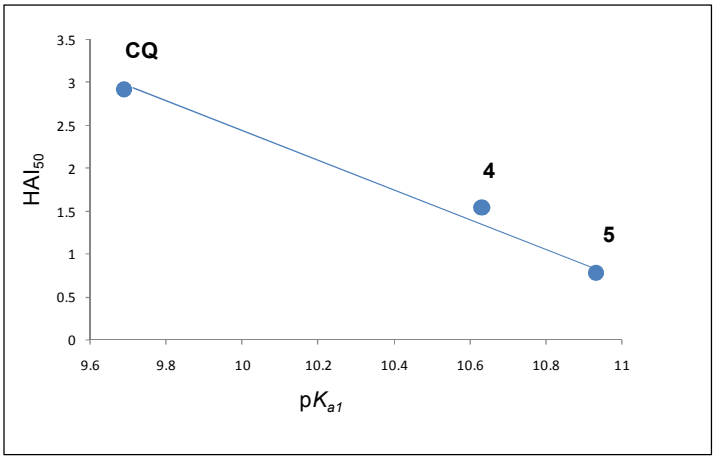

Figure 13. Correlation between pK_{a1} and heme aggregation inhibition activity of chloroquine diphosphate and compounds **4**, **5** at an aqueous acetate buffer (pH 4.9)/*n*-octanol interface.

The antiplasmodial activity measured on parasites also correlates with the basicity of the drugs, although not in a linear fashion (Figure 14). For the CQ-sensitive D6 strain the effect is small for compound **4** but marked for **5**.

On the other hand, for all the resistant strains the increase in basicity is accompanied by a sharp increase in antiplasmodial activity, with respect to CQDP, but little difference between them.

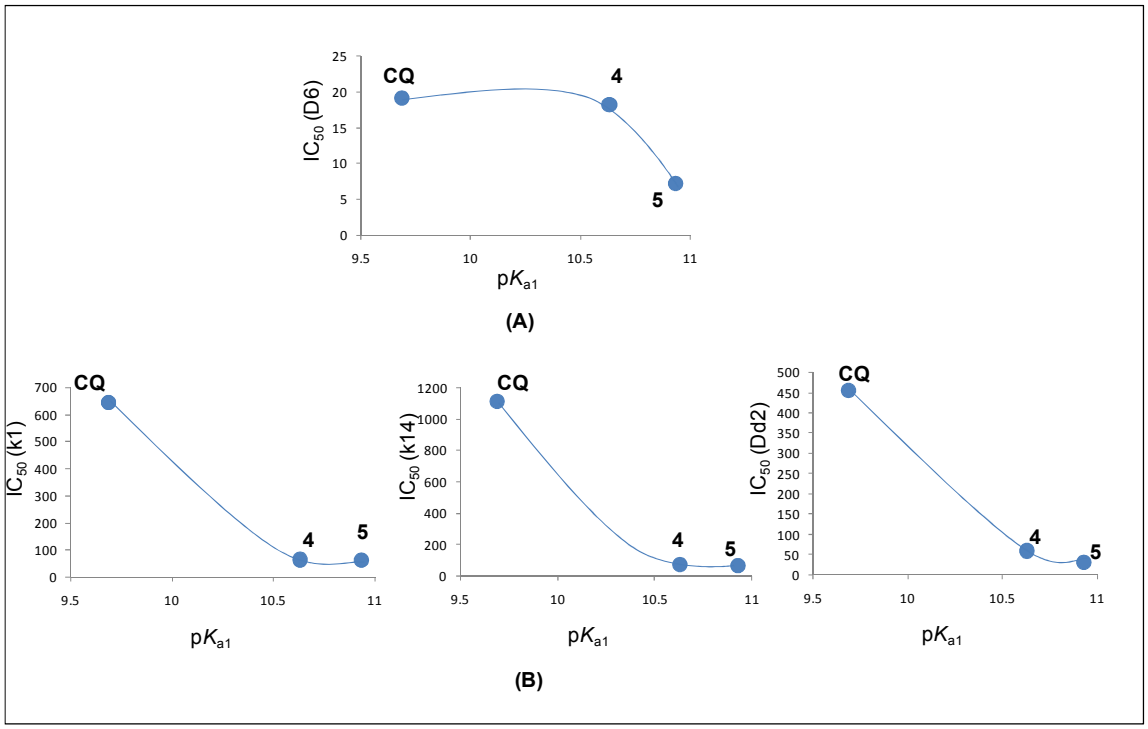

Figure 14. Correlation between basicity and antiplasmodial activity against (A) CQ - sensitive strain D6 and (B) CQ-resistant strains of *P. falciparum* K1 (left), K14 (center), and Dd2 (right) of compounds **4**, **5** and CQ. (Values for pK_{a1} from Table 5; values for IC_{50} from table 1)

These results can be interpreted in the following manner:

(i) In the case of CQ-sensitive parasites, compounds **4** and **5** may accumulate better than CQ at the acidic food vacuole and therefore they are more active. This effect combined with the influence of lipophilicity described above, may account for the difference in the behavior of **4** and **5**.

(ii) For CQ-resistant parasites, compounds **4** and **5** may not only accumulate better inside the food vacuole, but also they may not be extruded by PfCRT due to their modified structure and higher lipophilicity. In this case, the effective concentration of CQ will be drastically diminished by resistance and therefore the activity of **4** and **5** is much higher than that of CQDP.

One additional factor that may be taken into account is the vacuolar accumulation ratio, (VAR) another parameter that is sometimes used to predict the exent of drug accumulation inside the acidic food vacuole of the parasite. In general, higher VAR values are associated with better accumulation within the acidic food vacuole. The VAR values of compounds **4**, **5** and CQDP were calculated by using the equation of Henderson-Hasselbach, as described by Biot et al [23] and included in Table 6.

$$VAR = 10[\log D\ (6.6) - \log D\ (4.9)]$$

Table 6. The calculated VAR of compounds **4**, **5** and CQDP

Compound	VAR
CQDP	45
4	40
5	14

The calculated VARs for compounds **4** and **5** are lower than that of CQDP. This would suggest that in spite of their higher basicity and lipophilicity, these drugs would accumulate to a lesser extent inside the heme aggregation site (food vacuole) of the parasite in the absence of other effects. Concerning this apparent inconsistency, Hawley et.al [24] pointed out that although amodiaquine (AQ) has a higher lipophilicity than CQ at pH 5.0, its calculated cellular accumulation ratio (CAR) value is lower than that of CQ, but the experimentally measured parasite CAR of AQ is much higher than that of CQ (see Table 7).

Table 7. A comparison of predicted and experimentally measured CAR's for both AQ and CQ in *P. falciparum* (HB3 strain)

Compound	CQ	AQ
Predicted parasite CAR (HB3 strain)	1720	587
Experimentally measured parasite CAR	1823	4336

CAR = VAR * fractional cell volume occupied by acid vacuole

They further pointed out that the experimentally derived levels of drug accumulation were between 2- and 300-fold greater than could be predicted by the drug's weak base properties across the four isolates they have studied. It would thus seem that calculated VAR or CAR values may not be very good predictors of actual drug accumulation at the site of action of antimalarial drugs. Unfortunately we do not have the capabilities for measuring CAR or VAR values, in order to compare experimental data with our calculated values, but for our discussion we rely on the relations between the observed IC_{50} values against malaria parasites and the experimentally measured lipophilicity, basicity and HAI_{50} values.

5.4 Conclusion

Two new organic compounds **4** and **5** were synthesized and characterized by 1D/2D NMR spectroscopy, elemental analysis and mass spectrometry.

Both compounds are more active than CQ in *in vitro* tests against CQ-resistant strains of *P. falciparum* (K1, K14 and Dd2) as well as a CQ-sensitive strain (D6).

As other aminoquinoline drugs and our first series of Ru-CQ complexes, the new 4-aminoquinoline derivatives **4** and **5** share heme aggregation as the main target. In comparison to the standard drug CQ, the presence of the 1, 4-cyclohexadiene or benzene moieties in compounds **4** and **5** modifies the pharmacological behavior of the parent drug by enhancing the lipophilicity and basicity, which are responsible for a high accumulation of the drugs inside the acidic food vacuole of the parasite and for overcoming CQ resistance. This leads to improved antimalarial activity against CQ-resistant strains of *Plasmodium falciparum*, and to a lesser extent, against CQ-sensitive parasites.

In conclusion, our studies demonstrate the validity of our hypothesis: that the structural and physicochemical modifications of 4-aminoquinoline imposed by the presence of a lipophilic substituent as a side chain lead to an enhanced activity against malaria parasites, while retaining heme aggregation as the main target of action.

5.5 Further Prospects:

Compounds 4 and 5 as potential ligands for ruthenium

Since the new molecules **4** and **5** could also serve as ligands for metals, as an additional aim we attempted to coordinate them to ruthenium.

Biot and his coworkers[25] have shown that ferroquine (Figure 2A) is able to overcome CQ resistance. In FQ, the organoiron moety is covalently linked to the side chain of CQ through a C-C link without blocking the basic N atoms. Moss also achieved variations of metalloquines by introducing organic groups in the side chain of the structure (Figure 15 - M = Fe, Ru) [26] but their antiplasmodial activities were lower than those of ferroquine although higher than the standard drug CQ.

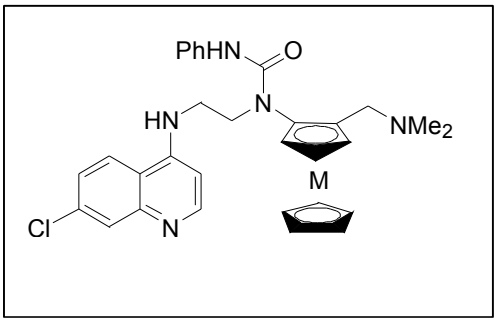

Figure 15. The structure of Moss' metalloquines; M = Fe, Ru

Although the concept of covalently linking metal containing fragment to the side chain of CQ-like molecules is very interesting, the molecular design of ferroquine and related compounds suffers a notable disadvantage, which is that the coordination sphere of the metal is not amenable to easy modification, due to the stability of the "sandwich" structure. Therefore, it is difficult to produce families of compounds for structure-activity correlation studies or for drug improvement. Consequently, ***there is a***

need for other covalently linked metal derivatives offering wider design possibilities for CQ-derived drugs targeting heme aggregation.

Our target compounds, generically represented in Figure 16, represent an innovative and more promising approach. Two particular advantages must be noted:

(1) The design retains the benefit of incorporating Ru to CQ through a covalent C-C link, which will increase the lipophilicity without reducing the basicity of CQ; and

(2) The structure includes additional ligands at Ru (L_1-L_3 in Figure 16) that can be systematically varied, thereby opening the way to structure-activity correlation studies.

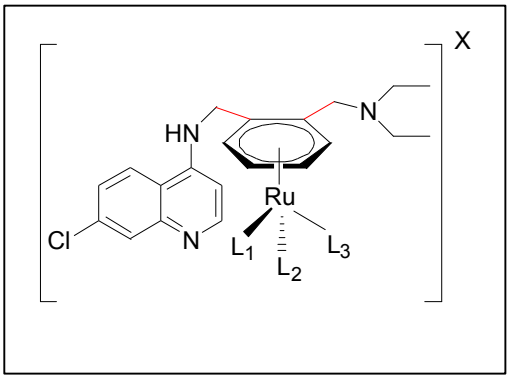

Figure 16. Covalent link molecular design; our target compounds

Retrosynthesis of starting material and synthesis of target complexes

The first approach would be to synthesize the desired $[RuCl_2(\eta^6\text{-arene})]_2$ complex (scheme 6- structure **6**) as a starting material to synthesize a variety of target molecules **7**, **8** and **9** as shown in scheme 7. The most general method for preparing ruthenium complexes of the $[RuCl_2(\eta^6\text{-arene})]_2$ type is the reaction of the corresponding 1,4-cyclohexadiene derivatives with ruthenium(III) chloride in alcoholic media.[27] The dimeric π-arene-Ru derivative **6,** which would serve as our main starting material, might

be prepared through dehydrogenation of the cyclohexadiene **4** by $RuCl_3.3H_2O$ in boiling alcoholic medium (Scheme 6).

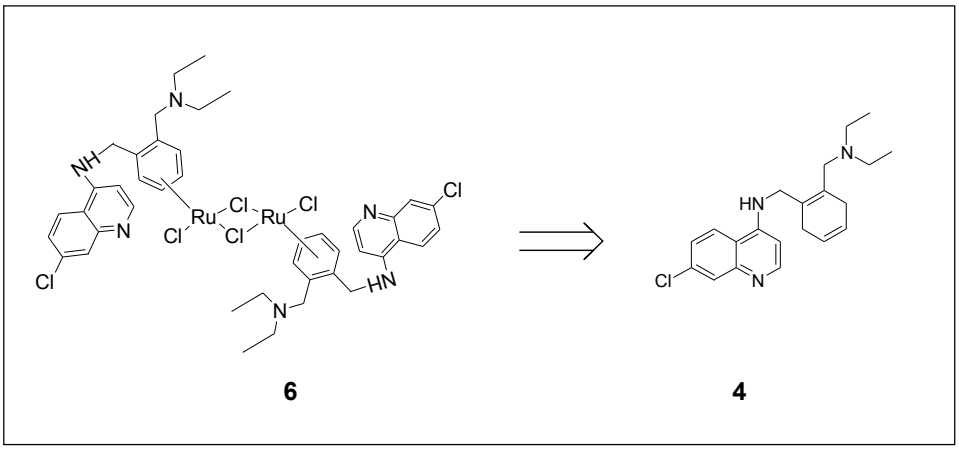

Scheme 6. Proposed retrosynthetic pathway of the starting material **6**

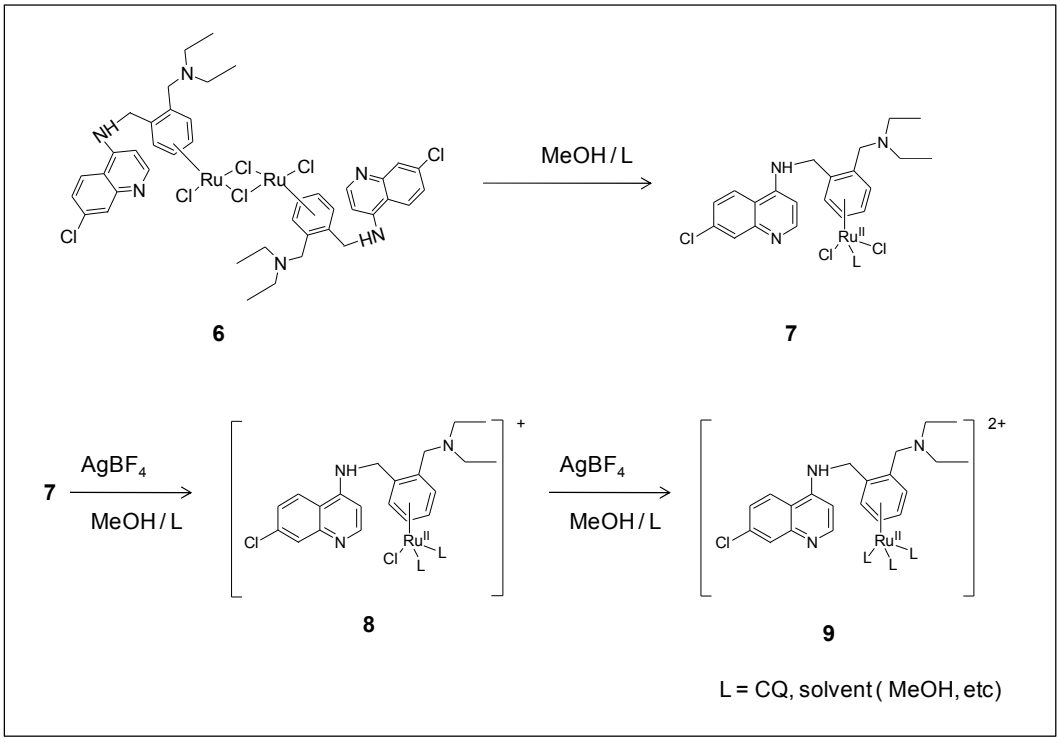

Scheme 7. Proposed synthesis of covalently linked arene bonded Ru-CQ complexes.

This method was first published by Bennett (Chapter 2, Figure 3). Haquette and his coworkers also followed Bennett's method successfully to synthesize this type of complexes bearing η^6-arene ligands with pendant maleimide or chloroacetamide groups.[28]

The synthesis of the starting material **6** through dehydrogenation of the cyclohexadiene derivative **4** by $RuCl_3.H_2O$ in boiling ethanol was attempted, but unfortunately no sign of a reaction was observed even after the reaction mixture was refluxed for 48 h (recovered starting material). As a second attempt compound **4** was refluxed 4 h in 2-methoxyethanol which has a higher boiling point (125^0C) in the presence of $RuCl_3.H_2O$. According to the ^1H NMR spectrum of the crude product, the signals for the diene protons disappeared, indicating that a dehydrogenation reaction may have taken place, but the spectrum revealed a complex mixture. This may be due to the decomposition of the product at the high temperature employed. So the reaction was repeated by reducing the reaction time in 2-methoxyethanol. The separation of the reaction mixture was attempted using column chromatography, but this method was not successful, due to decomposition of the product on the column.

Since **4** contains three basic nitrogen atoms the probability of ruthenium to coordinate to any or all of them must be envisaged as side reactions. In order to suppress this possibility the nitrogen atoms in **4** were protonated by stirring in methanol for two hours with 3eq of HBF_4, followed by refluxing the reaction mixture in ethanol in the presence of $RuCl_3$ in order to promote diene dehydrogenation. However, there was no reaction under these experimental conditions and the protonated compound **4** could be recovered at the end of the reaction.

Since the dehydrogenation step was not applicable to this compound, an alternative approach was envisaged to synthesize target compounds **7**, **8** or **9**. Reducing agents like Zn powder have been successfully used by the group of Dr. Sanchez-Delgado in 1996 to reduce Ru(III) to Ru(II) in the presence of CQ when preparing $[RuCl_2(CQ)]_2$.[29] As shown in Scheme 8 two CQ molecules coordinate to two Ru(II) ions, when the reaction was carried out by refluxing the mixture in methanol in the presence of $RuCl_3$ and Zn.

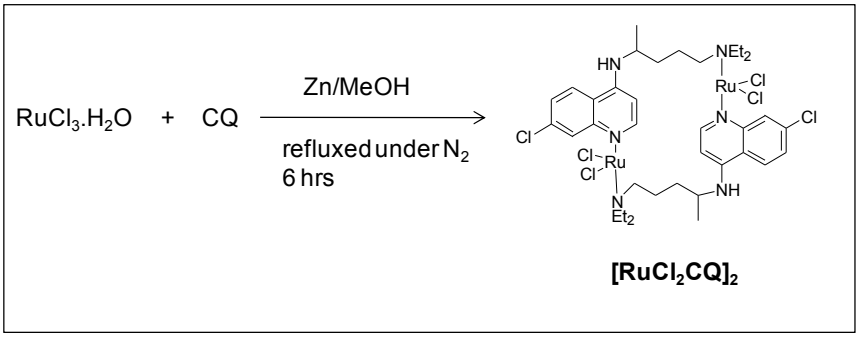

Scheme 8. Preparation of $[RuCl_2 (CQ)]_2$.[29]

Also, in the first phase of this project we synthesized an arene-Ru-CQDP complex (compound **10**) containing a π-bonded CQDP ligand, as shown in Scheme 9.[30]

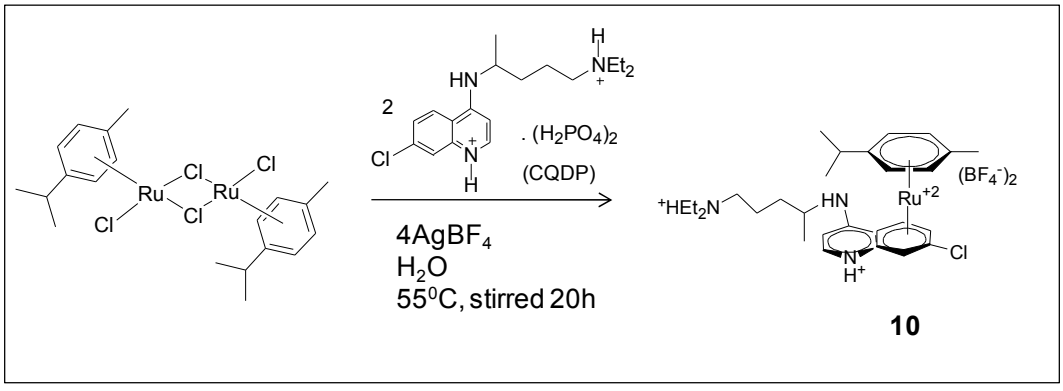

Scheme 9. Preparation of compound **10** [30]

Therefore, there is a possibility of synthesizing the target molecule **7** from **5** by using the reducing agent Zn and $RuCl_3.H_2O$, in the presence of a stabilizing ligand 'L' (e.g; L = MeOH). The synthesis of target compounds **8** and **9** from compound **7** can be envisaged by use of $AgBF_4$ and stabilizing ligands. The synthetic strategy proposed for compounds **7**, **8** and **9** from **5** is shown in Scheme 10.

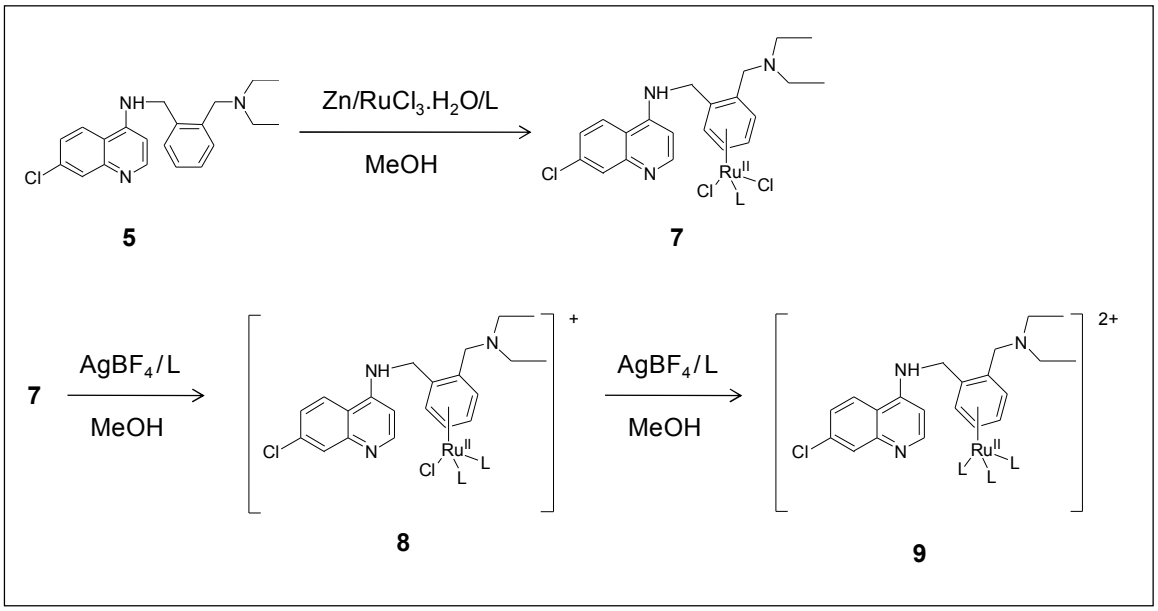

Scheme10. Proposed synthesis of complexes **7**, **8** and **9**

As a first attempt, compound **5** was refluxed in methanol for 52 h in the presence of $RuCl_3.H_2O$ and excess Zn. More than one product was observed in the NMR spectra, including a complex possibly having ruthenium bonded to the quinoline nitrogen atom. Separation of the product mixture using column chromatography, extraction or crystallization was unsuccessful.

Since the basic nitrogen atoms are available for coordination to ruthenium, it is possible that the N-bonded products are favored over the desired π-bonded species. In order to avoid nitrogen coordination, protonation of the basic nitrogen atoms of

compound **5** using HBF_4 was performed in methanol, to get compound **11** (Scheme 11). Then **11** was refluxed in methanol for 48h in the presence of Zn and $RuCl_3.H_2O$.

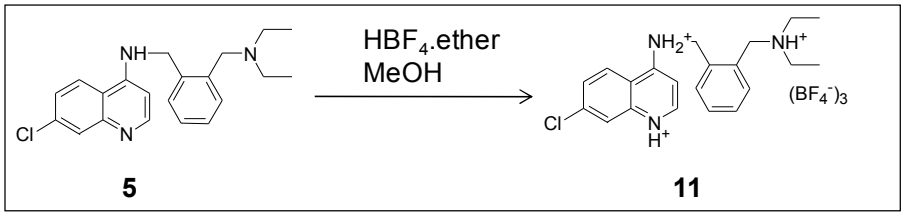

Scheme 11. Protonation of compound **5**

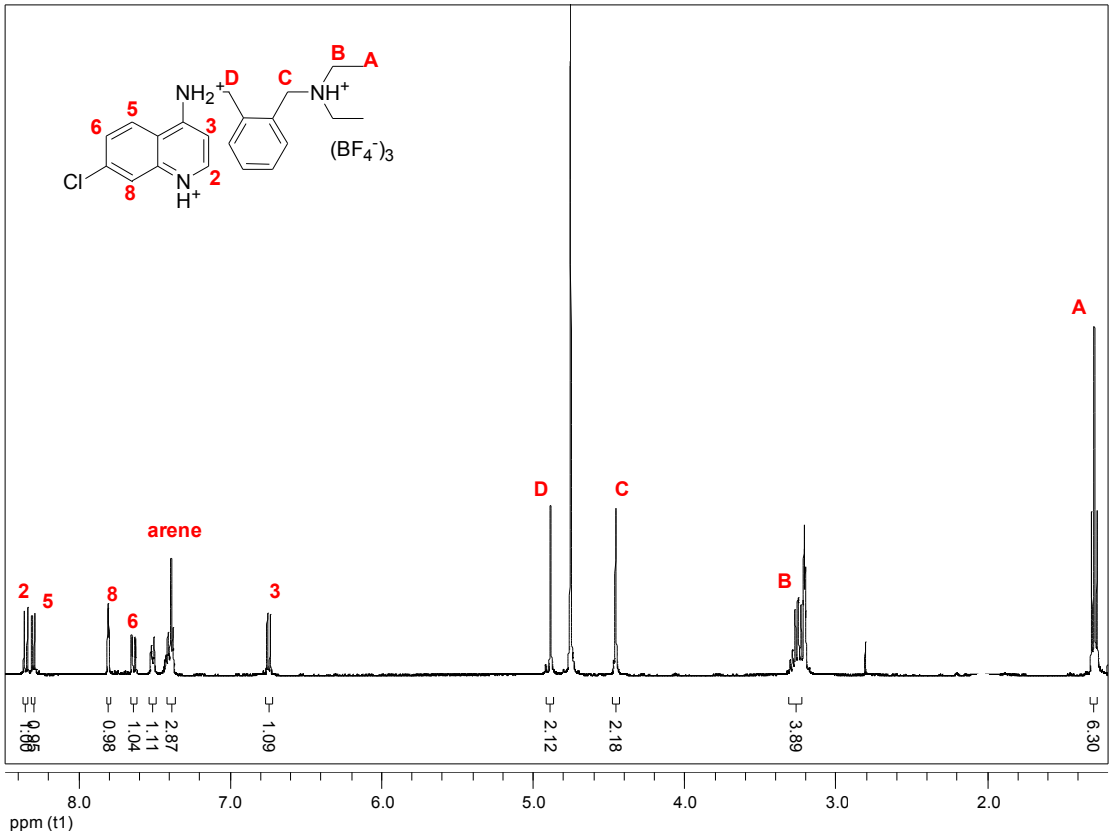

Figure 17. ^1H NMR of compound **11** in MeOD

The ^1H NMR spectrum obtained for the final product with the signal assignment is shown in Figure 18. The final product was yellowish green in color and the proton

signals are somewhat broader indicating that traces of ruthenium are present as paramagnetic Ru(III). The conductivity of a freshly prepared 1 mM solution of this compound in methanol was 124.7 μScm^2Mol^{-1}, a value typical of a 1:1 electrolyte. The IR spectrum of compound **11** clearly showed a peak for BF_4^- in the IR spectrum which disappeared for this unknown product.

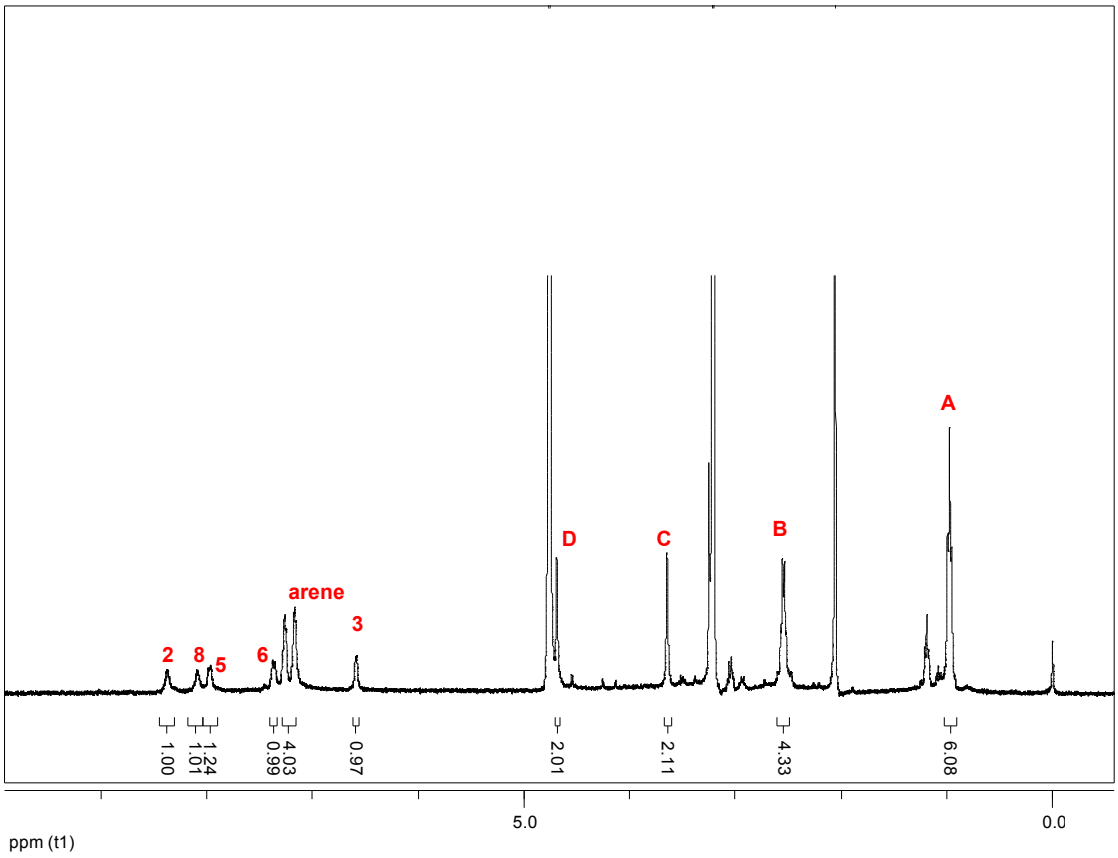

Figure 18. ^1H NMR of the product obtained by the reaction of compound **11** with $RuCl_3$ in the presence of Zn.

It was difficult to identify any protons in the NMR spectrum of the unknown compound in DMSO which were bonded to the quinoline nitrogen atom or the tertiary amine. All the other proton signals of the compound shifted upfield compared to the ^1H

signals of compound **11** in MeOD. All these observation suggest that, probably deprotonation took place due to the long reaction time in the presence of Zn metal.

Nevetherless, the proton signals for H2, H3 and H8 of the unknown compound shifted downfield by 0.155, 0.128 and 0.366 ppm, respectively, compared to those of unprotonated compound **5**, indicating that ruthenium might be binding to the quinoline nitrogen. The $\Delta\delta$ values of other signals are less than 0.09ppm, and there were no considerable chemical shift changes of the ^{13}C NMR signals of the unknown compound with respect to those of compound **5**. These data do not allow a correct identification of this complex.

Since the time allocated for this project ended, the bench work was stopped at this point and the aim of preparing Ru derivatives of **4** and **5** was left for future work in our laboratory.

5.6 References

1. Orvig, C.; *Inorgani.c chemistry*. **2005**, *44*, 2678
2. http://www.cmaj.ca/cgi/reprint/160/1/17.pdf
3. http://en.wikipedia.org/wiki/Amodiaquine
4. Hawley, S. R.; Bray, P. G.; Park, B. K.; Ward, S. A, *Molecular and Biochemical Parasitology*, **1996**, *80*, 15-25
5. Dive, D.; Biot, C. *Chem. Med. Che.* **2008**, *3*, 383-391
6. http://www.ifpma.org/fileadmin/pdfs/wennews/2009_07_07_status_RnD_for DDW
7. Biot, C.; Taramelli, D.; Forfar-Bares, I.; Maciejewski, L. A.; Boyce, M.; Nowogrocki,G. ; Brocard, J. S. ; Basilico, N.; Olliaro, P.; Egan, T. J. **2005**, *Mo.l Pharm. 2*, 185–193
8. Biot, C.; Chavain, N.; Dubar, F.; Pradines, B.; Trivelli, X.; Brocard, J. *J. Organomet. Chem.* **2009**, *694*, 845–854
9. Hine J et al. *J. Org.Chem*. **1975**, *40*, 290
10. Josefina et al. *Tetrahedron*, **2007**, *63*, 1372-1379
11. Biot et al.; *J. Med. Chem*. **1997**, *40*, 3715-3718
12. Blackie, M. A. L.; Yardley, V.; Chibale, K.; *Bioorg. Med. Chem. Lett*, **2010**, *20*, 1078- 1080
13. Egan, T. J.; Hunter, R. *J. Med. Chem*. **2000**, *43*, 283-291
14. Hawley, S. R.; Bray P. G.; Park, B. K. *Mol. Biochem. Parasitol* , **1996**, *80*, 15-25
15. Egan, T. J. *Mol Biochem Parasitol*, **2008**, *157*,127–136
16. Egan, T.J . **2008**, *J Inorg Biochem*, 102, 1288–1299
17. Van Schalkwyk, D. A.; Egan, T. J. **2006**, *Drug Resist Updat*, *9*, 211–226
18. Warhurst, D. C. **2003**, *Malar. J. 2*, 31–43

19. Warhurst, D. C.; Craig, J. C.; Adagu, I. S.; Meyer, D. J.; Lee, S. Y. **2003**, *Malar J 2*, 26–30

20. OECD guidelines for testing of chemicals, **1995**, no 107, OECD, Paris

21. Danielsson, L. G. ; Zhang, Y.H. *Trends Anal Chem.* **1996**, *15*,188–196

22. Rappel, C.; Galanski, M.; Yasemi, A.; Habala, L.; Keppler, B.; *Electrophoresi,* **2005**, *26*, 878–884

23. Biot, C.; Chavain, N.; Dubar, F.; Pradines, B.; Trivelli, X.; Brocard, J.; Forfar, I.; Dive, D.; **2008**. doi:10.1016/j.jorganchem.2008.09.33

24. Hawley, S.; R.; Bray, P.; G.; Park, B.; K.; Ward, S.; A, *Molecular and biochemical parasitology*, **1996**, *80*, 15-25

25. a) Biot, C.; Delhaes, L.; N' Diaye, C. M.; Maciejewski, L. A.; Camus, D.; Brocard, J. S.; Dive, D. *J. Med. Chem*. **1997**, *40*, 3715-3718

b) Biot, C.; Delhaes, L.; Abessolo, H.; Domarle, O.; Maciejewski, L. A.; Mortuaire, M.; Delcourt, P.; Deloron, P.; Camus, D. ; Dive, D.; Brocard, J. S. *J. Organomet. Chem.* **1999**, *589*, 59-65

26. Blackie, M. A. L.; Beagley, P.; Croft, S. L.; Kendrick, H.; Moss, J. R.; Chibale, K. *Bioorg. Med. Chem.* 2**008**, *15*, 6510-6516 (179)

27. a) Bennet, M. A.; Coord. *Chem. Rev.* **1997**, *166*, 225-254

b) Bennet, M. A.; Huang, T. N.; Matheson, T. W.; Smith, A. K. *Inorg. Synth.* **1882**, 25, 74-78.

28. Haquette, P.; Talbi, B; Canaguier, S; *Tetrahedron letters*, **2008**, 49, 4670-4673

29. Sánchez-Delgado, R. A.; Navarro, M.; Pérez, H.; Urbina, J. A.; *J. Med. Chem* **1996**, *39*, 1095-1099.

30. Rajapakse, C. S. K**.;** Martínez, A.; Naoulou, B.; Jarzecki, A.; Suárez, L.; Sánchez-Delgado, R.A.; Musi, E.; Ambrosini, G.; Schwartz, G.K. *Inorganic Chemistry*, **2009**, 48, 1122-1131.

Appendix
Chapter 2

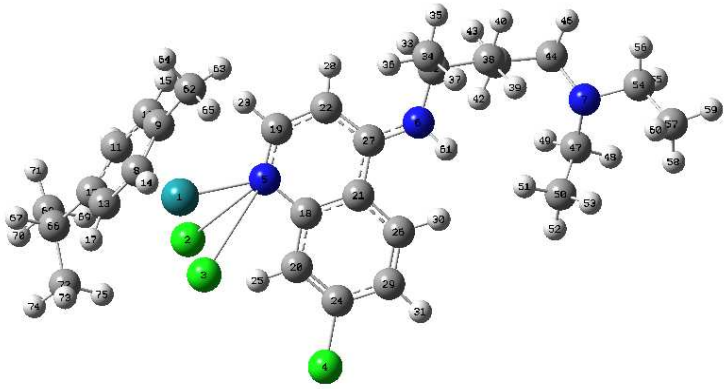

Optimized structure of complex **1** in gas phase (Ru binds through quinoline N)
Energy = - 1713018.76 kcal/mol

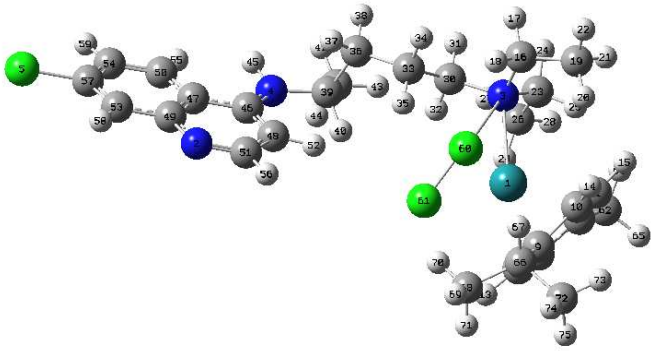

Optimized structure of complex **1** in gas phase (Ru binds through side chain N)
Energy = - 1713015.68 kcal/mol

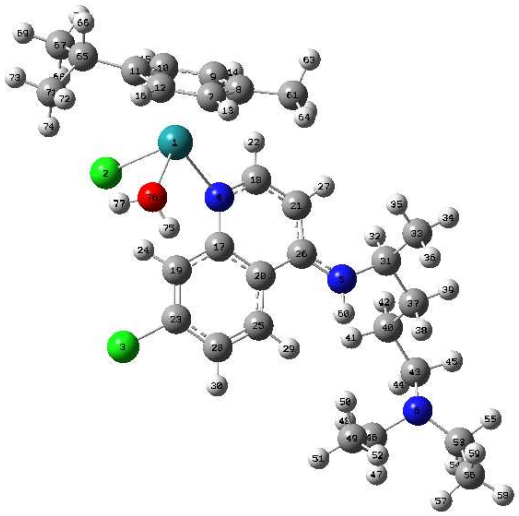

Optimized structure of complex **1'** in gas phase (Ru binds through quinoline N)
Energy = - 1472064.89 kcal/mol

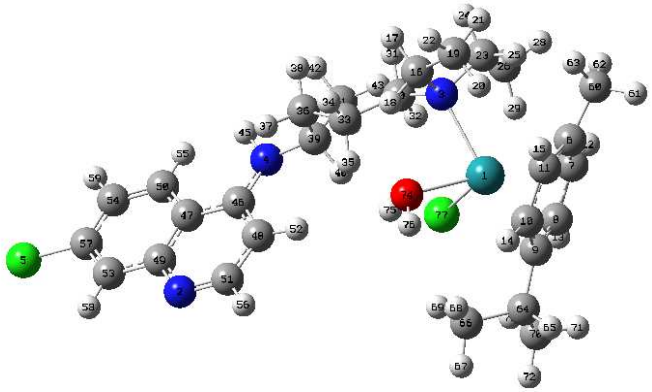

Optimized dtructure of complex **1'** in gas phase (Ru binds through side chain N)
Energy = - 1472046.75 kcal/mol

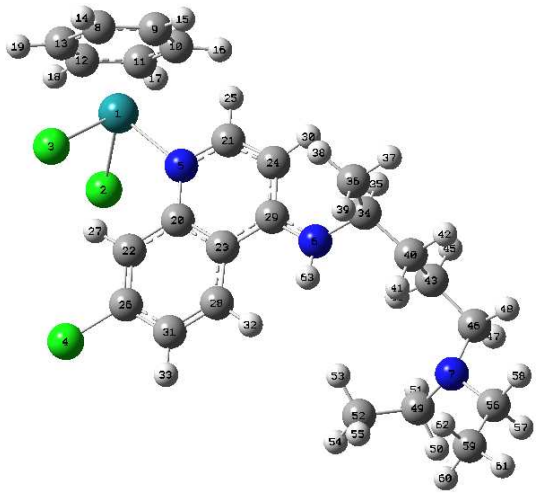

Optimized structure of complex **2** in gas phase (Ru binds through quinoline N)
Energy = -1614337.21 kcal/mol

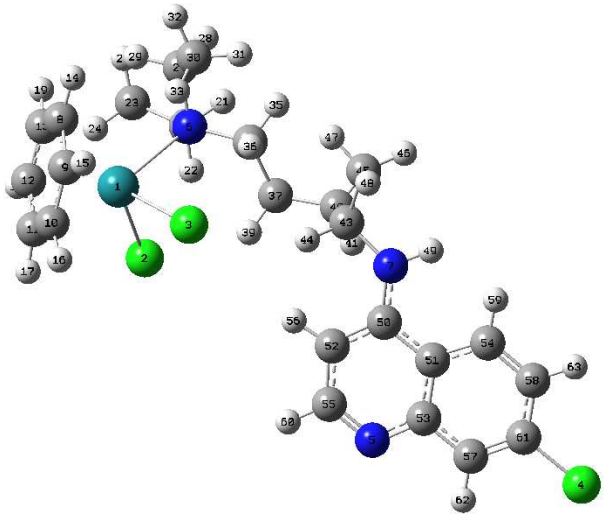

Optimized structure of complex **2** in gas phase (Ru binds through side chain N)
Energy = - 1614332.61 kcal/mol

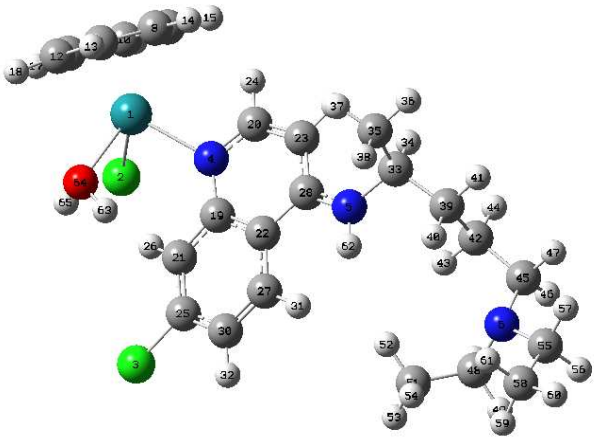

Optimized structure of complex **2'** in gas phase (Ru binds through quinoline N)
Energy = - 1373380.22 kcal/mol

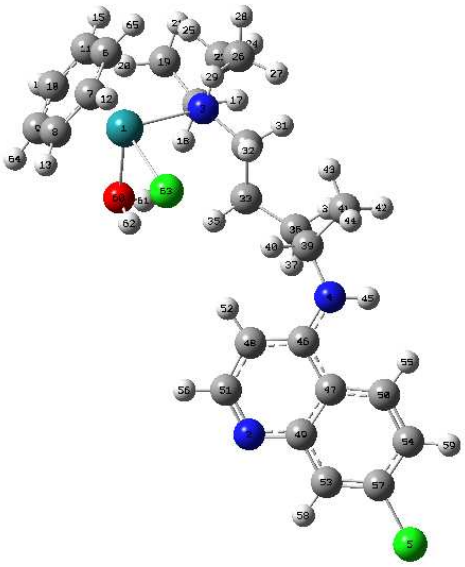

Optimized structure of complex **2'** in gas phase (Ru binds through side chain N)
Energy = -1373362.01 kcal/mol

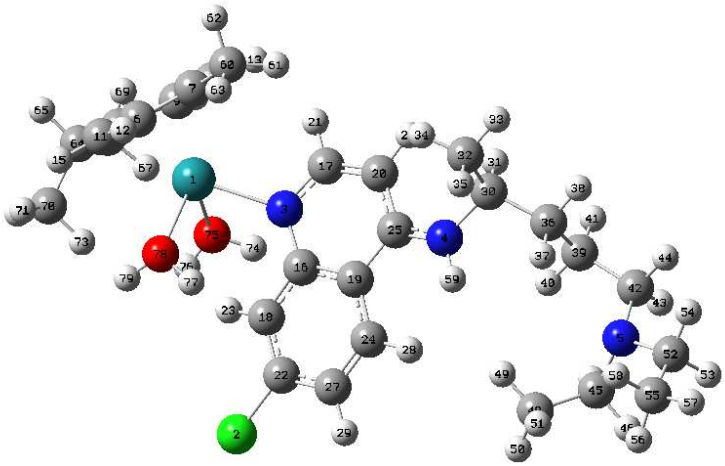

Optimized structure of complex **3** in gas phase (Ru binds through quinoline N)
Energy = - 1231029.08 kcal/mol

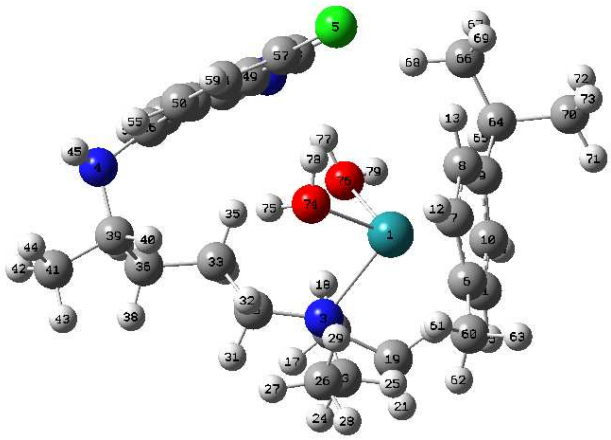

Optimized structure of complex **3** in gas phase (Ru binds through side chain N)
Energy = - 1231012.63 kcal/mol

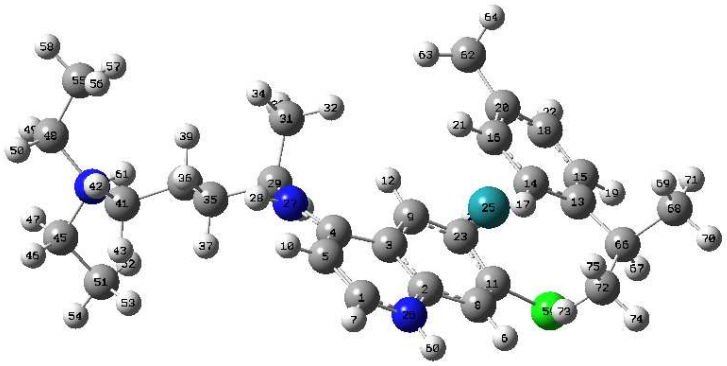

Optimized structure of complex **4** in gas phase (Ru binds through carbocyclic ring)
Energy = - 1135327.50 kcal/mol

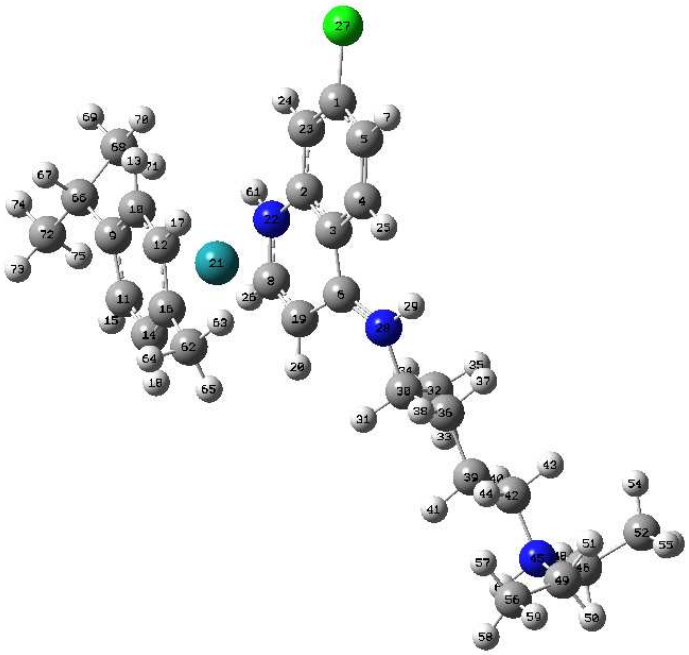

Optimized structure of complex **4** in gas phase (Ru binds through heterocyclic ring)
Energy = - 1135305.15 kcal/mol

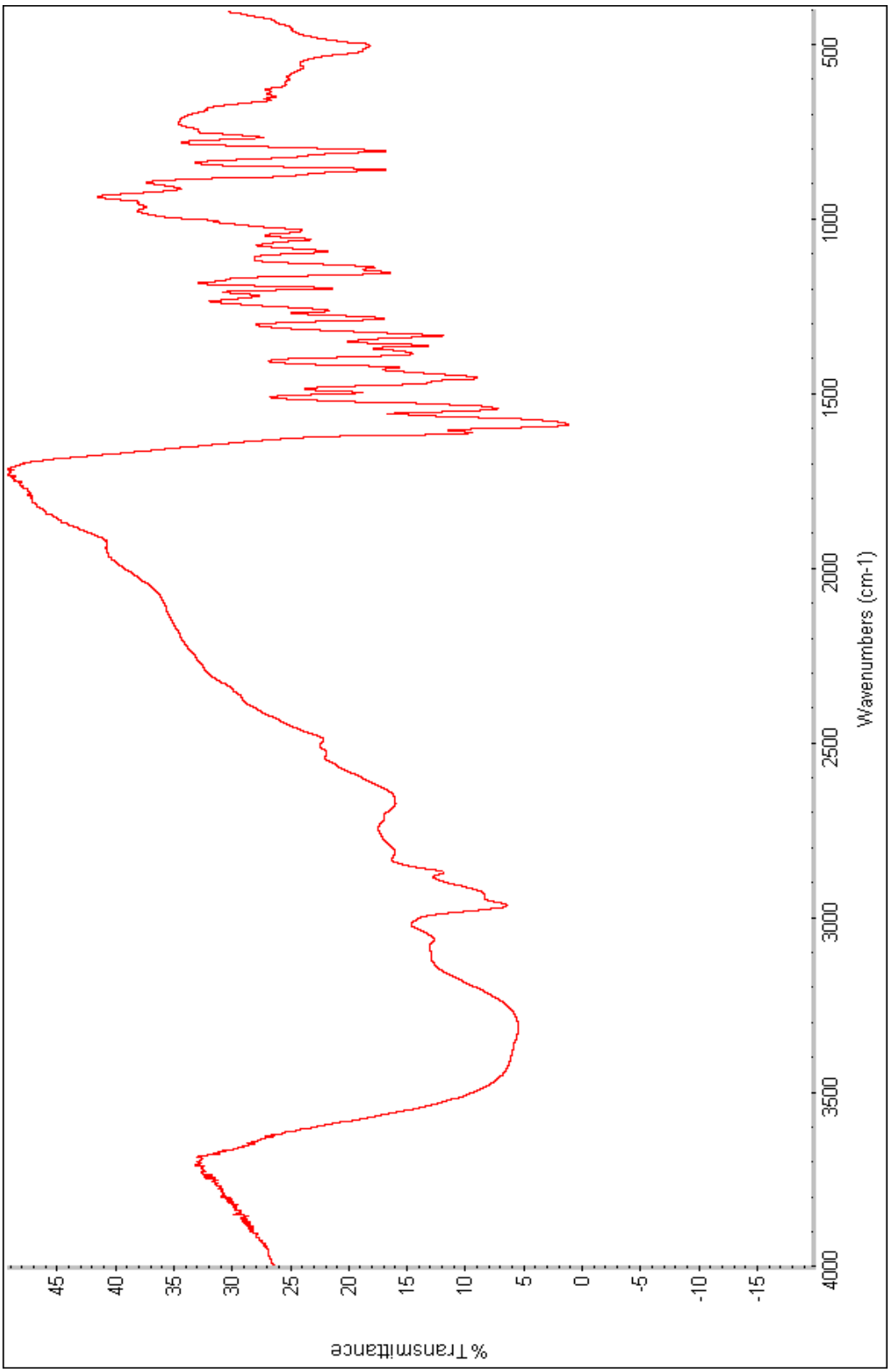

IR spectrum of complex 1

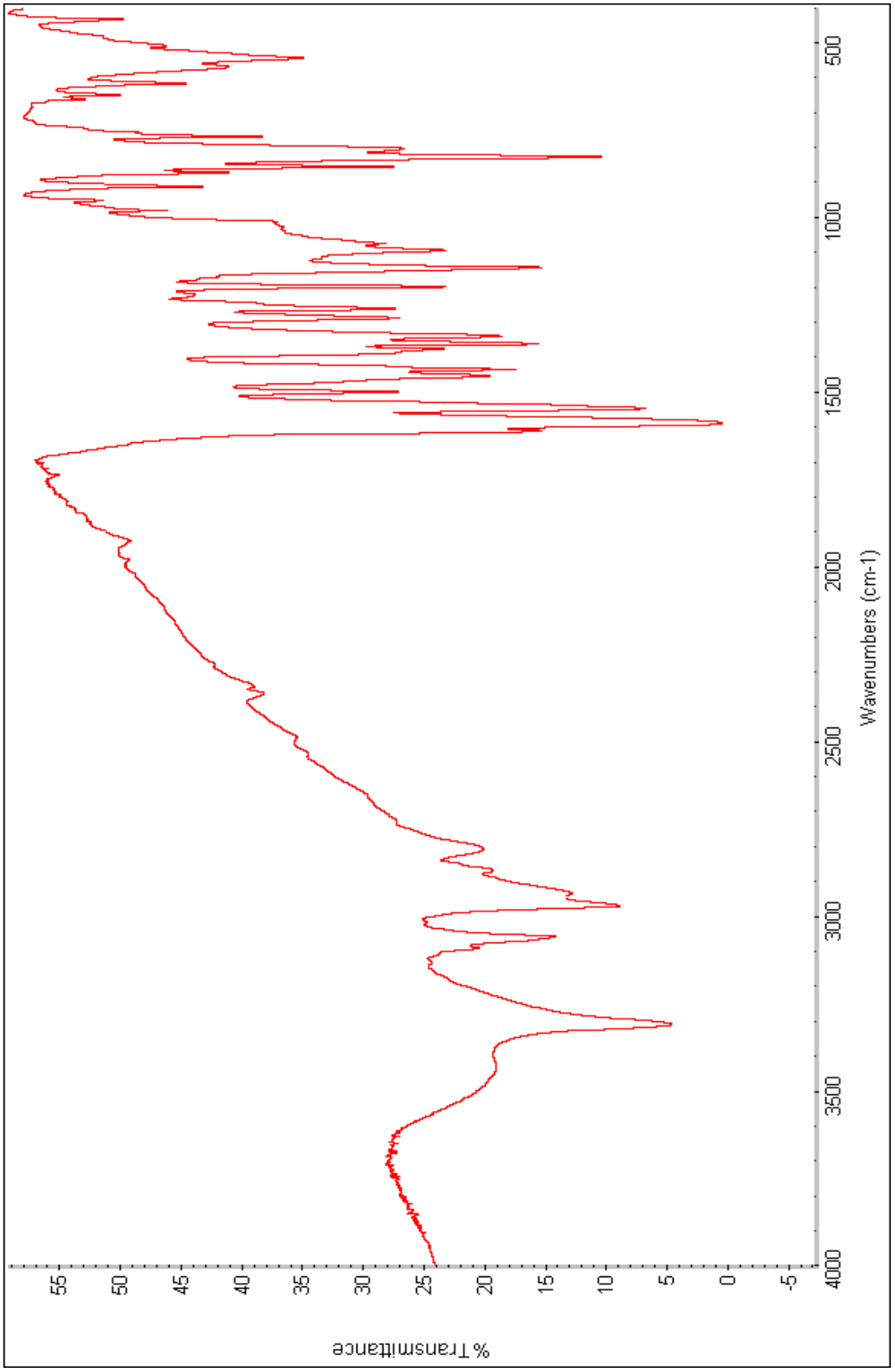

IR spectrum of complex 2

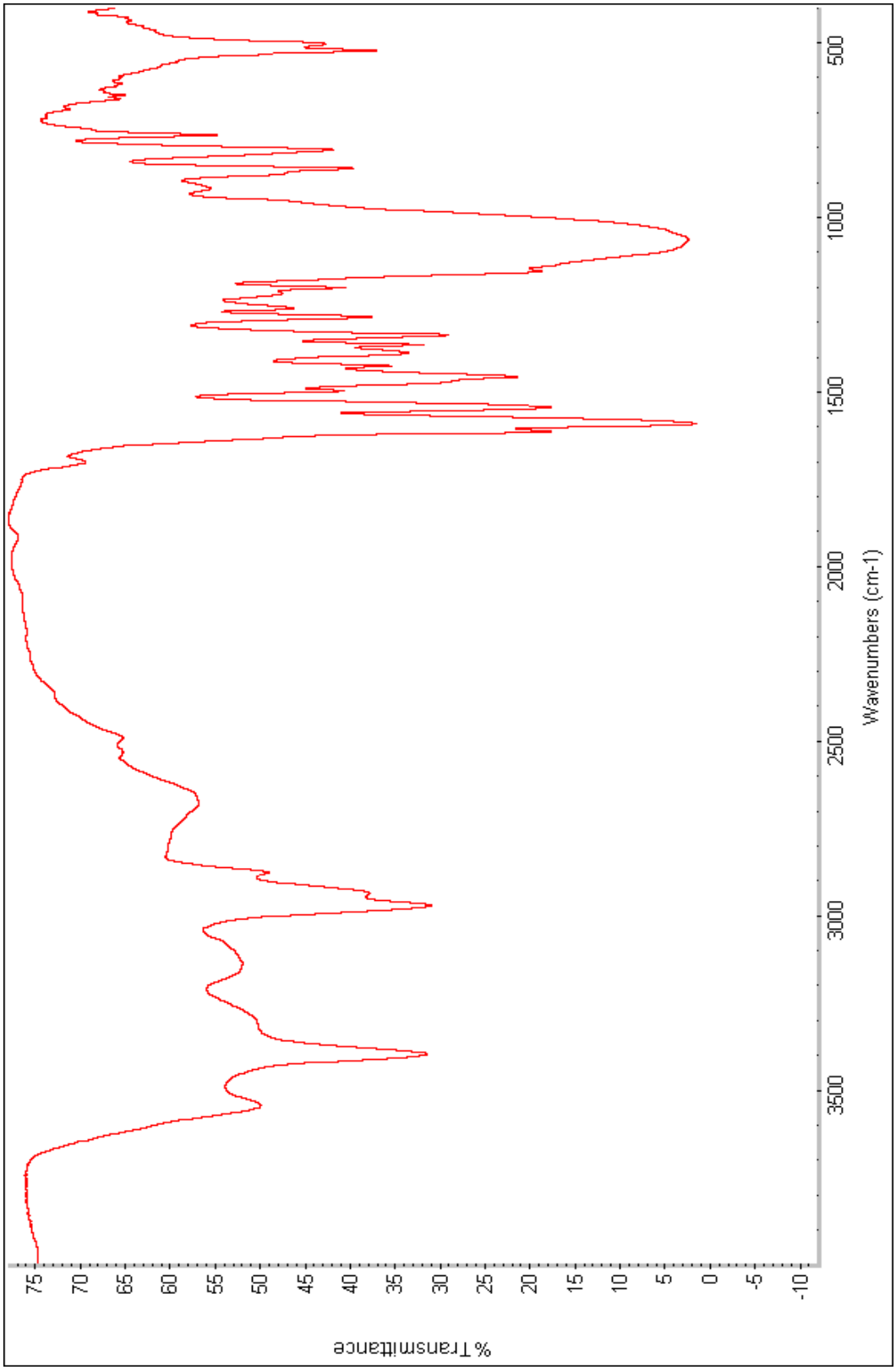

IR spectrum of complex 3

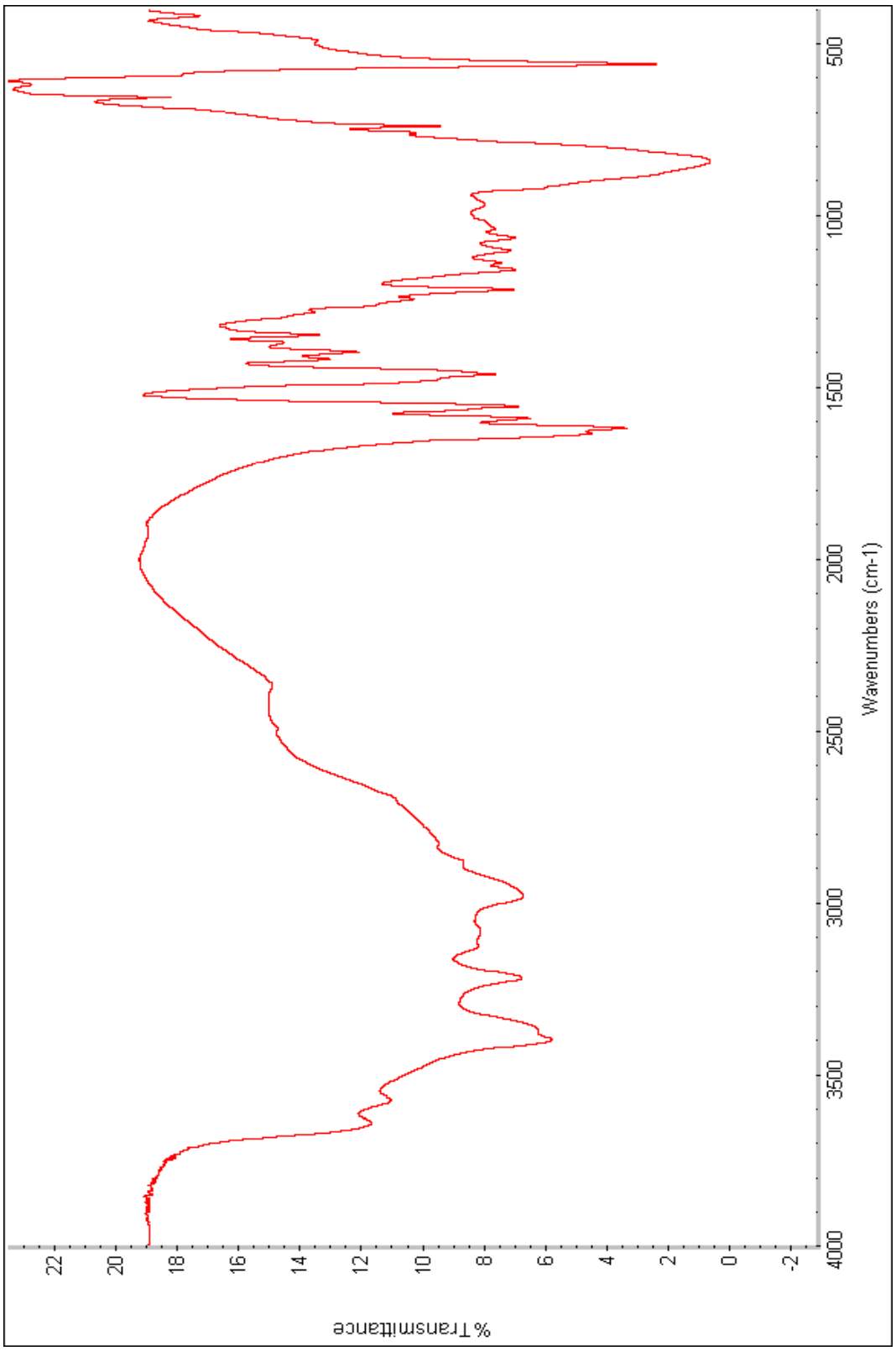

IR spectrum of complex 4

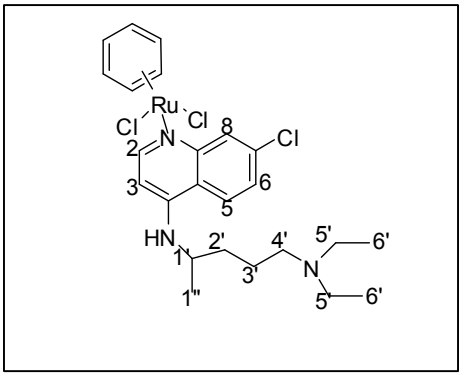

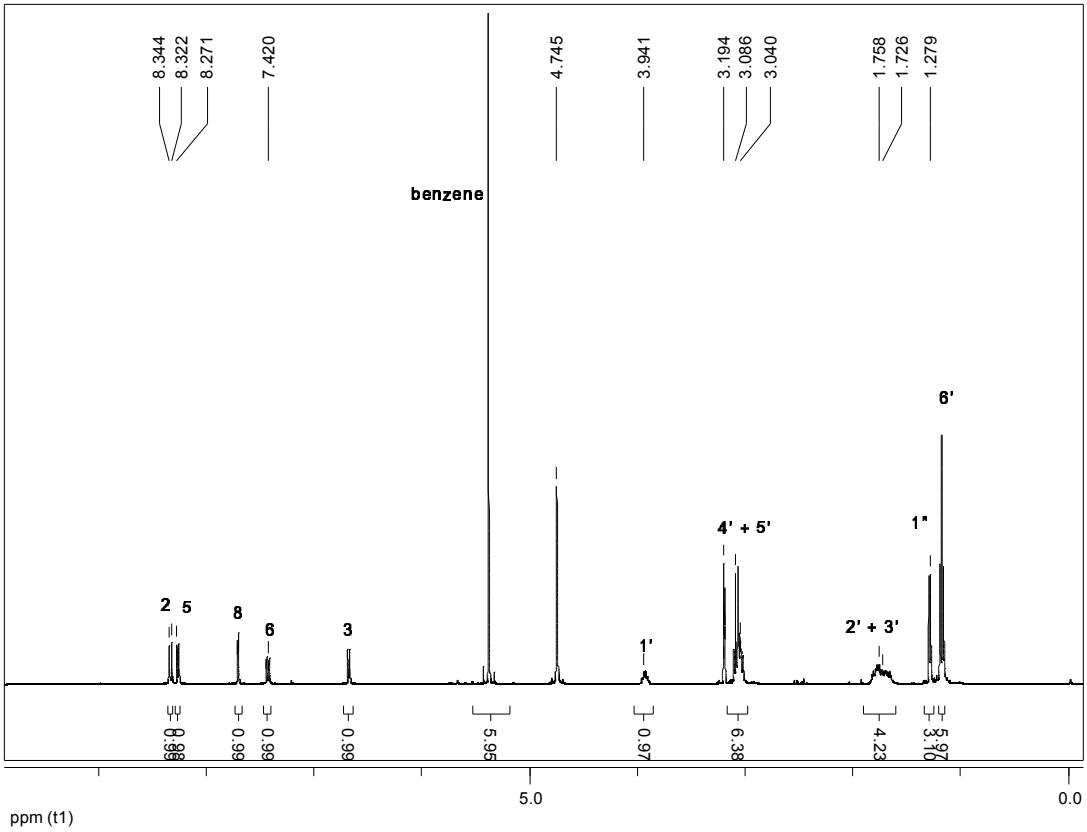

^{1}H NMR of complex **2** in MeOD

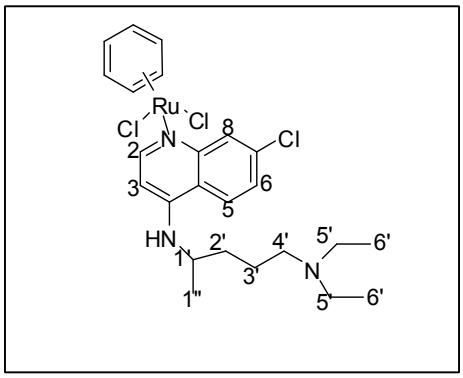

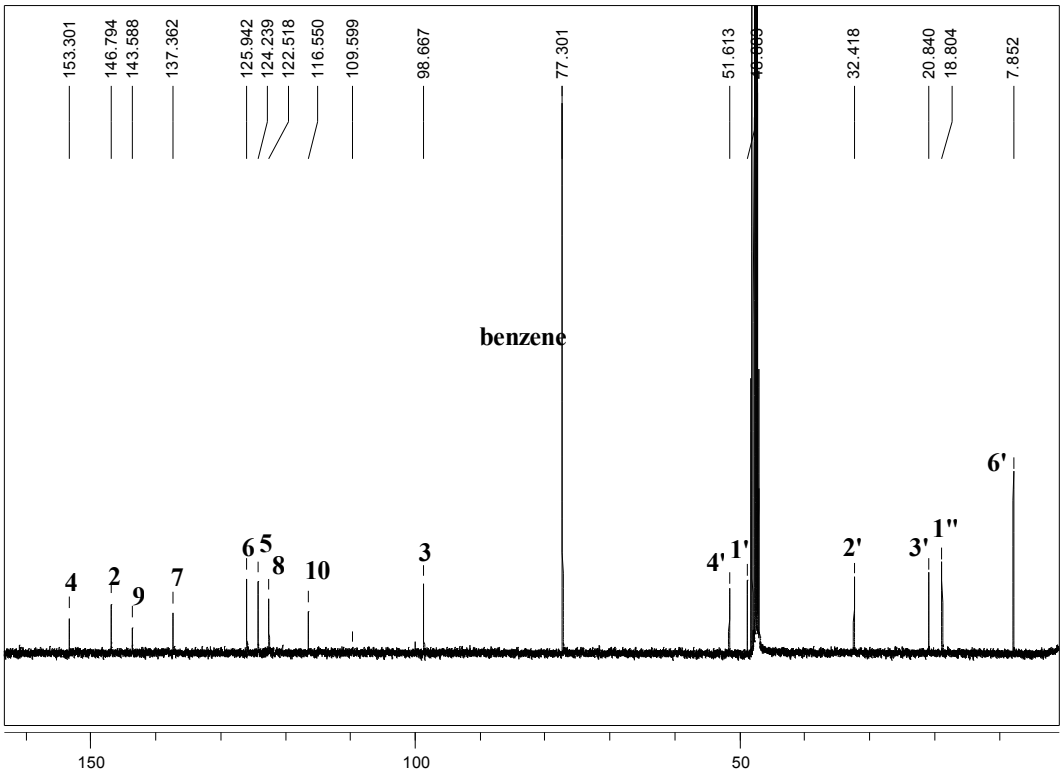

^{13}C NMR of Complex **2** in MeOD

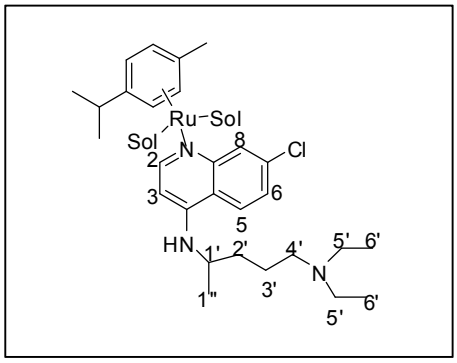

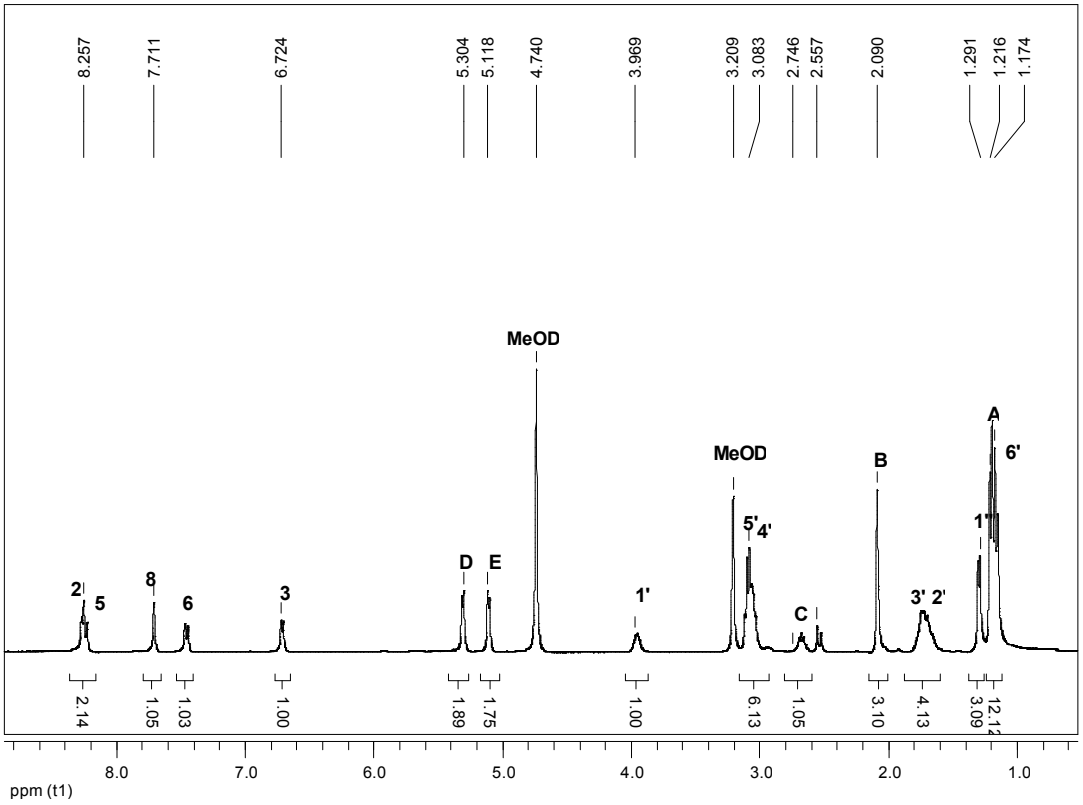

^{1}H NMR of complex **3** in MeOD

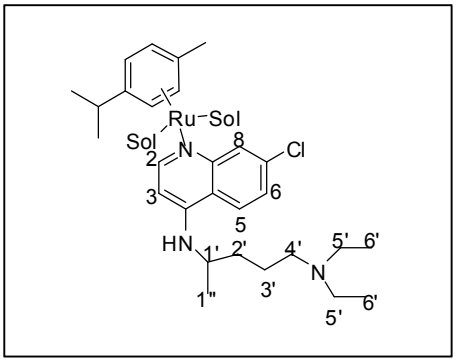

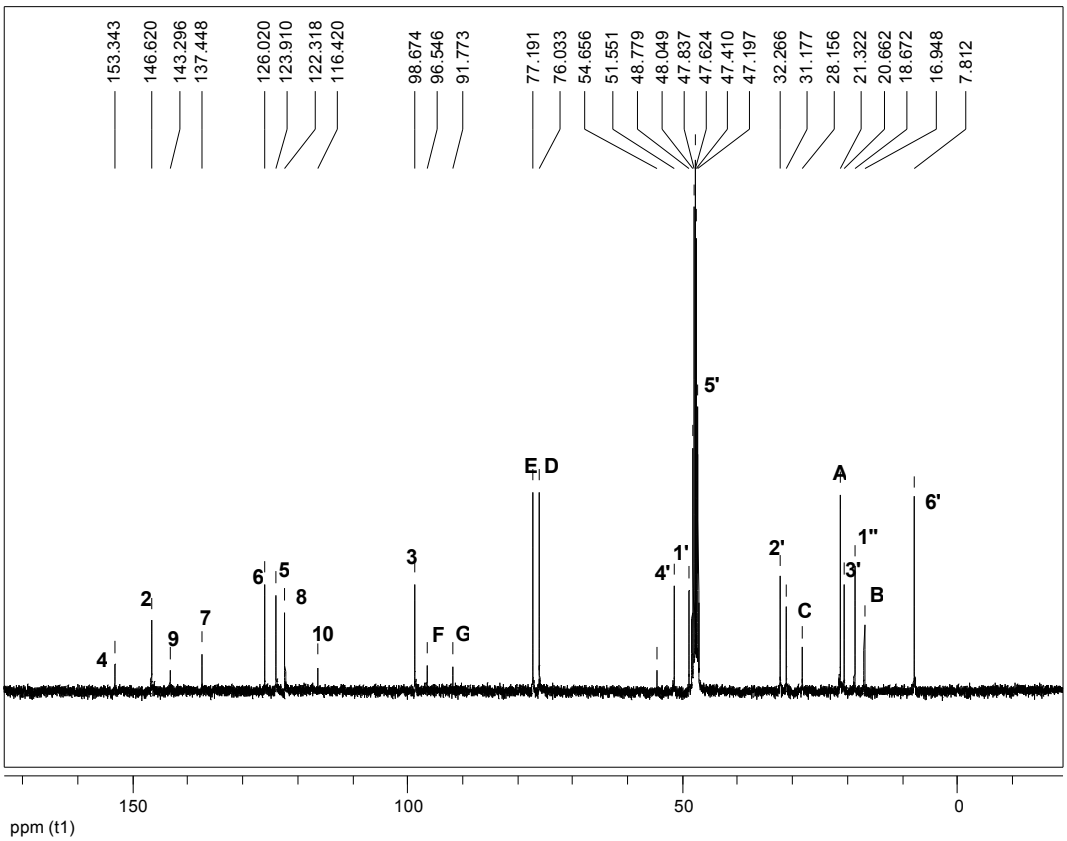

^{13}C NMR of complex **3** in MeOD

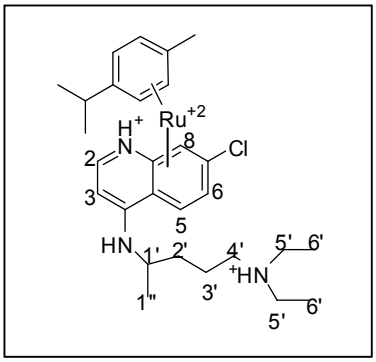

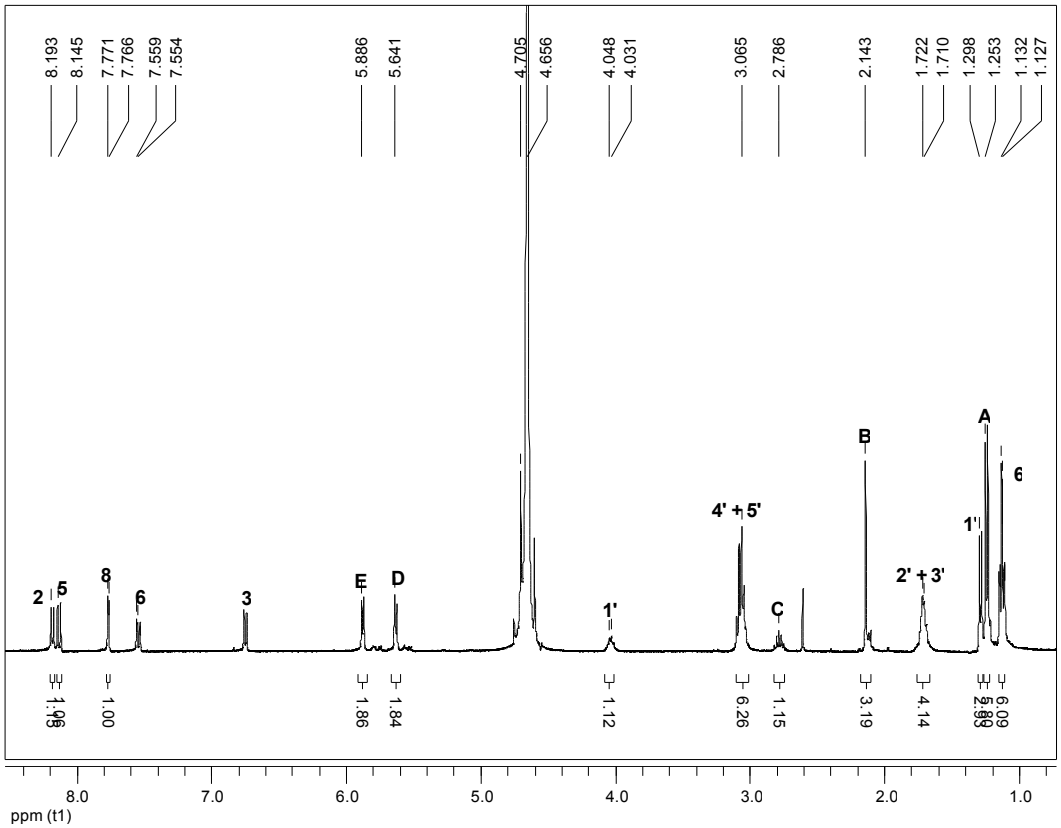

^{1}H NMR of complex **4** in D_2O

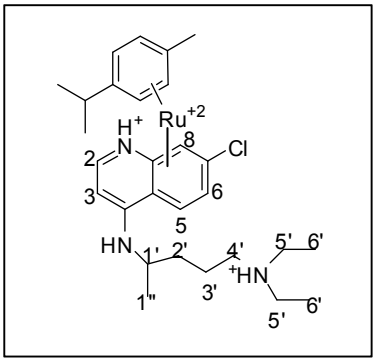

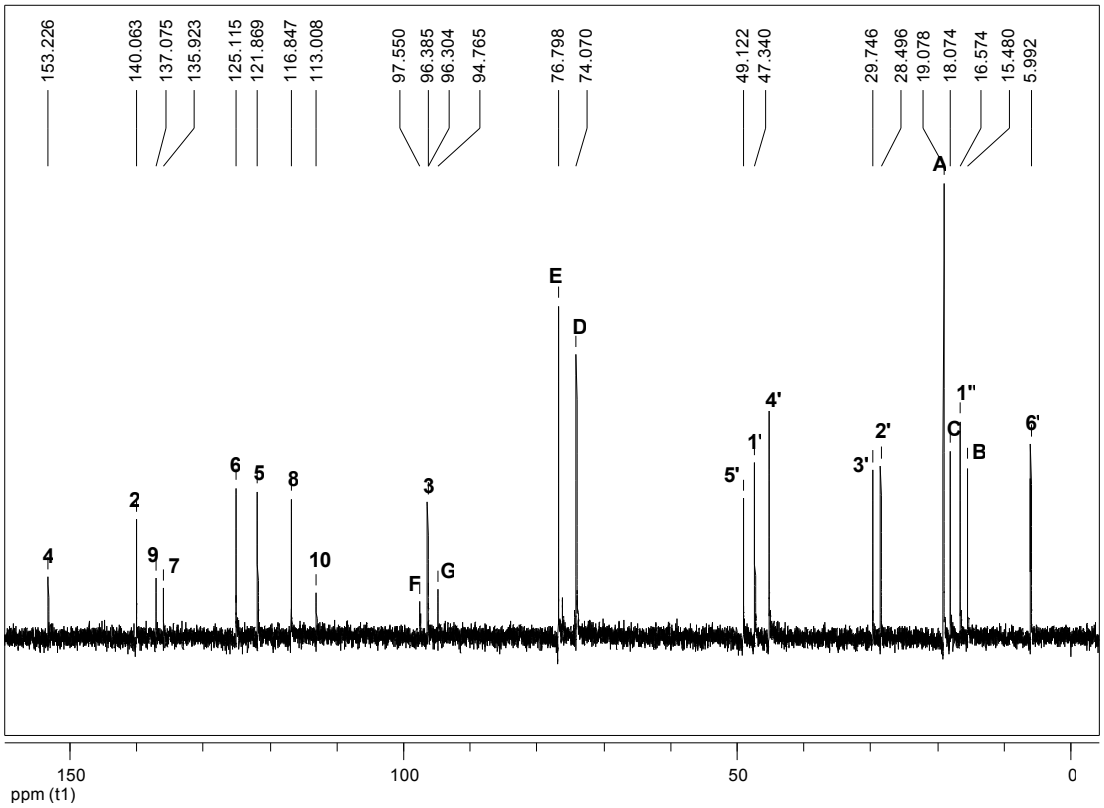

^{13}C NMR of complex **4** in D_2O

Chapter 3

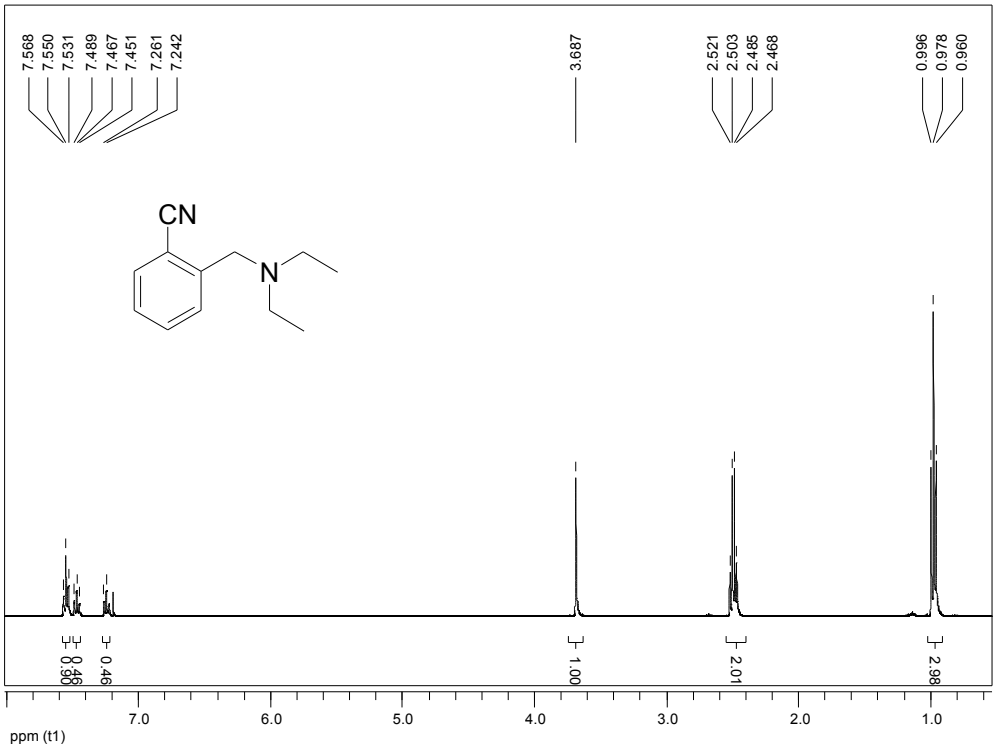

^{1}H NMR of compound **1** in $CDCl_3$

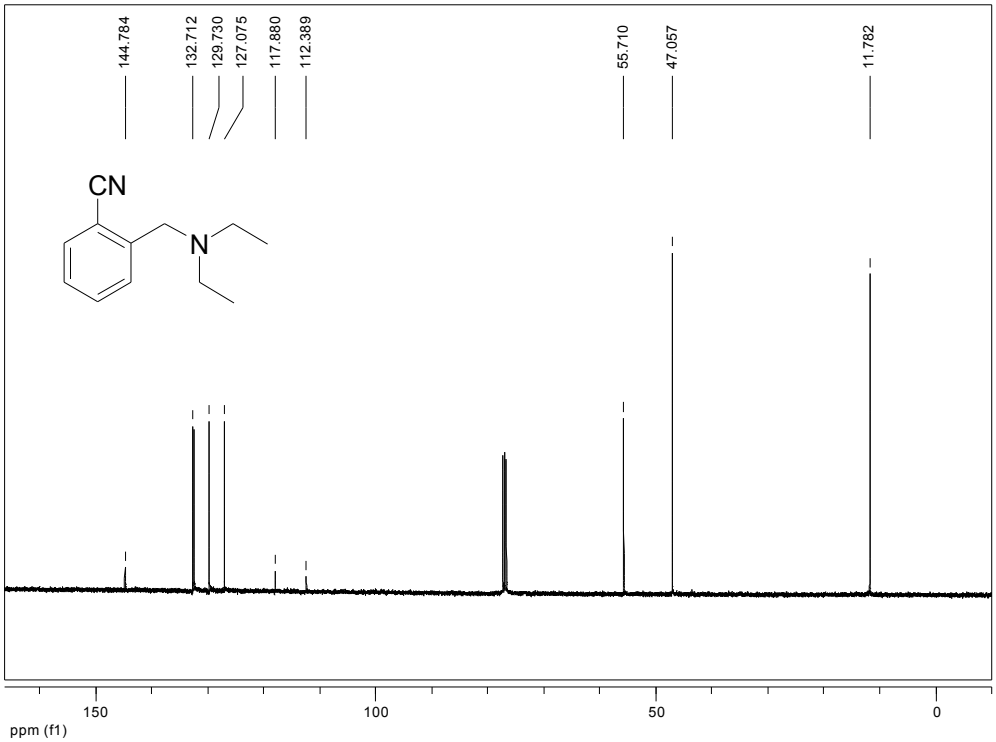

^{13}C NMR of compound **1** in $CDCl_3$

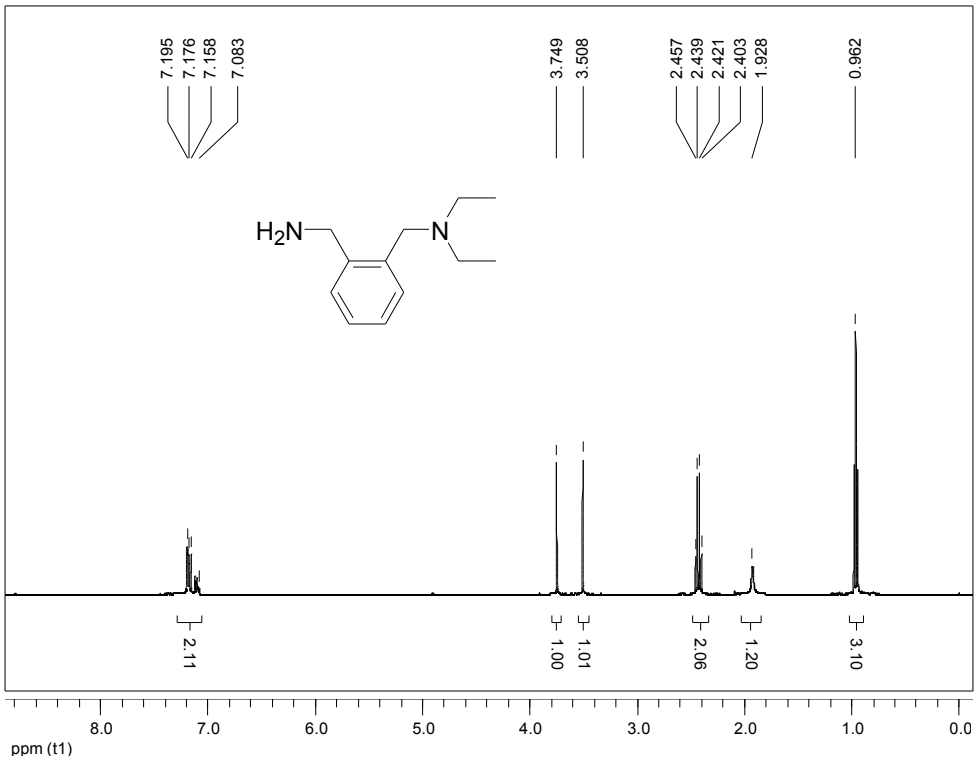

^{1}H NMR of compound **2** in $CDCl_3$

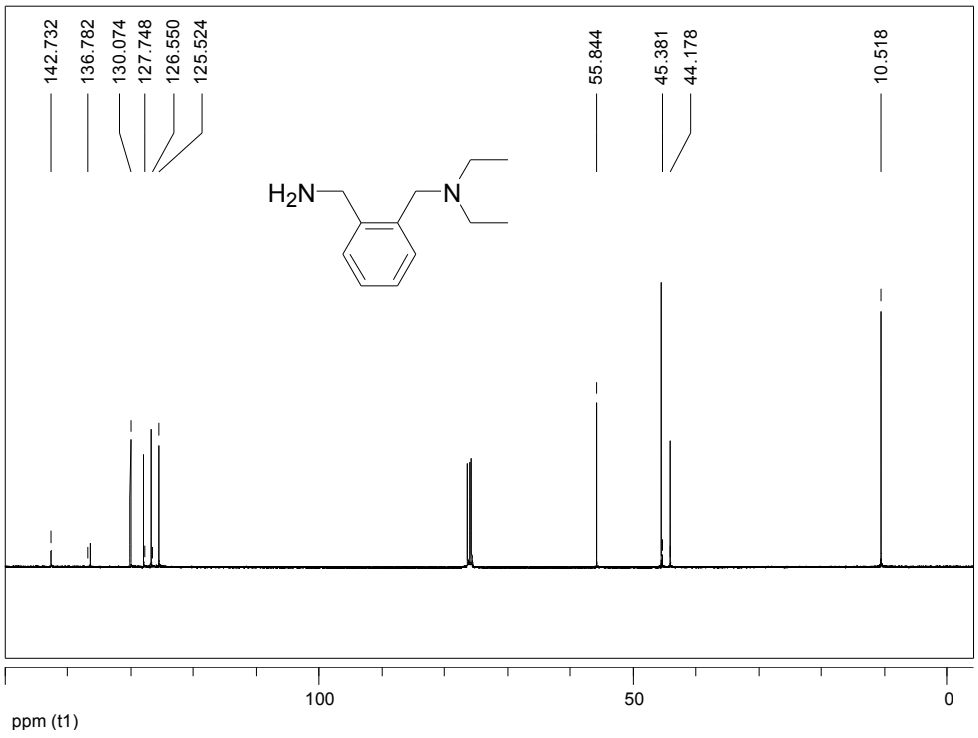

^{13}C NMR of compound **2** in $CDCl_3$

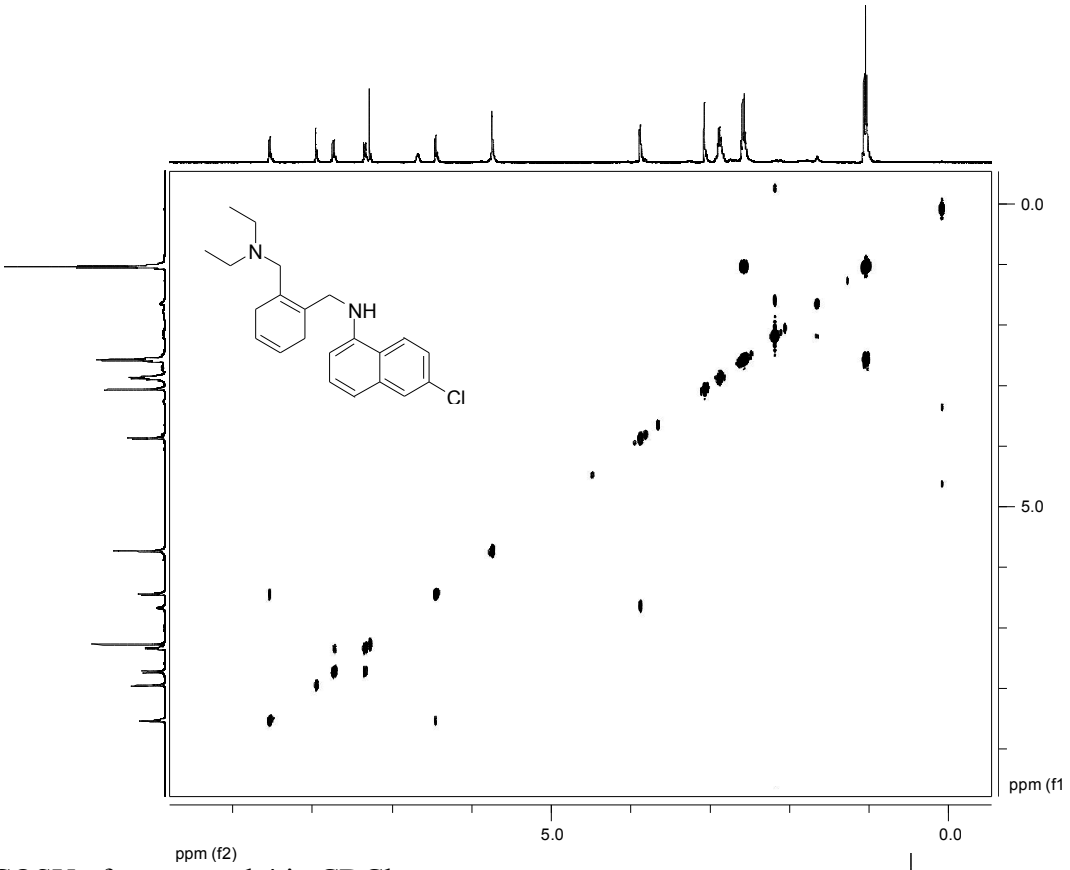

COSY of compound **4** in $CDCl_3$

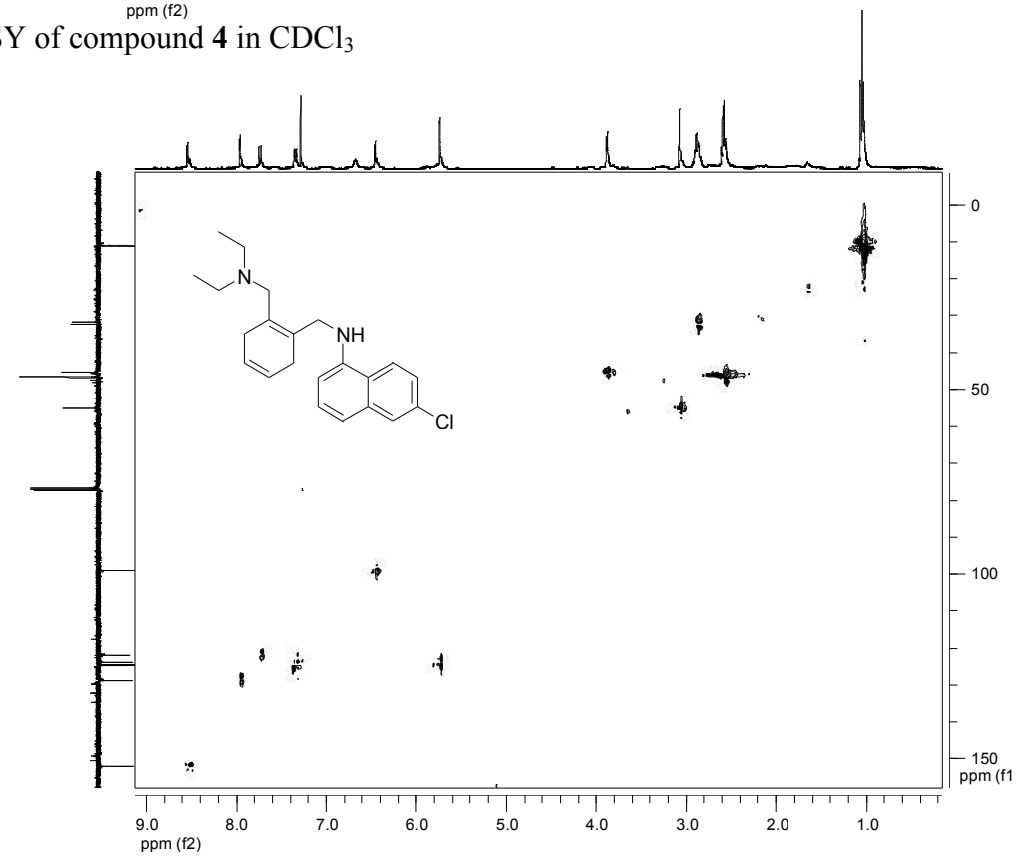

HSQC of compound **4** in $CDCl_3$

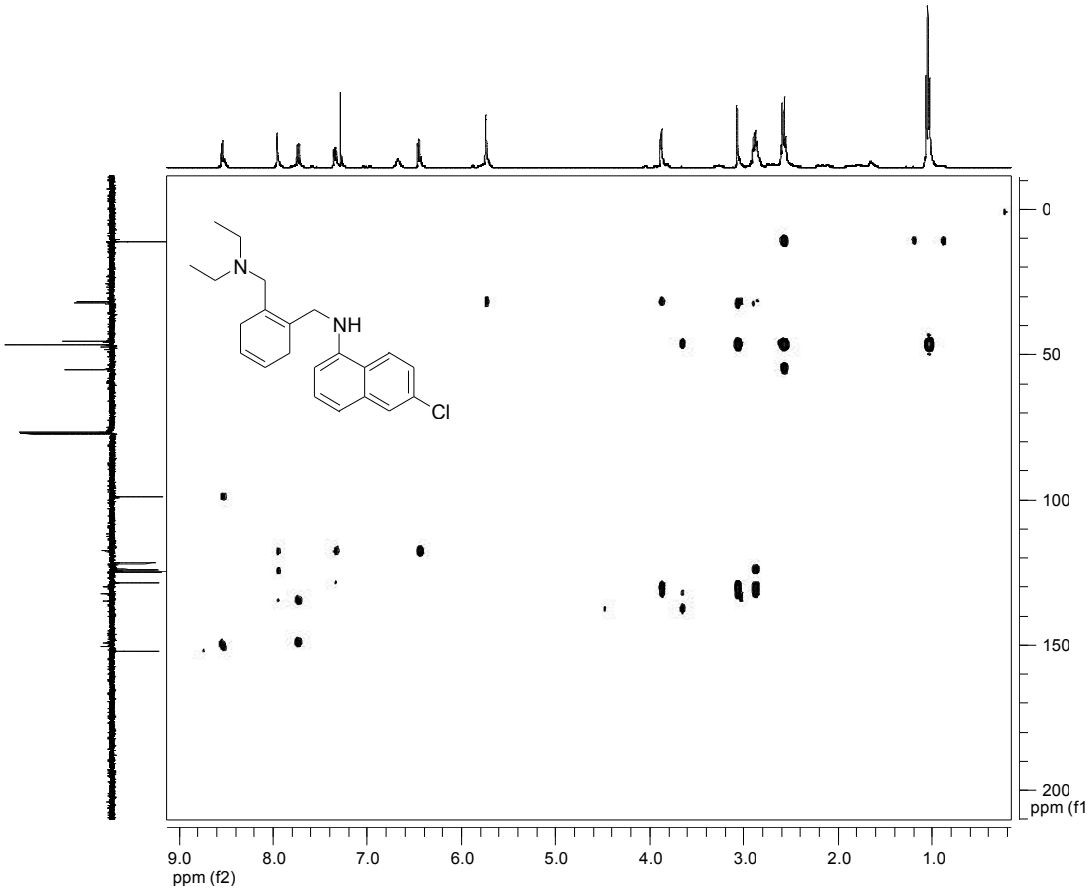

HMBC of compound **4** in $CDCl_3$

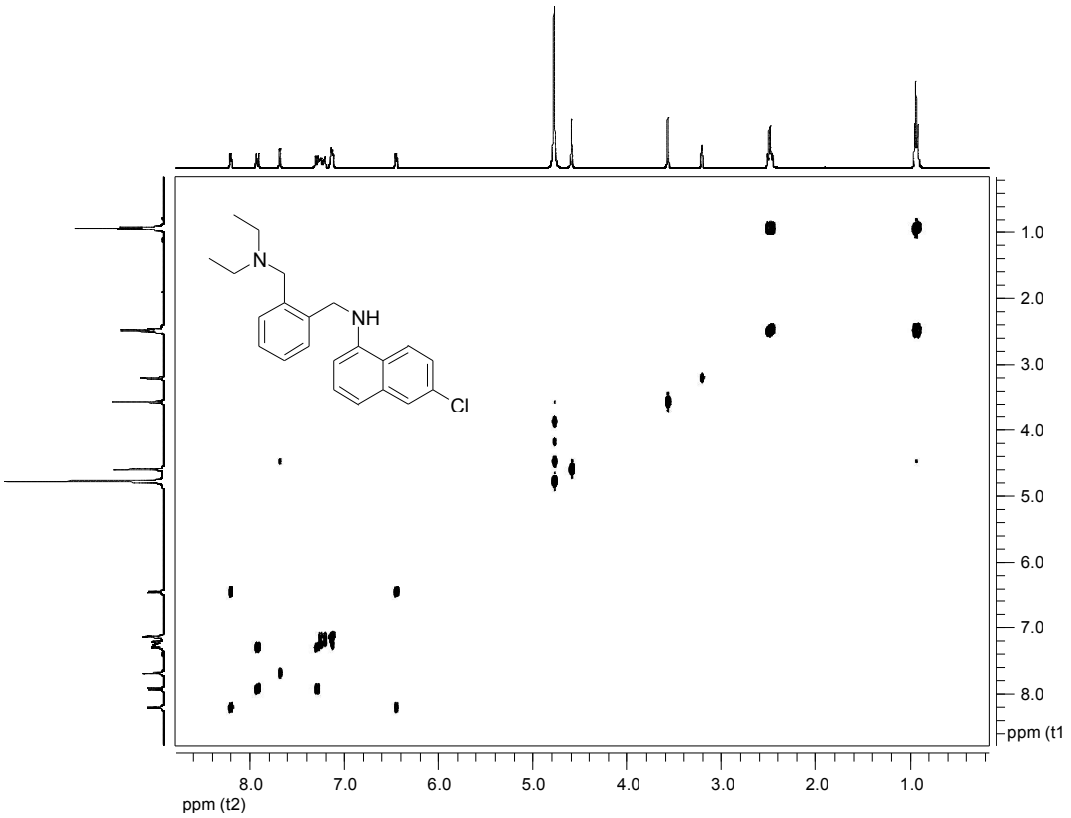

COSY of compound **5** in MeOD

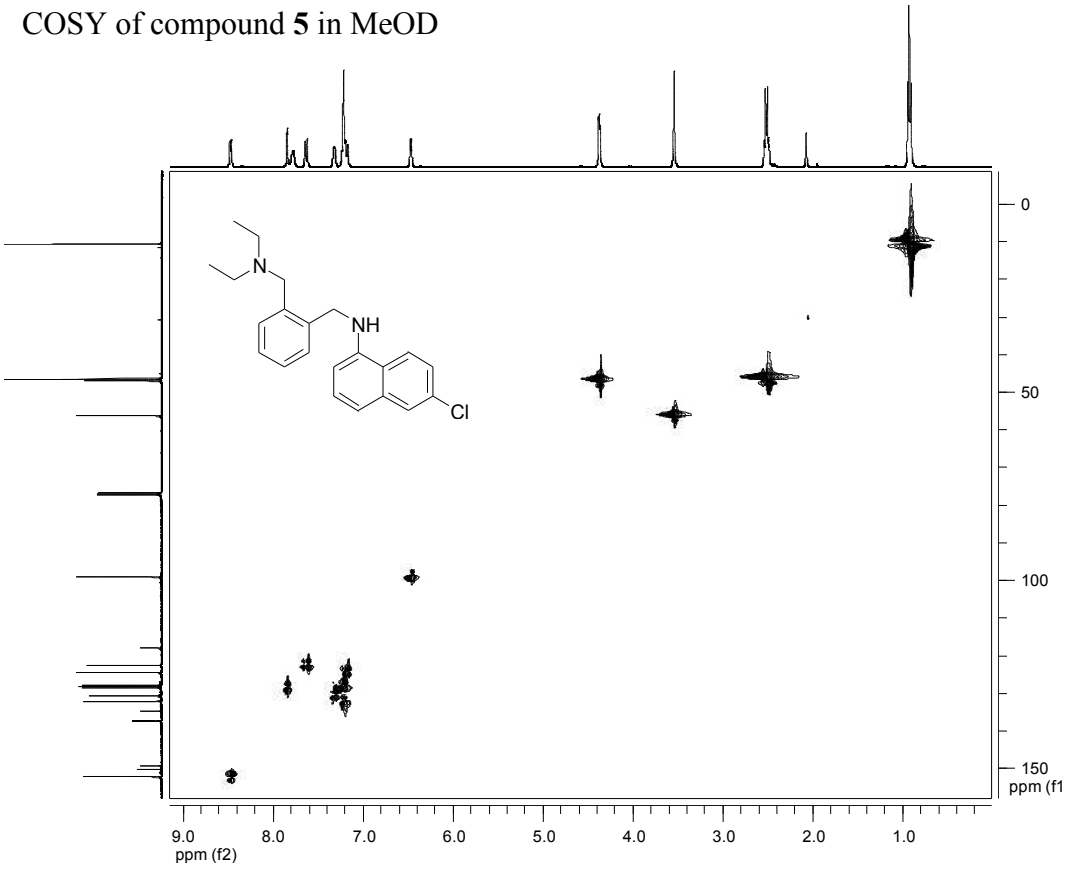

HSQC of compound **5** in $CDCl_3$

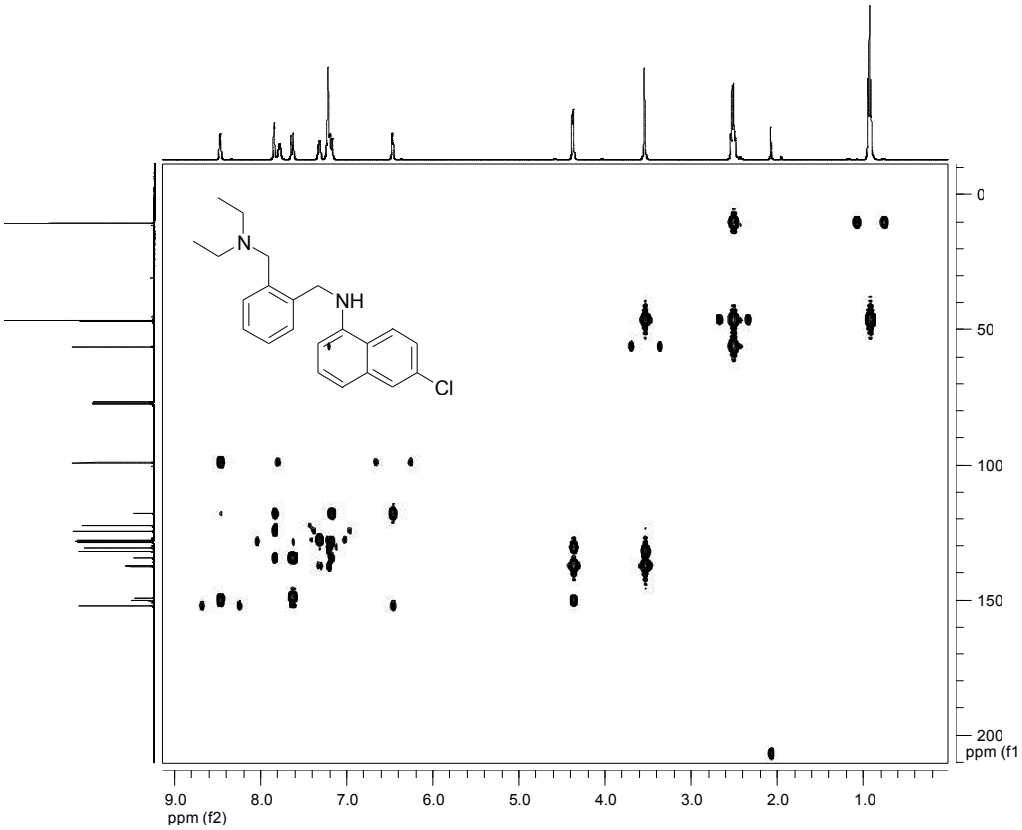

HMBC of compound **5** in $CDCl_3$